MECHANISMS OF CHROMIUM DEPOSITION AND DISSOLUTION UNDER DIRECT AND PULSE REVERSE PLATING CONDITIONS

NENAD VOJINOV MANDICH
Doctor of Philosophy

THE UNIVERSITY OF ASTON IN BIRMINGHAM

JUNE 1996

THE UNIVERSITY OF ASTON IN BIRMINGHAM

Title: MECHANISMS OF CHROMIUM DEPOSITION AND DISSOLUTION UNDER DIRECT AND PULSE REVERSE PLATING CONDITIONS

Author: Nenad Vojinov Mandich
Degree: Doctor of Philosophy
Date: JUNE 1996

SUMMARY

The mechanism of chromium electrodeposition and dissolution are not fully understood since chromium deposition proceeds through a specific cathode film containing complexes of chromium and catalysts.

In Part I of this thesis, different existing theories are discussed, and the sequences of chromium electrodeposition mechanism are presented. The present state of the theories for electrodeposition with periodic current reversal (PRC) are discussed and the existing theory of K. Popov was expanded by the introduction of variable charge ratio. This was found experimentally to be the governing factor for increased cathodic current efficiency (CCE) of chromium electrodeposition under PRC mode. Physical properties of chromium deposits under PRC regime were investigated for specific cases of equal anodic and cathodic current densities and variable time periods. Corrosion resistance was improved significantly, at the expense of lower deposit thickness and 14-28% reduction in hardness compared with DC deposits. Experiments with addition of nano-diamonds to three different plating baths resulted in improvements in wear properties of the deposits.

Baths containing sulphuric acid as catalyst and others with selected secondary catalysts (methane sulphonic acid - MSA, SeO_2, a $KBrO_3/KIO_3$ mixture, indium, uranium and commercial high speed catalysts (HEEF-25 and HEEF-405) were studied. The secondary catalysts influenced CCE, brightness and cracking.

Chromium deposition mechanisms were studied in Part II using potentiostatic and potentiodynamic electroanalytical techniques under stationary and hydrodynamic conditions. Sulphuric acid as a primary catalyst and MSA, HEEF-25, HEEF-405 and sulphosalycilic acid as co-catalysts were explored for different rotation speeds and scan rates. Maximum current was resolved into diffusion and kinetically limited components, and a contribution towards understanding the electrochemical mechanism is proposed. Reaction kinetics were further studied for H_2SO_4, MSA and methane disulphonic acid catalysed systems and their influence on reaction mechanisms elaborated. Charge transfer coefficient and electrochemical reaction rate orders for the first stage of the electrodeposition process were determined. A contribution was made toward understanding of H_2SO_4 and MSA influence on the evolution rate of hydrogen. Anodic dissolution of chromium in the chromic acid solution was studied with a number of techniques. An electrochemical dissolution mechanism is proposed, based on the results of rotating gold ring disc experiments and scanning electron microscopy.

Finally, significant increases in chromium electrodeposition rates under non-stationary conditions (PRC mode) were studied and a deposition mechanisms is elaborated based on experimental data and theoretical considerations.

Keywords: Electrodeposition Mechanisms, Chromium Electrodeposition, Pulse Reverse Plating, Catalysts.

DEDICATION

To Inga and

to Peter and Nikola

who can't remember when

Dad wasn't studying.

"My desire [was] to escape from trade, which I thought vicious and selfish, and to enter into the service of Science, which I imagine made its pursuers amiable and liberal....."

Michael Faraday, 1829

ACKNOWLEDGEMENTS

From the beginning of my tenure in the fields of Chemistry and Applied Electrochemical Engineering, I have had the good fortune to interact with a number of fine people, I take this opportunity to recognise some of the friends and colleagues with whom I have associated during my years in industry and academia.

I will always remember and strive to assimilate Dr. Bozidar J. Stipanovic's inquisitive and philosophical nature, which spans a phenomenally large number of subjects. He taught me the meaning of diligence - how it can greatly simplify seemingly complex situations - and taught me, above all else, how to approach solving technical and scientific problems. He gave me valuable tools that I shall always use.

I am grateful to my thesis advisor, Dr. J. K. Dennis, who stimulated me to start my Ph. D. work in the later stages of life and for his advice, interest, and encouragement throughout the course of study.

I am indebted to the professors at my *alma mater*, the University of Belgrade, Serbia, who instilled in me solid technical foundations and a love for engineering and Fatherland.

Lastly, I want to thank my family which is my foundation. Their continued encouragement and support have helped me through difficult times while doing Ph. D. research, running my own company which provides specialised plating technology and actively helping the Fatherland in the middle of a Civil War.

LIST OF CONTENTS

LIST OF TABLES

LIST OF FIGURES

PART ONE

THEORETICAL CONSIDERATIONS

I. AIMS

To study the complex nature of reactions occuring simultaneously during the depostion of chromium from hexavalent baths using direct current and pulse reverse current.

To study the behaviour of high efficiency catalysts and their effects on properties of chromium deposits.

To use modern experimental techniques to study mechanisms during the cathodic and anodic cycles of PRC deposition.

I.1 INTRODUCTION

For a long time it was considered that current interruption of any kind during chromium electrodeposition with Direct Current (DC) had detrimental effects on brightness and adhesion and it was considered as a nuisance to practical chromium platers. However, it was found that, if interruptions are short enough, as in the case of Pulse Current plating (PC) or, if a short anodic treatment is applied before cathodic treatment, as in Periodic Reverse Current plating (PRC), important beneficial effects result.

Pulse plating, or plating with unipolar cathodic pulses (PC), is treated in a number of papers with the common conclusion that, in general, the number of cracks is reduced or eliminated as a consequence of PC, but there is reduction of tensile stress, brightness, and current efficiency and somewhat less tendency to produce nodular deposits. Also, during the *off time* (when cathodic current equals zero), replenishment of the depleted cathode diffusion layer takes place. Nucleation is interrupted and started again, resulting in more small crystal nucleation sites with the net effect of having finer, denser and less porous metal deposits. Better throwing power and reduced tendency of "burning" at high current density are additional benefits. Due to the high current densities normally required for chromium plating, the cost of building PC power supplies most often outweighed benefits and this method of chromium plating found only limited specific applications.

While almost all commonly plated metals are deposited and dissolved at approximately the same rates , chromium dissolves (strips, etches, reverses) several times faster than it is deposited as a consequence of acute low cathode current efficiency. Early

research on Periodic Reverse Current (PRC) plating of chromium, mostly by Russians, produced crack-free deposits, which were softer than DC ones and semi-bright or dull in appearance. Due to the lack of satisfactory power supplies, cathodic and anodic current densities were kept the same and benefits were most often outweighed by drawbacks. However, recently, with the introduction of Silicon Controlled Rectifiers and Transistors as the components of DC power supplies, current modulation in forward and reverse cycles is simpler and less cost restrictive. Very few of theoretical treatments are available at this point. It is obvious that PRC plating has more variables than DC plating. More variables mean more complex plating equipment and controls but also wider choice of deposit characteristics which can be tailored for a particular application, e.g., increased corrosion protection, levelling, different hardness, ductility, stress values, alloy composition and in the case of chromium, results in higher cathode current efficiency.

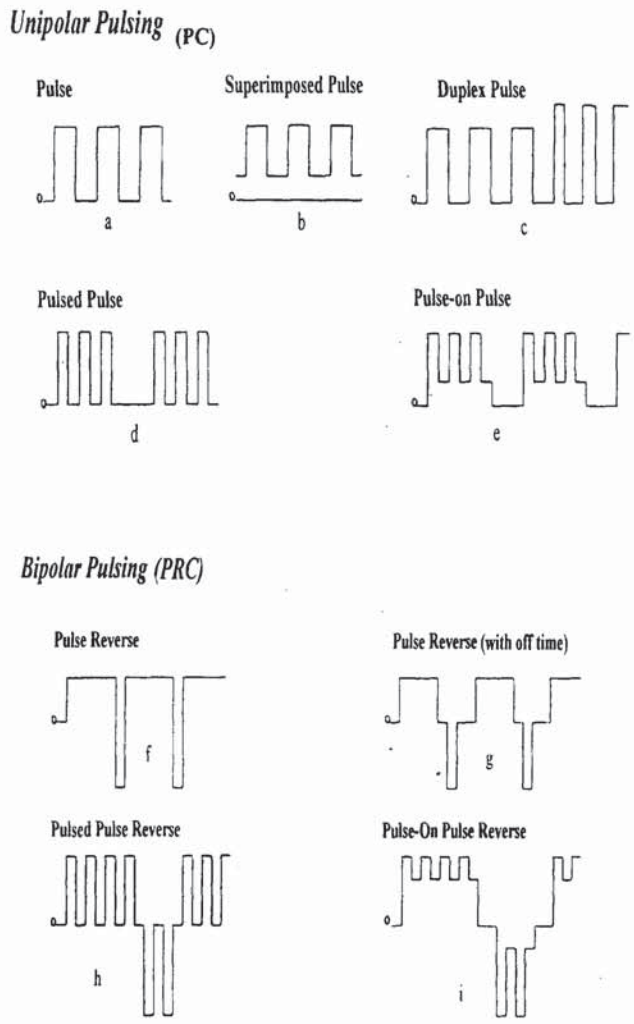

Figure 1. Non-Stationary Current Forms

I.2 CHEMISTRY OF CHROMIUM AND THEORY OF CHROMIUM DEPOSITION

I.2.1 CHEMISTRY OF CHROMIUM

I.2.1a. INTRODUCTION

Chromium, Cr, also loosely called Chrome, is the twenty-first element in relative abundance with respect to the earth's crust, yet is the seventh most abundant element because Cr is concentrated in the earth's core and mantle. It has atomic number 24 and belongs to the group 6(VI B) of the Periodic Table. On a tonnage basis, chromium ranks fourth among the metals and thirteenth among all mineral commodities in commercial production.

Chromium was discovered by Vauquelin in 1779 in Siberian red lead, the mineral *Crocoite*, $PbCrO_4$. In 1798 he isolated the new metal by reduction of CrO_3 with charcoal at high temperature. The name chromium (from Greek *chroma*, colour) was suggested for the new element because of its many coloured compounds. Chromium , relatively recently, was recognised as a biologically necessary trace element. The first conclusive evidence demonstrating a metabolic role for chromium was obtained by *Mertz* and *Schwartz*[1] in a series of investigations the first of which appeared in 1955.

Chromium has a ground state electronic configuration $1s^2$, $2s^2$, $2p^6$, $3s^2$, $3p^6$ $3d^5$, $4s^1$. This distribution of the outermost electrons is favoured over $3d^4$ $4s^2$ because of increased stability of the half-filled 3d shell with 1 electron in each of the orbitals. The half-filled shell leads to the "S" state (L=0) which is especially stable supposedly because of the large amount of exchange energy [2] . The *d* orbitals project close to the surfaces of the ions so that the electrons in them interact with the chemical environment.

A typical transition element, chromium forms many compounds that are coloured and paramagnetic. Chromium has oxidation states as follows: 2^-, 1^- , 0, 1^+, 2^+, 3^+ , 4^+, 5^+, 6^+; the highest oxidation state, 6^+, corresponds to the sum of the numbers of 3*d* and 4*s* electrons. The lowest 2^-, 1^- , 0 and 1^+ are formal oxidation states displayed by chromium in compounds such as carbonyls, nitrosyls and organometallic complexes.

b. DIVALENT CHROMIUM

Chromium in the oxidation state 2^+ was in the past not considered to be of particular great interest for electrodeposition mechanisms. However, it does play a role in the passivation of chromium and also recently it is accepted that possibly and probably plays a role in the deposition and dissolution mechanisms; this warrants that it be briefly introduced here. The outstanding characteristic of the Cr^{2+} ion (sky blue in aqueous solution) is its strength as a reducing agent $Cr^{3+} + e \Leftrightarrow Cr^{2+}$; $E_0 = 0.41$ V. Since it is easily oxidised by oxygen, preservation of the solution requires exclusion of air. Even under such conditions, the Cr^{2+} ion is oxidised by water with the formation of hydrogen. The rate of oxidation depends on several factors, including the acidity and the anions present.

It has been known for some time[3] that pure chromium (usually obtained electrolytically) dissolves in acids to form Cr^{2+} with no (or very little) Cr^{3+} , (if the solution is protected from air, of course); impurities apparently catalyse formation of Cr^{3+} . Chromium (2+) solutions may also be obtained by electrolytic reduction of chromium (3+)[4,5]. Recently *Leisner et al.*[6] proposed chromium dissolution mechanism during anodic dissolution of chromium in chromium plating solution, postulating $Cr^0 \rightarrow Cr^{2+}$ oxidation under these conditions. *Mandich and Vyazovikina*[7] contemplated Cr dissolution mechanism in CrO_3 solution as a seven steps mechanism under mixed diffusion-kinetic control. Six steps are single electron electrochemical steps while the seventh step is associated with desorption of Cr(6+). Dissolution of chromium in acid media (primarily H_2SO_4) is examined quite extensively in corrosion studies of chromium metal and alloys. Active dissolution yields chromous ions according to most of the models[8,9] while the active-passive transition is associated with the formation of the blocking passive layer.

c. TRIVALENT CHROMIUM

Chromium (3+) is the most stable and most important oxidation state of the element. The E^0 values[11] (Table 1) show that both the oxidation of Cr^{2+} to Cr^{3+} and the reduction of Cr^{6+} to Cr^{3+} are favoured in acidic aqueous solutions. The preparation of Cr^{3+} compounds from either state presents few difficulties and does not require special conditions[10]. In basic solutions, the oxidation of Cr^{3+} to Cr^{6+} by oxidants such as peroxides and hypohalites occurs with ease. The preparation of Cr^{6+} from Cr^{3+} in basic solutions

requires the use of powerful reduction agents such as hydrazine, hydrosulphite and borohydride; but Fe^{2+}, thiosulphate and sugars can be employed in acid solutions.

Half cell reaction	E^0, V
$Cr^{3+} + 3\,e^- \rightarrow Cr$	-0.740
$Cr(OH)^{2+} + H^+ + 3e^- \rightarrow Cr + H_2O$	-0 .058
$Cr^{2+} + 2\,e^- \rightarrow Cr$	-0.910
$Cr^{3+} + e^- \rightarrow Cr^{2+}$	-0.410
$Cr_2O_7^{2-} + 14\,H^+ + 6\,e^- \rightarrow 2\,Cr^{3+} + 7\,H_2O$	1.330
$Cr_2O_7^{2-} + 10\,H^+ + 6\,e^- \rightarrow 2\,Cr(OH)_2 + 3\,H_2O$	1.100
$CrO_4^{2-} + e^- \rightarrow CrO_4^{-3}$	0.100
$Cr^{6+} + e^- \rightarrow Cr^{5+}$	0.600
$Cr^{5+} + e^- \rightarrow Cr^{4+}$	1.300
$Cr^{4+} + e^- \rightarrow Cr^{3+}$	2.000

Table 1. Standard Reduction Potentials for Chromium Ions [11]

Reaction	Log *K*
$Cr^{2+} + H_2O \Leftrightarrow Cr(OH)^+ + H^+$	5.3
$Cr^{3+} + H_2O \Leftrightarrow Cr(OH)^{2+} + H^+$	-4.2
$Cr^{3+} + 2\,H_2O \Leftrightarrow Cr(OH)_2 + 2\,H^+$	-10.4
$Cr^{3+} + 3\,H_2O \Leftrightarrow Cr(OH)_3 + 3\,H^+$	-18.7
$Cr^{3+} + 4\,H_2O \Leftrightarrow Cr(OH)_4 + 4\,H^+$	-27.8
$2\,Cr^{3+} + 2\,H_2O \Leftrightarrow [Cr_2(OH)_2]^{4+} + 2\,H^+$	5.3
$3\,Cr^{3+} + 4\,H_2O \Leftrightarrow [Cr_3(OH)_4]^{5+} + 4\,H^+$	-8.7
$4\,Cr^{3+} + 4\,H_2O \Leftrightarrow [Cr_4(OH)_6]^{6+} + 6\,H^+$	-13.9
$Cr^{3+} + 3C_2O_4^{2-} \Leftrightarrow [Cr(C_2O_4)_3]^{3-}$	-15.4
$Cr^{3+} + H_2\,EDTA^{2-} \Leftrightarrow [CrEDTA]^- + 2\,H^+$	23.4
$Cr^{3+} + SO_4^{2-} \Leftrightarrow Cr\,SO_4^+$	1.8
$H_2CrO_4 \Leftrightarrow HCrO_4^- + H^+$	0.61
$HCrO_4^- \Leftrightarrow CrO_4^{2-} + H^+$	-5.9
$2\,HCrO_4^- \Leftrightarrow Cr_2O_7^{2-} + H_2O$	2.2
$H_2CrO_4 + Cl^- \Leftrightarrow CrO_3\,Cl^- + H_2O$	1.0
$HCrO_4^- + HSO_4^- \Leftrightarrow Cr_2\,SO_7^{2-} + H_2O$	0.60

Table 2. Hydrolysis, Equilibrium and Complex Formation Constants[11]

The chemistry of Cr^{3+} in aqueous solutions is coordination chemistry. It is demonstrated by the formation of kinetically inert outer orbital octahedral complexes.

The bonding can be explained by $d^2 sp^3$ hybridisations and a great number of complexes have been prepared. The kinetic inertness results from the $3d^3$ electronic configuration of Cr^{3+} ion[12] . This type of orbital charge distribution makes liquid displacement and substitution reactions very slow and allows separation, persistence and /or isolation of Cr^{3+} species under thermodynamically unstable conditions.

Hydrolysis of Chromium (3+) and related Processes.

Chromium (3+) is characterised by a marked tendency to form polynuclear complexes. Literally thousands of Cr^{3+} complexes have been isolated and characterised and, with a few exceptions, are all hexacoordinate. The principal characteristic of these complexes in aqueous solution is their relative kinetic inertness. Ligand displacement reactions of Cr^{3+} complexes have halftimes in the range of several hours. It is largely because of this kinetic inertness that so many complex species can be isolated as solids and that they persist for relatively long periods of time in solution even under conditions of marked thermodynamic instability.

The hexaaqua ion $[Cr(H_2O)_6]^{3+}$, which is a regular octahedral, occurs in numerous salts such as the violet hydrate $[Cr(H_2O)_6]Cl_3$ and in an extensive series of alumns $MCr(SO_4)_2\ 12 \bullet H_2O$, where M usually is NH^+_4 or K^+ ion. The aqua ion is acidic (pK = 4), and the hydroxo ion condenses to give dimeric hydroxo bridged species:

$$2\left[Cr(H_2O)_6\right]^{3+} \underset{H+}{\overset{-H+}{\rightleftharpoons}} 2\left[Cr(H_2O)_5OH\right]^{2+} \rightleftharpoons \left[(H_2O)_4Cr\left\langle{}^{OH}_{OH}\right\rangle Cr(H_2O)_4\right]^{4+} + 2H_2C \qquad <1>$$

On further addition of base, a precipitate is formed that consists of H - bonded layers of $Cr(OH)_3\ (H_2O)_3$ which readily redissolves in acid. Within a minute or less, however, this precipitate begins "ageing" to an oligomeric or polymeric structure that is much less soluble[13,14,15] .

Cr^{3+} ion also polymerises, as a result of hydrolysis and associated reactions, to form at bridged complexes with certain composition whose existence is indicated by indirect but substantial evidence. Complexes of this type range from dimers through polymers of colloidal dimensions to precipitated Cr^{3+} hydroxide. Except under special circumstances such reactions are inevitable in neutral and basic solutions and highly probable in slightly acid solutions.

What makes the chemistry of Cr^{3+} complexes interesting though intriguing and often torturous for researchers, is the number of steps and mechanisms possible. The processes include aquation, hydrolysis, olation, polymerisation, oxolation and anion penetration as described briefly in the following section:

Aquation

Chromium salts (chloride, sulphate, nitrate, etc.) are aqua complexes characterised by ions such as $[Cr(H_2O)_6]^{3+}$, $[Cr(H_2O)_5 Cl]^{2+}$ and $[Cr(H_2O)_4Cl_2]^{+}$. In aqueous solution, the replacement of co-ordinated groups by water molecules (*aquation*) is a common reaction:

$$[CrA_5 X]^{2+} + H_2O \leftrightarrow [CrA_5 H_2O]^{3+} + X^- \qquad <2>$$

where: A = Singly co-ordinated neutral molecule (e.g. H_2O, NH_3)

and X = Singly charged co-ordinated negative ion (e.g. Cl, CN, CNS)

The extent of aquation depends on several factors including the relative co-ordinating tendencies of H_2O and X and the concentrations of X. Thus, every aqueous solution of Cr^{3+} is actually potentially a solution of aqua complexes. The Cr^{2+} (whose complexes are labile) catalyses such reaction, which are usually quite slow otherwise. Electron-transfer reactions between Cr^{2+} and $[Cr(H_2O)_5 X]^{+}$ proceed predominantly through bridged intermediates $\{[Cr\text{-}X\text{-}Cr]^{4+}\}$. Ligand transfer accompanies electron transfer . In the investigations establishing these conclusions, the reaction conditions have generally been characterised by relatively low $[Cr^{2+}]$ and relatively high $[H^+]$. With relatively high $[Cr^{2+}]$ and relatively low $[H^+]$ another pathway is available[16] with the rate determining reaction involving hydroxy bridged complex: $[(H_2O)_4 X CrOH Cr]^{3+}$

. However, the role of Cr^{2+} is very important in industrial "hard" chromium applications when plating the thick layers of chromium or Cr-Ni and Cr-Ni-Fe alloys from trivalent chromium solutions as an alternative for Cr^{6+} based solutions. Failure to control the transient levels of Cr^{2+} is recognised as the reason for enabling Cr^{3+} based solution to sustain heavy deposition , with an appreciable deposition rate. Problems are recognised as massive olation catalysed by a build up of Cr^{2+} in the high pH region in the vicinity of the cathode.

Although, the bulk of electrolyte can be about pH =2 the diffusion layer can reach pH = 4. At this pH and with Cr^{2+} promoted catalysis, oligomeric species would be released into the bulk of the electrolyte, where they would build up and reduce the level of active species and hence the deposition rate.[17-20]

Hydrolysis

The behaviour of aquo complexes as acids leads to, far reaching consequences. The acidity of such solutions arises as follows:

$$[Cr(H_2O)_6]^{3+} \Leftrightarrow [Cr(H_2O)_5\ OH]^{2+} + H^+ \qquad <3>$$

The equilibrium will be displaced to the right by heating, and of course, by the addition of base. The order of magnitude of the first hydrolysis constant is $K = 10^{-4}$. As the pH of the Cr^{3+} solution is raised, the equilibrium is shifted and more of the co-ordinated water molecules may be converted to OH groups which brings into the picture the new process - olation.

Olation

Olated compounds are complexes in which the metal atoms are linked through bridging with OH groups. Such a group is designated as an *ol* group to distinguish it from the hydroxo group i.e., a co-ordinated OH linked to only one metal atom. The process of formation of ol compounds from hydroxo compounds is called *olation*. Olation results from the formation of polynuclear complexes consisting of chains or rings of Cr^{3+} ions connected by bridging OH groups. The first step of this process may be as follows:[21]

$$[Cr(H_2O)_6]^{3+} + [Cr(H_2O)_5\ OH]^{2+} \rightarrow [(H_2O)_5\ Cr\ \underset{H}{\overset{|}{O}}\ Cr\ (H_2O)_5]^{5+} + H_2O \qquad <4>$$

$$2[Cr(H_2O)_5\ OH]^{2+} \rightarrow [(H_2O)_4\ Cr\ \underset{O}{\overset{H}{\diagup\diagdown}}\ Cr\ (H_2O)_4]^{4+} + 2H_2O \qquad <5>$$

Since the *diol* produced by the reaction <5> is stabilised by the 4-member ring, there is a driving force tending to convert the singly bridged to doubly bridged complex. This diol

is produced by polymerisation of $[Cr(H_2O)_5 OH]^{2+}$, oxidation of Cr^{2+} by molecular oxygen. warming an equimolar mixture of Cr^{3+} and Na OH and boiling an aqueous solution of $[Cr(H_2O)_6]^{3+}$.

The diol and any other polynuclear products containing water molecules (or a group that can be displaced by water molecules) can still act as acids, releasing hydrogen ions and leaving co-ordinated OH groups.

The "Continued process of olation" - polymerisation.

Instead of reaching a definite termination, reaction <5> may continue with the formation of larger and larger molecules, the polymers. This may continue if the product of each successive step contains aqua or hydroxo groups. The ultimate consequence is precipitation of chromium hydroxide", $Cr(OH)_3 \ X \ H_2O$, a tri-dimensional olated complex[22]. Olation reactions are pH and time dependent. At moderate acidity they are quite slow. For higher oligomers to be formed after addition of the base to aqueous Cr^{3+} solution can take days but they can be subsequently decay contributing to pH stabilisation after a few weeks[23].

The continued process of olation starts with the hydrolysis of salts of such metals as Al or Cr. The acidity of solution of such salts is due to conversion of aqua to hydroxo groups:

$$[Cr(H_2O)_6]^{3+} \Leftrightarrow [Cr(H_2O)_5 OH]^{2+} + H^+ \qquad <6>$$

$$[Cr(H_2O)_5]^{2+} \Leftrightarrow [Cr(H_2O)_4 OH]^{+} + H^+ \qquad <7>$$

The degree of hydrolysis increases as the temperature is raised and depends on the nature of the anion and especially on the pH of the solution. If alkali is added to a warm solution of hydrolysed chromium salt but not enough for complete neutralisation, the polymerisation occurs instead of the precipitation of the basic salt or hydroxide.

This can be explained on the basis of a series of hydrolytic and olation reactions. The first step might be presented as :

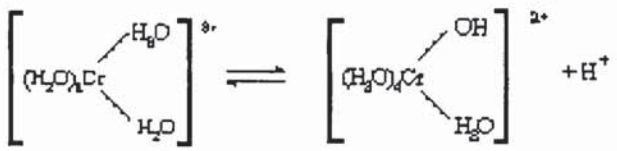

<8>

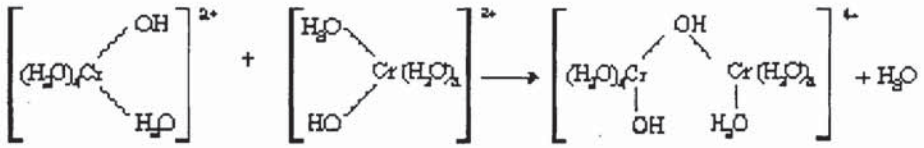

<9>

If the reacting groups in each ion are in the cis positions, a completely olated ion may be formed:

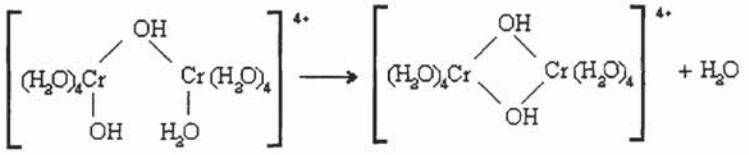

<10>

Further hydrolysis and olation might result in such polymetetrahydroxy-dodecaaquo hexachromium (III) ion:

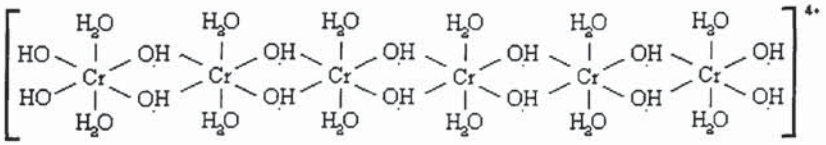

<11>

If the aqua groups are attached to the metal atoms at the end of the chain, *cross-linked* polymers are formed:

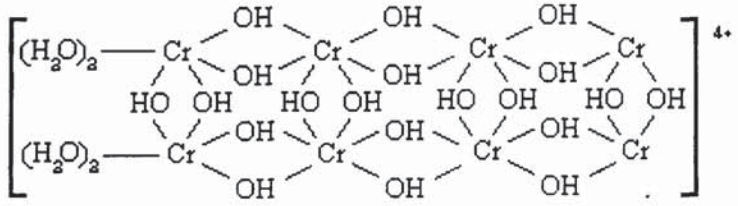

<12>

Because of the octahedral configuration of complexes of metals such as chromium, the bonds of a given metal occur in pairs, each of which lies in a plane perpendicular to the planes of the other two pairs. Thus, such cross-linked polymers are three-dimensional.

These processes account for the results obtained when a warm solution of a chromium salt is titrated with a base. With the addition of an increment of base, the pH rises immediately, but falls slowly if the solution is allowed to stand before more base is added. This continues with successive increments of base until enough base has been added to precipitate the hydrated oxide. As base is added to the solution, the hydrogen ions are removed. The equilibrium then shifts in the direction of further hydrolysis and olation, with the formation of more hydrogen atoms. In this way an amount of base can be added without precipitation, which would otherwise cause precipitation if it were added all at once.

The process of olation is favoured by an increase in concentration, temperature, and basicity. The process reverses slowly when the solution of olated complexes are diluted or when the solution is cooled; i.e., olation decreases the reactivity of co-ordinated OH groups.

Oxolation:

Oxolation may accompany or follow olation, particularly if the reaction mixture is heated. This reaction converts bridging OH^- groups to O^- groups.

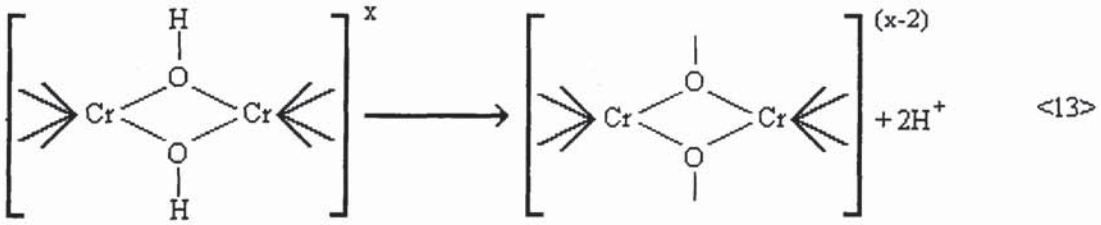

<13>

Olation and Oxolation account for changes in reactivity of chromium hydroxide as it ages. Freshly precipitated chromium hydroxide usually dissolves quite rapidly in mineral acids, but after standing some hours it becomes difficult to dissolve. Presumably, olation continues in the precipitate; since bridged OH^- groups react more slowly with acids than singly co-ordinated OH^- groups, the reactivity of the precipitated hydroxide progressively diminishes. If the hydrate is heated, there is a drastic decrease in reactivity due to oxolation, a process even more difficult to reverse than olation. While olation and oxolation are both reversible, the long time required for the acidity of solutions, which have been heated and then cooled, to return to the original value, leads to the conclusion that deoxolation is

extremely slow. In general, *ol* groups are more readily depolymerised than *oxo* compounds. since protons react more rapidly with *oxo* groups.

Anion penetration:

It is well known that the addition of neutral salts to a solution of basic sulphate changes the hydrogen ion concentration. Co-ordinated water molecules, OH^- group, OH^- bridges or other ligands are replaced by anions in the solution. The extent to which anion penetration occurs with *ol* complexes is determined by the relative coordination tendencies of the entering anions and the groups which it replaces, and the length of time which the solutions are allowed to stand[24] . Anions that can enter the co-ordinated sphere easily and displace OH groups can effectively prevent olation. Penetration by anions into basic chromium complexes decrease in the following order[25] :

Oxalate > glycinate > tartarate > citrate > glucolate > acetate > monochoracetate > formate > sulphate > chloride > nitrate > perchlorate.

Thus, if solution of $[Cr(H_2O)_6]^{3+}$ is required, the only anion should be weakly co-ordinated nitrate or perchlorate, since those of greater co-ordinating tendency may displace one or more of the co-ordinated molecules. In the stock solution of the basic chromium sulphate, *Serfas* et al.[24] found ionic species having molecular weights of 68.000.

Reaction Rates

After some parameter of a system containing Cr^{3+} complexes is changed, the corresponding change in composition of the complexes generally occurs only slowly. Heating a solution (or dispersion) of such complexes promotes olation and oxolation, both of which reverse at a low rate when the system is cooled; reversal of oxolation is much slower than reversal of olation. If the pH of a solution containing olated complexes is reduced to a value at which normally only monometric Cr^{3+} complexes would exist, it may take a long time for the state of aggregation corresponding to the new pH to be attained.

The complexity of chromium coordination chemistry is presented in Figure 2.

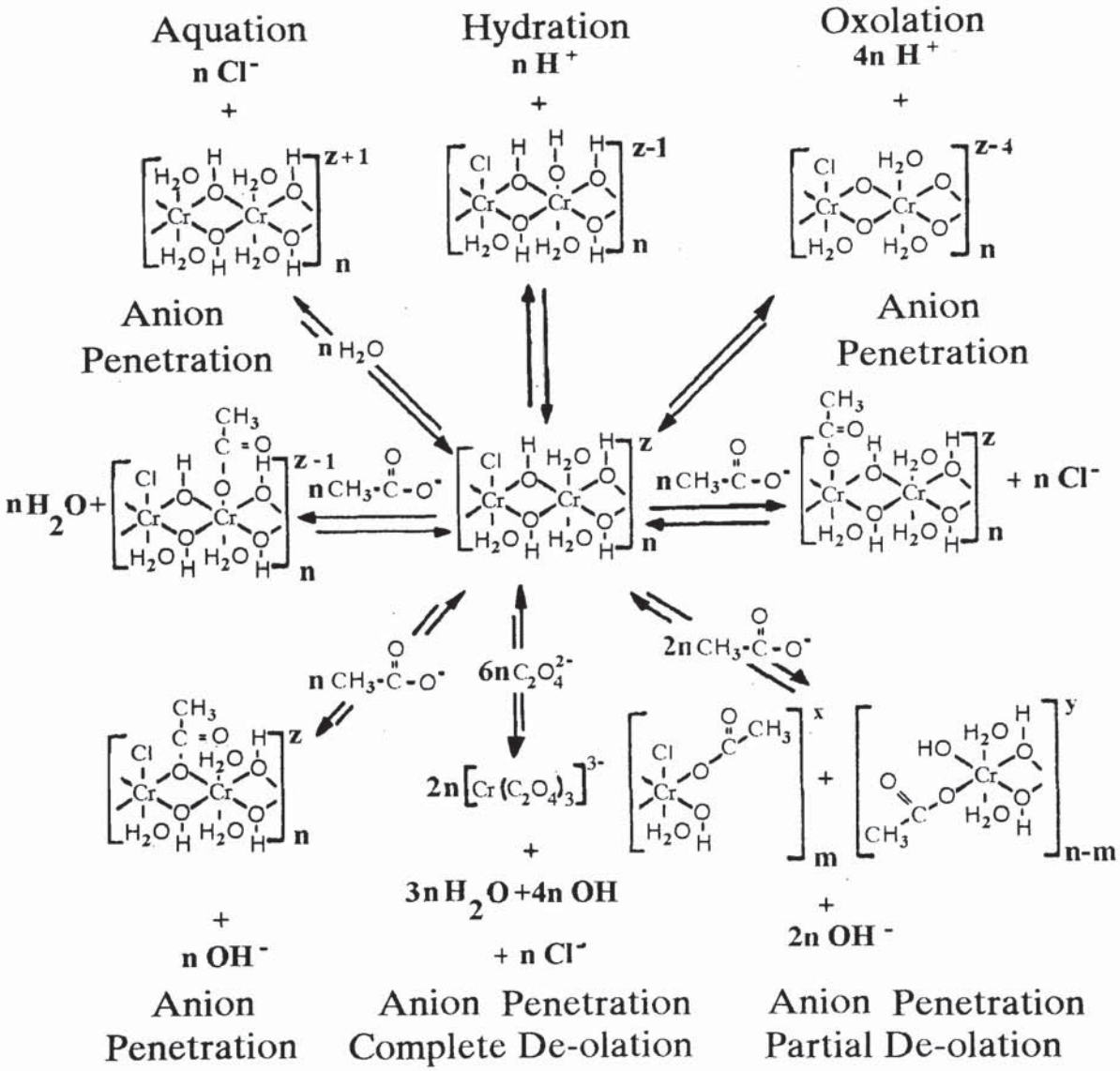

Figure 2. Reaction of Polymeric Cr (III) Complexes[21]

d. HEXAVALENT CHROMIUM

The mechanisms of the electroreduction of chromic acid are of great interest, not only from a theoretical point of view, but also for their application in industry. The vast majority of decorative and almost all hard chromium plating is carried out using CrO_3 as the electrolyte. The fact that chromium could be deposited from Cr^{6+} solution but not from simple aqueous solutions of lower valency salts is unfortunate for the following reasons:

a. Since the electrochemical equivalent of Cr in a CrO_3 solution is 0.3234 g/hr. and cathode current efficiency is 10-20%, one A hr yields only 0.032 to 0.064 g of metal. This is 15-30 times less than nickel, 18-36 times less than copper from acid solution and 63-126 times less than silver. The only way to offset this is to increase the current density and plating time.

b. The minimum current density at which electrodeposition takes place is two to three orders of magnitude larger than in the case of the other metals (Zn, Ni, Sn, Ag, Au, etc.).

c. The electrodeposition of chromium is more sensitive to operating conditions (temperature and current density) than any other deposition process.

d. In contrast to other processes, the cathodic current efficiency varies inversely with temperature but is proportional to current density (which causes low throwing power).

e. On the positive side, hexavalent chromium electrolytes are relatively less sensitive to the presence of impurities and the anode material is lead which can easily be made to conform to any shape.

Despite its paramount technological importance and with all the advances of modern science and instrumentation, exact mechanisms of the electrodeposition mechanism are still open to conjecture. The main difficulty is the necessary formation and presence of cathodic film on the surface of the metal being plated. The argument, whether the reduction of Cr^{6+} ions to chromium is direct or indirect, during the last decade developed into a discussion of whether the cathode film is useful or not (and how it should be modified to improve the process), since the existence of this film is no longer in question.

This is the reason it is important to understand the chemistry of chromium with all its intricacies of condensation, polymerisation, number of different valent states, ability to make anion/cation compounds (e.g. Cr_2 $(Cr_2$ $O_7)_3$), existence of a number of double-salts (alums), isomers, oxyhydrates, etc..

Virtually all Cr^{6+} compounds contain a Cr-O unit; the halide CrF_6 is the sole exception[26]. The other Cr^{6+} halides have formula CrO_2 X_2 , where X= F, Cl, or Br.

Chromic Acid.

The primary Cr-O bounded species is chromium (6+) oxide, CrO_3 , which is better known as chromic acid, the commercial and common name. This compound also has as aliases chromic oxide and chromic acid anhydride. Chromium (6+) forms a large number and considerable variety of oxygen compounds most of which may be regarded as derived from Cr^{6+} oxide. These include the oxy-halogen complexes and chromyl compounds, chromates, dichromates, trichromates, tetrachromates and basic chromates. All these Cr^{6+} compounds are quite potent oxidising agents, although kinetically they cover a wide range; Cr^{6+} does not appear to have anywhere the capability of forming isopoly anions so characteristic of molybdenum and tungsten.

Chromic trioxide has a molecular weight of 100.01 and forms dark red prismatic crystals which belong to the orthomorphic system, the bipyramidal subclass. Density of the solid is 2.79 g/cm^3 . It melts with some decomposition at 197^0 C. CrO_3 is very hygroscopic. Its solubility in water varies from 61.7% at 0^0 C. to 67.5% at 100^0 C. Oxidation potentials of CrO_3 and chromate solutions are augmented by increasing the acidity of the solution.

Oxidation potentials[26] at 23^0 C are listed in Table 3 and thermodynamic data[27] for some of the chromates at 25^0 C ions are in Table 4.

Reaction	E^0 ,V
$Cr^{3+} + 4\ H_2O \rightarrow\ HCrO_4^- + 7H^+ + 3e^-$	-1.3
$Cr^{2+} + 4\ H_2O \rightarrow\ HCrO_4^- + 7H^+ + 4e^-$	-0.9
$Cr^0 + 4\ H_2O \rightarrow\ HCrO_4^- + 7H^+ + 6e^-$	-0.4
$Cr^{3+} + 4\ H_2O \rightarrow\ CrO_4^{2-} + 8H^+ + 3e^-$	-1.5
$Cr^{2+} + 4\ H_2O \rightarrow\ CrO_4^{2-} + 8H^+ + 4e^-$	-1.1
$Cr^0 + 4\ H_2O \rightarrow\ CrO_4^{2-} + 8H^+ + 6e^-$	-0.6
$HCrO_4^- \rightarrow\ CrO_4^{2-} + H^+$	-0.2

Table 3. Oxidation Potentials for Chromate Ions[26]

Ion	Entropy, Cal/^{0} K/mol	Entropy of Formation Cal/^{0} K/mol	Heat of Formation Cal/mol	Free energy of Formation Cal/mol
CrO_4^{-2}	10.5 ± 1	−124.5 ± 1.0	−208,500	-171,400
$HCrO_4^{-1}$	-	-	-	-180,140
$Cr_2O_7^{-2}$	-	-	-	-305,800

Table 4 . Thermodynamic Data for Bichromate, Chromate and Dichromate Ions[27].

Chromic acid $HCrO_4^-$ or CrO_3 H_2O, is not known except in solution. Here it shows a marked tendency to form polyacids by elimination of water.[30]

$2\ H_2CrO_4 \rightarrow H_2O + H_2Cr_2O_7$ (dichromic acid) <14>

$3\ H_2CrO_4 \rightarrow 2\ H_2O + H_2Cr_3O_{10}$ (trichromic acid) <15>

$4\ H_2CrO_4 \rightarrow 3\ H_2O + H_2Cr_4O_{13}$ (tetrachromic acid) <16>

The change from H_2CrO_4 to $H_2Cr_2O_7$ is rapid, but the further polymerisation takes a measurable time.

The colour of CrO_3 indicates that it is itself highly polymerised for it is redder than the di- or trichromates and is approached in colour by the tetrachromates.

Depolymerization of CrO_3 solution in water is very rapid. It also seems to depolymerize on heating.

Chromic trioxide can be produced by the action of water on chromyl fluoride. It is most commonly produced, however, by action of concentrated sulphuric acid on a chromate, usually sodium dichromate.

A boiling persulphate solution, in the presence of silver ion as catalyst, oxidises chromic salts to chromic acid; this method can be used to rejuvenate spent $K_2Cr_2O_7$ / H_2SO_4 laboratory "cleaning" solution [28]

CrO_3 is a powerful oxidising agent. Bromine has no action on CrO_3 solutions. Iodine, however, turns a solution of CrO_3 black, probably forming a chromium hypoiodite. In the presence of sulphuric acid, iodine is oxidised to iodic acid by CrO_3.

Chromates and Dichromates

Chromates are salts of, the hypothetical chromic acid H_2CrO_4 . Salts of the hypothetical polybasic chromic acids, $H_2Cr_2O_7$, $H_2Cr_3O_{10}$, $H_2Cr_4O_{13}$, etc., are known as dichromates, trichromates, tetrachromates, etc., respectively. Basic salts, derived from hypothetical para and ortho chromic acids H_4CrO_5 and H_6CrO_6 also exist.

Acid solutions of chromic salts are also oxidised to chromates by permanganates and hydrogen peroxide. In alkaline solution, chromic salts are oxidised by hydrogen peroxide, persulfates, oxides of noble metals, hypochlorites, hypobromites, etc.

Electrolytic oxidation, in either acid or alkaline solutions, will also convert chromic salts to chromates.

The chromate ion and most of the normal solid chromates are yellow, but on acidifying, the solutions pass through orange to red. The dichromates are red in the solid state and in solution. The higher polychromates are even redder than the dichromate in the solid state. Although the various ions, CrO_4^{2-}, $Cr_2O_7^{2-}$, $Cr_3O_{10}^{2-}$, $Cr_4O_{13}^{2-}$, etc., exist together in equilibrium in solution, the ions higher than dichromate exist only in the most concentrated solutions[29]. Water is easily added to the higher polychromate ions, reverting them to the dichromate. On further dilution, even the dichromate ion adds water forming the chromates. The $HCrO^-_4$ ion exists in quantity only in dilute solution according to *Udy*,[30] but more recently[31], Raman spectroscopy proved non-existence of $HCrO^-_4$ ions.

The colours of the salts of chromic acid are interesting. With a few exceptions the monochromates are yellow. The exceptions already mentioned are dark red to black. The dichromatesas already mentioned are orange to red. The trichromates are redder and the tetrachromates still redder. The dark red colour seems to intensify with increasing polymerisation. Chromic anhydride, itself in solution, must be highly polymerised. It is approached in intensity of colour only by the tetrachromates. Most of the basic salts of chromic acid are yellow. There are exceptions, e.g., the basic lead chromates are scarlet.

In basic solutions above pH = 6, CrO_3 forms the tetrahedral yellow *chromate* ion CrO_4^{2-} .Between pH 2 and 6, $HCrO_4^-$ and the orange-red *dichromate* ion $Cr_2O_7^{2-}$ are in equilibrium; and at pH values < 1 the main species is H_2CrO_4 . The equilibriums are the following[30]:

$$HCrO_4^- \Leftrightarrow CrO_4^{2-} + H^+ \qquad K = 10^{-5.9} \qquad (F^0 = 8850 \text{ cal.}) \qquad <17>$$

$$H_2CrO_4 \Leftrightarrow HCrO_4^- + H^+ \qquad K = 4.1 \qquad - \qquad <18>$$

$$Cr_2O_7^{-2} + H_2O \Leftrightarrow 2\,HCrO_4^- \qquad K = 10^{-2.2} \qquad (F^0 = 2240 \text{ cal}) \qquad <19>$$

In addition there are the base-hydrolysis equilibriums

$$Cr_2O_7^{2-} + OH^- \Leftrightarrow HCrO_4^- + CrO_4^{2-} \qquad <20>$$

$$HCrO_4^- + OH^- \Leftrightarrow CrO_4^{2-} + H_2O \qquad <21>$$

which have been studied kinetically for a variety of bases.

The pH-dependent equilibriums are quite labile, and on addition of cation that form insoluble chromates (e.g., Ba^{2+}, Pb^{2+} and Ag^+), the chromates and not the dichromates are precipitated. Furthermore, the species present depend on the acid used, and only for HNO_3 and $HClO_4$ are the equilibriums as given. With the addition of sulphuric acid a sulphate complex with chromates is formed in essentially quantitative conversion[26] :

$$CrO_3\,(OH)^- + HSO_4^- \rightarrow CrO_3\,(OSO_3)^{2-} + H_2O \qquad <22>$$

With polychromates, heteropoly acid of $Cr_2O_6\,(OSO_3)^{2-}$ type is formed.[32] Conversion of chromates to dichromates involves formation of an oxygen linkage between chromium atoms. Electronic structure of dichromate ions is given in Figure 3.

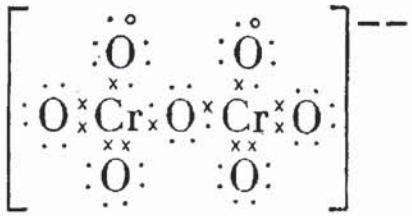

Figure 3. Electronic structure of $Cr_2O_7^{2-}$ ion:

Acid solutions of dichromate are strong oxidants.

$$Cr_2O_7^{2-} + 14H^+ + 6e = 2Cr^{3+} + 7H_2O \qquad E^0 = 1.33 \text{ V} \qquad <23>$$

The mechanism of oxidation of Fe^{2+} and other common ions by Cr^{6+} has been studied in detail and with one-and two-electron reduction respectively, Cr^{5+} and Cr^{4+} are initially formed. The reaction with H_2O_2 in acid solution has a very complex and imperfectly understood mechanism.

The chromate ion in basic solution, however is much less oxidising:

$$CrO_4^{2-} + 4H_2O + 3e = Cr(OH)_3\,(s) + 5\,OH^- \qquad E^0 = -0.13 \qquad <24>$$

The crystalline trioxide $(CrO_3)_\infty$ is built of infinite chains formed by the linking up of CrO_4 tetrahedra:[33]

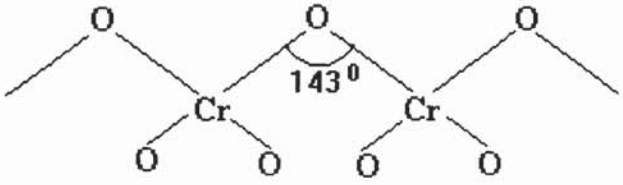

In this bridging Cr - O bond has the length of 1.75 Å and the end terminal length is 1.6 Å. There are only Van der Waals forces between the chains, consistent with the comparatively low melting point (197^0 C)

In simple crystalline chromates[34] there are tetrahedral CrO_4^{2-} ions in which the Cr O bond is around 1.6 Å, (Figure 4)

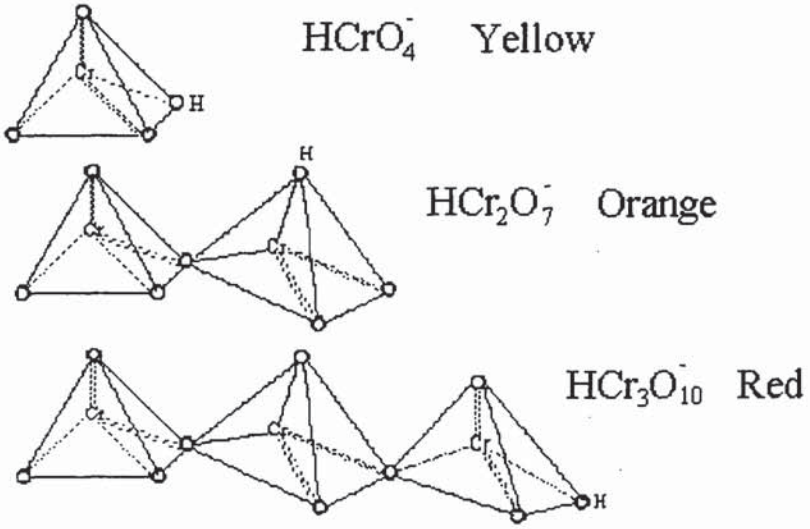

Figure 4. Chromates and Polychromates Structures.[35]

Polychromates

Polychromates result from sharing corners between CrO_4 tetrahedra. In $(NH_4)_2\ Cr_4O_7$ the anion[10] has the structure shown below:

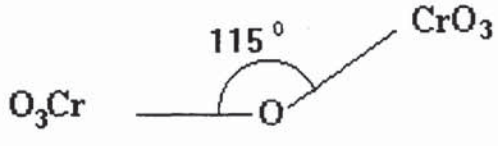

The central Cr O bonds are found to be much longer (1.91Å) than the terminal ones (1.6Å).

Polychromate ions are of particular interest due to their role in chromium plating from hexavalent solutions. It is recognised and accepted that chromium cannot be electrodeposited from Cr^{6+} solutions without the addition of catalyst usually in the form of the sulphate. Since the strength of commercial solutions is customarily 1-3 Molar, at this concentration, considering the low pH and taking into account the dark red colour of the solution, at least the tri and possible the tetrachromate ions are present. It should be noted that in the absence of electrical current, the pH of the chromium plating solution is subject to considerable variation, depending on the initial concentration of chromic and sulphuric acids. If the amount of CrO_3 is increased from 10 to 300 g/l (0.1-3 M), the pH changes from 1.4 to 0.08.

Martens and Carpeni[35] with the use of radioactive chromium measured the autodiffusion coefficients of isopolychromates at 25^0 C in aqueous solution as a function of concentration. Table 5 represents ionic equilibrium dependence on molar concentration. It is evident that in the plating operating ranges ($1.5 < C < 3.5$ mol/ℓ), the predominant species are di and trichromate ions.

C (mol/ℓ)	Ions in Equilibrium
$C < 10^{-2}$	$HCrO^-_4$
$10^{-2} < C < 10^{-1}$	$HCrO^-_4 \Leftrightarrow Cr_4O_7^{2-} + H_2O$
$10^{-2} < C < 1,5$	$Cr_4O_7^{2-}$
$1,5 < C < 3,5$	$3Cr_2O_7^{2-} + 2H^+ \Leftrightarrow 2Cr_3O_{10}^{2-} + H_2O$
$3,5 < C < 7,5$	$Cr_3O_{10}^{2-}$
$7,5 < C < 10$	$4Cr_3O_{10}^{2-} + 2H^+ \Leftrightarrow 3\ Cr_4O_{13}^{2-} + H_2O$

Table 5. Ionic Equilibrium of CrO_3 in Water.[3]

I.2.2 THEORY OF CHROMIUM DEPOSITION

The dominant role of trichromates is advanced by *Hoare*[34] According to his phenomenological model, in absence of the bisulphate ion (or sulphate - which at this low pH dissociates to bisulphate), trichromate ion in a successive steps (of electron transfers and loss of oxygen and reaction with H_3O^+ ion) will decompose to chromous hydroxide going through an intermediate step of formation of chromic (3+) and then chromous (2+) dichromates and will finally discharge at the cathode as black chromium at very low current efficiency:

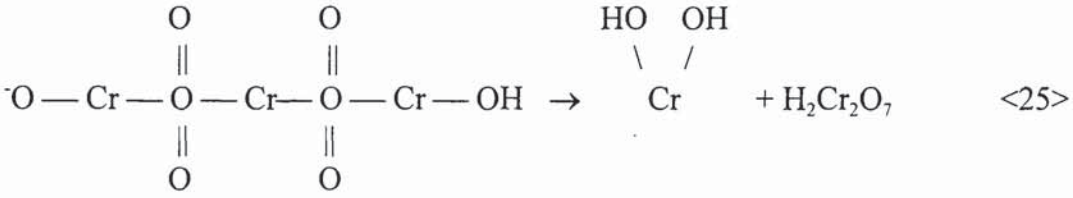

<25>

The next step of reduction mechanism is the formation of a complex between the Cr^{2+} hydroxide and the bisulphate through hydrogen bonding:

<26>

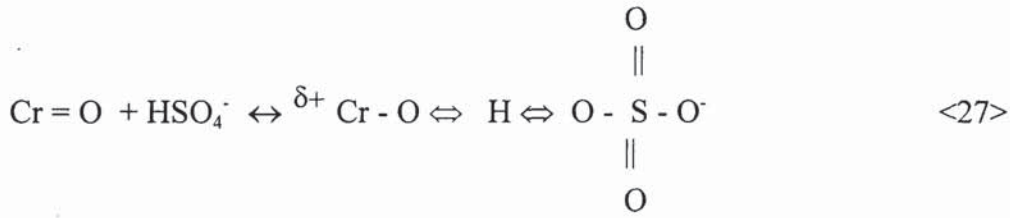

<27>

where ⇔ represents the hydrogen bond and δ+ represents a dipole generated on the chromium end (left side) of the complex. Now, the positively charged complex can be specifically adsorbed on the cathode, two electrons transferred to this end-on configuration with formation of metallic Cr and regeneration of HSO_4^-.

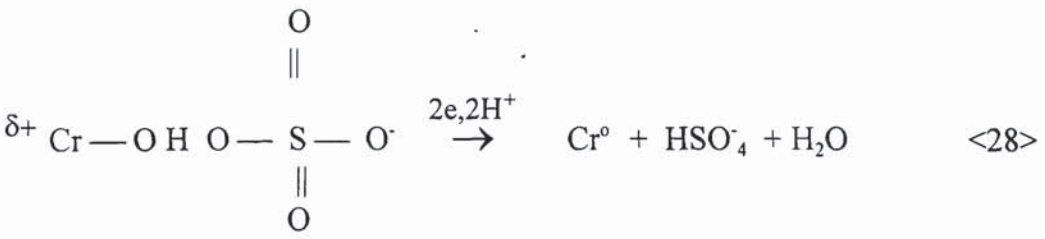

<28>

According to this model, the chromic-dichromate complex is necessary to protect Cr^{3+} from forming the stable Cr(III) aquo complexes. As a refinement of this model, HSO_4^- ion has a dual role: it also "blocks" other chromium atoms in the trichomate ions from being reduced (leading to Cr^{3+} aquo-complexes formation).

The ideally protected trichromate ion would be:

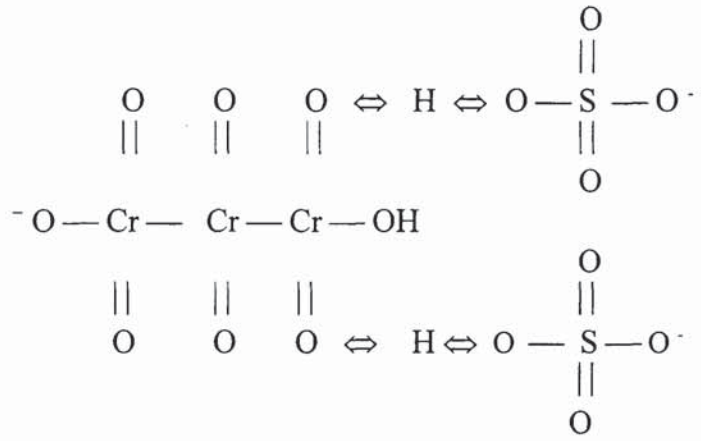

<29>

This would leave one end (the right side of <29>) protected, preventing formation of unwanted dichromic chromate complex which decomposition would lead to unwanted $[Cr(H_2O)_6]^{3+}$ formation. This also explains the narrow range (CrO_3:HSO_4 = 100:1) of bisulphate concentration in the chromium plating solution: too little of HSO_4^- will bring insufficient protection of Cr on the right end of the trichromate ion (undercatalyzation) or too much would block the left end Cr which is necessary for reactions <25-28> and Cr deposition (overcatalyzation).

According to *Hoare*[36], for fluoride catalysed CrO_3 based plating systems almost the identical mechanism is proposed in which F^- plays a role of blocking agent and catalyst.

Although not complete, this mechanism is most recognised to date. The incompleteness of his remarkable theory is that he treated the chromium deposition mechanism without elaboration on the structure of and influence of liquid layer adjacent to the cathode (L-film) which is formed at the beginning of the cathodic process and continuously forming and reforming at a steady-state conditions.

Luckily enough, both older and newer Russian research is extensive on the L-film formation and reactions that occur in the film since they quite early recognised its decisive

importance on the deposition mechanism in general and current efficiency in particular.

On the other hand, it is well known fact that halide ions (X^-) such as Cl^- and F^- have a marked improving effect on the cathode current efficiency of chromium electrodeposition are recently collaborated[37]:

As the hydration of halide anions is incomplete, they can penetrate the hydrogen layer and be absorbed onto the metal surface. XPS results show that F^- and Cl^- ions, which are stable in the chromic acid bath may participate in the film formation.

The probable activation steps of halides are as follows: the absorbed halide first penetrates at the hydration layer at the chromium surface and forms a bridged transition surface complex:

$$[Cr_2O_7\ (H_2O)_2Cr^{3+}\text{-}X^-\text{-}Cr^{3+}(OH_2)_2Cr_2O_7]^{++} \qquad <30>$$

The electrons on the cathode are transferred to Cr^{3+} through halides, and Cr^{3+} is reduced to metallic chromium. By the formation of the transition complex, the activation energy of the reduction of Cr^{3+} to Cr^0 is decreased. The overpotential of chromium deposition apparently is decreased, which facilitates chromium electrodeposition.

The rate of reaction follows a first order rate equation[38]. In the case of a rotating cylinder, the specific reaction rate constant was found to increase with increasing rotation speed until a limiting value was reached with further increase in the rotation speed. A study of the reaction mechanisms has shown that, at a relatively low rotation speed, the reduction of chromium is partially diffusion controlled; at higher speeds the reaction becomes chemically controlled. Agitation (cylinder rotation) increases the rate of chromium reduction through decreasing the degree of cathode coverage by hydrogen bubbles and consequently increases the effective cathode area[39,40].

In this sense, it seems that non-stationary currents can be of great advantage, since the current interruptions and/or current reversal can promote the hydrogen liberation. Also, the use of current pulses interrupts the nucleation and resulting crystal growth. Each pulse gives room for fresh renucleation with the net effect of refining the structure and size of grains. Grain consolidation seems to interfere with the accumulation of internal stresses and acts as an inhibitor for crack formation, as noted in early papers[41].

In a recent paper[32], the x-ray diffraction study was carried out in order to identify the predominant species in an industrial CrO_3-H_2O system. Structural analysis showed that dichromate ions have maximum likelihood, but linear-shaped trichromate ions may also exist in significant concentrations. They also concluded that formation of complex given in <29> can be hardly assumed because of steric hindrance and that it is more realistic that *one* HSO_4^- ion reacts with polychromate.

A very recent paper[42] by Russian researchers studied the existence of various chromium complexes in CrO_3/H_2SO_4 plating solutions for different X = CrO_3/H_2SO_4 ratios. They concluded that although five different chromium complexes exist, the reduction to metal proceeds only from the following type of complexes:

$$[HSO_4]_n^- \bullet [Cr_2O_7]_m^{2-} \qquad <31>$$

where $n = 1$; $m = 1$ and $25 < X < 150$ to 200.

They concluded that those complexes are characterised by a single hydrogen bond between two ions in the complex.

Another recent paper on chromium mechanisms is the latest contribution of a group headed by *Z. A. Soloveva*[43] from Institute of Physical Chemistry of Russian Academy of Science. Potentiodynamic and impedance measurements are used to further collaborate their mechanism of deposition based on formation of cathode film (with solid and liquid phase) consisting of oxide-hydroxide Cr^{3+} compounds. A few other Russian groups headed by Professors Shluger, Vargamyan, Levin, N. V. Kudriavtsev, Matulis, Falicheva, etc., among others contributed a significant amount of research, but the problem of a final and definite answer is still open.

It is clear at this point that for successful approach and significant further contributions, an *in situ* method is needed to study the deposition mechanisms under both transient and steady state conditions.

High pressure from environmentalists is recently stirring up new research in the area of replacing Cr^{6+} solutions by less harmful Cr^{3+}. At the same time, it becomes more and more obvious that mechanisms of deposition from trivalent and hexavalent solutions are deeply intertwined and that, in both cases, chromium coordination chemistry is deeply involved.

Despite the flurry of the research on chromium deposition mechanisms in the 1950's, 1960's and 1970's, eventually the flow of the papers on chromium reduced to a mere trickle. The reason is obvious: the complexity of the problem and difficulties involved with highly coloured, highly concentrated solutions of chromium salts used; the number of different valence states involved; and general lack of in-depth knowledge of chromium coordination chemistry.

What further complicates the matter is that in the beginning (onset) of the deposition process (first 1-3 sec), one set of reactions occur - formation of the film, more or less compact and independent of the anions present and rather thin (5 mg/m^2). Russian workers use the term "product of partial reduction of $Cr^{6+} \rightarrow Cr^{3+}$ " and this film forms in the first branch of the chromium polarisation curve at potentials up to about 700 mV.

Once this film is formed (the C-film, short for *compact* film), another cathodic film (layer) is formed on the surface of C-film and closer to the bulk of the solution: the L-film (short for *liquid* film).

Significant Japanese contributions toward explanation of discussed mechanisms (unfortunately) passed mainly unnoticed due to language barriers. The author went to considerable labour, pain, and expense to obtain correct translations of some of the Japanese papers. Due to their apparent importance, a portion of this chapter is devoted to them.

Japanese School of Thought on Chromium Deposition Mechanisms

Yoshida, Suzuki, Doi and Arai[44] studied the behaviour and composition of a cathode film with the help of radioactive tracers in the form of S^{35} radioactive-labeled sulphuric acid and over-the- counter high grade CrO_3 treated with radiation to obtain Cr^{51} as a tracer. A special (but a rather simple) plating cell is constructed with a rapid rinsing station. In essence, a steel cathode will be plated for a short period of time so that the C- and/or L-films will be formed and can be analysed. Since the L-film is liquid and dissolvable in either hot plating solution or hot alkali, by dissolution or simple brushing of the L-film, its formation and influence on deposition of metallic chromium was studied. By initially forming the C- and L-films with labelled Cr or H_2SO_4 and plating in pure (unlabeled) solution and vice versa, they came to the important conclusions that:

(1) The cathode film is composed of two layers with different forming properties in terms of thickness and composition. The outer layer, referred to as the L-film, and the inner layer, referred to as the C-film, differ in that the L-film contributes the majority of the cathode film, contains sulphate ions and dissolves easily in the electrolyte and is about 10 times thicker than C film.

(2) The C-film has a thickness of about 5 mg/m^2, contains very few sulphate ions and does not dissolve easily in electrolyte.

(3) The cathode film itself does not reduce to metallic chromium. The metallic chromium is deposited from a separate chromium complex compound that passes through the cathode films (C and L) from the bulk of the solution.

(4) In the electrolyte, the L-film vigorously repeats the dissolving and forming cycles, while the C-film remains constant, once formed.

(5) The cathode film may be a chromium hydroxy aquo complex , as shown in Figure 5 or primarily an oxolated version of this compound. Assuming that the cathode film is formed from such chromium complexes, the author feels that the L-film is a compound with lower molecular weight, such as in structures (*i*) and (*ii*), while the C-film is more like structure (*iv*), a large complex with a high degree of polymerisation.

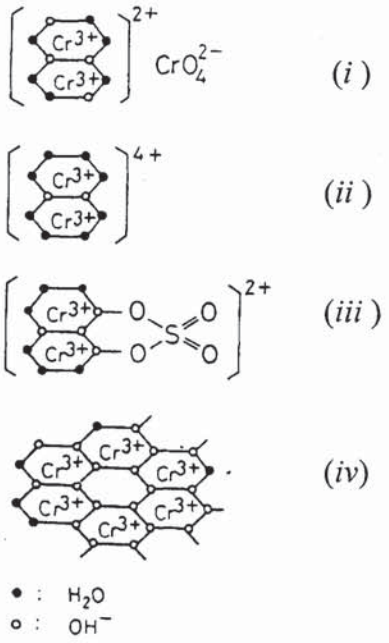

Figure 5. The Structures of the Chromium Complexes in the Cathode Film Layer[44].

Kimura and Hayashi [45] also used sulphates labels with radioactive ^{35}S in order to overcome difficulties of determining the amount of sulphate in the cathode film by standard analytical methods (due to its relatively small content) and to study sulphate content in the cathodic film formed during potentiostatic polarisation of 0.4, 1.5 and 2.5 M CrO_3 baths on Fe, Au and Pt cathodes. They found that sulphate content is directly related to the potential in the region of between -0.6 to -1.0 V which in turn is controlling the state of the cathode surface (L-film formations) and accompanying electrochemical reactions. In the region of -0.2 to -0.8 V where current is increasing (C-film), sulphate content was negligible for Pt, Au and Fe cathode. In the region >-0.8 V where current starts to decrease and L-film starts to form, sulphate concentration increases sharply. In the potential regions between -1.0 and -1.1 V (beginning of Cr deposit region), sulphate concentration in the film drops due to the liberation of sulphates from the complexes. At potentials of > -1.1 V sulphate concentration increases slightly again due to the inclusion in the cracks and imperfections in metallic chromium deposit. They also found that as sulphate concentration in 0.4 M CrO_3 bath is increased from 0.002 M (200:1) to 0.008 M (50:1), sulphate content in L-film tended to increase. Temperature increase has a similar effect, while an increase in CrO_3 concentration at constant ratio has the opposite effect. At every CrO_3 concentration the maximum amount of sulphates in the L-film is predictably at 100:1 ratio of sulphuric acid. The authors also investigated the influence other anions as additions to H_2SO_4 ; HCl or KBr (0.01 M) added to 1.5 M CrO_3 + 0.01 M H_2SO_4 solution considerably increased the sulphate amount in the L-film while 0.01 M Na_2SiF_6 addition had the opposite effect, demonstrating the substantial film dissolution effect of Na_2SiF_6. Effects of HCl , KBr and Na_2SiF_6 on film were also proportional to increases in their respective concentrations.

Nagayama and Izumitani [46] studied coordination chemistry of chromium complexes as related to deposition mechanisms. They started with observations made by *Levitan*[47] that during galvanostatic (I = 75 mA/cm^2) chromium deposition from Sargent type bath, chromic acid *dimer* of the type like one presented in Equation < 11 > is formed together with *polymer* of unknown structure as well as mono-nuclear $[Cr(H_20)_6]^{3+}$, the stable aquo complex. But rather than to use the galvanostatic method where current is kept constant and potential changes, they choose to keep potential fixed at -0.75V (vs SCE), where only $Cr^{6+} \rightarrow Cr^{3+}$ and $2H^+ \rightarrow H_2$ reaction are under the progress (for $Cr^{6+} \rightarrow Cr^0$ reaction to happen,

this potential is too positive). During the electrolysis (0-60 min) they took the samples at different time intervals and with the use of anion and cation exchange chromatography. they separated mononuclear (a) binuclear, (b) and polynuclear Cr^{3+} complexes. (c) Their formation rates are presented in Figure 6 and reproduced from this paper. They found that the complex formation rate for mononuclear complexes increases linearly with time while for the other two complexes, the rate increase is more gradual. Since formation rates were straight lines (at least at the beginning), they can be expressed as the corresponding slopes. Noting that the sum of the slopes for a, b, and c lines add up to the slope of line d (total Cr^{3+} - complex formation line), they concluded that each (a, b, and c) complex is forming at its own, constant, rate. For complexes a, b, and c, they found the growth rates to be: 0.90, 0.519, and 0.311 mg/cm^2 min respectively. After the completion of the electrolysis, the binuclear and polynuclear complexes were found to be decomposing to monomers in the absence of the current.

By measuring, now, the decomposition rates, of a, b and c complexes they found that overall decomposition rate is of the first order and can be expressed as:

$$\frac{dC}{dt} = r - k\,C \qquad <32>$$

After integration they obtained:

$$C = \frac{r}{k}\,(1 - e^{-kt}) \qquad \text{where,} \qquad <33>$$

C = overall formation rate of binuclear or polynuclear complexes,
r = formation rate (slopes of dotted lines from Figure 6),
k = decomposition rate constant and t = time of electrolysis

They also repeated the same experiment at -1.10 V (Cr^0 formation region) and obtained similar results. Authors concluded in this rather important paper that the cathode layer consisting of the dense film of various Cr^{3+} - complexes is necessary condition for deposition reaction $Cr^{6+} \rightarrow Cr^{3+} \rightarrow Cr^{2+} \rightarrow Cr^0$ to happen. Catalyst (e.g., H_2SO_4) promotes formation on dissolution of binuclear and polynuclear soluble Cr^{3+} complexes, thus maintaining the film of the constant thickness where deposition proceeds via intermediate Cr^{2+} (inner orbital) complex rather through extremely stable $[Cr\,(H_2O)_6]^{3+}$ (outer orbital) complex.

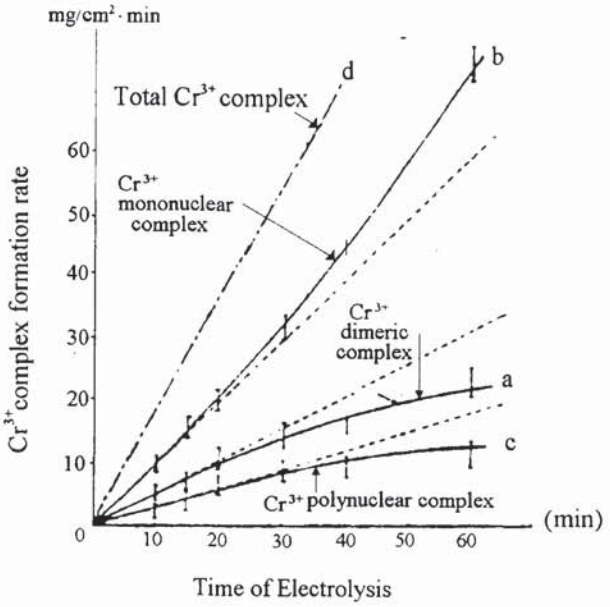

Figure 6. Formation Rates for C^{3+} - Complexes.

Nagayama et al, has also assumed that the $Cr^{3+} \rightarrow Cr^{2+}$ step of overall deposition mechanism , is reduction within the cathode film; Cr^{2+} reacts with polynuclear hydroxy aquo complex and that portion of the Cr^{2+} obtained in this fashion reacts with Cr^{6+} and is oxidised to Cr^{3+} ($Cr^{2+} + Cr^{6+} \rightarrow 2\ Cr^{3+}$), with the remainder being reduced to metallic chromium.

Okada[48] holds that SO_4 ions will penetrate an olated compound such as that shown in Figure 5 as structure (*iv*) to form a complex such as that in structure (*iii*) and that from this complex metallic chromium is deposited. According to him, reduced solubility of L-film causes OH- cross linking level to rise together with the pH increase.

Yoshida, Tsukahara and Koyama[49] used ESCA analysis to further elaborate their previous research[37], where they noted that there are two layers, the L- and C-films, within the cathode film. With ESCA analysis, they obtained depth profiling of C- and L-films and demonstrated that C-film is a highly polymerised complex with very few anions present, if any. The L-film appears to be mostly in Cr^{3+} state but the exact valence could not be accurately established, suggesting the possibility of also two- and four-valence states.

They suggested that Cr^{3+} complexes are the main constituents of L-film and that metallic chromium does not deposit from this cathode film but from the Cr^{6+} state, which contributes to the formation of cathode film but also forms olated complexes, hydroxy aquacomplexes and polymers of higher molecular weights. These olated complexes will

penetrate the cathode film from the bulk of the solution before reducing to metallic chromium.

Nishihara et al.[50] studied Cr^{3+} complexes and reaction $Cr^{3+} + e^- \rightarrow Cr^{2+}$ in relationship with pH and temperature using the aqueous solution of chrome alum: [(NH_4) $Cr(SO_4)_2$ $12\ H_2O$].

As the temperature of the solution is raised from room temperature to 80^0 C, pH values of the solution decrease proportionately to the temperature, the halfwave of $Cr^{3+} + e^- \rightarrow Cr^{2+}$ reaction, moves toward more negative potentials , and reaction changes from reversible to irreversible with the colour of solution changing from violet to green. From these results it is postulated that the degree of hydrolysis of Cr^{3+} complexes is temperature dependant. The structure of Cr^{3+} aquo complexes are estimated at > 40^0 C, as $[Cr(H_2O)_6]^{3+}$ and $[Cr(H_2O)_5\ OH]^{2+}$; at 40 to 70^0 C as $[Cr(H_2O)_5\ OH]^{2+}$, $[Cr(H_2O)_4\ (OH)_2]^+$ and olated polymer as presented in equation <11> on page 27; at > 80^0 C mostly as olated polymer like one in <11>.

At the conclusion, the whole complicated situation revolved around the exact mechanism can be, for reasons of clarity, described in Figure 7, noting again that this is a simplification of one complicated mechanism that happens in different steps and electrochemically and kinetically is still poorly understood. Explanation of CrO_3 electrodeposition mechanisms will undoubtedly benefit closely related fields like electrodeposition from trivalent decorative and hard plating chromium plating baths as well as chromium conversion coatings.

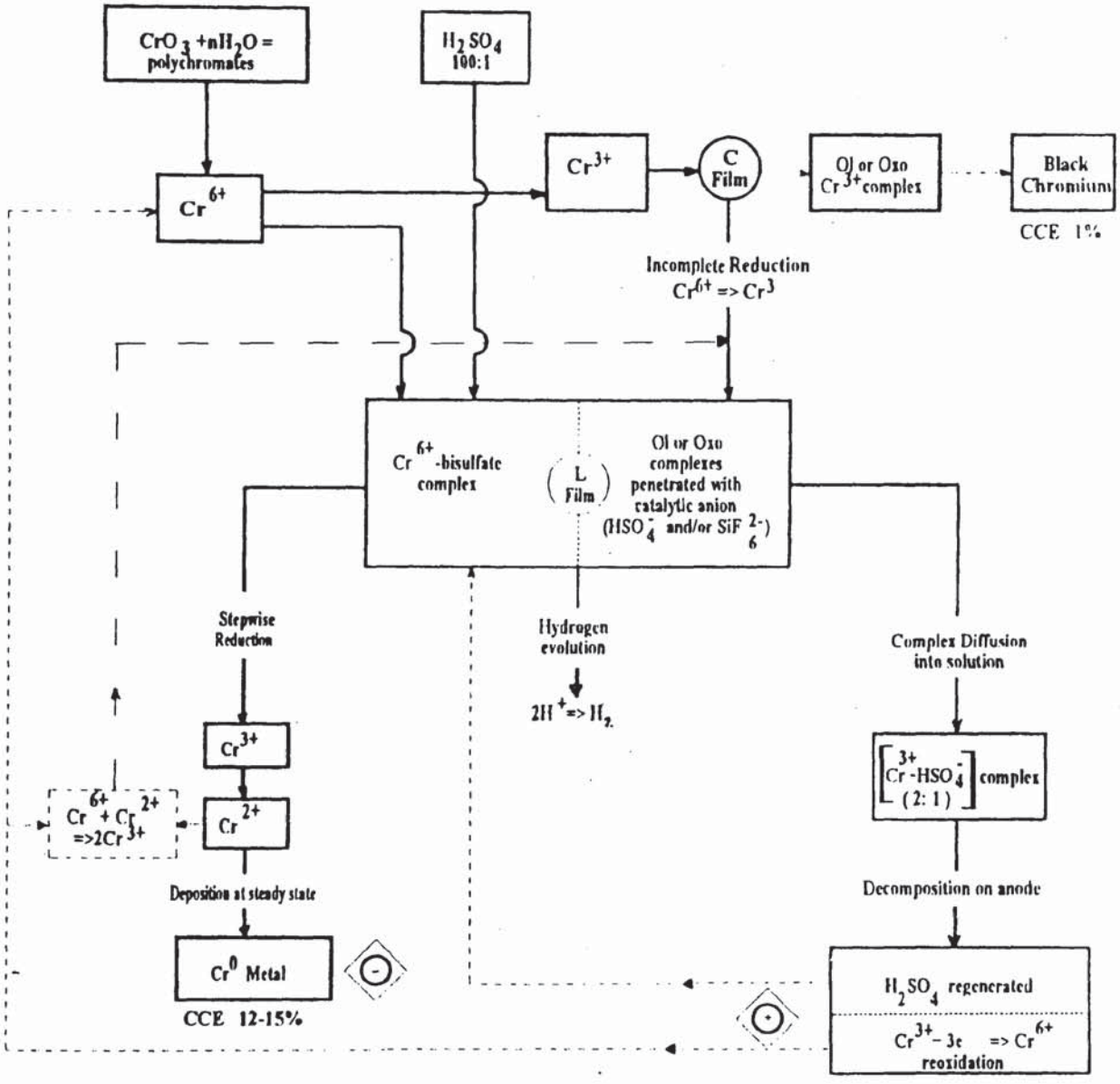

Figure 7. Sequences of the Chromium Electrodeposition Mechanism .

1.3 THE THEORY OF PERIODIC CURRENT REVERSAL

a. INTRODUCTION

Periodic current reversal (PRC) plating is the bipolar electrodeposition process where DC current is continuously changing its direction (polarity). Quite popular in the 1950s, found then its major use in improving levelling action in hot cyanide copper plating baths[51-55]. However, the use of these baths was drastically reduced due to environmental problems and inherent build-up of carbonates and PRC was relegated to secondary duties such as for very effective electrocleaning as well as for derusting and desmutting. Theoretical studies were therefore not pursued.

In the 1970s new theoretical contributions were introduced and in the 1980's and 1990's it became quite obvious that PRC can give answers to many complicated electrodeposition problems. Theory became much more complex and intriguing. The essence of current reversal, is that, during the metal electrodeposition, the polarity automatically changes, and the duration of the reverse (anodic) current is, normally a small fraction, *e.g.*, 20% or less, of the duration of the current in the direct (cathodic) direction.

Figure 1 shows different kinds of non-stationary currents and Figure 8 the shape of the PRC form used throughout most of this work. Periodically reversed current is characterised by the following properties: a current in the forward direction (cathodic polarisation current) i_c; a time for the metal deposition (cathode period) t_c; anodic polarisation (reverse) time period t_a and a total period of the current reversal: $T = t_a + t_c$.

The average current is given by:

$$i_{av} = \frac{i_c t_c - i_a t_a}{i_c t_c} \qquad <34>$$

and for $i_c = i_a = i$; it follows that: <35>

$$i_{av} = i \quad \frac{1-r}{1+r} \qquad <36>$$

$$r = \frac{t_a}{t_c} \qquad <37>$$

In the electrodeposition of metals by a reversed current, the electricity q_c flowing through the electrodes during the cathode period t_c must be greater than the amount of electricity q_a flowing during the time of the anode period t_a, i.e., $i_c t_c > i_a t_a$. Consequently, in this method of deposition, the whole quantity of electricity is not consumed in the formation of the deposit. A significantly smaller portion is expended for the anode polarisation (deplating, stripping, reversing) of the plated products. During each total period **T** of plating with current reversal, a layer of metal of a determined thickness is built up on the surface of the products and, during anodic polarisation (t_a), part of the deposited layer can be dissolved.

To increase the rate of metal deposition, conditions in the electrode double layer must be created under which the limiting current density and passivating anodic current are significantly increased. During this time a high metal-to-current efficiency must be maintained and the protective properties of the electrodeposits must satisfy the requirements. As was noted earlier, until relatively recently, these conditions were met mainly by changing DC variables: the metal concentration, temperature and agitation of the bath, as well as by introducing various additives.

Despite the fact that PRC deposition occurs with the *incomplete* use of the whole quantity of electricity applied on the electrodes, this method of metal deposition permits acceleration of the electroplating rates. Faster deposition can be accomplished by using a higher working current density than with a direct current. Initially this is caused by the prevention of depletion of metal ions in the cathode double layer, to which the anodic dissolution of the deposit contributes. The upper limit of the working current density during the metal deposition is a function of the parameters of the reversed current t_a and i_a and also of the length of the total period **T**. The limiting current density usually increases with an increase of the ratio t_a/t_c, and with a decrease in **T**.

A higher working current density during the PRC deposition as compared with DC plating is also a result of the periodic depolarisation of the electrodes. Such an effect of the current reversal on the electrode processes, as well as the electropolishing action of the current on the deposit during the period of its anode polarisation, permits ensuing electrocrystallisation on the cathode surface in the preferred direction under a higher working (practical) current density. During the cathodic period, this leads to grain refinement normally associated with unipolar, pulse plating, PC, which is further supported

by the disturbance of growth steps by the periodic inversion of the current. In a number of processes, for example, in the electrodeposition of certain metals from solutions of their simple salts, the upper limit of the working current density can be, under certain conditions, close in magnitude to the limiting current; however, under **real** conditions, the working current density of the cathode is often limited to the admissible upper limit of the anode current density. Exceeding this limit causes anode passivation when the electroplating bath is operating in a DC mode (e.g. Ni, brass, cyanide and acid copper baths). Current reversal prevents passivation of the anodes during the period of cathode polarisation and sometimes contributes to a significant increase of the upper limit of the anode working current density, and thus also increasing the working cathode current density.

The use of a current of alternating polarity permits not only increasing the working current density but as a result of the periodic action of the anodic current on the deposited layer of metal, the deposit acquires better protective properties as demonstrated for acid copper,[56-61] nickel,[62-68] gold,[69-71] chromium[72,75] and zinc[76,77]. For a number of processes, current reversal is the means of achieving smooth and even bright deposits, better current distribution and less porous deposits with lower internal stresses, and in the case of chromium plating, higher current efficiency.

b. THEORETICAL ASPECTS OF PERIODIC CURRENT REVERSAL

Reversal of current in electrolytic processes was first mentioned in 1893[78] and revived again in the 40 's. *Baeyens*[79] published a comprehensive article on pulsed current electroplating which included a review of the literature and patents on PRC plating up to 1954. Rudimentary treatment of PRC is given back in 1957 by *Hickling and Rothbaum*[80] who investigated effects of PRC upon concentration overpotential and current efficiencies for metal deposition reactions which are purely diffusion controlled. In the cathodic part of the cycle, the onset of limiting diffusion conditions is deferred, and the current efficiency and average rate of the metal deposition are increased. The magnitude of the effect depends upon the ratio of the anodic to cathodic charges ($Q_a/Q_c = i_a t_a/i_c t_c$) passed in anodic and cathodic pulses. It is the greatest under conditions such when diffusion away from the electrode of anodically formed ions is minimised. *Dini*[81] reviewed the literature available up to 1963. In the seventies, the sudden increase in the price of gold initiated new applied and theoretical research for methods of improving electrodeposition technology, and a number of important papers with new models were published..

LIMITED RATE OF DEPOSITION BY RECTANGULAR PC AND PRC PULSES

A model was presented by *Cheh*[82-84]. The PRC diffusion model is a complete analogy to that of Pulse Plating (PC). The only difference appears in the boundary conditions involving the form of the applied current density at the electrode surface. Using notation as in Figure 8, Cheh expressed applied current density for PRC plating as:

$$i = i_c \qquad \text{for} \qquad 0 < t \leq t_1;\ t_2 < t \leq t_3, \text{ etc.} \qquad \text{<38>}$$

$$i = i_a = \tfrac{1}{r} i_c \quad \text{for} \quad t_1 < t \leq t_2;\ t_3 < t \leq t_4, \text{etc} \ . \qquad \text{<39>}$$

The total cycle period (θ) is given by:

$$\theta = \theta_1 + \theta_2 = t_2 = (t_4 - t_2) = (t_6 - t_4), \text{ etc.} \qquad \text{<40>}$$

The mathematical model was solved first in 1910 by *Rosenbrugh and Miller*[85] and, similar to PC plating, the ratio of instantaneous cathodic limiting current density for PRC plating, $(i_{pr})_l$, to that of DC plating, $(i_{dc})_l$, can be expressed as[85]:

$$\frac{\left(i_{pr}\right)_l}{(i_{dc})_l} - = \frac{1}{1-\frac{8}{\pi^2}\left(\frac{r-1}{r}\right)\sum_{j=1}^{\infty}\frac{1}{(2j-1)^2}\frac{\left(\exp\left[(2j-1)^2 a\theta_2\right]-1\right)}{\left(\exp\left[(2j-1)^2 a\theta\right]-1\right)}} \qquad <41>$$

The asymptotic form for: $a\theta << 1$ where $a = \frac{\pi^2 D}{4\delta^2}$ is, therefore,

$$\left[\frac{\left(i_{prc}\right)_l}{(i_{dc})_l}\right]_{a\theta<<1} = \frac{1}{1-\left(\frac{r-1}{r}\right)\frac{a\theta_2}{a\theta}} \qquad <42>$$

The overall plating rate which can be calculated by integrating over the entire cycle is:

$$\frac{\text{max overall rate of plating}}{\text{max rate of DC plating}} = \frac{(i_{prc})_l\left(\theta_1+\frac{1}{r}\theta_2\right)}{(i_{dc})_l\,\theta} = \frac{\frac{\left(\theta_1+\frac{1}{r}\theta_2\right)}{\theta}}{1-\frac{8}{\pi^2}\left(\frac{r-1}{r}\right)\sum_{j=1}^{\infty}\frac{1}{(2j-1)^2}\frac{\left(\exp\left[(2j-1)^2 a\theta_2\right]-1\right)}{\left(\exp\left[(2j-1)^2 a\theta\right]-1\right)}} \qquad <43>$$

Cheh obtained numerical results for equations <42> and <43> for various values of $a\theta$ and $1/r = -0.20$. He also carried out experimental investigation using gold plating solution, and satisfactory agreement was observed between theory and experimental results.

GENERALISED THEORY OF PERIODIC ELECTROLYSIS WITH RECTANGULAR CURRENT PULSES, PERIODIC PULSE REVERSE AND PULSE -PULSE REVERSE

This theory was presented by *Chin*[87] in his fundamental paper. To simplify rather complex equations, he split the current flowing across the electrode/electrolyte interface into elements composed of time-averaged DC component, i_{dc} and a fluctuating alternating current AC component, iac :

$$i(t) = i_{dc} + i_{ac}(t) \qquad <44>$$

For rectangular periodic reverse pulse (Figure 8), the time averaged DC current component may be obtained from the following expression:

$$i_{dc} = \frac{1}{T}\int_0^T i(t)\,dt = \frac{1}{T}\left(i_1 t_1 + i_2 t_2\right) \qquad <45>$$

Likewise, he split the concentration, C, into time invariant, steady-state $\bar{C}$ component, and a fluctuating $\tilde{C}$ component, .

$$C(y,t) = \bar{C}(y) + \tilde{C}(y,t) \qquad <46>$$

Also, he considered that potential responses of an electrode during activity are also periodically fluctuating with time, and it can be considered to consist of time -averaged DC component, η_{dc}, and fluctuating AC component, $\tilde{\eta}$. $\eta(t) = \eta_{dc} + \tilde{\eta}(t)$ <47>

The DC overpotential component may be obtained by carrying out the time-averaging of the total overpotential profile over one pulse period:

$$\eta_{dc} = \frac{1}{T} \int_{(p\text{-}1)T}^{pT} \eta(t)dt \qquad <48>$$

Introducing the following dimensionless variables and parameters:

dimensionless overpotential $\eta^* = \frac{zF}{RT}\eta$ <49>

dimensionless exchange current density $i_o^* = \frac{i_0}{|i_{\lim}|}$ <50>

ohmic resistance $(\rho l)^* = \frac{zF}{RT}\rho\, l\, |i_{\lim}|$ <51>

the governing equations for the potential responses may be expressed in the dimensionless form as:

surface overpotential $i^* = i_0^* C_s^{\gamma}[\exp(\alpha\eta_S^*) - \exp(-\beta\eta_s^*)]$ <52>

overpotential concentration $\eta_{conc}^* = \ln C_s^*$ <53>

ohmic overpotential $\eta_{ohm}^* = (\rho l)^* i^*$ <54>

total overpotential $\eta^* = \eta_s^* + \eta_{conc}^* + \eta_{ohm}^*$ <55>

DC overpotential $\eta_{dc} = \int_{p-1}^{p} \eta^* dt^*$ <56>

Equations <52> to <56> permit calculation of the instantaneous overpotential components η_s^*, η_{conc}^* and η_{ohm}^* , once the surface concentration of the diffusing ion is calculated. The total overpotential wave η_{dc}^* , and the DC overpotential component η_{dc} are then obtained from Equations <55> <56> respectively. For the given pulsating current waveform, the calculation can be made at various DC current densities to generate a DC polarisation curve in the form of η_{dc}^* vs. log i^*_{dc} The apparent electrokinetic parameters for pulse electrolysis can be then evaluated from DC polarisation curves.

Figure 9 shows the dimensionless limiting pulse current density, $i_{pl}^* = \frac{i_{pl}}{|i_{lim}|}$, which is defined as the current density at which the surface concentration of the reacting species becomes zero at the end of the cathodic pulse time as a function of the dimensionless pulse period $T^* = \frac{DT}{\delta^2}$ for rectangular pulse reverse ($i_3^* = 5.0$). The parameter in the figure is the cathodic duty cycle $\theta_1 = t_1$ /T. The value of i_{pl}^* increases with decreasing T^* and θ_1 . At very small pulse periods and cathodic duty cycles, a very high limiting pulse current density corresponding to 100 times the DC current density is obtained.

Effect of anodic pulses on limiting pulse C.D.

The average C.D. (or DC current density where electrode is being operated) can be calculated from the following equation:

$$i_{dc}^* = i_{pl}^* \theta_1 + i_3^* \theta_3 \qquad <57>$$

i_{pl}^* represents a cathodic process and has a negative value, i_3^* represents anodic current density and has a positive value. The value of i_{pl}^* represents a net rate of an electrode reaction. Equation <57> has been numerically solved for the pulse wave shown in Figure 9 and is plotted in the figure as a dashed curve.

The curve can serve as a guideline to practical electroplaters to determine the correct value of i_1^* and i_3^* in pulse plating. It should be noted that i_{pl}^* represents a maximum cathodic pulse limit for the outset of mass transfer-controlled conditions. Since the anodic current pulse causes an increase in the surface concentration of the reacting ion during the anodic duty cycle, the value of i_{pl}^* for the pulse waves with anodic duty cycle is generally greater than when using only the rectangular cathodic pulses.

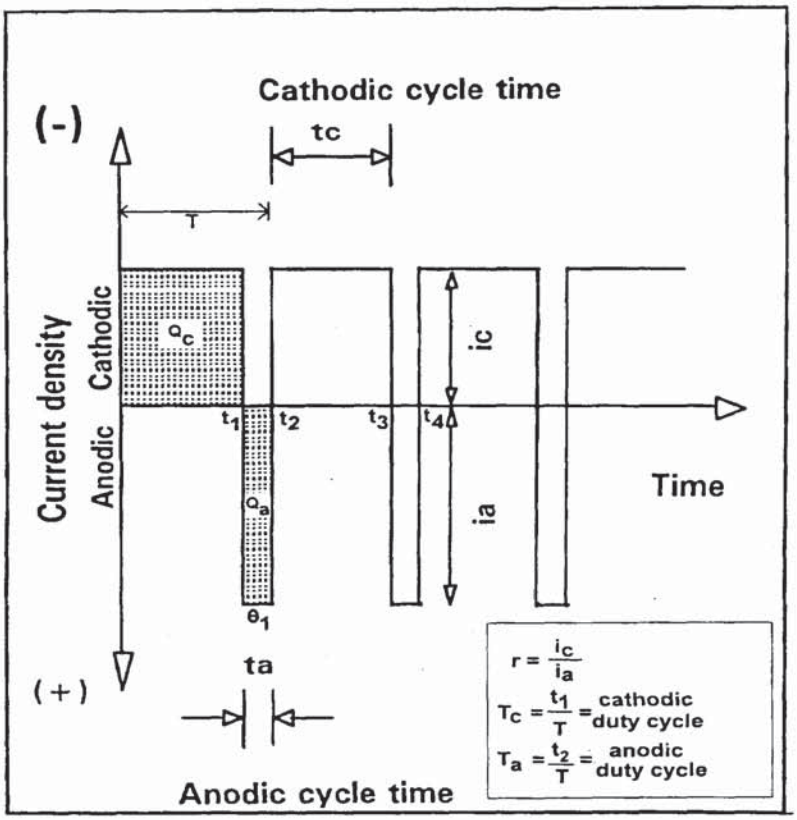

Figure 8. Typical current waveform for periodic-reverse (PRC) plating.

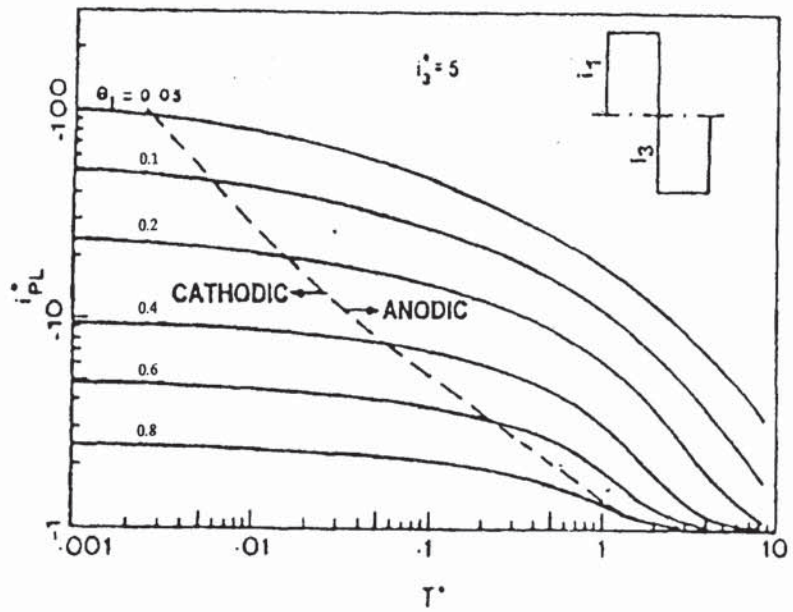

Figure 9. The dimensionless pulse limiting current density as a function of a dimensionless pulse period.[87] The results are given for a rectangular pulse reverse with i_3= 5.0.

Surface Concentration and Potential Fluctuation. For electrolysis with a current wave having an anodic pulse reverse[87], the surface concentration C_s^* generally undergoes a rapid increase during the current reversal period. Also, C_s^* undergoes a decrease during the cathodic duty cycle. Under certain conditions, the surface concentration of the reactive ion becomes greater than the bulk concentration, even though the overall process (as represented by $\bar{C}_s^* < 1$), is cathodic and there is a net consumption of the reactive ion at the electrode surface.

THE THEORY OF THE EFFECT OF ELECTRODEPOSITION AT PERIODICALLY CHANGING RATE ON THE MORPHOLOGY OF METAL DEPOSITS

This theory was presented by *Popov*[88,89] and co-workers from the University of Belgrade, Serbia. They described the electrodeposition with periodic reverse current in terms of time and distance dependent concentration:

$$\frac{\partial C}{\partial t} = D\frac{\partial^2 c}{\partial x^2} \qquad <58>$$

$$C(o,x) = C_o \qquad <59>$$

$$C(t,\delta) = C_o \qquad <60>$$

$$\frac{\partial C}{\partial x}\Big\|_{x=0} = \frac{i(t)}{zFD} \qquad <61>$$

Equations <58> to <61> are solved for different $i\,(t)$ and the solutions applied to different types of problems, e.g. by *Chin*[86], *Cheh*[82] *and Viswanathan and Cheh.*[89]

The current density $i\,(t)$ is the periodic function of time given by:

$$i\,(t) = \begin{cases} i_c & \text{for } mT < t \leq \left[\frac{m+1}{r+1}\right]T \\ -i_a & \text{for } \left[\frac{m+1}{r+1}\right]T < t \leq (m+1)T \end{cases} \qquad <62>$$

For i(t) given by Equation <62>, the solution of Equations <58> to <61> for surface concentration for x = 0, and m $\rightarrow \infty$ (at the ends of cathodic pulses) and similarly for x = 0, t = (m+1) T (end of anodic pulses), results in rather lengthy and fairly complex equations However, after a sufficiently long period), T (T>> t_0 where $t_0 = \frac{\delta^2}{\pi^2 D}$) the system behaves as under DC conditions. For T $\rightarrow \infty$, the expression for surface concentrations becomes:

$$\lim_{T\to\infty} C_c = C_o - \frac{\delta i_c}{zFD} \qquad <63>$$

$$\lim_{T\to\infty} C_a = C_o - \frac{\delta i_a}{zFD} \qquad <64>$$

The average current density in PRC is given by:

$$j_{av} = \frac{i_c t_c - i_a t_a}{t_c + t_a} \qquad <65>$$

or

$$j_{av} = i_A \frac{1-r}{1+r} \qquad \text{for} \quad i_c = i_a = i_A \qquad <66>$$

It follows from Equation <66> that the deposition current density, j_A during is larger than j_{av} (since: r = < 1;). In this way, rougher deposits can be expected than in DC deposition, assuming that the electrode dissolves uniformly and no electropolishing conditions are obtained.

For sufficiently small total period T, (T << t_0):

$$\lim_{T \to 0} C_c = C_o - \frac{\delta}{FD} \frac{i_c - r i_a}{r+1} \qquad <67>$$

$$\lim_{T \to 0} C_a = C_o - \frac{\delta}{FD} \frac{i_c - r i_a}{r+1} \qquad \text{or} \qquad <68>$$

$$\lim_{T \to 0} C_c = \lim_{T \to 0} Ca \qquad <69>$$

This means the surface concentration becomes constant and its value depends only on average current density. *In such conditions, the surface roughening will be the same,* at the same *effective current density.* Hence, less rough deposits in PRC will be expected than in DC

Reversing Current in the seconds range. For *T* close to the conditions in which the distribution of the concentration inside the diffusion layer at the end of the cathodic pulse is close to that given to Equation <59> is to be found. That will happen at $C_a = C_o$ or:

$$\sum_{k=0}^{\infty} \frac{1}{(2k+1)^2} \left[j_c \frac{\exp\{-\lambda_k r T/(r+1)\} - \exp(-\lambda_k T)}{1 - \exp(-\lambda_k T)} - j_a \frac{1 - \exp\{-\lambda_k r T/(r+1)\}}{1 - \exp(-\lambda_k T)} \right] = 0 \qquad <70>$$

It is known that[85] for $\frac{rT}{(r+1)} \geq 1.5\ t_0$, series ($\Sigma$) in the above equation can be approximated with respect to the first term (k = 0). Hence,

$$\exp\left(-\frac{r}{r+1} \bullet \frac{T}{4 t_0}\right) - \exp\left(-\frac{T}{4 t_0}\right) = 1 - \exp\left(-\frac{r}{r+1} \bullet \frac{T}{4 t_0}\right) \qquad <71>$$

for $i_c = i_a$, it follows:

$$r = \left[\frac{4t_0}{T} \ln \left\{ \frac{2}{1+\exp(-T/4t_0)} \right\} \right] \left[1 - \frac{4t_0}{T} \ln \left\{ \frac{2}{1+\exp(-T/4t_0)} \right\} \right]^{-1} \qquad <72>$$

It can be shown that for $T = 3t_0$ r = 0.7 and for $T = 16t_0$ r = 0.2 by assuming that for $T = 3t_0$, the equation <69> is valid and that at $T > 16t_0$ the system behaves as under DC conditions. Therefore, the optimal ratio is given by Popov as:

$$1.5 \leq \frac{t_c}{t_a} \leq 5 \qquad <73>$$

for period T such that: 3 seconds $\leq T \leq$ 16 seconds <74>

Reversing current for the case of variable PRC charge ratio $R = Q_a / Q_c$

At this point in the discussion of the theoretical treatment by Popov et al.[88], the author of this thesis now expanded their approach by offering a mathematical solution for the case of *variable coulombic charge ratio*, designated as $R = Q_a / Q_c$.

a.) Approximate solution.

Equation <70> derived by *Popov et al.*[88] for the simplest case when $J_c = J_a$ and is in good agreement with older references. However, the newer publications[71,72,91] stress the importance of the *charge ratio*, $R = Q_a / Q_c$ over the *time ratio* t_c / t_a. To introduce this the following mathematical treatment is offered: It is necessary to return to equation <71> for replacing r with $R = Q_a / Q_c$. Equation <70> follows immediately from the original treatment produced in 1910 by *Rosebrugh and Miller*[85].

It gives the condition for re-establishment of the concentration inside the diffusion layer at the end of the anodic pulse. If all the terms except the first one (k=0) can be neglected, then expression <70> simplifies to:

$$i_c \frac{\exp\{-\lambda_0 rT/(r+1)\} - \exp(-\lambda_0 T)}{1 - \exp(-\lambda_0 rT)} = i_a \frac{1 - \exp\{-rT/(r+1)\}}{1 - \exp\{-rT\}} \qquad <75>$$

Hence, it follows that:

$$\left(\frac{i_a}{i_c}\right)_{opt} = \frac{\exp\{-\lambda_0 rT/(r+1)\} - \exp(-\lambda_0 T)}{1 - \exp(-\lambda_0 rT/(r+1))} = \frac{\exp\{-rT/4t_0(r+1)\} - \exp(-T/4t_0)}{1 - \exp\{-rT/4t_0(r+1)\}} \qquad <76>$$

(for $\lambda_o = 1/4t_o$)

After multiplying both sides by r

$$R_{opt} = \left(\frac{j_a}{j_c}\right)_{opt} \bullet \frac{t_a}{t_c} = \left(\frac{j_a}{j_c}\right) r = r \frac{\exp\{-rT/4t_0(r+1)\} - \exp(-T/4t_0)}{1 - \exp\{-rT/4t_0(r+1)\}} \qquad <77>$$

This equation shows that optimal R depends not only on T/t_0 but also on the given value of r. Therefore, one can find R_{opt} for different T/t_0 and r by numerical calculation.

b. The exact solution:

In real conditions one has to take more than one term in the series in <70>. Neglect of the second, third, etc., terms (especially in the denominator) would cause in many cases inexact assumptions. The point is that only the factor at j_c in Equation <70> decays rapidly; but the factor at j_a approximates to 1. Therefore, the factor is summation containing:

$$\sum_{k=l}^{\infty} \frac{1}{(2k+1)^2} \qquad <78>$$

i.e. (...+ 1/25 + 1/49 +1/81 + 1/121....), where is the number of the first neglected term, giving, as a result, some considerable quantity.

For this reason the values for r of 0.2 and 0.7 in Equation <72> (forT/t_0 = 16 and T/t_0 = 3 correspondingly) are too large. In actuality, more precisely they will be:

$$0.5 > r > 0.1 \qquad <79>$$

In the general case, it is necessary to use the general formula instead of < 77>:

$$j_c \sum_{k=0}^{\infty} \frac{1}{(2k+1)^2} \frac{\exp\{-\lambda_k rT/(r+1)\}-\exp(-\lambda_k T)}{1-\exp(-\lambda_k T)} = j_a \sum_{k=0}^{\infty} \frac{1-\exp\{-\lambda_k rT/(r+1)\}}{1-\exp(-\lambda_k T)} \qquad <80>$$

For convenience let us denote:

a) $\frac{(2k+1)^2}{4} = m_k$;

b) $\lambda_k = (2k+1)^2$; $\pi^2 \frac{D}{4\delta^2} = \frac{m_k}{t_0}$ (since $t_o = \frac{\delta^2}{\pi^2}/D$)

and taking into account that: $\frac{rT}{(r+1)} = t_a$ it follows that:

$$j_c \sum_{k=0}^{\infty} \frac{\exp(-m_k t_a/t_0)-\exp(-m_k T/t_0)}{4m_k(1-\exp(-m_k T/t_0))} = j_a \sum_{k=0}^{\infty} \frac{1-\exp(-m_k t_a/t_0)}{4m_k(1-\exp(-m_k T/t_0))} = 0 \qquad <81>$$

After multiplying both sides by r and rearranging we can now obtain for $R_{opt,}$, instead of equation <77>, the exact solution in the form:

$$R_{opt} = r \sum_{k=0}^{\infty} \frac{\exp(-m_k t_a/t_0)-\exp(-m_k T/t_0)}{m_k(1-\exp(-m_k T/t_0))} \Big/ \sum_{k=0}^{\infty} \frac{1-\exp(-m_k t_a/t_0)}{m_k(1-\exp(-m_k T/t_0))} = 0 \qquad <82>$$

Considering that T, t_a, t_o, and r are known for each particular case R_{opt} may be calculated numerically.

The calculations show that if, $r = 0.1$, then R_{opt} becomes smaller than 0.32 (for T/t_0 . = 16) If $r = 0.01$, the corresponding values for R_{opt} are 0.13 and 0.06, and if r = 0.001 then R_{opt} is close to 0.2 over a wide range of T/t_0 .

If it is desired, more detailed calculations can be made for any range of parameters.

It is essential to note that <76> takes into consideration only the concentration near the electrode surface and has no association with current efficiency . The results reported in the literature for chromium PRC deposition (R_{opt}= 0.007) were deduced from the maximum obtainable current efficiency and are connected with peculiarities of the rather complex and multistep cathode reduction process rather than the concentration field.

Amplification of Surface Irregularities by PRC in the Seconds Range.

Popov et al[92] explained the amplification mechanism by starting with a general relation for the rate of growth of a protrusion:

$$\frac{dh}{dt} = \frac{VD}{\delta^2} h(C_o - C_s) \qquad <83>$$

Using Equations <61>, <66> and expressing $i\ (t) = i_a$ and with further mathematical treatment, Popov and co-workers obtained for the situation an expression that the same effect on the morphology in PRC and PC conditions can be expected if:

$$P_{eff} = \frac{T}{\frac{T}{1-r} - \frac{8}{\pi^2}\frac{1+r}{1-r}\sigma} \quad \text{where} \quad \sigma = \sum_{k=0}^{\infty} \frac{4t_0}{(2k+1)}\left[1 - \exp\left(-\frac{(2k+1)^2 T}{4\,(r+1)t_0}\right)\right] \qquad <84>$$

For (pause-to-pulse ratio) lower than P_{eff}, rougher deposits can be expected under PC than under PRC and vice versa.

Maximum Deposition Rate by PRC in the seconds range.

Solutions of Equations <58> to <61> for: $i\ (t) = i_a$ are given by *Popov* et al.[87]:

$$C_o - C_s = \frac{i_A \delta}{zFD}\left\{1 - \frac{8}{\pi^2}\sum_{k=0}^{\infty}\frac{1}{(2k+1)^2}\exp\left[-\frac{(2k+1)^2 t}{4t_0}\right]\right\} \qquad <85>$$

It follows from Equation <85> that the surface concentration of depositing ions for $t \geq 1.5$ is given by:

$$C_s = C_o - \frac{i_A \delta}{zFD}\left[1 - \frac{8}{\pi^2}\exp\left(-\frac{t}{4\,t_0}\right)\right] \qquad <86>$$

The maximum amplitude of current density variation, $i_{A,max}$, corresponding to $C_s = 0$ after a deposition time t_c, is given by:

$$i_{A,\max} = \frac{i_L}{1-\left(\frac{8}{\pi^2}\right)\exp\left(\frac{-t_c}{4t_0}\right)} \qquad <87>$$

The relation between i_A and i_{av} is given by Equation <36> and t_c is given by $T/(r+1)$. Now, Equation <52> can be written in the form:

$$i_{av,\max} = \frac{1-r}{1+r}\,\frac{i_L}{1-\frac{8}{\pi^2}\exp\left[-\frac{T}{4(r+1)t_0}\right]} \qquad <88>$$

The average maximum current density, which is considerably lower than i_L, depends strongly on r, the anodic-to-cathodic time ratio. An increase in r leads to an increase in i_{av}. It is obvious that $i_{av,max}$ depends on r (which depends on t_0) and t_0; $t_0 = \delta^2/(\pi^2 D)$ and depends on the deposition conditions. For this reason, different shapes of the PRC wave are to be applied for different plating conditions, according to those authors.

DISCUSSION:

Theoretical considerations offered in this section are intended to help in understanding fundamental relations and the rather cumbersome equations involved in this field of electrochemistry. As understanding of these relations develops, new practical solutions are offered for practising electrochemical technologists.

It is obvious that periodic plating with anodic pulses (PRC) offers new dimensions in the electrodeposition field. Limiting current densities can be greatly increased, resulting in higher practical current densities[93-95]. Anode passivations are reduced or eliminated, *e.g.*, in cyanide copper plating[96,97]. The mechanical and chemical properties of alloys are changed, usually for the better (Ni-P amorphous alloys, Ni-Zn, Ni-Fe)[98-101]. Possibility of obtaining powder particles with different properties, depending on conditions of electrolysis are reported[102]. Hydrogen adsorption is minimised in the case of chromium plating, producing less stressed, crack-free deposits and much higher current efficiencies[72-75]. In the case of acid zinc plating, reduced hydrogen evolution results in reduced polarisation and finer-grained deposits[76.77]. This effect is similar to that observed in alkaline zinc plating solutions and explains the decreased tendency for dendritic growth and better levelling. For PRC nickel deposits, under specific PRC pulses, the deposits become bright and smooth, even without organic brighteners, due to the change in surface morphology[62-68]. The yield and tensile

strengths can be increased by a factor of three. The coefficient of friction was reduced. Even in gold plating, PRC found application although unipolar pulse plating (PC) is commonly commercially used.[69,70]

In the case of acid copper plating[56-61], pulse reverse current in additive-containing solutions can improve dramatically the metal distribution in low current density areas. Deposition rates and ductility are improved, too. Use of low frequency (about 1Hz), PRC current instead of DC, caused no significant change in the current efficiency, alloy composition, hardness or wear, but the key property, the porosity, was reduced.

New developments in rectifier technology and the use of primary SCR's (Silicone Controlled Rectifiers) as diodes are making the new generation of PRC rectifiers more affordable and easily interfaced with the computers. This, in turn, can make dialling appropriate R_{opt} quite simple. There is no doubt that the plating with periodically reversed current has a bright future

The theory behind the influence of PRC variables is much more complex than encountered with DC or PC. With the growing contributions to understanding how the control of the additional variables can improve the properties of the products increasing popularity will come to this technology.

I.4 CHROMIUM PLATING UNDER PERIODICALLY REVERSED CURRENT

It is usually cheaper and faster to apply thicker chromium plating to restore worn surfaces as well as to increase the surface hardness of parts which operate under serious wear and abrasion conditions.

Chromium plating is therefore the main industrial method of restoring worn-out parts. Despite the number of positive qualities of chromium deposits obtained with a direct current, a serious drawback is a lack of levelling and an increase of surface roughness when plating for a long time (usually in the order of hours) to obtain thick chromium deposits.

During the last few decades, a number of attempts have been made to find new plating baths and conditions to accelerate the chromium plating process and to improve the properties of deposits. New catalysts were introduced that were more efficient in comparison to the usual two-component CrO_3 - H_2SO_4 baths; however, during DC chromium plating poor throwing power, high internal stresses, low efficiencies and other disadvantages are still not fully minimised.

After the original publications on PRC deposition, for a long time it was believed that the electrodeposition by PRC, which permitted changes in the properties and improvement in the quality of many metal deposits, could not be successfully extended to chromium plating; during the anodic period of current reversal intensive metal dissolution could occur as the anode current efficiency exceeded the cathode efficiency by 10 to 20 times, depending on the cathode current efficiency of the bath in question.

In later studies, it was found that through periodic current reversal under appropriate conditions an increased rate of chromium deposition became possible, resulting in somewhat smoother deposits, more uniform thickness distribution and nonporous deposits, mainly due to the use of higher current densities and electropolishing action.

PRC chromium plating was first carried out in France by *Audubert*[103], in Germany by *Cohen*[78] and in the USSR by *Rykova*[104] and *Bogorad*[105]. Much of the earlier work on PRC chromium plating originated with the Russians.

Rykova studied the effect of current reversal on the internal stresses and on the quality of the electrodeposited chromium. She claimed that PRC chromium deposits have reduced internal stresses in comparisons with DC deposits; that the surface of PRC deposition chromium-plated surface is smoother, without dendrites and nodules, even after longer deposition times.

Bogorad studied nonporous and porous PRC chromium deposits in a bath containing chromic acid (250 g/l) and sulphuric acid (2.5 g/l) at 55° C. In each cycle of reversal, he used a gradual build up of cathodic current density ("ramping"), with a subsequent determined period at a given working current density, after which the electrode was anodically polarised (reversed) for 40-60 seconds. When porous chromium deposition was needed, electrodeposition begins with anodic treatment for 5-10 seconds and also ends with a 2-minute reversal. According to Bogorad, PRC chromium plating has a number of advantages in comparison with direct current. The internal stresses are lower. The uniformity in thickness of chromium plating and the wear-resistance (over cast iron) are increased as well as the smoothness of the surface of the plated objects being noticeably improved.

Pamfilov et al.[106] studied the effect on cathodic current efficiency and the quality of the chromium deposits in a 250 g/l Sargent bath. They found that current reversal with exceptionally short periods of cathode and anode polarisation increases the brightness and current efficiency. Decrease in bath temperature decreases the porosity. They assumed that anodic current causes a change in the cathode film, which affects the physical properties of the chromium deposits and the current efficiency.

Shluger and Kazakov[107] studied the effect of PRC on the rate of deposition and on the properties of deposits, *e.g.*, porosity, throwing power, microhardness, internal stresses and others. They discovered that during PRC chromium plating, each change of polarity is accompanied by an increase of the current in comparison with the given working current. This is clearly evident in the current-time oscillogram taken at a constant potential. Parts **ab** and **ef** correspond to the cathode period, and part **cd** to the anode period of the current reversal (Figure 9). By determining the rate of deposition as a function of the anode current density for different conditions of reversal ($i = 60\ Adm^{-2}$, temperature 60° C): t_c = 2 min., t_a = 0.5 sec.; t_c = 1 min., t_a = 1 sec.; t_c = 3-5 min., t_a = 10 sec.; t_c = 4-10 min., t_a = 30 sec., the investigators came to the conclusion that in the PRC mode the rate of chromium deposition decreases according to the *decrease* of the ratio t_c/t_a. However, with certain conditions of current reversal, the authors obtained smooth deposits with current densities of 100 Adm^{-2}. This allowed them to assume that current reversal can contribute to an increase

of the efficiency due to the use of high *working* current densities. For chromium plating in DC mode, too high current densities lead to the formation of rough deposits with nodular growths. In their opinion, even and smooth PRC deposits are related to the formation of new centres of crystallisation during each new cathode current pulse as well as to changes in the cathode process.

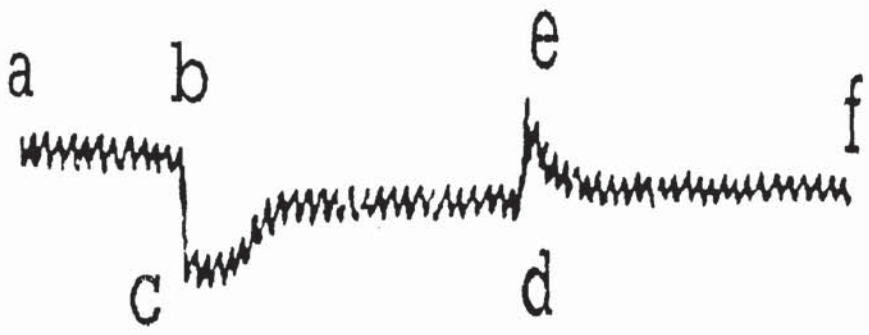

Figure 10. Current-time oscillogram for PRC chromium plating[107].

Determination of the internal stresses in chromium deposits showed that increasing the solution temperature to a certain limit (to 50° C), periodic current reversal causes a definite increase of the internal stresses; however, at temperatures of 60° and 70° C, a sharp reduction is observed, especially with a decrease of the anodic pulse. PRC plating permitted them to obtain practically nonporous deposits with a thickness of 30-40μ , although in the initial period of deposition (to 10μ), they had a greater porosity compared to DC. The authors also established that the throwing power of the bath improves noticeably with the increase of the frequency of current reversal. The wear-resistance of the deposits obtained under DC and PRC, measured with a load of 50 kg/cm^2 for 50 hours, was practically identical.

Maslov[108] established that the current, during the cathodic cycle, does not remain at the same magnitude as during the anode cycle, but increases by 1.5 to 2 times and attains the fixed value only after a relatively long time (25 seconds and longer). The degree of increase and fall of current during the anodic period depends on the distance between the electrodes . He assumes that PRC chromium plating should logically be conducted with separately regulated cathode and anode currents. From the study of the different conditions of current reversal, he found a decrease in the rate of deposition and current efficiency with a decrease of the ratio t_c / t_a . For a given current density of 50 Adm^{-2} and a decrease of t_c from 10 to 6 minutes at t_a = 15 seconds, the thickness of the plating is decreased from 40 to

26μ ; but for t_a = 5 seconds, a decrease of 40 to 36μ : Thickness distribution is also found to be a function of the ratio t_c / t_a . With a significant reduction of this ratio, intensive dissolution of the chromium deposits is observed, especially at the edges of the electrode or the projecting parts of the surface. The best results for throwing power were obtained at t_a = 10 and 15 seconds and t_c= 9 and 15 minutes, respectively. Increasing the working current density, the chromium current efficiency is increased in both polarities. With DC at a current density of 80 Adm^{-2} and higher, an intensive formation of dendrites (roughness) occurs at the edges of the electrode, impairing the smoothness of the surface, increasing the brittleness and wear. In the PRC mode, those disadvantages are not observed even at current densities up to 140-160 Adm^{-2} (t_c / t_a = *9 min./10 sec).* The microhardness of the deposits decreases with an increase of the ratio t_c / t_a due to the reduction of internal stresses and a partial elimination of the hydrogen absorption. During PRC deposition, the optimal bath temperature for maximal wear reduction depends on the ratio t_c / t_a .

Filin[109] tried to find the optimal values of t_c and t_a to establish the effect of current reversal on the smoothness, current distribution, and the effects of current reversal on the fatigue strength of the plated parts. The smoothness is mainly affected by the initial smoothness of the base and by the chromium thickness. When applying thick layers of chromium (*e.g.*, of the order of 0.2 mm) with DC, the smoothness of the surface was made 3-5 times worse, indicating negative levelling and the fatigue strength of the base metal is impaired, sometimes by 30-50%. Tests were carried out in standard, Sargent, or self-regulating electrolyte baths with i = 56 Adm^{-2} at 55° C. For PRC, at t_c = 15 min. and t_a = 10 sec., the results showed that, after plating 0.14 - 0.15 mm thick chromium deposits (on the diameter), the smoothness of the surface was unchanged in both baths.

Kryzhanovskiy[111] studied PRC electrodeposition with a different ratio t_c / t_a . The author did not find conditions necessary for obtaining a bright range. The deposits obtained were a grey colour. Increase of the anode component of the periodic current resulted in decreased current efficiency.

Shluger, a well known Russian authority on chromium plating in one of his classical papers[112], determined some general principles for choosing PRC conditions during chromium deposit. He assumes that a great difference is characteristic for the values of the cathode and anode current efficiencies. Effective results can be achieved by making t_c and t_a as short as possible. Reduction of t_c must be accompanied by a corresponding reduction

of t_a . An unusual dependence of current on time for the anodic dissolution of chromium is observed. During the polarity change of the chromium-plated part as the anode, the current at the first moment is several times larger than the steady state current value. To study the plating rate, the author used a Sargent type bath at 50-60° C and $i_c = i_a =$ 50-60 Adm^{-2} and varied t_c / t_a from 0 to 50 seconds. It was found that the plating rate depends sharply on the ratio t_c / t_a and that a ratio > 30 is most favourable. With significant increase in t_c / t_a , although the rate of deposition is also increased, the effect of the positive influence of current reversal on the deposits is also reduced. Along with this ratio, i_a has a considerable effect on the current efficiency and an increase of i_a causes its decrease. Studying the throwing power of the bath, the author conducted tests with and without the two conditions of current reversal at 60° C and $i_c = i_a = 60\ Adm^{-2}$. He established that current reversal noticeably improves the throwing power and it inversely depends on the t_a Thus at t_c 1 min. and $t_a = 1$ sec., the throwing power of the bath is higher than with $t_c = 2$ min. and $t_a = 2$ sec. The author presumably explains the improvement of the throwing power with reduction of t_c by the fact that the non-uniformity of electrodeposition characteristic to chromium plating is not present when plating thin metal layers. Increase in the concentration of hexavalent chromium in the electrode cathode layer during the anodic period of the current reversal also contributes to the improvement of the throwing power of the electrolyte by increasing the cathodic layer conductivity. The author did not succeed in obtaining bright deposits by PRC conditions indicated above. Most frequently, the chromium deposited was semi-bright or milky. However, an important advantage of PRC in comparison with DC was noted: with DC plating, roughness is rapidly generated on the surface but improved in the PRC mode. The author explains this by the electropolishing action of the anodic current. Shluger studied also the effect of current reversal on internal stresses by the "flexible cathode" method. It was established that periodic change of the current direction does not always reduce the internal stresses. Depending on the conditions of deposition (current density, temperature, reversal conditions), PRC in isolated cases, increase the internal stresses. He confirmed that, with the increase of the bath temperature, current reversal altogether has positive effects on the reduction of internal stresses which, in turn, is a function of the decrease of the porosity of the deposits with an increase of the temperature. Reduction of the t_c or increase of t_a , as well as increase of the i_a , contributes to internal stress reduction. In a study of the effect of PRC on porosity with increase of chromium thickness, the same dependence was observed, as in nickel plating,

namely, with PRC plating of relatively thin layers, the porosity is higher than in DC. but deposits of less thickness are nonporous for PRC. Corrosion tests done by total immersion of steel samples, chromium plated to a thickness of 30 microns, in a 3% NaCl solution at room temperature showed that the deposits obtained with the PRC method at t_c = 2 min. and t_a = 2 sec. have better protective properties as compared to those using the DC method. *Golubov et al.*[113], use PRC to produce bright, adherent chromium deposit (5-8 μ thick) in a bath consisting of NaOH = 10, CrO_3 = 375, Cr_2O_3 = 0.5, sugar = 1.0 and H_2SO_4 = 2 g/l at 20°-30° C at i_c 10-12 Adm^{-2}, t_c = 25-30 sec. and t_a = 1-1.5 sec. with total deposition time being 20-25 min.

Vagramyan[114] showed that deposition from a Sargent bath (250 gr/l, 100:1), carried out with and without the reverse current, did not affect the degree of uniformity of the chromium deposition. Keeping the temperature between 40° and 60° C also did not have an effect on uniformity (covering -power).

Colombini[115] in a more recent paper used the same Sargent bath at 50° C. at i_c = 40 Adm^{-2} and constant anodic time, t_a = 20 msec. He used three different anodic current: i_a = 15%, 25%, and 40% of i_c. By varying intervals between negative pulses (t_c) between 15 and 60 sec., he claimed the following results:

- As t_c decreases, hardness and probability of crack formation decrease but efficiency increases.
- As i_a increases from 16 to 60 Adm^{-2}, hardness and probability of crack formation decrease and efficiency increases.

Sutter et al.[116], used i_c = 30-50 Adm^{-2}, i_a = 5-50 Adm^{-2}, t_c = 1-15 sec., and t_a = 30-50 msec. Without significant change of deposition rate, they obtained deposits with a greyish look, crack-free but with a spectacular increase in corrosion resistance; 15 microns of chromium plating on steel will withstand 200 hours of salt spray exposure vs. 24 hours for conventional chromium.

Colombini[117] eliminated the problem of inferior hardness and dullness associated with PRC chromium by plating the first chromium layer by PRC and the top one with DC from the same Sargent type bath. Efficiency was also increased.

Leisner et al.[72] recently used the Taguchi statistical method to optimise current efficiency. He varied t_a, i_a and i_c showing that efficiency can be doubled when the ratio

of anodic to cathodic charges (Coulombs) lies within a certain range. *Leisner*[106] in his later paper again investigated the current efficiency of chromium under PRC conditions. Using the Sargent type bath, he found that current efficiency increases with the cathodic CD and decreases with temperature and that the ratio of anodic to cathodic charge Q_a /Q_c is a dominant factor. Optimal current efficiency is obtained for Q_a /Q_c value between 0.0020 and 0.0085. On the basis of the results for his work and the literature data, crystallisation mechanisms for deposition of chromium under PRC conditions has been proposed.

Petrovic et al.,[118] used the PRC regime and standard 100:1 Sargent solution. Applying the Simplex method for experimental design, they established functional correlation between cumulative mass loss (abrasion resistance) in relation to optimal temperature (45° C), current density (73 Adm^{-2}) and frequency (1900 Hz). Deposits were bright and crack-free.

Krishman et al.,[119] used self-regulating, high speed chromium bath. Using the equal $i_c = i_a$ = 31, 46.5, and 62 Adm^{-2} , they plated electropolished steel specimens under Direct current, Pulse current (175 sec. on, 5 sec. off) and PRC (t_c = 175 sec, t_a = 5 or 10 sec.; $ic = i_a$) regimes. They found that CCE's are approximately the same for Direct current and Pulse current (17.9% as 18.2% at 46.5 Adm^{-2}) but lower for PRC (11.8% at i_a = 5 sec and 9.3% at i_a = 10 sec). Low CCE's are obviously a result of too long anodic current and consequently high Q_a / Q_c 0.003 or 0.057 ratios. Interestingly enough, PRC increased (!) the microhardness from 750 (Direct current) and 800 (Pulse current) to 1020 kq/mm at 46.5 Adm^{-2}. Appearance under PRC was uniformly bright with few cracks.

I.5 CHROMIUM ANODIC REACTIONS

Considering the amount of chromium metal used world-wide and its importance, it is surprising to find how little information is available on anodic reactions and the mechanisms involved. Actually, there are no definite data on the dissolution reactions or anodic current efficiency even for such important reactions as chromium passivation and dissolution in an acid environment as a part of chromium corrosion studies. The mechanism of anodic oxidation is still insufficiently studied and several practical and fundamental problems of a purely electrochemical nature remain to be solved.

Caveth and Curry[120] back in 1905 suggested that chromium in chromic acid was not a reversible electrode, since from chromate solutions it is impossible to obtain metal and that chromium when used as an anode goes to solution at different valences according to conditions used. At lower temperatures the rate or dissolution showed the Cr^{6+} while at higher temperatures it tended to become bivalent.

Mitskus and Skenikaite [121] postulated that electrolytic reduction of chromic acid depends on the state of the electrode and that the reduction of chromic acid to Cr^{3+} at positive potentials occurs on activated chromium cathodes only. The common phenomena occurred during the dissolution of the cathodes and the electrolytic deposition of chromic acid: auxiliary anions (e.g. sulphates) are needed in both cases. They also found that anodic dissolution of chromic acid is proportional to time, temperature and H_2SO_4 concentrations . They postulated that the generally accepted electrochemical reaction for reduction of chromic acid can be considered in two stages:

$$6\,Cr^{3+} + 6e = 6\,Cr^{2+} \qquad \text{(electrochemical reaction)} \qquad <89>$$

$$6\,Cr^{2+} + Cr_2O_7^{2-} + 14\,H^+ = 8\,Cr^{3+} + 7\,H_2O \qquad \text{(chemical reaction)} \qquad <90>$$

$$Cr_2O_7^{2-} + 14\,H^+ = 2\,Cr^{3+} + 7\,H_2O \qquad \text{(total)} \qquad <91>$$

The anodic behaviour of chromium with respect to its passivity has been studied for many years, with most studies carried out in acidic solutions, mostly based on sulphuric acid. It has been reported[122-124] that solution-soluble Cr^{2+} and or Cr^{3+} species are formed on chromium electrodes in the active-passive region. Colorimetric analysis of the solution after anodic polarisation of chromium[125], indicated that the active dissolution of chromium is preceded by a two-electron process to form Cr^{2+}.

Cherkez[126] studied anodic etching of chromium and its influence on porous chromium plating. He found that anodic current efficiency does not depend on the CD (from 1 - 100 Adm^{-2}), on duration of the anode etching (from 2.5 - 30 min.), on the temperature of the electrolyte (17 - 80^0 C), or on the content of the chromic acid in the Solution. The anode current efficiency is 104 - 106%, as related to Cr^{6+} . He experimentally determined that the potential of the chromium anode is gradually decreased with time. During the first 3 - 4 minutes of etching, the potential drop was considerably more rapid than later, when all potentials approached a certain constant magnitude after which no changes could be noted.

Shluger[127] found that dissolution of chromium does not depend on CD but on the amount of anodic charge used $(t_a \cdot i_a)$. It is temperature dependent and also depends on the temperature at which the chromium is plated as a cathode.

Delombe et al.[128] studied electrochemical properties of chromium with the use of potential - pH equilibrium diagrams. By examining the chemical and electrochemical properties of chromium, the essential point is brought out that the metal behaves as though it existed in two clearly different states: active and passive. In acid solutions of pH around 1 to 2 (e.g. 0.1 and 0.01 M H_2SO_4) the polarisation curves display at first a section corresponding to the dissolution of metal as chromous ions, Cr^{2+} , for potentials around -0.5 to -0.6 V. An increase in the current density then produces a sharp increase in the potential to a value above +1.2 V. This abrupt increase in the potential corresponds to a change from the active state to the passive state. Increasing the CD further, a new section of activity is encountered, also corresponding to the dissolution of the electrode, but this time in the form of chromic acid.

Hurlen et al.[129] from steady state and transient polarisation data and corrosion data found that the active dissolution of chromium in the presence of sulphate ions occurs primarily by transfer of univalent ions mainly on the kink sights and by solution components. The dissolution reaction is pH indépendent to values below about 2, but is stimulated by hydroxide ions at a higher pH. A possible overall reaction for the anodic dissolution of active chromium electrodes may then be:

$$Cr + H^+ = Cr^{2+} + 1/2\ H_2 + e \qquad <92>$$

and this implies that Cr^+ species are too unstable to survive noticeably.

Vyazovikina et al.[130] studied temperature effects upon kinetics of chromium dissolution in acidic sulphate solutions under non-stationary conditions.

(1). Using the fast chronovoltametry, they have obtained new experimental data, which give evidence of the possibility of the Cr anodic dissolution in the acidic sulphate solutions as Cr^{2+} and Cr^{3+} in the active and in the transpassive regions of the potential.

(2). They found that the rate of anodic dissolution of monocrystalline chromium of crystallographic orientation {100} in 0.5 M H_2SO_4 solution under non-stationary conditions depends upon temperature. According to the electrochemical data, at $T \geq 308^0$ *K*, chromium dissolves mainly as Cr^{2+} ions; at $T \geq 284^0$ *K* as Cr^{3+} ions; and at T between 289 and 303^0 *K* as both Cr^{2+} and Cr^{3+} ions. The temperature range, where Cr dissolves anodically as both Cr^{2+} and Cr^{3+} at sufficient rates, depends on the metal structure and purity.

(3). The observed temperature dependence or the rate of Cr anodic dissolution as Cr^{2+} and Cr^{3+} ions is governed by the interplay of the thermodynamic and kinetic factors that affect the partial anodic processes.

Lou and *Ogura*[131] studied anodic polarisation of 304 stainless steel in dilute H_2SO_4 containing CrO_3 and accompanying current oscillations. The occurrence of current oscillations was rationalised in terms of periodic sequence of dissolution and reformation of the $M(OH)_3$ film which was formed by the reaction of divalent metal ions dissolved in the earlier stage of the polarisation of the stainless steel according to the reaction:

$$6\ M^{3+} + Cr_2O_7^{2-} + 11\ H_2O \rightarrow 6\ M(OH)_3 + 2\ Cr^{3+} + 4\ H^+ \qquad <93>$$

The addition of small amount of CrO_3 accelerates the reaction <93>. The progress of this reaction leads to the lowering of pH and ultimately $M(OH)_3$ dissolves into solution. (M = divalent metal ions Fe^{2+}, Ni^{2+}, Cr^{2+}, etc.). Thus, periodic formation and dissolution of $M(OH)_3$ will be repeated. The induction time observed for the occurrence of the oscillations in the conditions of the electrolysis at the constant potential is related to the time required for the build-up of adequate amounts of H^+ ions to dissolve in the precipitated film. At higher temperatures ($>60^0$ C), the solubility of $M(OH)_3$ becomes greater, leading to further tranquillisations of current oscillations.

Seo[132] studied dissolution behaviour of precipitated chromium oxide in perchloric solution containing SO_4^{2-} from electrochemical point of view. Although they were concerned mostly on amorphous passive oxide film formed on passivated stainless steel in acidic solution, it is relevant to chromium deposition mechanisms. It is established by number of authors that in the initial stage of chromium deposition, amorphous chromium oxide film is formed, but his structure was mostly referred as "amorphous chromic oxide" or "hydrated chromic oxide" film and its dissolution rate was never explained. According to this author, the dissolution rate is determined by superimposing the following two coupling and coupled reactions whose rates depend on potential difference at the hydrous oxide solution interface:

$$OH^-_{(O.H.)} + H^+_{aq} \rightarrow H_2O_{aq} \qquad <94>$$

$$[\text{chromium complex}]^{n+}_{(H.O.)} \rightarrow [\text{chromium complex}]^{n+}_{aq} \qquad <95>$$

where H.O. denotes hydrous chromium oxide. An electrochemical dissolution mechanism is proposed which involves an intermediate sulphate complex $CrSO_4^+$ for perchloric acid solution containing SO_4^{2-}.

Mandich and *Vyazovikina*[133] studied dissolution mechanism of chromium anode in a standard plating strength (2.5 M CrO_3 + 2.5 mM H_2SO_4) solution. By using rotating ring-disc electrode, Auger spectroscopy and SEM methods they offered plausible mechanism of Cr dissolution. Multistep anodic dissolution mechanism is postulated as the charge transfer of single electron steps associated with separation of first electron. The suggestion is offered about changes in the mechanism of chromium anodic dissolution in the transpassive region. From 1.07 to 1.35 V chromium dissolves with formation of Cr^{3+} and Cr^{6+} under mixed diffusion-kinetic control and with the rising fraction of kinetic component with the increase of the potential. In the potential range from 1.35 V to 1.50 V chromium dissolves with the formation of only Cr^{6+} through seven sequential steps. In the range of limiting anodic currents, the transfer of Cr^{3+} to solution proceeds according to CrO_3 formation-dissolution reactions that are in dynamic equilibrium.

It is suggested that the stationary diffusion of reacting ions to the oxide/metal interface through CrO_3 film of a constant thickness limits the anodic process under these conditions. Anodic Current Efficiencies were calculated taking into account the fractions of the metal dissolving as Cr^{3+} or Cr^{6+} ions, and totalling 100%.

I. 6 QUARTZ CRYSTAL MICROBALANCE (QCM)

It has only recently been demonstrated that QCM, commonly employed for mass measurements in vacuum, will operate in solution[134-137] These piezoelectric devices are very sensitive to mass changes at the surface of the crystal and provide the capability of detecting extremely small amounts of deposited material. The operation of the device relies on the excitation of a normal mode of oscillation by the application of a radio frequency field across a thin disc of the material[138]. For AT cut crystals, the resonant condition corresponds to a shear oscillation in which the shear wave propagates through the bulk of the material, perpendicular to the faces of the disk. The atomic displacements corresponding to this shear motion are thus parallel to the disk faces. If material is deposited on either or both faces of the crystal, the resonant frequency decreases. The first quantitative investigation of this effect was that by *Sauerbrey*[139] , who derived the relationship between the frequency change (Δf) caused by the added mass (ΔM) Sauerbrey argued that the elastic properties of the deposited film cannot contribute to the resonant frequency since the film is thin and located entirely within the antinodal region of the resonator, where no shear deformation occurs either in the film or in the quartz crystal near the surface. The unloaded resonant frequency f_o , is found[140] from the condition that the bulk material thickness d is an integral multiple n of half wave length λ_Q, ie, $d = n\lambda_Q/2 = nV_Q\ 2f_o$, where V_Q is the shear wave velocity in quartz. Therefore:

$$f_o = nV_Q / 2d \qquad <96>$$

and if one assumes that at the fundamental frequency (n = 1), $N_{AT} = df_Q$ is the frequency constant of the commonly used AT-cut crystal and is 0.1666 $MH_Z \cdot cm$[141] . A change of thickness of the quartz plate will cause a change of frequency as given by:

$$f/f_o = \Delta d/d \qquad <97>$$

The density, mass, and thickness of the quartz are related by $d = M_Q /A\rho$ where A is the surface area, and this yields:

$$f/f_o = M_Q/dA\ \rho \qquad <98>$$

The change in frequency resulting from the deposition of a thin, uniform film of any foreign substance would be equal to that resulting from a layer of quartz of the same mass[139,140]. Using the relationship between the thickness and N_{AT} , one obtains:

$$\Delta f = \Delta M f_o^2 / A \rho N_{AT} \qquad <99>$$

where ΔM is the mass of film of any substance added to the quartz plate. Using values of the constants quoted, and for the density of quartz ($\rho = 2.648$ g/cm^3) it follows:

$$\Delta f = -2.275 \times 10^6 f_o^2 \ (\Delta M/A) \qquad <100>$$

where Δf is the change in frequency due to the added film (Hz), f_o is the resonant frequency of the quartz plate without deposited film (MHz), ΔM is the mass of deposited film (g), and A is the area (cm^2) for a 5 MHz crystal, one finds:

$$\Delta M = -1.74 \times 10^{-8} A \Delta f \qquad <101>$$

so that the mass sensitivity is -1.74×10^{-8} g/cm^2 Hz. Equation <101> is the fundamental relationship which relates the frequency decrease to the increase of mass loading on the quartz crystal, and the mass sensitivity can be calculated from first principles.

Equations <100> and 101> predict that the QCM is sensitive to submonolayer amounts of material deposited on the quartz plate, and that the sensitivity increases as the square of the frequency of the plate, f_o .

I. 7 FUNDAMENTALS OF LINEAR POTENTIAL SWEEP, CYCLIC VOLTAMMETRY AND ROTATING DISC ELECTRODES

I.7.1 LINEAR POTENTIAL SWEEPS VOLTAMMETRY

One of the aspects of electroanalytical chemistry that can be intimidating for non-electrochemists is a large number of techniques that are available. For example, there are 38 techniques available for the BAS-100 potentiostat used among others in this thesis. However, many of these techniques are related, and these relationships can be easily understood by using a rational approach to these techniques.

In an electroanalytical experiment, there are three important components:

(a) the excitation signal

(b) the system (the particular electrode solution composition and geometry)

(c) the response

The excitation signal is user-defined potential or current wave form, such experiments are deemed potentiostatic (or controlled potential) or galvanostatic (controlled current) experiments. Current-potential experiments are also referred to as voltammetric experiments, whereas current-time experiments are referred to as chronoamperometric experiments.

There are two broad classifications for the system used in electroanalytical experiment - stationary solution or hydrodynamic. The essential difference is the mode of mass transport - in the stationary solutions experiments the only available mode of mass transport is diffusion, whereas, in hydrodynamic experiments, the rate of mass transport is controlled by the user, e.g., by stirring the solution (rotating disc voltammetry). In any experiment, it is important to know what data can be obtained from the experiment and how it can be extracted from the experimental output. This later point is particularly relevant for electroanalytical techniques such as cyclic voltammetry and chronoculormetry, since the measuring of the experimental response for these experiments is not immediately apparent.

The complete electrochemical behaviour of a system can be obtained through a series of steps to different potentials with recording of the current-time curves to yield a three-dimensional I-t-E surface. However, the accumulation and analysis of these data can be tedious, especially when a stationary electrode is used. Also, it is not easy to recognise the presence of different species (i.e., to observe waves) from the recorded I-t alone, and

potential steps that are very closely spaced (e.g., 1 mV apart) are needed for derivation of well-resolved I-E curve. More information can be gained by a single experiment by sweeping the potential with the time and recording the I-E curve directly. Usually, the potential is varied linearly with the time with sweep rates ranging from 0.04 V/s (1 V traversed in 25 s) to about 100 V/s. In this experiment, it is customary to record the current as a function of the potential, which is obviously equivalent to recording current versus time. The technical name for this method is linear sweep chronoamperometry, but most workers refer to it as a linear potential sweep voltammetry (LPS). The resulting I-E curve is bell-shaped. For the reversible (e.g., diffusion controlled), the shape of the curve and the peak potentials are independent on scan rate, but peak current is proportional to $\sqrt{v}$. Since peak current is proportional to the concentration, an LPS can be used for analytical purposes.

1.7.2 CYCLIC VOLTAMMETRY

a. Introduction

Cyclic voltammetry (CV) is a modern electrochemical technique[142-155] which provides the means to examine the nature or "pathway" of an electrochemical reaction in detail. From a detailed investigation of an electrochemical reaction an electrochemist obtains information which not only provides a firmer basis for control of the reaction but also opens the door to study the fundamental chemistry that underlies the reaction system of interest. All electrochemical experimentation involves the application of some perturbation to the system, monitoring the results and interpreting the data thus obtained. In CV the primary concern is related to those fundamental parameters: current, potential and time. Consider a system of reversible redox couple, the oxidised form of which is present in a solution containing excess of supporting electrolyte. A stationary working electrode is employed, the potential of which is monitored versus some reference electrode and through the use of appropriate instrumentation, there is no IR drop in solution. If the potential of the electrode is made increasingly more cathodic (more negative) and at an infinitesimally slow rate current is measured, the familiar *S - shaped* current - potential curve will be obtained.

Repeating the experiment but using potential at a finite rate as a linear function of time results in a significantly different response with a *hysteresis* type curve which is the "trade mark" of CV experiments. Current - potential is no longer S - shaped but exhibits peaks and curves as forward and reverse processes are no longer identical. This further illustrates the effect of variable time on the nature of the electrochemical process and its magnification of the responses obtained. The CV curve provides four measurable parameters: the net current and potential at the peak of cathodic response, and the corresponding parameters for the anodic or reverse response; it is with these parameters and the parameters of time that we deduce the kinetic and the mechanistic information from the data.[143,144]

b. Diagnostic Criteria for CV Experiment.

The basic features of a voltammogram (i.e. a plot of current vs. potential during a cyclic voltammetric or linear potential sweep) is the appearance of a current peak at a potential characteristic of the electrode reaction taking place. The position and shape of a given peak depend on such factors as sweep rate (v), electrode material, solution composition and the concentration of reactants. In Figure 10 is a summary of diagnostic criteria[143]. Also, by way of summary Figure 10 shows the effect of charge transfer rate constant on the cyclic voltammetric response as the state is varied from essentially reversible (diffusion controlled) behaviour to irreversible behaviour. Cyclic voltammograms can result in three kinds of curves indicating reversible, quasi-reversible and irreversible behaviour as presented in Figure 11.

Diagnostic Criteria for *Reversible* Charge Transfer

$$\mathbf{O + ne^- \leftrightarrow R}$$

E_p is Independent of v.

$E^c_p - E^a_p = 59/\text{ mV}$ at 25^0 C and is indepent of v.

Properties of the current function:

$i_p / v^{1/2}$ is independent of v.

Properties of the anodic to cathodic ratio:

i^a_p / i^c_p is unity and independent of v.

Diagnostic Criteria for *Irreversible* Charge Transfer

$$\mathbf{O + ne^-} \xrightarrow{k} \mathbf{R}$$

Properties of the potential of the response:

E_p shifts cathodically by 30 n mV for a ten fold increase in v.

Properties of the current function:

$i_p / v^{1/2}$ is constant with scan rate.

Properties of the anodic to cathodic ratio:

There is no current on the reverse scan.

Diagnostic Criteria for the *Quasi-Reversible* Charge Transfer:

$$\mathbf{O + ne^- \leftrightarrow R}$$

Properties of the potential of the response:

E_p shifts with v.

$E^c_p - E^a_p$ may approach 60/**n** mV at low V but increases as v. increases.

Properties of the current function:

$i_p / v^{1/2}$ is virtually independent of v.

Properties of the anodic to cathodic ratio:

i^a_p / i^c_p equal to unity only for = 0.5.

Others: The response visually approaches that of the irreversible charge transfer as v increases.

Figure 11. *DIAGNOSTIC CRITERIA FOR CYCLIC VOLTAMMETRY* [143]

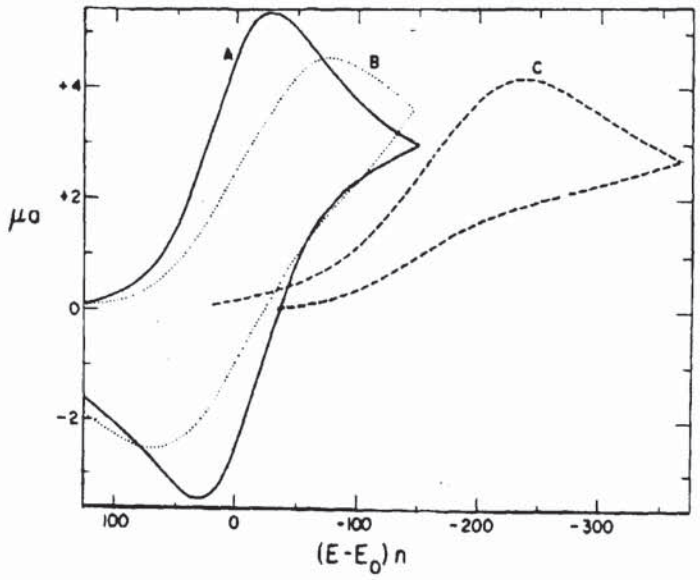

Figure. 12 Theoretical CV curves[143] showing the effect of the charge transfer rate constant on the CV response as the rate is varied from essentially reversible (diffusion controlled) behaviour to irreversible. A = 0.02 cm^2 , $C_0 = 10^{-6}$ M, $D_0 = D_R = 10^{-6}$ cm^2 /s, = 1 V/s, E^0 = 0. A, *reversible curve*; B, *quasi-reversible curve*, $k_s = 0.03$; C, *irreversible curve*; $k_s = 10^{-4}$ cm/s.

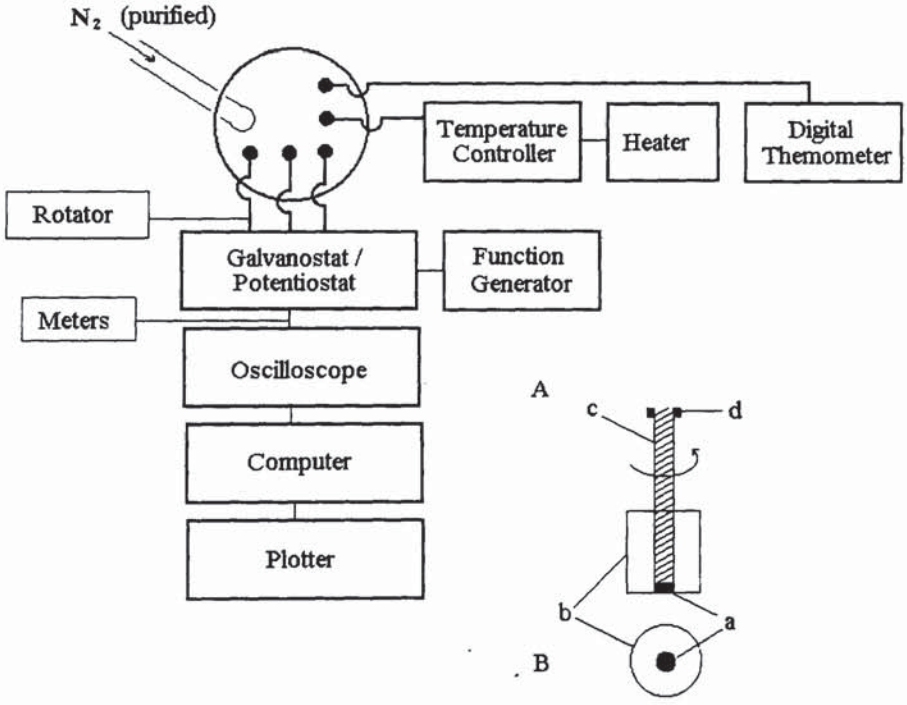

Figure 13. Expeimental Equipment for RDE Experiments. Left figure: *schematic illustration ofthe electrochemical cell and peripherials.* Right figure: *schematic illustration of the rotating disk electrode. (A) Side View (B) Bottom View, (a) disk, (b) insulator, (c) shaft, (d) brush contact.*

I. 7.3 ROTATING DISC ELECTRODE (RDE)

a. Introduction

Voltammetry at the rotating disc electrode (RDE) is a widely used method for the study of electrode processes at solid electrodes. The benefits of RDE are:

(1) A diffusion layer is developed with a thickness that does not change with time
(2) Double-layer charging has a minimal effect on the measurement.
(3) The theoretical basis of the mass transfer process has been solved and equations are available to relate the experimental parameters to the mass transfer of reactants to the electrode surface.

The RDE as shown in Figure 13 is constructed from a disc of electrode material (e.g., glassy carbon, gold or platinum) embedded in a rod of an insulating material (e.g., glass , Teflon, Kel-F). The electrode is attached to a motor and rotated at a *certain rate,* ω, where ω is the angular velocity (s^{-1}). Electrical contact is made to the electrode by means of a brush contact or by copper wire submerged in a mercury pool. Details of construction of RDE's are given by *Adams*[147] .

When an electrode is rotated, mass transfer of reactants and products is governed by convective-diffusional mechanisms. The theory of convective flow at the RDE is identical with the theory of flowing fluids hydrodynamics[148], and thus the methods are termed *hydrodynamic voltammetry.* At the RDE the hydrodynamic flow pattern results from centrifugal forces that move the liquid horizontally out and away from the centre of the disc while fresh solution continually replaces it by a flow normal to the electrode surface.

The mass transfer equations for the RDE under laminar flow are given by *Levich*[148-150]. The hydrodynamic boundary layer, γ, as described above can be given as:

$$\gamma = 3.6 \left(\frac{\nu}{\omega}\right)^{\frac{1}{2}}$$

where ν is the kinematic viscosity of the fluid (cm^2s^{-1}), and δ represents the thickness of the layer of fluid dragged by rotating disc. For water ($\nu \approx 0.01 cm^2\ s^{-1}$ at 20^0 C) at a rotation rate

of 100 rpm (ω =1000s^{-1}), γ is 0.036 cm. If concentration gradients are included the convection-diffusion equation can be determined. The equation for the limiting current that is derived by Levich for a reaction controlled by mass transfer is:

$$i_l = 0.620\, nFAC_0\, D^{\frac{2}{3}}\, \nu^{-\frac{1}{6}}\, \omega^{\frac{1}{2}} \qquad <102>$$

where i_l is the limiting current (amps), n is the number of electrons transferred (eq mol^{-1}), A is the electrode area (cm^2), C_0 is the solution concentration (mol cm^{-3}), D is the diffusion coefficient (cm^2s^{-1}), and F is the Faraday constant 96,485 C eq^{-1} . Thus for the RDE, the diffusion layer thickness, $\delta = 1.61 D^{\frac{1}{3}}\, \omega^{-\frac{1}{2}}\, \nu$. For water, $D \approx 10^{-5}$ cm^2 s^{-1} , $\delta \approx 0.05\gamma$ More complete accounts of the Levich equation are available[149,150]. The limiting current is that which is obtained when the potential of the RDE is adjusted to be on the plateau of the corresponding current-potential curve for the reactant. Following the application of a potential in the plateau region, the limiting current at the RDE quickly approaches the steady-state value, i.e., independent of time, as predicted by the Levich equation. For the case of a rotating disc, laminar flow is obtained when critical Reynolds number (Re) is > $1 \cdot 10^{-5}$. For a typical radius of RDE of, say, 0.3 cm this Re number corresponds to a rotation rate of $1 \cdot 10^5$ rpm. It should be noted that the critical Re represents as a rule the upper limit for laminar flow at ideally smooth surfaces. If the surface is rough, turbulence may set in at a lower Re number. For this reason most RDE's are operated at a maximum speed of $1 \cdot 10^4$ rpm, well within the range of laminar flow. The lower limit for the rotation rate is determined by the requirement that the limiting current density resulting from the rotation rate be large when compared to that which would exist in a stagnant solution due to natural convection. In practice this corresponds to a lower limit of about 400 rpm, which can be extended to 100 rpm under carefully controlled experimental conditions.

Information about a redox system that can be obtained by rotating disc voltammetry includes redox potentials and reversibility . The angular velocity of rotation of the RDE is an adjustable parameter. Thus electrode mechanisms that involve coupled homogeneous chemical reactions and cause deviations of the experimental currents from the Levich equation are amenable to study with the RDE[147-150].

b. Application of CV and RDE in Electrodeposition

Due to its relative simplicity and ease of operation, CV has become a useful tool for practising electroplaters in recent years. *Abys*[156] demonstrated very clearly the usefulness of this technique for finding conditions where the separation of palladium from Pd complex and hydrogen deposition is at a maximum. Another noteworthy application of CV was developed by *Tench* and *Ogden*[157-161] for the determination of additives in copper plating baths. The maintenance of additive concentrations in the low-ppm range is critical to obtain deposits acceptable for printed circuit boards. The method is based on the fact that the rate of copper deposition at a given potential is a function of additive concentration.

Paunovic[162] used CV in the study of electroless copper baths. *Horkans*[158] applied the same technique for the study of the Pd-Sn catalyst. Lyn and Selman[159] used CV to study Ni-Zn alloy. *Mimani*[165] et al. applied CV in the study of the influence of additives on the electrodeposition of Ni from "Watts" bath. *Vales*[166] et al. investigated the relation between the presence of inhibitors and deposit morphology in nickel deposition. *Bertazzoli and Pletcher*[167] applied this method to study Fe-Co alloy. *Crousier and Bimaghra*[168] studied the effect of Ni on Cu deposition.

Several authors have used Cyclic Voltammetry to investigate chromium. *McCormick* and *Dobson*[169] studied performance of 450 g/l CO_3 bath (100:1) on steel, Cu, Au, Cr and C cathodes. *Hoare*[170] investigated reduction of CrO_3 on Pt electrode . *Lin-Cai and Pletcher*[161] studied electrode reactions occurring at C, Cr, Au and Ni cathodes for $Cr^{6+} \rightarrow Cr^{2+}$ reaction and demonstrated that this reaction is mass transport controlled. They also studied[171-a] the roll of surface film formation . *Hoare*[172] also performed ring-disk study of chromium electrodeposition and concluded that cathodic film is strongly adsorbed on the electrode surface and that the electrode reaction is increased with the rotation rate of the disk. Since the scan patterns are independent of rotation speeds from 400 - 2000 rpm he concluded that electrode processes are surface processes under kinetic and not diffusion control. *McCormick et al.*[173] studied by linear and cyclic voltammetry influence of additives in 450g/l CrO_3 standard bath. *Popov et al.*[174] investigated reduction of Cr^{6+} in the presence of organic additives in a black chromium plating bath.

I. 8 DERIVATION OF EXACT EQUATION FOR CURRENT EFFICIENCY UNDER PERIODIC REVERSE CURRENT CONDITIONS.

To determine the effect of the PRC mode on cathode current efficiency during chromium deposition (ζ_{PRC}) it is desirable to compare the *effective* current of metal deposition and accompanying efficiencies, during the cathodic cycle with ones that would be obtained during DC conditions. In the DC mode, Cathode efficiency ξ_{DC} can be simply expressed as $\zeta_{DC} = \frac{I_d}{I} \bullet 100$ where I_d is *effective* current (current used only for chromium deposition) and I is t*otal* current passing through the plating bath and that can be measured:

a. By an Amp-hour meter, as is often used in actual practice.

b. By an Integrator (electronic coulometer), if experiments are done with the use of a galvanostat.

c. With classical method, e.g. silver coulometer connected, in series, with the plating bath under experiment.

Let us denote cathodic and anodic time periods and currents as t_c , I_c and t_a, I_a .
It follows that an increase of the mass at e.g. coulometer cathode is proportional to:

$$\Delta m \propto I_c t_c - I_a t_a = q_c - q_a \qquad <103>$$

The increase of actual, electrodeposited chromium mass is proportional to:

$$\Delta m \propto \xi_c t_c I_c - \xi_a t_a I_a = \xi_c q_c - \xi_a q_a \qquad <104>$$

where ζ_c is the current efficiency of chromium deposition reaction and ζ_a is the current efficiency the chromium dissolution reaction, which in the case of the most commonly PRC plated metals (e.g. Cu, Ag or Ni) is about 1 (100 %). However, for chromium ζ_a can vary, depending mainly on anodic current density, temperature and bath composition. q_a and q_c are anodic and cathodic coulombic charges and q_a / q_c = ρ is the *charge ratio*, experimentally established later in this thesis to be a governing factor for maximizing the current efficiency of PRC deposited chromium.

Now, for *effective* current efficiency, ζ_{prc} we obtain expression <105> by dividing equation <104> by <103> and rearranging:

$$\xi_{prc} = \frac{\xi_c q_c - \xi_a q_a}{q_c - q_a} = \frac{\xi_c - E\xi_a \frac{q_a}{q_c}}{1 - \frac{q_a}{q_c}} = \frac{\xi_c - \rho\xi_a}{1-\rho} \qquad <105>$$

or, $\xi_c = \xi_{prc}(1-\rho) + \xi_a \rho$ <106>

If anodic process proceeds with 100% dissolution efficiency ($\xi_a = 1$) then <106> simplifies to:

$$\xi_{prc} = \frac{\xi_c - \rho}{1-\rho} \quad \text{or} \quad \xi_c = \xi_{prc}(1-\rho) + \rho \qquad <107>$$

In our experiments it was found that optimal value of ρ is usually about 0.005. Substituting this value in <106> we obtain:

$$\xi = \xi_{prc}\ (1\text{-}0.005) + 0.005 = 0.995\,\xi_{prc} + 0.005 \quad \text{or,}$$

$$\xi_{prc} = \frac{\xi_c - 0.005}{0.995} \qquad <108>$$

If we use for chromium cathodic current efficiency, the typical value of 20% ($\xi_c = 0.20$), from <108> we obtain:

$$\xi_{prc} = \frac{0.20 - 0.005}{0.995} = 0.196 \text{ or } 19.6\%$$

with difference in efficiency (error) of 2%. For the situation that is closer to the actual efficiency, when ξ_a is different than 1 (e.g. 0.95), from < 102> we now obtain:

$$\xi_{prc} = \frac{0.20 - 0.005 \cdot 0.95}{1 - 0.005} = 0.193$$

or 19.3% with an error of 3.5%.
(0.193/0.20 = 0.965; 1 -0965 = 0.035).

Although equations <106> and <107> are relatively simple derivations, surprisingly enough a literature search did nor reveal an equation like <106> or <107>, probably due to the fact that PRC deposition is a relative new-comer and that ξ_a a are in most of the cases equal or close to 1. Only *Hickling* and *Rothbaum*[80] offered an equation somewhat similar to <107>, when $\xi_a = 1$, in rather elaborate forms: .

$$\xi = \xi_{prc} + (100 - \xi_{prc}) \cdot \frac{t_c I_a}{t_c I_c} \quad \text{and} \quad \frac{\xi_{prc}}{100} = \frac{\left(\frac{E}{100} \cdot t_c I_c - t_a I_a\right)}{t_c I_c - t_a I_a} \qquad <109>$$

PART TWO

EXPERIMENTAL WORK

II. 1 PHYSICAL PROPERTIES OF CHROMIUM DEPOSITS UNDER PRC REGIME

II.1.1 Experimental set-up

In order to obtain independently controlled anodic and cathodic current densities and time periods, a system with two pulse plating rectifiers, one connected to the cathode side of the plating tank and the other to the anode side with a Time Switching Module between was chosen (Figure 14). In this way a variety of Direct Current (DC), Pulse Current (PC), and Pulse Reverse Currents (PRC) wave forms can be generated as well as a combination of them in msec., sec. and min. time range. A system of two rectifiers is contemplated, keeping in mind eventual scaling-up for production size systems. The price of a single large periodic plating rectifier with separately controlled cathodic and anodic Current Densities is prohibitive for almost all production plating shops. However, it is much more affordable and realistic to use two rectifiers with solid state current controls and connected as described for the above mentioned laboratory set up with a Time Switching Module to sequentially engage them. This way it is possible to plate in DC mode (with the second rectifier as a spare standby) or use both for PRC plating when higher speed and superb corrosion resistance are required. A thermostatically controlled 6 litre lead lined tank with exhaust is a scaled down replica (800:1) of a (1200 gallon) production tank and was also used for small production jobs when high speed or corrosion resistant deposits were required using experimental solutions. The tank is bussed for reversible 2 buss bar plating rack system. An anode holder is made from PVC block to make the anode area equal to the cathode. Anode to cathode distance was kept constant at 3 cm. A cathode holder was designed for the plating of standard Hull Cell panels (7.5 x 10 cm) due to their easy availability and reproduction. Only one side of the panel was used for plating. Particulars are depicted in Figure 15.

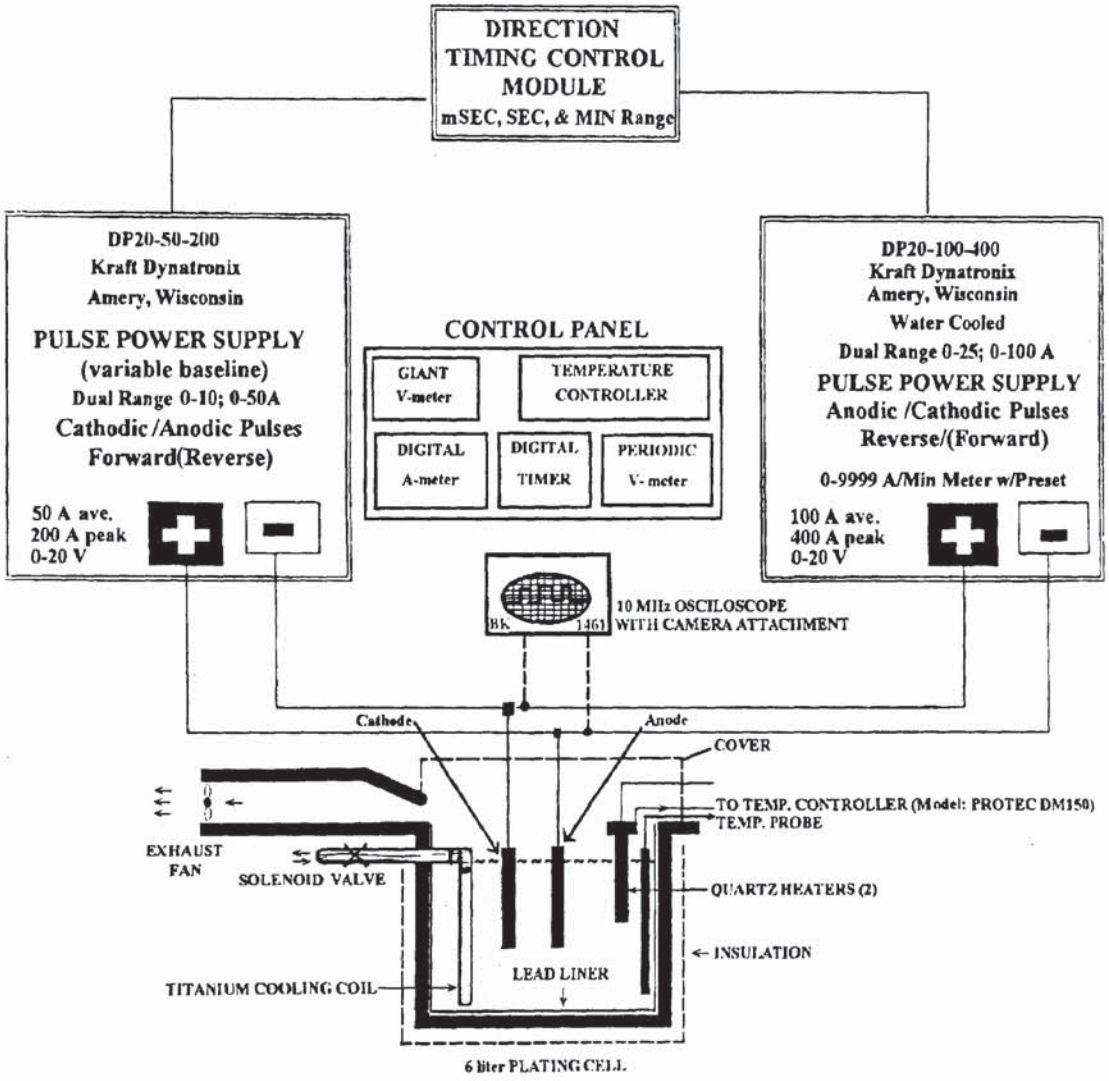

Figure 14. Experimental Arrangement for Producing Pulse, Periodic Reverse, Pulse Reverse and Combination of Pulses in m Sec, Sec or Minute Range.

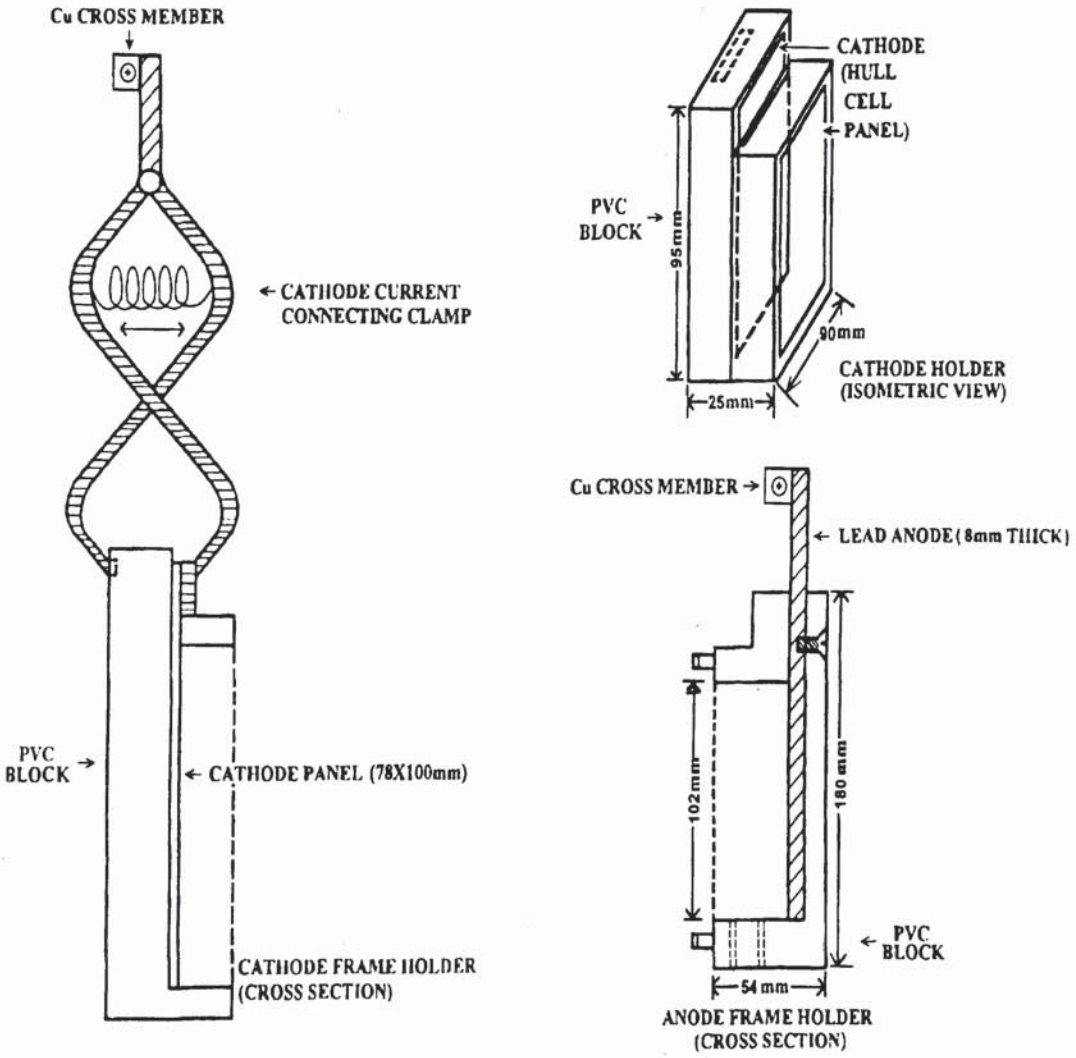

Figure 15. Anode and Cathode Assembly

II.1.2 Experimental Procedure And Results

Variables chosen for investigation were: Hardness, Corrosion Resistance and Deposit Thickness. Hardness was measured with a Vickers Hardness Tester (Rockwell System, model 900-330). Corrosion resistance was measured in the Salt Spray Cabinet (Chicago Industrial Filter model 411-2ACD) according to the ASTM:B117-73. Thickness was determined by measuring the weight of the panels before and after plating and calculating the thickness from the surface area and chromium density data.

Total deposition time was varied from 10 to 60 min. Cathodic time (t_c =6 sec.) and anodic time (t_a = 60 sec.) as well as the current density (40 Adm^{-2} 400 ASF) were kept constant. The solution used was standard sulphate catalysed, Sargent type bath (240 g/l; 100:1 Ratio) at 58^0 C. Protective zinc coating from Hull-cell panels was dissolved in 50% HCl, triple rinsed, dried with acetone and weighed to 0.001 gr. accuracy. After mounting the cathode panels they were anodically etched for 1 min. at the same current density (40) and plated. Three additional experiments **7, 8 & 9** were done with different Q_a / Q_c ratios for comparison purposes; Corresponding SEM's (Figures 16 and 17) are presented for experiments 7 and 8 in order to illustrate the influence of Q_a and Q_a / Q_c on the cathode current efficiency (CCE) and compared with DC experiment (experiment No. 9) in Figure 18. Results are summarised in Table 6:

Exp. no.	Temp. ^{0}F /^{0}C	i_c Adm^{-2}	i_a Adm^{-2}	t_a sec.	t_c sec.	Dep.Tk μ	Q_a / Q_c x 1000	Tot Dep Time min.	CCE %
1	136 / 58	40	40	0.6	60	7.00	10.0	10	23.3 (!?)
2	136 / 58	40	40	0.6	60	8.80	10.0	20	14.6
3	136 / 58	40	40	0.6	60	10.10	10.0	30	11.2
4	136 / 58	40	40	0.6	60	12.10	10.0	40	10.1
5	136 / 58	40	40	0.6	60	15.20	10.0	50	10.1
6	136 / 58	40	40	0.6	60	20.00	10.0	60	10.1
7	136 / 58	30	30	0.26	60	7.80	4..3	15	22.5
8	136 / 58	30	30	0.04	60	12.80	0.7	30	18.5
9	136 / 58	30	0	-	-	1.08	0.0	3	15.4

Table 6: Deposit Thickness vs. Total Deposition time for PRC Plated Chromium.

II.1.3 Corrosion Resistance And Deposition Thickness Vs. Deposition Time At Equal Anodic And Cathodic Current Densities And Variable Anodic Time.

Most of the earlier research was done with equal anodic and cathodic current densities since less sophisticated rectifiers are needed for this approach. A set of experiments were performed to verify this approach.

Physical properties under $\mathbf{i}_c = \mathbf{i}_a = 40\ Adm^{-2}$; $t_c = 60$ sec. with variable anode dissolution time, $\mathbf{t}_a$ are graphically represented in Figures 19-21.

Figure 19 shows that thickness is directly proportional to total deposition time-as in the case of DC plating. However, due to high t_c/t_a ratio (6sec/6sec = 0.01), total thickness after 60 min. is less than under DC (20 vs. 28), indicating that efficiency is lowered under this set of PRC conditions.

Figure 20 represents the dependence of Salt Spray Resistance on total deposition time and corresponding thickness. While DC chromium will resist corrosion only for a few hours, after one hour of PRC plating and 2 of thickness, a spectacular increase in corrosion resistance resulted (500 + hours), indicating that in order to have the same corrosion resistance the thickness of the PRC chromium applied layer can be significantly reduced with corresponding economic advantages.

Figure 21shows the dependence of hardness on total PRC time. Hardness is lower compared to DC although not significantly when using short deposition times and plating thin deposits (e.g. for 10 min of total deposition time is 900 vs. 1050 Vickers or 14.3% lower). At 60 min of total plating time hardness is 28.5% less than under DC conditions. It should be noticed that hardness is only one variable of three and that it is inversely dependent on the total deposition time; compromise has to be chosen for maximum performance of chromium deposit under this particular set of PRC conditions.

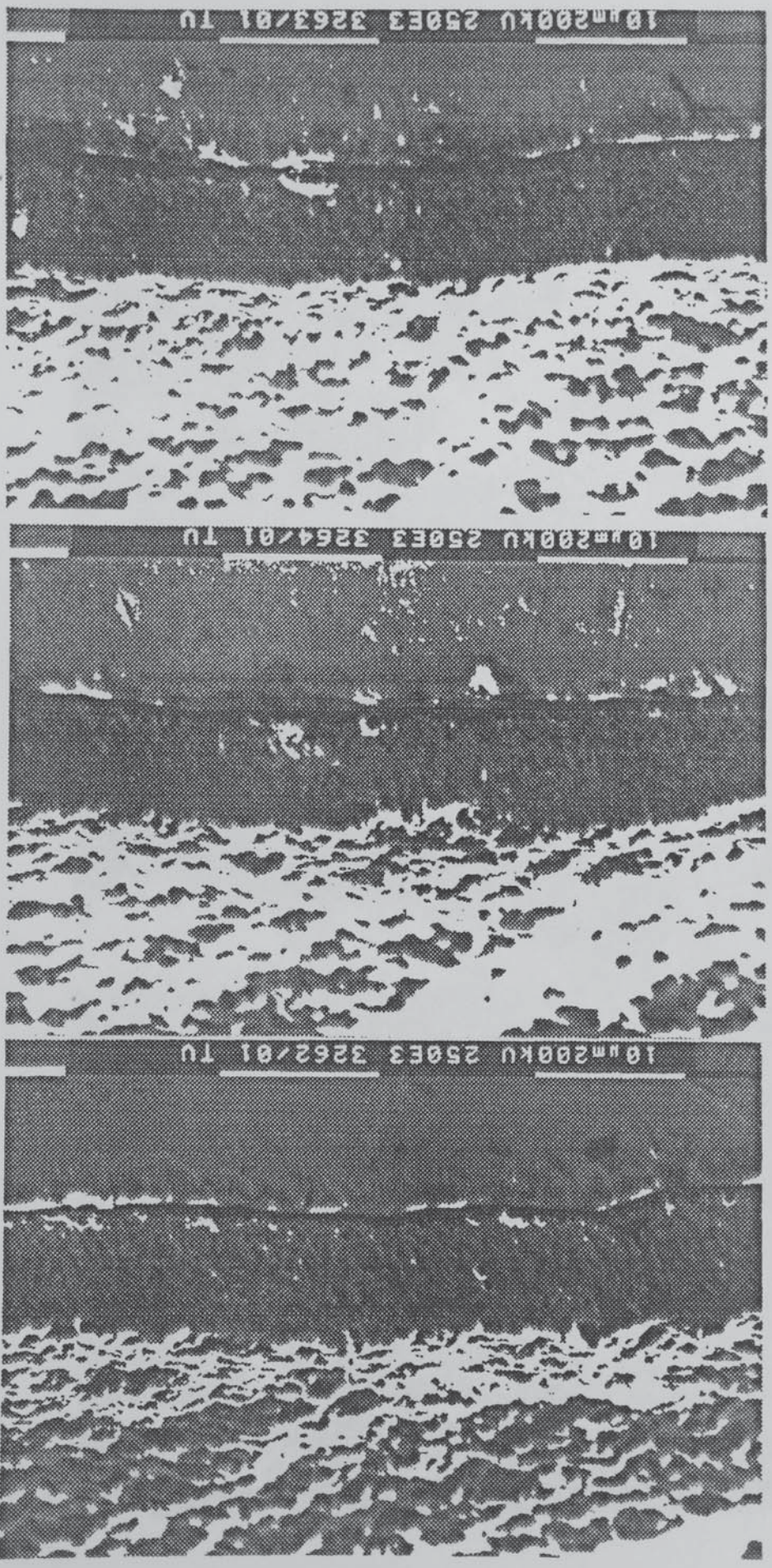

Figure 16. SEM'S of PRC Chromium deposits at $i_a = i_c = 30\ Adm^{-2}$ Q_a/Q_c x 1000 = 4.3

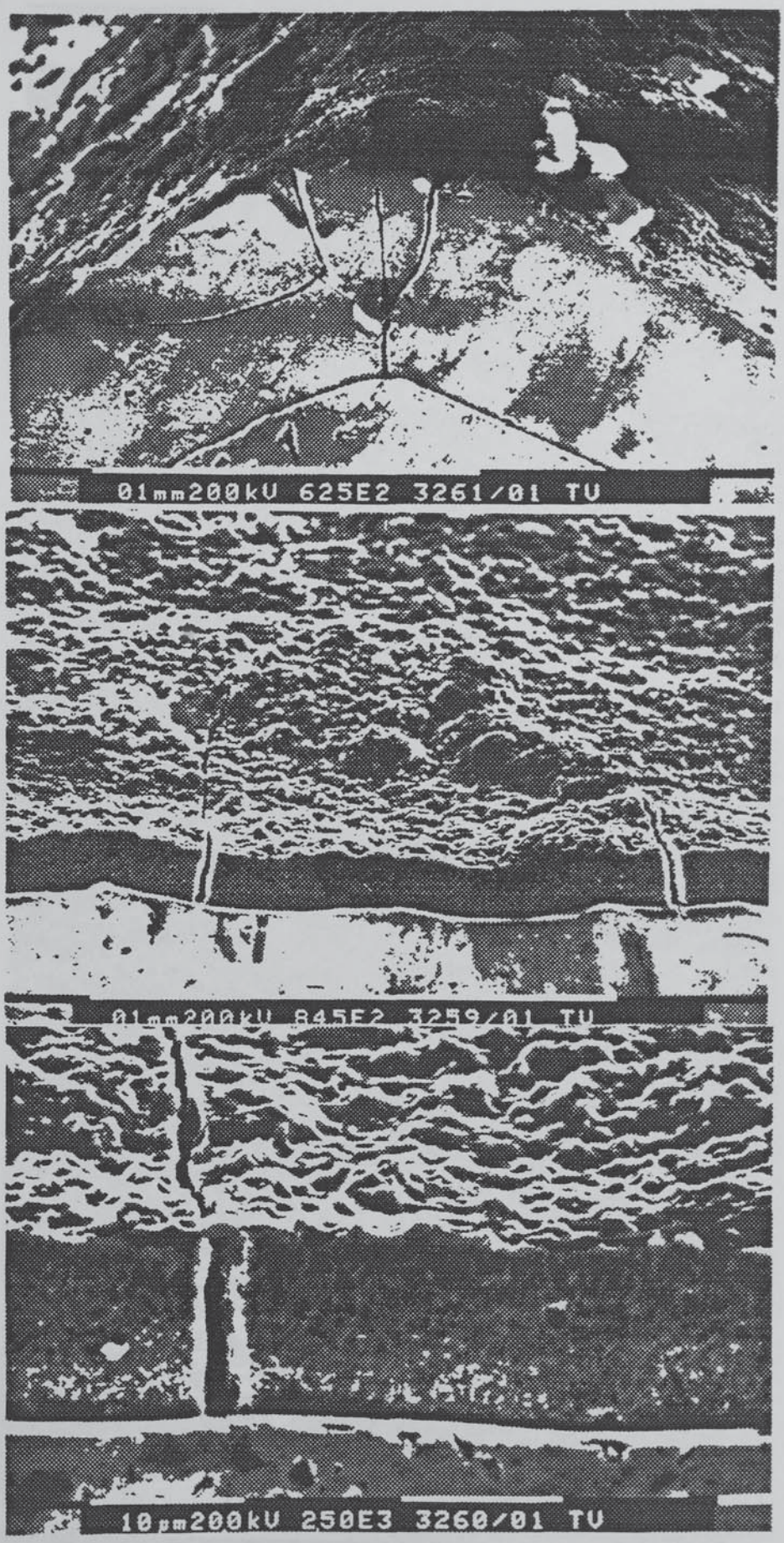

Figure 17. SEM'S of PRC Chromium deposits at $i_a = i_c = 30\ Adm^{-2}$ Q_a/Q_c x 1000 = 0.7

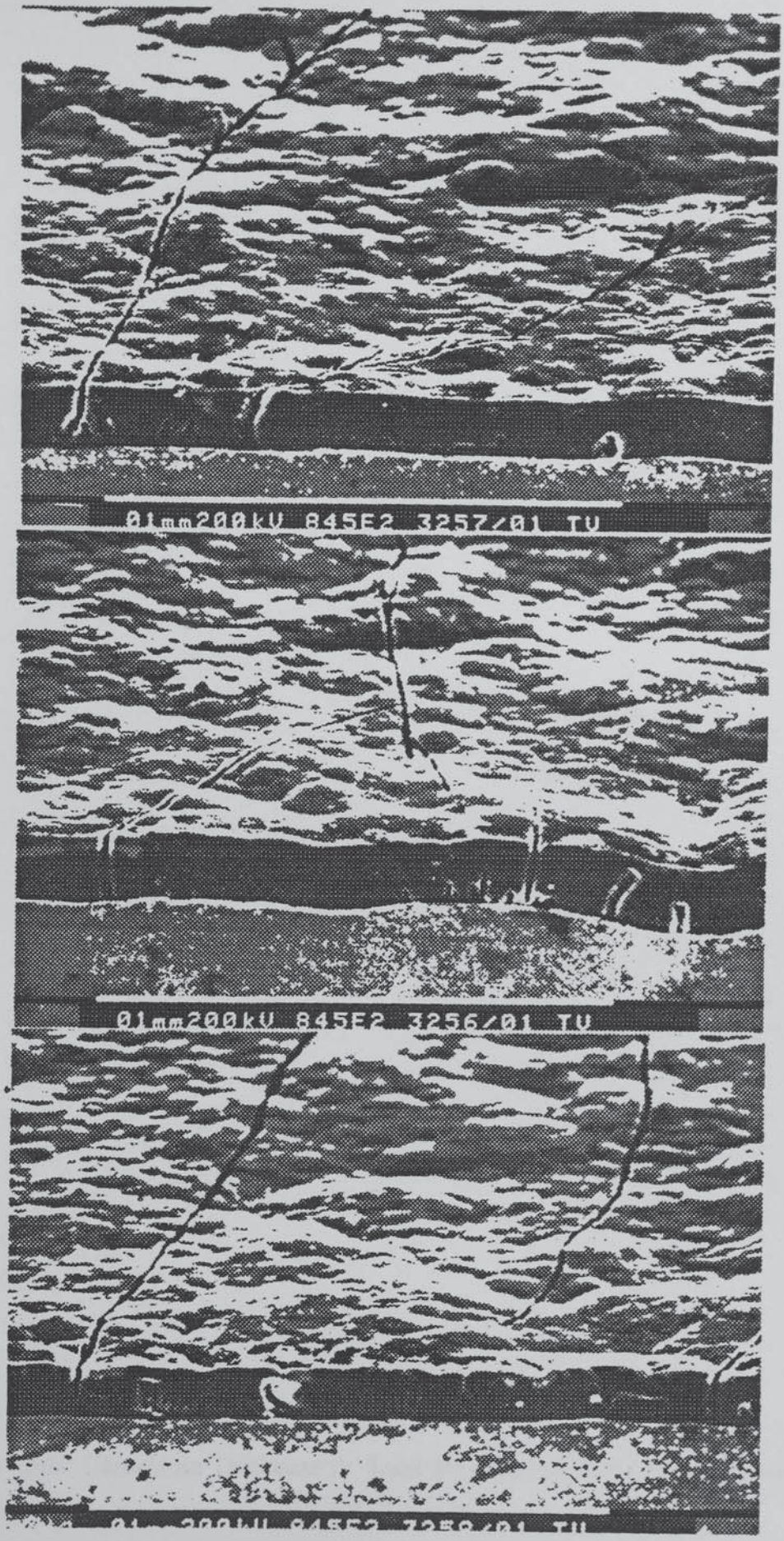

Figure 18. SEM's of DC Chromium Deposits at $i = 30\ Adm^{-2}$ for 3 min.

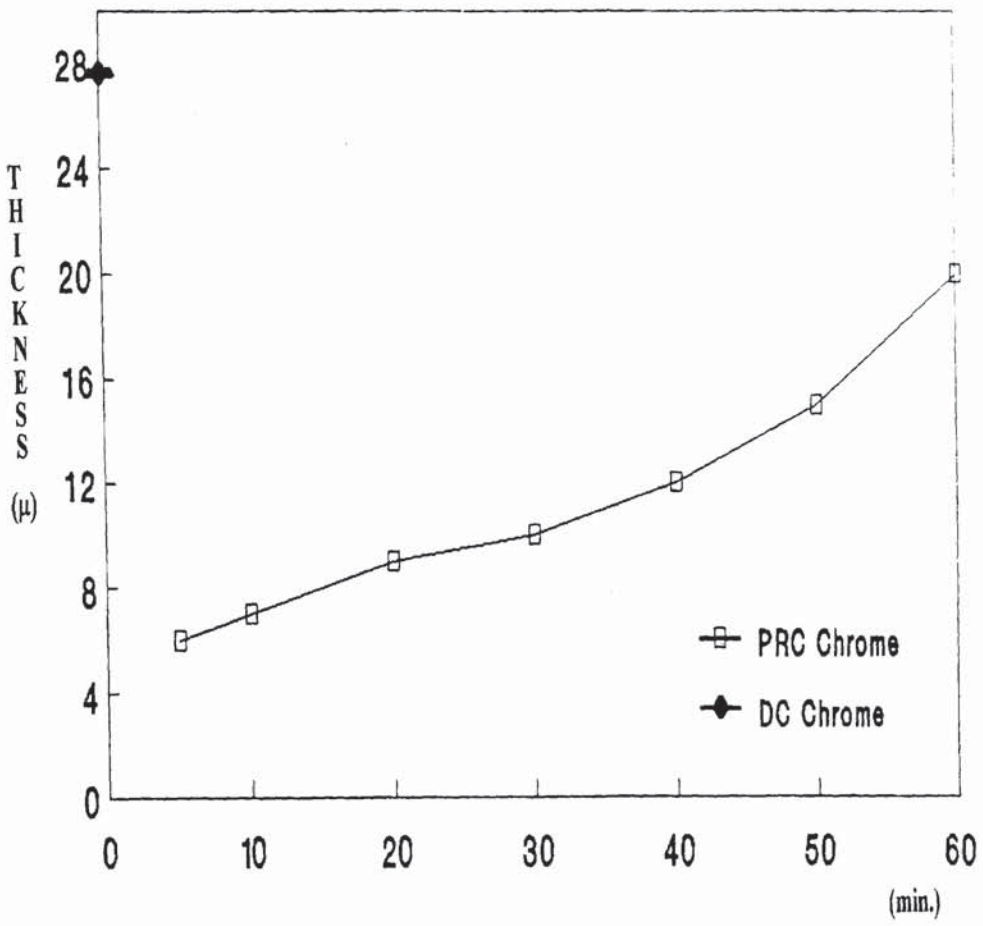

Figure 19. PRC Chromium Thickness vs. Total Deposition Time. $i_c = i_a = 40\ Adm^{-2}$.

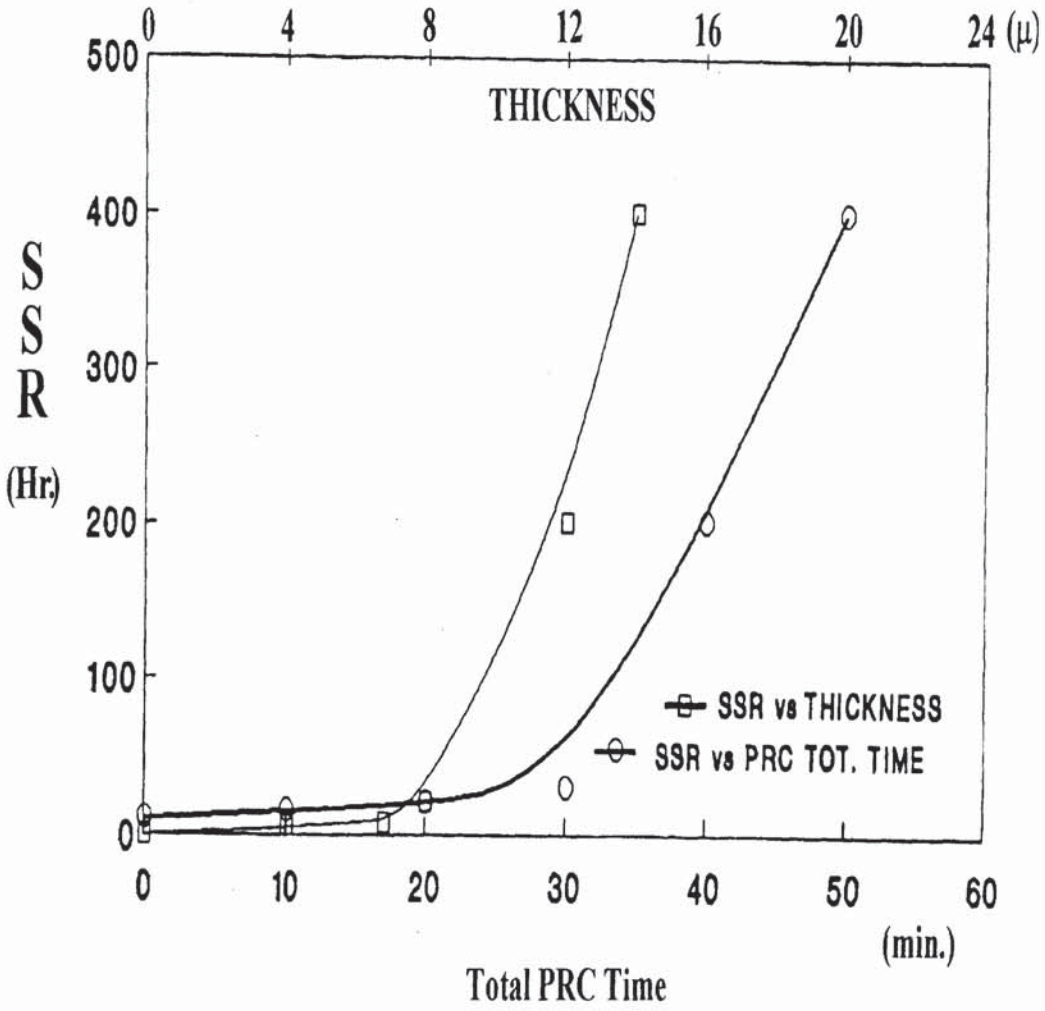

Figure 20. PRC Chromium Salt Spray Resistance (SSR) vs. Time and vs. Thickness. $i_c = i_a = 40\ Adm^{-2}$.

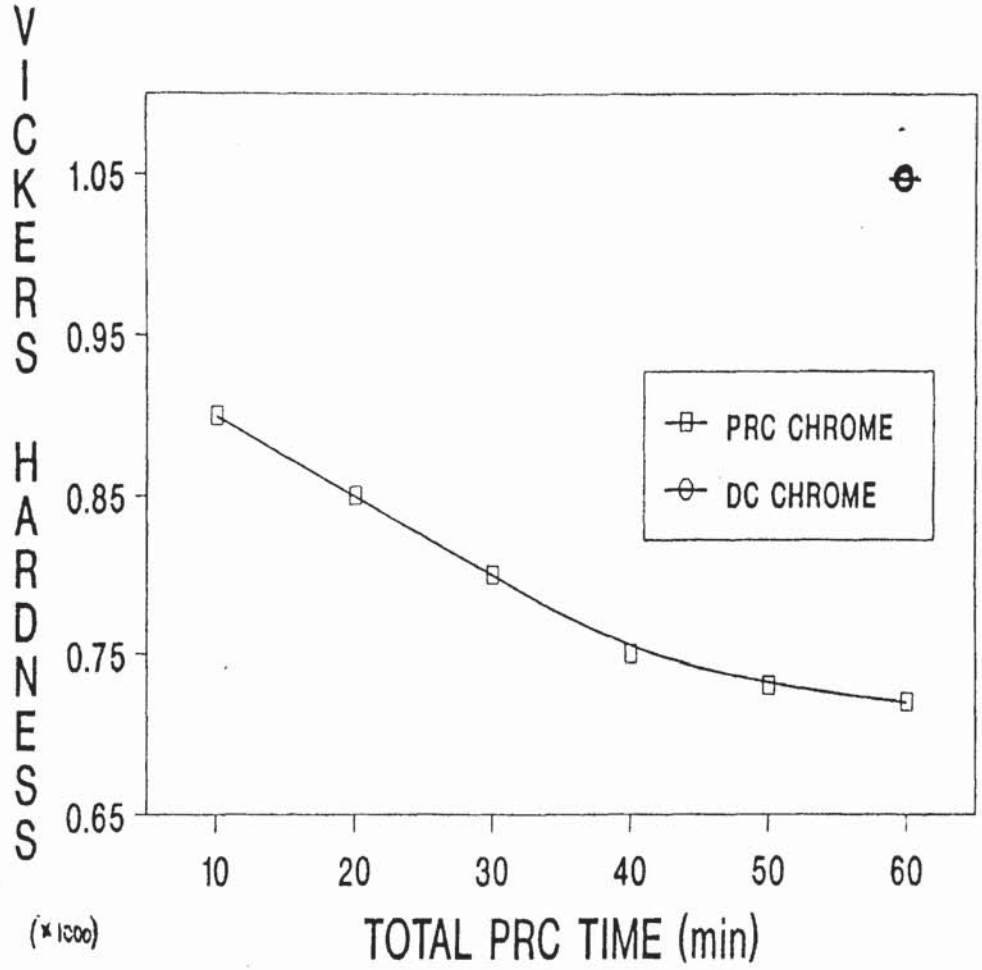

Figure 21. PRC Chromium Hardness vs. Total Deposition Time. $i_c = i_a = 40\ Adm^{-2}$.

II.1.4 Discussion

Plating of chromium under Periodic Reverse Conditions (t_c = 60 sec and t_a = 60 i_c = 40) resulted in dramatic improvement in Salt Spray Corrosion resistance, somewhat but not significantly lower deposition thickness and a 14-28% reduction of hardness, compared to DC plated deposits. Keeping the same cathodic and anodic current densities (4 Adm^{-2}) for $\mathbf{t_a/t_c}$ = 100, it is possible to obtain sound, commercially reproducible chromium deposits from standard Sargent type baths especially when improved corrosion resistance is required. By increasing the $\mathbf{t_a}$ /$\mathbf{t_c}$ ratio and using different cathode and anode current densities it is found that current efficiencies will exceed the DC ones. This will be reported in future chapters, where it will be clearly demonstrated that it is imperative to find optimal ratio of anodic/cathodic coulombic charges to gain higher cathode current efficiencies.

II.2 EXPERIMENTS WITH NANO DIAMONDS

a. Introduction

The possibility of codepositing inert particles from electrolytic baths in order to obtain composite layers of metal matrix containing finely dispersed particles has long been known[165,166] . In more recent years, this technique has received increasing attention in view of the interesting possibilities it offers, for example, the electrodeposition of coatings characterised by desirable properties like wear and abrasion resistance.

Why diamond? The old song may say "Diamonds are a Girl's Best Friend," but considering the uncommon blend of properties, diamonds have a lot to offer everyone:

-- highest hardness
-- highest thermal conductivity
-- low coefficient of thermal expansion
-- low coefficient of friction
-- high chemical inertness

Its hardness suggests an ideal material for coating the objects that are exposed to heavy wear. High thermal conductivity coupled with low coefficient of expansion suggests a material that is resistant to strong thermal shocks. It's hardness and inertness offer a durable material for cutting tools and wear resistant parts like turbine blades. Durability and low coefficient of friction suggest a "lubricating" coating suitable for highly reliable moving parts. Suffice is to say, one can imagine a myriad of applications ranging from the mundane to the most sophisticated that could take advantage of many of diamond's properties. However, they are not as widely used as one would expect. This is mainly because, up until now, synthesis of diamond was expensive. However, recently synthetic diamonds are available from Russia in very fine particle sizes ("nano-diamonds") at affordable prices (about $3,000 /pound), opening new areas for its applications.

Chromium is attractive as a matrix metal in a number of ways, although primarily for its good wear and oxidation properties. However, when depositing from chromium hexavalent baths, electrolyte is a strong oxidant and as a consequence a choice of materials for codeposition is drastically reduced. Also, the low cathodic current efficiency of this bath produces heavy gas evolution at the cathode, which acts as a barrier to particles entry and the presence of the cathodic film has an inhibiting effect, as well as, high electrolyte surface tension. Successful codeposition of hard particles with chromium such as, TiO_2[175-17

SiO_2 [176,177] , B_4C [177,178] , TiC[177], Cr_3C_2,[180] ZrB_2[176], TiB_2[181], WC[181] CeO[183], graphite and diamond with chromium has been claimed by various investigators. Codeposition "stimulators" can reduce the surface tension and /or be adsorbed on the cathode and partial, changing the partial surface charge and adsorbability are recently discussed[184] . Mechanisms involved are not fully understood. Four different models are in existence: by *Saifullin and Khalilova*[185] , *Blazzard and Boden*[186] , *Guglielmi*[187] , *Kariapper and Foster*[188] and *Valdes and Cheh*[189].

Diamonds and diamond-like additives, as mentioned when added to hexavalent chromium bath, offer, in principle, promising results due to their high hardness, low coefficient of friction, high thermal conductivity (about five times that of copper), chemical inertness and high electrical resistance. Nevertheless, the literature on diamonds as additives to chromium plating baths is minimal and sketchy.[170,190-192]

Takaya et al.[190,191] used natural and synthetic diamond products (0.5 micron average partial size). It was possible to obtain chromium deposits containing 0.05-0.11 wt % of diamond particles at a range of 10-40 g/l. Deposits were not as hard as hexavalent chromium films, but wear characteristics were superior. *Berkh*[184] briefly discussed the role of codeposition "stimulators", e.g., $ThSO_4$ in tri and hexavalent chromium baths.

Vashenko et al recently studied[192] electrodeposition of wear-resistant coatings from different chromium plating baths (temperature 55^0 C, 60 Adm^{-2}, containing a dispersion of an ultra-fine diamond (UFD) particles (particle size 50 A). They found that UFD addition into a high-deposition-rate self-regulating chromium plating bath slightly decreases the metal current efficiency, while coating brightness, micro-cracking and microhardness remain unchanged. On the other hand, in a standard chromium bath current efficiency does not depend on the addition of UFD while deposit brightness and microhardness decrease and micro-cracking increases. The quantity of diamond particles included in chromium deposit is very low (~0.01-0.03 wt %) and does not depend on the nature of catalytic ions and solution agitation. Inclusion of UFD in chromium deposit is enhanced by a decrease of CrO_3 concentration (from 250 to 150 g/l) UFD in chromium deposits obtained at 70^0 C is about 50% of those in deposits obtained at 55^0 C. Wear-resistance of chromium deposits obtained from various baths was quite different, but after addition of UFD the deposits wear resistance decreases and becomes similar for all types of baths. Wear reduction of deposits from a sulphate high-speed self-regulating and

diluted (150 g/l) baths containing UFD is respectively ~ 40, 30 and 10%. It does not depend on the UFD content in the deposit. Coating wear reduction is possibly associated with a change in the structure of chromium deposits.

b. Experimental

Panels 9 x 10 cm. Plating area: 0.9 dm^2 = 36 A/panel for 40 Adm^{-2}. Panels were reverse etched for 1 min. at 40 Adm^{-2}.

1. *Bath chemistry: Baths chosen are listed in Table 7.*

Components (g/l)	Sargent bath	Fluoride bath	HEEF-25 bath
CrO_3	240	240	240
H_2SO_4	24	0.5	2.4
K_2SiF_6	--	200-	--
$BaSO_4$	--	6.0	--
HEEF-25	--	--	20.0

Table 7: *Bath formulations for nano-diamond experiments.*

Two types of nano-diamonds (15g/l) were used in the experiments: (1) Dupont Co. and (2) Straus Chemical Corporation (SCC)

2. *Experimental Conditions:*

A. The chromium coating was performed on the cleaned and pretreated steel panels with the surface area of 4" x 4".
B. Operating coating bath temperatures (a) 50^0 C and (b) 60^0 C.
C. Current density 40 ADS.
D. Anodes: lead /tin (7%); anode/Cathode area ratio 2/1.
E. Plating thickness 25-40 microns
F. Agitation: thorough agitation for 30 seconds before plating and interrupted mechanical agitation for 10 seconds after each 10 minutes.

3. *Taber Abrasion Testing Procedure*

The Taber abrasion testing was performed on the Standard Taber Abrasion Tester (Federal Test Standard 141, Method 6192) with the load of 1 Kg and using abrasive wheels Calibrase CS-10. First 1000 revolutions were applied on each panel to clean and unify the surface before measuring the abrasion resistance. The abrasion resistance was evaluated by the weight loss of the coating after each 3000 revolutions. Then the Calibrase wheels were completely cleaned by the special Abraser Refacing Discs and the next 3000 cycles were applied. The total number of measured cycles was 6000 (excluding the first 1000 cycles)

The results of the Taber Abrasion Wear Index (average weight loss in milligrams per 1000 cycles) are presented in Table 8.

BATH TYPE	RESULTS @ 50°C					RESULTS @ 60°C				
	Panel no.	Loss wt.	CDE (%)	Time (min)	Thick (m)	Panel no.	Loss wt.	CDE (%)	Time (min)	Thick. (m)
SARGENT										
(a) without nano-diamonds	[26]	1.65	16.9	60	32.7	[25]	1.47	16.2	60	29.0
(b) with SCC nano-diamonds	[24]	1.28	18.2	60	--	[23]	138	14.7	60	---
(c) with DuPont nano-diamonds	[31]	1.61	15.14	60	30.8	[30]	1.63	14.9	60	28.7
FLUORIDE										
(e) without nano-diamonds	[34]	1.52	*	50	27.5	[33]	1.65	*	50	27.0
(f) with SCC nano-diamonds	[39]	1.00	*	50	--	[38]	1.05	*	50	--
(g) with DuPont nano-diamonds	[37]	0.83	*	57	--	[36]	1.35	*	50	--
HEEF-25										
(i) without nano-diamonds	[21]	0.83	22.5	60	--	[22]	1.10	21.0	60	--
(j) with SCC nano-diamonds	[27]	0.95	19.6	60	47.2	[20]	0.85	21.6	60	--
(k) with DuPont nano-diamonds	[29]	1.04	21.6	60	43.7	[28]	0.83	20.2	60	38.2

Table 8: Wear loss results for Nano-diamond experiments

Wear-loss experimental results indicated a few interesting findings.

a). With the exception of experiments resulting in panel no. [25], Sargent Bath and fluoride baths with and without diamonds and HEEF-25 without diamonds had more weight loss at higher temperatures, which is in accord with results in plating practice. Diamond additions decreased the weight loss.

b). HEEF-25 bath showed much higher wear resistance compared with the other two baths. At the lower temperature, diamond additions decreased wear resistance, but reversed at the higher temperature, indicating unique behaviour of this bath with respect to temperature.

c). Cathode current efficiency measurements did not reveal any appreciable influence of diamond additions.

d). The difficulties for diamonds to enter the cathode film are due to vigorous hydrogen generation during chromium deposition. This is the probable cause for not having a more significant decrease in wear.

II.3 DEVELOPMENT OF HIGH EFFICIENCY CATALYST

II.3.1 **Introduction:**

As a part of this research program, development work was done in order to obtain a catalyst that will exceed cathode current efficiency (CEE) and possibly throwing power of customary sulphate ion catalyst in applied electroplating practice. Due to the enormous usage and consumption of chromium and its chronic low CEE, any single percent of CEE increase translates directly into billions of KWA saved. Also ecologically important is the reduction of chromium mist generated by hydrogen bubbles as a by-product of low efficiency and usually exhausted into the atmosphere. In the U.S.A., savings in chromium are of particular importance because it is 100% imported from Russia, China and South Africa. Both inorganic and organic catalyst systems are investigated. Criteria used in choosing the catalyst system are based on the premise that compounds used for trials should be "non-exotic" or, in other words, relatively easily available and inexpensive, while keeping in mind that the ultimate goal is to identify industrially usable catalyst with at least 20% efficiency. Other significant characteristics considered are stability, ease of controlling the concentration, as well as toxicity.

The commercial, high-efficiency catalysts HEEF-25 and HEEF-405 (Autotec Co, Somerset, N.J.,USA) are investigated for comparison purposes. It is accepted in chromium plating circles that HEEF-25 is, at the present time, the most efficient catalyst for plating over steel, claimed by its manufacturer to produce CEE's in the 25% range; HEEF-405 produces CEE's in the 40% range for plating over aluminium but has serious adhesion problems when plating over steel. The experimental set-up and procedure is detailed in Chapters 1 and 2 of Section One, Part Two. A number of experimental setups, racks, anodes, etc., have been tried; proposed setup is suggested as close to an optimal one.

All catalytic systems under investigation started with Sargent bath as the base solution. Its sulphate content can be considered the "primary catalyst". "Secondary catalysts" as a term is used for any additional catalyst(s) added into the Sargent bath.

II.3.2 CATHODE CURRENT EFFICIENCY OF SARGENT BATH. DC

a. Introduction

In order to have a meaningful comparison of Cathode Current Efficiencies (CCE's) of the Catalysts under investigation and to eliminate the influence of the measuring method, rather than using the published data, a set of experiments were performed to obtain the CCE's of Sargent Bath catalyzed with sulphates at 100:1 ratio.

b. Experimental Details

Solution: 240 g/l Chromic Acid + 2.4 g/l Sulphuric Acid; 100:1 ratio.

Make up for 6 litre solution: 1440 g CrO_3 + 33 ml 30 Be H_2SO_4 (35%, d =1,260)

Plating area of the panels = $3^{11}/_{32}$ x 4 = 10 in^2 (85 x 78mm aprox. 0.7 dm^2).
Current density range explored: 14-70 Amps per panel; 7 Amps per panel represents 10 Adm^{-2}, 14 Amps per panel = 20 Adm^{-2}, etc.

Cathode Current Efficiencies (CCE's) were calculated from Faraday's Law:

$$CCE = \frac{m}{\frac{ItM}{96.500z}} = \frac{m}{\frac{It52.01}{96.500 \bullet 6}} = \frac{m}{It}\ 0.3234 \qquad <110>$$

where **I** is *applied current* in Amps, **t** is *time* of *electrolysis* in hours, **z** *is number of electrons* for Chromium reduction (6) , **m** *is deposited mass* (gr), **M** *is molecular mass of chromium* (52.01 g/mol.), **96.500** is *Faraday's Constant* (Coulumbs/mol) and **0.3234 (g/A hr)** is *Electrochemical Equivalent*, for Cr^0 -6e $\rightarrow$ Cr^{+6} reduction reaction.

Cathode Current Efficiency results are presented in Table 9. These results are represented in Figures 22 and 23, plotted together with results from later experiments for the Sargent Bath with HEEF-25, MSA (1%) and MSA (2%) as a secondary catalysts.

b. Experimental results

Table 9. summarizes data generated from Cathode CE determinations for chromium deposition from Sargent Bath for eight currrent densities. Method used is weight gain determination for different CD's at constant temperature (Anodic etch time = 17 A min.).

Exp. no.	Temp. ^0F / ^0C	i_c Adm^{-2}	i_a Adm^{-2}	t_a ms	t_c min	Dep. Wt.. g/h	Q_a / Q_c x 1000	CCE %	Note:
74	130 / 55	10	0	0	60	0.191	0	8.4	
75	130 / 55	10	0	0	60	0.188	0	8.3	Repete # 74
76	130 / 55	20	0	0	60	0.622	0	13.7	
78	130 / 55	30	0	0	60	1.020	0	15.0	
80	126 / 52	40	0	0	60	1.535	0	16.9	
82	129 / 54	50	0	0	60	1.829	0	16.1	
83	131 / 55	60	0	0	60	2.104	0	15.5	
84	131 / 55	70	0	0	60	2.278	0	14.3	
85	128 / 53	35	0	0	60	1.297	0	16.4	

Table 9. Cathode CE of Sargent Bath, 240 g/l. 100:1 DC. t_c = 60 Min;

b. Discussion:

Figure 22 shows, as expected, non-linear relationship of CD vs. cathode weight gain expressed as CCE's at given temperature. When plotted at semi-logarithmic scale as CCE vs. CD, (Figure 23) a straight line is obtained, and can be presented with the following general expression:

$$E = a \log D + b \qquad <111>$$

Where **a** and **b** are constants for a given temperature. **a** is the slope and **b** is the intercept. This is reducible to the form:

$$\mathbf{D^a = A \bullet 10^E} \qquad <112>$$

At 55^0 C (130^0 F), for example, for solution from Table 9 the slope can be read from the Fig. 166 and is as follows:

$$\mathbf{a} = \frac{16.95 \quad -8.8}{\log \quad 400 - \log 100} = 13.53 \qquad <113>$$

A is a constant, which proves to be $1.8 \cdot 10^{18}$ when **D** is expressed in ASF, and the expression simplifies to:

$$\mathbf{D^{13.53}} = 1.8 \bullet 10^{(1.8+E)} \qquad <114>$$

If desired, the slope of this line **a**, can be plotted against temperature and the resulting expression will give, for a fixed bath composition, the relationship between the variables: CD, CCE and temperature.

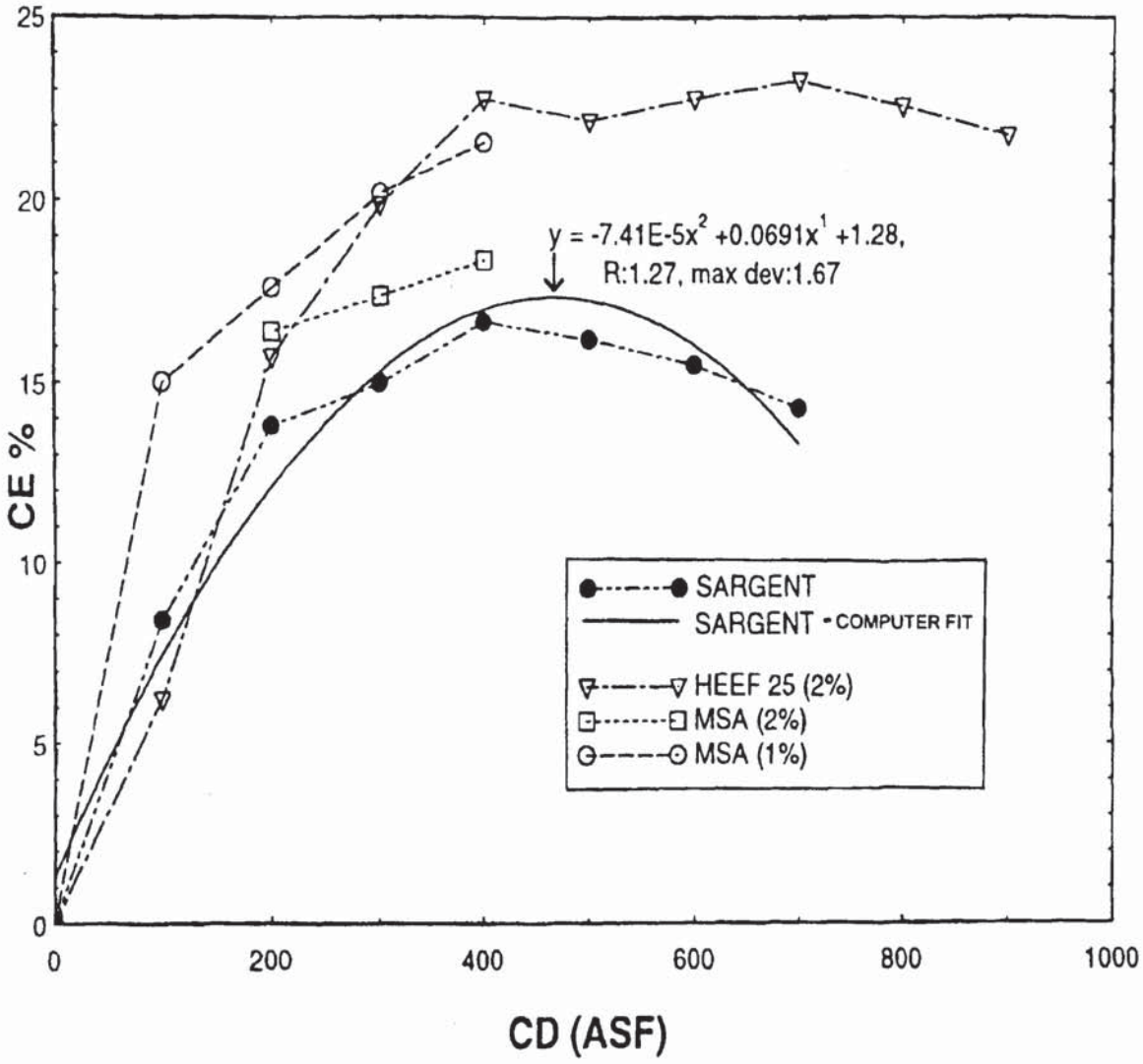

Figure 22. CE vs. CD for SB, HEEF-25, MSA (1%) and MSA(2%) Bath.

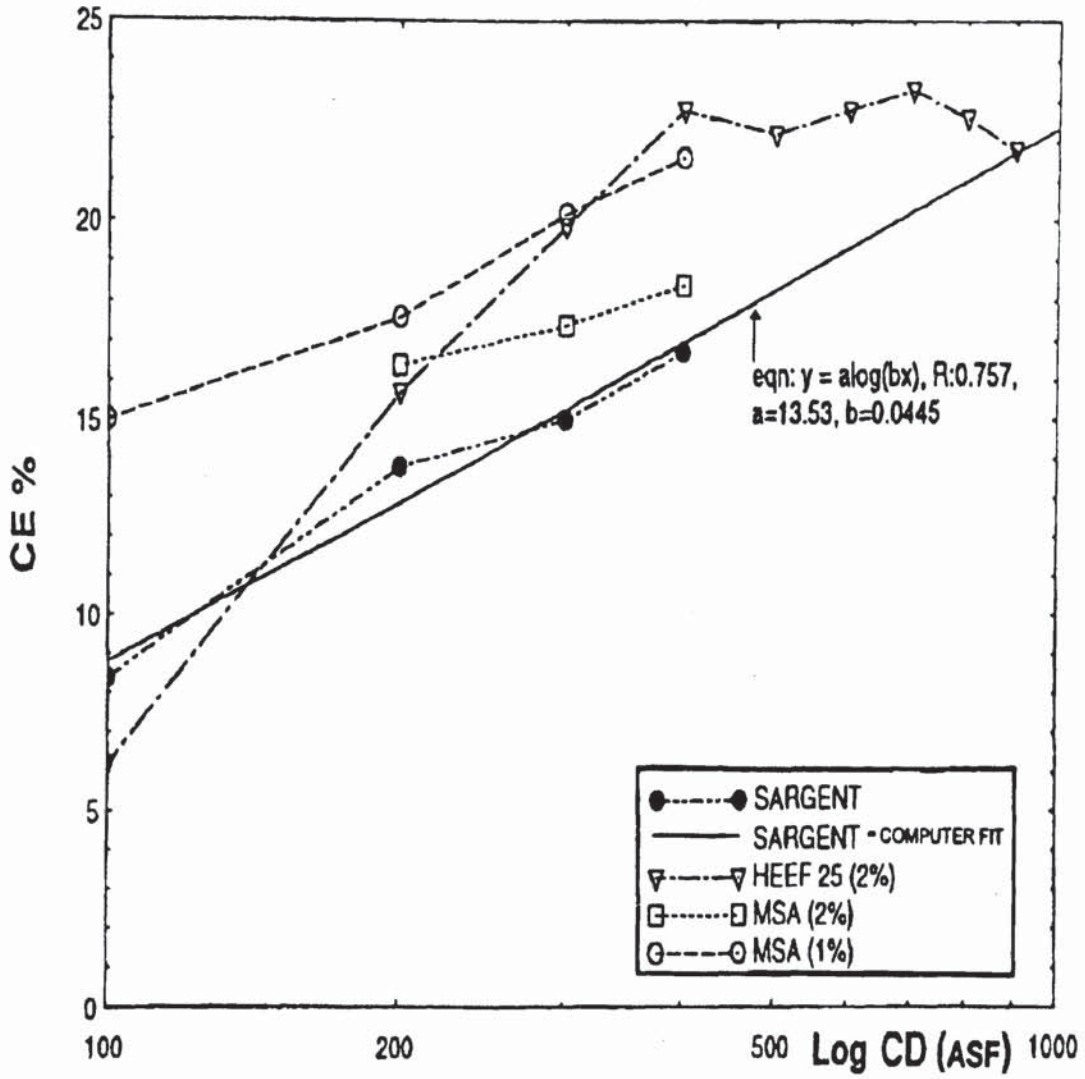

Figure 23. Figure 22 in semi-log scale.

II.3.3 PRC DEPOSITION AT CONSTANT i_a / i_c = 15% and 39% ratios.

a. Introduction:

Colombini[115,117] introduced the concept that in order to obtain sound and efficient PRC Chromium deposits from Sargent Bath anodic current density ($\mathbf{i_a}$) should be a fraction of cathodic current density ($\mathbf{i_c}$) and that ratio, $\mathbf{i_a / i_c}$ should be constant and within 15-40% range. In order to verify this, the following experiments were carried out:

b. Experimental Details

Solution: 240 g/l Sargent Bath 100:1 i_c = 40 Adm^{-2}, i_a = 6 Adm^{-2} Temperature : 53^0 C (118^0 F); Rev. etch. = 14 A min. Total deposition time 1 hr.

c. i_a = 15% i_c :

i_c = 40 Adm^{-2}, i_a = 6 Adm^{-2}, t_c = 15sec.; t_a = 0.1 - 1.1 sec.

Exp. no.	Temp. ^{0}F / ^{0}C	i_c Adm^{-2}	i_a Adm^{-2}	t_a s	t_c s	Dep. Wt g/h	Q_a / Q_c x 1000	CCE %	Note:
305	128 / 53	40	0	0	60 x 60	1.111	0	12.3	DC
306	128 / 53	40	6	0.1	15	1.884	2	20.8	PRC
307	128 / 53	40	6	0.2	15	1.761	1	19.4	PRC
309	128 / 53	40	6	0.3	15	1.784	3	20.4	PRC
310	127 / 53	40	6	0.4	15	1.891	4	20.9	PRC
311	128 / 53	40	6	0.5	15	1.907	5	21.1	PRC
312	126 / 52	40	6	0.6	15	1.961	6	21.6	PRC
313	126 / 52	40	6	0.6	15	1.888	6	20.9	PRC
314	126 / 52	40	6	0.7	15	1.894	7	20.9	PRC
315	126 / 52	40	6	0.8	15	1.876	8	20.7	PRC
316	126 / 52	40	6	0.9	15	1.894	9	20.9	PRC
317-a	126 / 52	40	6	1.0	15	1.886	10	20.6	PRC
318	126 / 52	40	6	1.1	15	1.873	11	20.9	PRC
319	126 / 52	40	6	0.5	15	1.898	5	21.0	Repeat # 311

Table 10: PRC deposition at i_a = 0.15 i_c ratio.Sargent Bath; 100:1 ratio.

d. $i_a = 39\%\ i_c$; $i_a = 15.6\ Adm^{-2}$, $i_c = 40\ Adm^{-2}$, $t_a = 0.1\text{-}0.6s$; $t_c = 15s$.

Exp. no.	Temp. ^0F / ^0C	i_c Adm^{-2}	i_a Adm^{-2}	t_a s	t_c s	Dep. Wt.. g/h	Q_a / Q_c x 1000	CCE %	Note:
365	128 / 53	40	15.6	0.0	51 x 60	1.650	0.0	18.2	DC
367	128 / 53	40	15.6	0.0	16 x 60	1.713	0.0	18.9	DC
366	128 / 53	40	15.6	0.1	15	2.335	2.6	25.1	PRC
368	128 / 53	40	15.6	0.2	15	2.298	5.2	24.2	PRC
369	**128 / 53**	**40**	**15.6**	**0.3**	**15**	**2.172**	**7.8**	**24.0**	**PRC**
370	128 / 53	40	15.6	0.4	15	2.183	10.4	24.0	PRC
372	128 / 53	40	15.6	0.5	15	1.991	13.0	22.0	PRC
373	128 / 53	40	15.6	0.6	15	1.884	15.6	20.8	PRC

Table 11: PRC deposition at $i_a = 0.39\ i_c$ Sargent Bath; 100:1.

Discussion:

It is obvious from the Tables 10 and 11 that with proper i_a/i_c ratio and with the appropriate t_a it is possible to increase CCE of Sargent type bath in magnitude of approx. 30-40%, compared to DC, as long as Q_a / Q_c x 1000 is between 3-6. Deposits are grey, but they can be polished bright and they are crack-free, indicating increased corrosion resistance.

II.3.4 SECONDARY CATALYST: Methane Sulphonic Acid - MSA

a. Introduction:

Survey of patent literature[103,194] revealed that *Atotech - USA* patented secondary catalyst- probably in combination with additional additive(s) is Alkane sulfonic acid,e.g. Methane Sulphonic Acid (MSA). For initial cathode current efficiency (CCE) trials, technical grade (70%) solution from Aldrich Co. is used.

b. Experimental Details

c. MSA (tech) 1%, 100:1; DC:

14.4g/6ℓ of MSA as 100% or 20.57 gr as 70%; CrO_3 = 240 g/ℓ;100:1

Reverse etch = 7 A-min.

CCE results are converted from g/h to 0.001 in/hr (mls/hr) and microns/ hour according to the following calculation: (example-experiment no. 87; 10 in ^{2} panel.):

0.366 gr/10 in^2 h = 3.66 gr/in^2 h • 0.155 in/cm = 5.673 g/cm h

$$\frac{5.673\ g/cm \bullet h}{7.19\ g/cm} = 0.789 cm/h = 7.89\ mm/h \bullet 0.0394\ in/mm = 0.00031\ in/h = 0.31 \text{ mil/h}$$

0.31 mil/hr •25μ/mil= 7.7μ/hr.

Exp. no.	Temp. ^0F / ^0C	i_c Adm^{-2}	i_a Adm^{-2}	t_a ms	t_c min	Dep. Wt. g/h	Q_a / Q_c x 1000	CCE %	Note:
87	127 / 53	12.8	-	-	60	0.366	0	12.5	7.7 μ/h
88	130 / 54	20.0	-	-	60	0.668	0	15.2	14.5 μ/h
89	129 / 54	30.0	-	-	60	1.212	0	17.8	25 μ/h
90	129 / 54	40.0	-	-	60	1.835	0	20.2	39 μ/h
91	130 / 54	50.0	-	-	60	2.444	0	21.6	52.5 μ/h

Table 12: Cathode Current Efficiency; MSA (tech) = 1%; 240 g/ℓ CrO_3; 100:1 DC.

d. MSA (tech.) = 2%; 100:1, DC.
Additional 21 cc of MSA(t) added (42 ml/l total).

Exp. no.	Temp. ^0F / ^0C	i_c Adm^{-2}	i_a Adm^{-2}	t_a s	t_c s	Dep. Wt.. g/h	Q_a / Q_c x 1000	CCE %	Note:
93	132 / 55	20	-	-	60	0.741	-	16.3	0.63 mil/h
92	130 / 54	20	-	-	60	0.724	-	16.0	0.61 mil/h
94	131 / 55	30	-	-	60	1.317	-	19.4	1.12 mil/h
96	135 / 57	40	-	-	60	1.754	-	19.3	temp. high
97	130 / 54	40	-	-	60	1.758	-	19.4	1.50 mil/h

Table 13: Cathode Current Efficiency, 240 g/l CrO_3; MSA(t) = 2%, 100:1 DC.

e. MSA (tech.) = 3%

Experiments with 3% concentration of MSA (tech.) produced very low CCE's (6.0-8.9%) Current Density ranges from 10-60 Adm^{-2} with brown smut at the surface, indicating overcatalyzation.

f. 3% MSA(t) + 7g/l H_3BO_3 in 240 g/l Chromic Acid bath , 100:1 ratio, PRC.

Following patent claims[195] and literature data[196.196-a] that boric acid has beneficial effects and some catalyst properties for chromium deposition, 7 g/l of boric acid is added to the previous bath. DC and Periodic Reverse Current modes were explored.

Exp. no.	Temp. ^0F / ^0C	i_c Adm^{-2}	i_a Adm^{-2}	t_a s	t_c s	Dep.Wt. g/h	Q_a / Q_c x 1000 1	CCE %	Note:
108	128 / 53	60	-	-	60x 60	0.754	-	5.50	DC
109	128 / 53	60	-	.2	60	0.970	11	7.14	PRC
110	128 / 51	60	20	.3	60	1.073	3	7.90	PRC
111	128 / 53	60	20	3	66	0.783	23	-	Peal
112	128 / 53	60	30	3	33	1.073	45	7.90	
113	128 / 52	60	10	2	99	0.658	33	-	Peal
115	128 / 53	60	20	9	60	0.613	5	4.50	

Table 14. Cathode Current Efficiency: 240 g/l CrO_3; MSA (t) 3%; H_3BO_3 = 7 g/l. PRC.

Addition of 6 g/l boric acid to 3% MSA solution did not add significant benefits, either in DC or PRC mode, indicating that the bath is still over-catalyzed. However. it was further explored for MSA (tech.) = 1 and 2% concentrations.

g. 3% MSA(tech.) + 6g/l H_3BO_3 in 360g/l Chromic Acid bath; 150:1 ratio. PRC

Assuming that over-catalyzation at least partially contributed to high sulfate effective catalyst ratio, CrO_3 concentration is raised to 360g/l (730 g/l added) and ratio increased to 150:1. PRC mode is explored.

Exp. no.	Temp. ^0F / ^0C	i_c Adm^{-2}	i_a Adm^{-2}	t_a s	t_c s	Dep. Wt g/h	Q_a / Q_c x 1000	CCE %	Note:
117	130 / 54	30	10.0	9	60	0.433	50	6.5	
118	128 / 53	60	10.0	2	90	2.000	3.7	12.9	
121	128 / 53	40	10.0	2	90	1.994	5..5	17.6	Bright
122	128 / 53	50	10.0	2	90	1.462	4.4	12.9	Peel
123	128 / 53	50	12.5	2	90	-	5.5	-	Missing
124	128 / 53	50	12.5	2	90	-	55	-	Missing

Table 15: 3% MSA(t) + 6g/l Boric Acid; 360 g/ℓ CrO_3 ;150:1 ratio, PRC.

Increasing the ratio to (150:1) via increased concentration of chromic acid, reduced overcatalyzation and, if the Q_a/Q_c ratio is correct, can result in higher CCE's at high current densities. However, the results are not conclusive enough at this point; as the Q_a/Q_c ratio is changed from 5.0, 3.7, to 5.5, CCE's are increased from 6.5%, 12.9% to 17.6%, indicating the importance of Q_a/Q_c (charge ratio), but at the same charge ratio (5.5) for longer t_a, plating produced only partial chromium deposit on the panels indicating overcatalyzation, and the importance of proper anodic charge.

h. 3% MSA (t) in 320 g/l Chromic Acid bath, 200:1 ratio, PRC.

The ratio is further increased to 200:1. New solution is used, consisting of 320 g/l CrO_3 (or 1840 g/5.75ℓ) + 9.2 g H_2SO_4 (5cc); MSA = 3% [1840 x 0.03 = 55.2 g = 79g (70%) = 60cc (d= 1.3)]

Exp. no.	Temp. ^0F / ^0C	i_c Adm^{-2}	i_a Adm^{-2}	t_a s	t_c s	Dep. Wt g/h	Q_a / Q_c x 1000	CCE %	Note:
128	125 / 52	50	12.5	2	90	2.060	5.7	18.2	
129	125 / 52	50	12.5	2	90	1.995	5.7	17.6	
131	128 / 53	60	12.8	2	90	2.356	3.7	17.3	
139	128 / 53	60	12.8	2	90	2.003	3.7	14.7	
136	126 / 52	60	12.6	2	90	1.499	3.7	11.0	Bright
138	126 / 52	50	12.6	2	90	1.906	5.7	16.8	Bright
139	129 / 54	50	12.9	2	90	1.680	4.4	14.0	Bright

Table 16: Experimental results. 3% MSA (t), 320 g/ℓ CrO_3 200:1 ratio; PRC.

Reduction of the amount of the sulfate catalyst (200:1), in PRC mode resulted in the increase in CCE's, indicating that the previous baths with 100:1 and 150:1 ratios were overcatalysed in regard to sulfate. Also, CCE's were constantly higher at Q_a / Q_c ratio of 5.7. It is important to note that Periodic Reverse mode consistently had higher CCE's compared with DC and with proper Q_a / Q_c ratio will also result in bright deposits.

i. 3% MSA (t) in 360 g/l Chromic Acid bath 300:1, DC

Exp. no.	Temp. ^0F / ^0C	i_c Adm^{-2}	i_a Adm^{-2}	t_a ms	t_c m	Dep. Wt g/h	Q_a / Q_c x 1000	CCE %	Note:
133	126 / 52	60	-	-	60	1.222	-	9.0	Brown Smut
135	126 / 52	60	-	-	60	1.518	-	11.2	Bright
137	126 / 52	60	-	-	60	1.639	-	12.0	Bright
104	126 / 52	50			60	0.800		7.4	100:1

Table 17: 3% MSA (t) 360 g/l; 300:1 DC.

Reduction of the amount of the sulphate catalyst to 300:1 ratio in DC mode did somewhat increase CCE (see Experiment No.104 for 100:1 ratio) but it is still lower than in solutions with lower concentrations of MSA, indicating an upper level of MSA concentration.

j. Subsequent experiments with 4% MSA (t) at 200:1 ratio and $Q_a / Q_c = 0.0057$ resulted in rough, burned or pealed deposits in PRC or DC modes, indicating *overcatalysations* by MSA and resulting in low CCE's (9-12%).

II.3.5 HEEF-25 (2%) and HEEF-405 as SECONDARY CATALYSTS

a. HEEF-25 (2%), 240 g/ℓ CrO_3 100:1; DC

Bath Composition:

240 g/ℓ CrO_3 (1440 g/6 l) + 2.4 g/l H_2SO_4 (7.8 ml/6 l) + 2% HEEF-25 (120 cc/6 l)

Exp. no.	Temp. ^0F / ^0C	i_c Adm^{-2}	i_a Adm^{-2}	t_a ms	t_c min	Dep. Wt.. g/h	Q_a / Q_c x 1000	CCE %	Note:
177	128 / 53	90	-	-	60	4.450	0	21.8	
176	128 / 53	80	-	-	60	4.101	0	22.6	
175	128 / 53	70	-	-	60	3.703	0	23.3	
162	122 / 50	60	-	-	60	3.100	0	22.8	
163	125 / 52	50	-	-	60	2.520	0	22.0	
164	125 / 52	40	-	-	60	2.066	0	22.8	
165	125 / 52	40	-	-	60	2.201	0	22.0	
167	128 / 53	45	-	-	60	1.872	0	20.6	
168	128 / 53	40	-	-	60	1.357	0	19.9	
169	128 / 53	30	-	-	60	0.980	0	17.8	
172	128 / 53	25	-	-	60	0.961	0	17.5	
170	128 / 53	20	-	-	60	0.713	0	15.7	
173	128 / 53	15	-	-	60	0.364	0	12.2	
174	128 / 53	10	-	-	60	0.140	0	6.2	

Table 18: HEEF-25 (2%); 240 g/ℓ CrO_3; 100:1, DC.

b. HEEF-25 (1%) in actual (used) production plating solution; 240 g/ℓ CrO_3; 100:1

Rather than using freshly made chromic acid plating solution, actual solution, taken from production bath is used in order to investigate influence of hard chrome plating bath impurities on Cathode Current Efficiency.

Bath composition:

240 g/l CrO_3 ; 98:1 ratio. Impurities: Cr^{3+} = 1.2% ; Fe + Cu = 9000 ppm.

Exp. no.	Temp. ^0F / ^0C	i_c Adm^{-2}	i_a Adm^{-2}	t_a s	t_c min	Dep. Wt. g/h	Q_a / Q_c x 1000	CCE %	Note:
269	127 / 53	40	-	-	60	1.458	0	16.1	as is
270	125 / 52	30	-	-	90	0.800	0	11.8	as is
271	125 / 52	20	-	-	46	0.502	0	11.5	as is
272	125 / 52	30	-	-	60	1.121	0	16.5	1% HEEF-25
273	125 / 52	20	-	-	60	0.580	0	12.8	1% HEEF-25
274	126 / 52	20	-	-	60	0.771	0	17.0	2 % HEEF-25
275	126 / 52	30	-	-	50	.0904	0	12.0	2% HEEF-25
276	128 / 53	40	-	-	60	1.542	0	17.0	2% HEEF-25
279	124 / 51	20	-	-	60	0.653	0	14.4	2% HEEF-25
280	126 / 52	30	-	-	60	1.174	0	17.3	3% HEEF-25

Table 19: HEEF-25 (1%) in the production (used) solution 240 g/ℓ CrO_3; 100:1. DC.

c. HEEF-405 (2%) 240 g/l of CrO_3; DC, PC and PRC modes.

New Solution; 240 g/l of CrO_3; 100:1 ratio

Exp. no.	Temp. ^0F / ^0C	i_c Adm^{-2}	i_a Adm^{-2}	t_c min	t_{on} ms	t_{off} ms	Dep.Wt g/h	Q_a / Q_c x 1000	CCE %	Note:
202	127 / 53	50	-	60			2.341	0	20.7	Rev.Etch.-30s, 9A
203	128 / 53	50	-	60			3.661	0	32.2	Peel, DC
204	129 / 54	50	-	60			3.647	0	32.2	Peel, DC
205	126 / 52	50	-	60			3.276	0	28.7	R.Etch 9A min. DC
207	128 / 53	50	125	60			3.004	8.2	26.5	Peel, PRC
208	128 / 53	50	-	60	60	2		-		Peel., PC
209	129 / 54	50	-	60	60	2	3.900	-	34.4	PC, R. Etch 8A min
210	128 / 53	40	-	60	60	2	2.069	-	22.8	Peel, PC.

Table 20: HEEF-405 (2%). 240 g/l of CrO_3; 100:1; DC, PC and PRC conditions.

d. **Discussion:**

In the new freshly made bath, HEEF-25 behaves approximately as the manufacture's literature suggests at high CD's (25-90 Adm^{-2}). However, at low range CD's (10-15 and 20 Adm^{-2} CCE's are rather modest. This presents drawbacks for the hard chromium platers when plating large parts where anode current carrying capacity, rectifier sizes and cooling limitations would restrict practical current densities, in most cases toward the lower ends, where HEEF-25 is not as efficient. It is obvious that impurities have strong effects on HEEF-25.

Private communication with platers from the field indicate that HEEF-405 had serious adhesion problems and its application was restricted to plating on aluminium only. Nevertheless, a set of experiments were conducted to verify adhesion problems. Previous reports from practising electroplaters proved to be correct, that HEEF-405 can not be used for plating over steel using customary reversing techniques. It was found that adhesion problems do exist when using standard reversing techniques and that also CCE's are not in the claimed 40% range. Some preliminary experiments with Pulse and Pulse Reversed Current were not encouraging. It is left to future experiments to try to optimise reverse etch. One way would be to pulse in a reversing (etching) cycle with longer *off* periods with resulting higher average currents. MSA as a catalyst behaved approximately as HEEF-25.

For both MSA and HEEF-25 baths it is observed that anodes used in experiments did appear much more corroded as compared to the anodes used in the Sargent Bath.

II.3.6 SECONDARY CATALYST: $KBrO_3$ and $KBrO_3$ /KIO_4 mixture.

a. Introduction

It was assumed for a long time that from the non-sulfate group of catalysts such as halogen catalysts, only the fluorides are suitable. The chlorine ion was considered too active, difficult to control and corrosive to plating equipment. Bromine and related bromates and perbromate compounds are considered unstable in the presence of strong oxidizers such as CrO_3 at pH < 1 and high temperatures.

Older [197] and newer patent[197-a] and literature data[173], however, do indicate the possible use of bromate or bromate/periodate mixture.

The following results, clearly demonstrate that it is possible to use bromates and Periodates as effective secondary catalysts.

Solution: Sargent Bath, 240g/ℓ 100:1; 1% $KBrO_3$ (2.4 g/ℓ).

Reverse etch = 7 A min.

b. $KBrO_3$ (1%); DC.

Exp. no.	Temp. ^0F / ^0C	i_c Adm^{-2}	i_a Adm^{-2}	t_a s	t_c min	Dep. Wt.. g/h	Q_a / Q_c x 1000	CCE %	Note:
223	118 / 48	**50**	-	-	60	1.634	0	14.4	
230	126 / 52	50	-	-	60	1.816	0	16.0	
231	126 / 52	**40**	-	-	60	1.433	0	15.8	
232	126 / 52	**30**	-	-	60	1.028	0	15.1	
233	125 / 52	**20**	-	-	60	0.564	0	12.5	
235	126 / 52	20	-	-	60	0.630	0	13. 9	

Table 21: 1% $KBrO_3$ as secondary catalyst; 240 g/ℓ CrO_3 . 100:1. DC.

c. $KBrO_3$ (1%) as secondary catalyst; t_a / t_c = 2s/91s; PRC

Exp. no.	Temp. ^0F / ^0C	i_c Adm^{-2}	i_a Adm^{-2}	t_a s	t_c s	Dep. Wt.. g/h	Q_a / Q_c x 1000	CCE %	Note:
229	127 / 53	50	10.0	2.0	91.0	1.742	4.4	15.4	
224	127 / 53	50	10.0	2.0	91.0	1.792	4.4	15.8	
225	126 / 52	40	8.5	2.0	91.0	1.410	4.7	15.5	
226	127 / 54	30	7.1	2.0	91.0	1.092	5.2	16.0	
227	128 / 52	20	5.7	2.0	91.0	0.964	6.3	21.2	(!)
228	125 / 54	20	5.7	2.0	91.0	0.913	6.3	21.7	(!)
235	**130 / 52**	20	-	-	1.0 hr.	0.630	-	13.9	DC

Table 22: 1% $KBrO_3$ as secondary catalyst; 240 g/ℓ CrO_3;100: 1 ratio; PRC.

d. $KBrO_3$ / KIO_4 : - DC. 20 - 60 Adm^{-2}.

In order to increase catalytic effect of halogen ions, 2 g/ℓ of potassium periodate is added in excess of 2.4 g/ℓ of $KBrO_3$ previously added to a solution under **a**.

Exp. no.	Temp. ^0F / ^0C	i_c Adm^{-2}	i_a Adm^{-2}	t_a s	t_c s	Dep. Wt.. g/h	Q_a / Q_c x 1000	CCE %	Note:
237	127 / 53	20	-	-	60	0.589	0	12.9	
238	126 / 52	30	-	-	60	1.027	0	15.1	
240	126 / 52	40	-	-	60	1/625	0	17.9	
242	126 / 52	50			60	2.927	0	20.0	
244	126 / 52	50	-	-	60	2.351	0	20.7	
243	128 / 53	60	-	-	60	2.992	0	20.3	

Table 23: $KBrO_3$ / KIO_4 mixture as secondary catalyst 240 g/ℓ CrO_3;100: 1ratio; DC.

e. $KBrO_3$ / KIO_4 as secondary catalyst; t_a / t_c = 2s/91s; PRC

Exp. no.	Temp. ^0F / ^0C	i_c Adm^{-2}	i_a Adm^{-2}	t_a s	t_c s	Dep. Wt.. g/h	Q_a / Q_c x 1000	CCE %	Note:
244	127 / 53	50	10.0	2.0	91.0	2.224	4.4	19.6	
245	127 / 53	50	10.0	2.0	91.0	2.337	4.4	20.3	
246	126 / 52	60	10.0	2.0	91.0	2.764	3.6	20.3	
247	127 / 53	40	10.0	2.0	91.0	1.627	5.5	17.9	
249	128 / 53	30	10.0	2.0	91.0	1.210	7.3	17.8	
250	125 / 52	30	7.1	2.0	91.0	1.136	5.2	16.7	
259	**130 / 54**	143	40.0	0.1	2.1	5.574	1.3	17.2	Bright

Table 24: $KBrO_3$ / KIO_4 mixture as secondary catalyst; t_a / t_c = 2s/91s -PRC;

f. $KBrO_3$ / KIO_4 as secondary catalyst -PRC i_a / i_c = 140%; t_a = 0.1 - 0.6 sec. PRC.

This set of experiments with the same bromate/periodate mixture (2.4 + 2.0 g/l) is done with three sets of constant anodic (70 Adm^{-2}) and cathodic (40 Adm^{-2}) current densities as well as with constant cathodic period: t_c = 60 sec. The anodic period was varied from 0.1, 0.2, 0.3 and 0.4 sec. with different Q_a / Q_c ratios.

Two additional "odd" experiments were done with i_a = i_c (No. 256) and i_c = 156% i_a (No. 258) in order to get a rough idea: should i_c be greater than, equal to, or smaller than i_a (?). From Experiment No. 258 the indication is that i_c should be greater than i_a This is further elaborated under subsections **f-1** and **f-2**.

Exp. no.	Temp. ^0F / ^0C	i_c Adm^{-2}	i_a Adm^{-2}	t_a s	t_c s	Dep. Wt.. g/h	Q_a / Q_c x 1000	CCE %	Note:
253	126 / 52	50	70	0.1	60	2.198	2.3	19.4	
254	126 / 52	50	70	0.1	60	2.600	2.3	23.0	
257	128 / 53	50	70	0.2	60	2.157	6.6	18.1	Semi bright
255	120 / 49	50	70	0.4	60	2.038	9.3	18.0	
256	122 / 50	40	40	0.6	60	1.561	10.0	17.2	
258	128 / 53	50	32	0.3	60	2.650	6.4	25.4	Dark gray

Table 25: $KBrO_3$ / KIO_4 as secondary catalyst; i_a = 140% i_c ; 240 g/l CrO_3 100:1; PRC.

f-1 $\mathbf{i_a}$ **= 57%** $\mathbf{i_c}$; $i_a / i_c = 40 / 70\ Adm^{-2}$; $t_c = 60$ sec.; $t_a = 0.1 - 0.4$ sec.

Exp. no.	Temp. ^0F / ^0C	i_c Adm^{-2}	i_a Adm^{-2}	t_a s	t_c s	Dep. Wt.. g/h	Q_a / Q_c x 1000	CCE %	Note:
252	125 / 52	40	70	0.1	60	1.910	2.9	21.1	
259	126 / 52	40	70	0.2	60	1.186	5.8	20.5	
251	125 / 52	40	70	0.3	60	1.774	8.7	19.6	
260	126 / 52	40	70	0.4	60	1.745	11.6	19.3	

Table 26: $KBrO_3$ / KIO_4 as secondary catalyst; $i_a = 0.57\ i_c$; 240 g/ℓ CrO_3; 100:1; PRC.

f-2. $\mathbf{i_a}$ $= 43\%\ i_c$; $i_a / i_c = 30 / 70$; Adm^{-2} $t_c = 60$ sec.; $t_a = 0.1 - 0.4$ sec.

Exp. no.	Temp. ^0F / ^0C	i_c Adm^{-2}	i_a Adm^{-2}	t_a s	t_c min	Dep.Wt. g/h	t_{on} ms	t_{off} ms	Q_a / Q_c x 1000	CCE %	Note:
261	128 / 53	30	70	0.1	60	1.742	-	-	3.8	25.7	PRC
262	128 / 53	30	70	0.2	60	1.842	-	-	7.7	**27.1**	PRC
263	124 / 51	30	70	0.3	60	1.753	-	-	11.6	25.8	PRC
264	127 / 53	30	70	0.4	60	1.458	-	-	7.7	21.5	PRC
268	127 / 53	30	70	0.2	60	1.787	-	-	7.7	19.7	PRC
266	125 / 52	30	70	0.2	60	1.905	-	-	7.7	**28.0**	PRC
267	127 / 53	30	70	0.2	60	1.787	-	-	5.8	19.7	PRC
265	127 / 53	40	70	0.2	60	1.488	-	-	7.7	21.5	PRC
281	126 / 52	100	-	-	60	1.334	100	40	-	16.1	PRC
267	127 / 53	30	73	-	60	3.564	-	-	0.0	21.5	DC

Table 27: $KBrO_3$ / KIO_4 as secondary catalyst; $i_a = 0.43\ i_c$; 240 g/ℓ CrO_3; 100:1; PRC.

g. Discussion:

From Tables 21-27 it follows that $KBrO_3$ / KIO_4 mixture even under DC conditions can produce rather high CCE's (e.g. 21.5% - exp. 267). Under PRC conditions, CCE's in 20% plus range are obtained under moderate current densities (30-40 Adm^{-2}) making it suitable for hard chromium plating.

h. $KBrO_3$ / KIO_4 + 3-Pyridine-Sulphonic Acid (PSA); DC, PC and PRC.

Following the patent literature claim[198] that pyridine compounds are stable and have catalytic effects as chromium electrodeposition catalysts 1g/ℓ of PSA were added to $KBrO_3$ / KIO_4 mixture [(2.4 g/ℓ)/(2 g/ℓ) used as a secondary catalyst. 100:1 ratio; CrO_3 240 g/ℓ 7 A min. reverse etch is applied]. DC, PRC and PC modes were explored.

Exp no.	Temp. ^0F / ^0C	i_c Adm^{-2}	i_a Adm^{-2}	t_a s	t_c min	Dep.Wt g/h	t_{on} ms	t_{off} ms	Q_a / Q_c x 1000	CCE %	Note:
287	123 / 50	40	-	-	30	1.452	-	-	-	17.1	DC
288	123 / 50	40	70	0.2	61	2.088	-	-	4.6	18.5	PRC
289	125 / 52	40	0	0	30	1.616	60	20	-	17.8	PC; T = 0.750
290	118 / 48	40	0	0	60	1.718	60	20	-	19.0	PC; T = 0.750
291	127 / 53	40	0	0	61	1.512	60	10	-	16.7	PC; T = 0.857
292	127 / 53	40	0	0	66	1.530	80	10	-	16.8	PC; T = 0.888
293	128 / 53	40	0	0	60	1.678	85	10	-	16.8	PC; T = 0.947
294	128 / 53	40	0	0	66	1.397	90	10	-	15.4	PC; T = 0.900
295	127 / 53	40	0	0	60	1.588	60	10	-	17.5	PC; T = 0.857

Table 28: $KBrO_3$ / KIO_4 + 1% PSA as secondary catalyst; 100:1; DC, PC and PRC.

As seen in Table 28, no noticeable improvement resulted from the addition of 3-Pyridine-Sulphonic Acid to the Sargent Bath already catalyzed with $KBrO_3$ / KIO_4 mixture.

II.3.7 SeO_2 AS SECONDARY CATALYST

a. Introduction:

Two U.S. Patents[199,200], a British Patent[201] , a Russian paper[202] and a U.S. paper[203] mention selenium as a catalyst or co-catalyst for chromium deposition. Chemical similarity to sulfur warrants a closer look at its catalytic properties. Although highly toxic, selenium concentrations used are in the ppm range and experiments were performed to explore its catalytic influence.

b. Experimental Results

Solution: Sargent Bath, 240 g/l, 100:1 ratio; 100,200,300 and 400 ppm SeO_2.

Exp. no.	Temp. ^0F / ^0C	i_c Adm^{-2}	i_a Adm^{-2}	t_a s	t_c min	Dep. Wt. g/h	Se O_2 ppm	Q_a / Q_c x1000	CCE %	Note:
347	127 / 53	70	-	-	5	3.156	100	0	19.9	Light gray
348	127 / 53	70	-	-	5	3.564	200	0	22.5	Dark gray
353	127 / 53	70	-	-	5	3.960	300	0	25.0	Darker gray
355	127 / 53	70	-	-	5	2.064	400	0	13.0	
356	127 / 53	70	-	-	5	2.580	400	0	16.3	+ 1% MSA
375	127 / 53	70	-	-	5	3.588	400	0	22.6	

Table 29: Selenium Oxide as Secondary Catalyst; 240 g/ℓ CrO_3; 100:1; DC.

c. Discussion:

It is obvious that selenium acid (also called Selenium Oxide, SeO_2) in the 100-400 ppm range has definite catalytic effect in the presence of sulfuric acid and that the bath can be easily overcatalysed. Optimal concentration is 300 ppm.

II.3.8 INDIUM AS A SECONDARY CATALYST

a. Introduction:

The decision to try indium as an ingredient of the chromium bath is based on published observations that indium deposits easily from sulphate baths , makes Ni-In alloy when added to $NiSO_4$ based on nickel plating solution[204], and as an electroplated alloy - although alone it is a very soft metal - can produce alloys of unexpected properties . It is reported[205] , that in spite of its softness small amounts of indium harden and increase the strength of Cu, Sn, or Pb alloys. In-Au and In-Ag alloys are used in dentistry because the indium increases hardness, strength and smoothness.

Electrochemistry of deposition of indium from sulphate solutions is well described in the literature[206,207]. In a similar way to chromium deposition, the deposition is multistep electron transfer:

$$In^{3+} \underset{e}{\overset{r_3}{\rightleftharpoons}} In^{2+} \underset{e}{\overset{r_2}{\rightleftharpoons}} In^{1+} \underset{e}{\overset{r_1}{\rightleftharpoons}} In^{0} \qquad <115>$$

Rate determination is the 'first step' (r_3) at lower CD's. At higher CD's, there is a fusion of the first two steps and the reaction:

$$In^{1+} \underset{2e}{\longleftrightarrow} In^{3+} \qquad <116>$$

is the slowest (and rate determining) step.

Determination of the electrode reaction order for I^-, Br^-, Cl^-, and SO^{2-}_4 (all known catalysts for chromium deposition) show that they participate in the process of discharge and ionisation of Indium, forming reactive complexes[207-210]. The composition of the reactive complexes often differs from those of the complexes prevailing in the bulk solution and consequently, the charge-transfer is accompanied by chemical reaction of the formation and dissociation of complexes[208,211].

b. Experimental

Standard 240 g/ℓ Sargent bath is made with different additions of $In_2(SO_4)_3$ to bring the sulphate level to different ratios. Cathode Current Efficiency determinations are presented in Tables 30-36.

Exp. no.	Temp. ^0F / ^0C	i_c Adm^{-2}	i_a Adm^{-2}	t_a s	t_c min	Dep.Wt. g/h	t_{on} ms	t_{off} ms	Q_a / Q_c x 1000	CCE %	Note:
400	130/54	10	-	-	5	0.108	-	-	0	-	no plate
401	130/54	20	-	-	5	0.144	-	-	0	3.2	Brite
402	130/54	30	-	-	5	0.716	-	-	0	10.9	Brite
402-a	130/54	40	-	-	5	1.056	-	-	0	11.7	Brite
403	130/54	50	-	-	5	1.332	-	-	0	11.8	Brite
415	130/54	50	-	-	15	1.736	-	-	0	15.1	Brite
416	130/54	50	-	-	15	1.668	-	-	0	14.7	Brite
404	130/54	60	-	-	5	2.112	-	-	0	15.5	Brite

Table 30. Indium Sulphate at 4.2 g/ℓ; 240 g/ℓ CrO_3; 100:1; DC.

Exp. no.	Temp. ^0F / ^0C	i_c Adm^{-2}	i_a Adm^{-2}	t_a s	t_c s	Dep.Wt. g/h	t_{on} ms	t_{off} ms	Q_a / Q_c x 1000	CCE %	Note:
405	129/54	50	30	0.1	50	2.292	-	-	1.2	20.2	Brite
406	129/54	50	30	0.1	50	2.376	-	-	1.2	21.0	Brite
407	129/54	70	50	0.1	60	3.012	-	-	1.2	19.0	Brite
408	129/54	50	70	0.1	60	1.848	-	-	2.3	16.3	Brite
409	129/54	50	70	0.3	60	1.584	-	-	7.0	13.2	Brite
410	129/54	50	10	0.2	91	1.824	-	-	0.4	16.1	Brite
411	130/54	70	50	0.1	60	2.856	-	-	1.2	18.0	Brite
413	130/54	25	-	-	15	1.668	1	1	-	12.7	PC;T=.5

Table 31. Indium Sulphate at 4.2 g/ℓ; 240 g/ℓ CrO_3; 100:1; PRC.

Exp. no.	Temp. ^0F / ^0C	i_c Adm^{-2}	i_a Adm^{-2}	t_a s	t_c min	Dep.Wt. g/h	t_{on} ms	t_{off} ms	Q_a / Q_c x 1000	CCE %	Note:
417	130/54	50	-	-	15	1.932	-	-	0	17.1	v. smooth
418	130/54	50	-	-	5	1.704	-	-	0	15.1	v. smooth
418-a	130/54	50	-	-	60	2.073	-	-	0	18.3	v. smooth

Table 32. Indium Sulphate at 8.2 g/ℓ; 240 g/ℓ CrO_3; 50:1; DC.

Exp. no.	Temp. ^0F / ^0C	i_c Adm^{-2}	i_a Adm^{-2}	t_a s	t_c min	Dep.Wt. g/h	t_{on} ms	t_{off} ms	Q_a / Q_c x 1000	CCE %	Note:
419	130/54	50	-	-	5	1.584	-	-	0	14.0	
421	130/54	50	-	-	15	1.769	-	-	0	15.9	
422	130/54	50	-	-	60	1.791	-	-	0	15.9	

Table 33. Indium Sulphate at (16.49 g/ℓ) as catalyst; 240 g/ℓ CrO_3; 25:1; DC.

Exp. no.	Temp. ^0F / ^0C	i_c Adm^{-2}	i_a Adm^{-2}	t_a s	t_c min	Dep.Wt. g/h	t_{on} ms	t_{off} ms	Q_a / Q_c x 1000	CCE %	Note:
422	130/54	50	-	-	5	1.344	-	-	0	11.9	
423	130/54	50	-	-	15	1.480	-	-	0	13.1	
424	126/52	50	-	-	60	1.473	-	-	0	12.9	

Table 34. Indium Sulphate at (25.2 g/ℓ) as catalyst; 240 g/ℓ CrO_3; 16.7:1; DC.

Exp. no.	Temp. ^0F / ^0C	i_c Adm^{-2}	i_a Adm^{-2}	t_a s	t_c s	Dep.Wt. g/h	t_{on} ms	t_{off} ms	Q_a / Q_c x 1000	CCE %	Note:
419	130/54	70	50	0.1	60	1.860	-	-	1.2	11.7	t_{tot} = 5'
420	130/54	70	50	0.2	60	1.866	-	-	1.2	11.8	t_{tot} = 10'
421	126/52	70	50	0.1	60	1.920	-	-	1.2	12.1	t_{tot} =5'

Table 35. Indium Sulphate at (25.7 g/ℓ) as catalyst; 240 g/ℓ CrO_3; 16.7:1; PRC.

By further addition of indium sulphate its concentration was increased to 41.9 g/ℓ and the sulphate ratio decreased to 11.1:1. Very smooth, bright panels were produced. Cathode

current efficiencies could not be measured at this point due to the dissolution of the back of the panels caused by acid attack on the steel from very high sulphate levels.

The ratio was then increased back to 50:1 by addition of barium carbonate and the experiment continued in both DC and PRC modes. Results are presented in Table 36.

Exp. no.	Temp. ^0F / ^0C	i_c Adm^{-2}	i_a Adm^{-2}	t_a s	t_c min	Dep.Wt. g/h	t_{on} ms	t_{off} ms	Q_a / Q_c x 1000	CCE %	Note:
430	129/54	50	-	-	5	1656	-	-	0	14.5	DC
431	125/52	50	-	-	15	1660	-	-	0	14.7	DC
										14.7	
437	129/54	70	50	-	60	3252	-	-	1.2	20.5	PRC
436	130/54	70	50	-	60	3108	-	-	1.2	19.6	PRC
438	126/52	70	50	-	60	3240	-	-	1.2	20.4	PRC
439	132/55	70	50	-	60	3140	-	-	1.2	19.8	PRC
440	130/54	70	50	-	60	3072	-	-	1.2	19.4	PRC

Table 36. Indium Sulphate at (25.7 g/ℓ) as catalyst; 240 g/ℓ CrO_3; 50:1; PRC.

c. Discussion:

From Tables 30-36 it is obvious that indium sulphate has a unique role as a catalyst for chromium plating, Although it did not appreciably change the cathode current efficiency it did permit plating with extremely high concentrations of sulphates (from 100 to 11.1 ratios) Plated surface is bright and smooth with few cracks, if any,. A bending test revealed excellent adhesion.

It is generally accepted that in concentrated chromic acid plating baths (e.g. 240 g/ℓ), the lowest ratio possible is about 25:1, but in our case the addition of indium as indium sulphate exerts what appears to be a profound effect on the character of the electrodepossition process. It could be only hypothesised at this point that the indium ion acts as a internal regulator of sulphate ion activity in the cathode film formation and/or that it possibly modifies the Cr^{2+} concentration and the role of Cr^{2+} in the deposition mechanism by influencing the equations <27> and/or <28> presented in the section on chromium deposition mechanism.

II.3.9 Uranium as Secondary Catalyst

One early reference[212] mentioned that addition of uranium salts as secondary catalyst produces very bright deposits.

To verify this, experiments were performed and the uranium salts chosen were: a) carnotite (natural uranium ore) and b) Uranium sulphate ($UO_2 SO_4 \bullet 3 H_2O$)

a. *Carnotite*: $K_2O_2UO_3 \bullet V_2 O_5 \bullet 3 H_2O$

Solution: Standard 240 g/ℓ Sargent Bath with 100:1 ratio (except Experiment No. 499 with 200:1 ratio) were explored at 54^0 C with 0.5 and 1% of carnotite. Since plates exhibited brittleness (cracking sounds when bending plates) additional experiments were conducted with different additions of Methyl disulphonic acid (DMSA). Results are tabulated in Tables 37 and 38.

Exp. no.	Temp. ^0F / ^0C	i_c Adm^{-2}	i_a Adm^{-2}	t_a s	t_c s	Dep.Wt. g/h	DMSA %	Q_a / Q_c x 1000	CCE %	Note:
508	130/54	30	0	0	1260	1.077	0	0	15.8	very bright
509	130/54	16	40	0.1	77	1.567	0	0.52	17.3	semi. bright
510	130/54	10	40	0.1	50	1.639	0	0.5	18.1	semi. bright
511	130/54	56	0	0	1620	1.080	0.5	0	19.0	semi. bright
512	130/54	15.6	40	0.1	15	2.102	0.5	2.6	23.2	dull (c)
513	130/54	15.6	40	0.2	15	2.051	0.5	5.2	22.6	dull (c)
514	130/54	15.6	40	0.2	15	2.264	1.5	5.2	25.0	dull
515	130/54	40	0	0	1860	1.726	1.5	0	19.0	blisters (a)
516	130/54	40	0	0	3600	2.062	1.5	0	22.2	bright (a)
517	130/54	20	0	0	3600	0.653	1.5	0	14.4	bright (a)
518	130/54	40	0	0	6660	1.859	2	0	20.5	bright (b)
519	130/54	28	11	0.2	15	2.131	2	5.2	23.5	dull (c)
520	130/54	40	0	0	3600	1.720	3	0	19.1	bright (a)
521	130/54	40	0	0	6300	1.766	3	0	19.5	bright (a)
522	130/54	15.6	40	0.2	15	1.908	3	5.2	21.1	dull (c)

Table 37. CEE's of SB + 1 % Carnotite + DMSA; DC and PRC modes.

Notes: (a) No cracking sound when bending a plated panel.
(b) Slight cracking sound when bending a plated panel.
(c) Cracking sound when bending a plated panel.

Exp. no.	Temp. ^0F / ^0C	i_c Adm^{-2}	i_a Adm^{-2}	t_a s	t_c s	Dep.Wt. g/h	DMSA %	Q_a / Q_c x 1000	CCE %	Note:
499	130/54	30	-	-	600	0.984	0	0	14.2	bright DC
500	130/54	30	-	-	1500	1.077	0	0	15.9	bright DC
501	130/54	30	30	0.1	99	1.444	0	1	21.2	bright PRC
502	130/54	30	60	0.1	99	1.152	0	2	16.9	bright PRC
503	130/54	30	60	0.1	99	1.130	0	2	16.3	bright PRC
504	130/54	30	60	0.2	99	1.061	0	4	15.6	bright PRC
505	130/54	30	60	0.2	99	1.057	0	4	15.5	bright PRC
506	130/54	30	30	0.1	99	1.086	0	1	15.7	bright PRC
507	130/54	30	30	0.4	99	1.085	0	4	15.7	bright PRC

Table 38. CCE's of Sargent bath + 0.5 % Carnotite; 240 g/ℓ CrO_3 (100:1); DC and PRC.

b. *Uranium Sulphate*

Exp. no.	Temp. ^0F / ^0C	i_c Adm^{-2}	i_a Adm^{-2}	t_a s	t_c s	Dep.Wt. g/h	DMSA %	Q_a / Q_c x 1000	CCE %	Note:
550	126/52	30	-	-	10	.600	0	0	8.8	630:1 Bright
551	132/55	30	-	-	10	.792	0	0	11.6	100:1 Bright

Table 39. CCE's of Sargent bath + 0.39 % of Uranium Sulphate. DC mode.

Russian research[213] claimed that Vanadium salts not only substantially increase CCE's in the Sargent bath (e.g. from 15 to 22% at 40^0 C), but also narrows down the bright plating range and increases the stress. In order to separate the influence of the vanadium, uranium is added as a secondary catalysts in the form of the simple salt.

c. *Discussion.*

Results presented are quite unusual: when compared to the standard Sargent bath, brightness of the DC plated panels improved with relatively small amounts of carnotite: 0.5 and 1% - relative to CrO_3 content (or 1.2 and 2.4 g/l).

On the other hand, panels plated in PRC mode exhibited loud, cracking sounds when bent, indicating stressed, brittle deposit - opposite to DC plated panels. Almost as a rule, with all previously investigated catalysts, PRC plating produced softer deposits

compared with DC produced deposits. Addition of DMSA, however, reduced drastically the amount of brittleness in the PRC plated panels and also increased the cathode current efficiencies in DC and PRC conditions.

From the results of experiments No. 499-522 it can be concluded that PRC strongly influences this inorganic catalyst by modifying the Uranium and/or Vanadium content and making conditions suitable for alloy plating. To rule out the influence of vanadium in the experiments Nos. 550 and 551 uranium sulphate is used.

In experiment 550 the only sulphate present, originated from the addition (0.34%) of uranium sulphate, thus bringing the ratio to a high 630:1 level. Surprisingly, the panels were bright and CCE higher than that expected for such a ratio. In experiment 551 the ratio was adjusted to 100:1 with $H_2 SO_4$ and CCE was increased to 11.6% , still it resulted in a bright deposit.

After all the uranium sulphate on hand was spent for these experiments it was found that **no** USA chemical supply houses carry any of this compound consequently no further experimentation could be made to investigate the influence of higher uranium content. Salts found available were acetates and uranil and uraneous oxides. The unusually high brightness of deposits obtained warrants a closer look by interested future researchers.

II.3.10 Cyclohexane Carboxylic Acid as Secondary Catalyst.

It is already recognised that the addition of an organic acid containing carboxylic group can benefit the chromium deposition process. For example, *Kassaaian and Dash,*[214] *Hoshino et al.*[215] *Tsai et al.,*[216] and *Vashcenko and Soloveva*[227] used formic acid. *Formichev et al.*[218] used gallic acid, *Korbach et al.*[219] and *Chessin et al.*[220] sulphoacetic acid, *Woodsand and Moul*[221] oxalic acid, *Gabriel*[222], melitic and tartaric acids and *Doskar et al.*[223] cyanuric acid. However, *Hoshino et al.*[224] later recognised a problem with the stability of organic acids in the presence of a strong , hot chromic acid and used cyclopropane carboxylic acid due to its stability against oxidation. They obtained bright chromium deposits of *bcc* structure with increased cathodic current efficiencies (but decreased corrosion resistance), at an optimum concentration of CPA which they found to be 4 ml/l. Oddly, they used an unconventional solution: 100g/l (1.0 M) CrO_3 + 5 g/l of H_2SO_4 (20:1 ratio) with a 0-30 ml/l of CPA.

To verify these potentially important results a more conventional 240 g/l Sargent bath was used with 178:1, 100:1 and 50:1 ratios. As presented in Table 40, no increase in cathode current efficiencies was found using 1,2, and 3 ml/l of CPA in DC mode.

Exp. no.	Temp. ^0F / ^0C	i_c Adm^{-2}	i_a Adm^{-2}	t_a s	t_c min	Dep.Wt. g/h	Q_a / Q_c x 1000	CCE %	Note:
491	132/55	50	0	0	11	2.105	0	18.6	178:1; 1ml/l CPA
492	130/54	50	0	0	11	1.975	0	17.4	100:1; 1ml/l CPA
493	131/54	50	0	0	11	2.051	0	18.1	100:1; 1ml/l CPA
494	129/54	50	0	0	11	1.974	0	17.4	100:1: 2ml/l CPA
4 95	130/54	50	0	0	11	2.062	0	18.2	100:1; 3 ml/l CPA
496	126/52	50	0	0	11	2.094	0	18.9	3 ml/l + 0.5%; MSA
497	132/55	50	0	0	11	2.094	0	18.9	3 ml/l + 1%; MSA
516	130/54	50	0	0	5	1.956	0	17.3	67:1; 1m l/l CPA
52 7	132/55	50	0	0	5	2.028	0	17.9	50:1; 1m l/l CPA
528	130/54	50	0	0	5	2.076	0	18.3	50:1; 1m l/l CPA
529	131/54	50	0	0	5	2.028	0	17.9	50:1; 1m l/l CPA

Table 40. Cyclohexane Carboxylic Acid (CPA) as Secondary Catalyst. DC mode.

Exp. no.	Temp. ^0F / ^0C	i_c Adm^{-2}	i_a Adm^{-2}	t_a s	t_c min	Dep.Wt. g/h	Q_a / Q_c x 1000	CCE %	Note:
530	130/54	50	0	0	5	2.232	0	19.7	50:1; 2m l/l CPA
531	126/52	50	0	0	5	2.244	0	19.8	50:1; 2m l/l CPA
532	132/55	50	0	0	5	1.956	0	17.3	50:1; 2m l/l CPA
533	130/54	50	0	0	5	2.052	0	18.1	50:1; 2m l/l CPA
534	132/55	50	0	0	5	2.136	0	18.9	50:1; 4m l/l CPA
535	130/54	50	0	0	5	2.136	0	18.9	50:1; 4m l/l CPA
536	131/54	50	0	0	5	2.508	0	22.1	100:1 +1% MSA +4 ml/l CPA
536-a	129/54	50	0	0	5	2.160	0	19.1	100:1 +2 % MSA +4 ml/l CPA
545	130/54	62.5	0	0	5	2.832	0	20.8	100:1 +0.5% MSA +3 ml/l CPA
246	126/52	62.5	0	0	5	2.892	0	21.3	Repeat No. 545

Table 40. Continued

II. 4 ON THE CHROMIUM DEPOSITION AND DISSOLUTION MECHANISMS

II.4.1 DEPOSITION MECHANISM

II.4.1a Introduction:

Despite being one of the most widely used metals for electrodeposition, the exact deposition mechanisms for chromium are still open for conjecture. Almost non-existent is an explanation of the role of organic sulpho acids as modern high efficiency catalysts. Brief and veiled bits of information are available only in patent literature.[193,194]

Deposition mechanisms were studied with the use of linear potential sweep (LPS) and cyclic voltammetry (CV) on stationary and rotating disc electrodes (RDE).

Experiments were conducted, most of the time, at two different temperatures: 20^0 C and 55^0 C with five different plating baths used:

1. Standard, Sargent type bath: (240 g/l CrO_3, 2.4 g/l H_2SO_4) designated as SB.
2. SB plus HEEF-405, as secondary catalyst.
3. SB plus HEEF-25, as secondary catalyst.
4. SB plus SSA (sulpho salicylic acid), as secondary catalyst.
5. SB plus MSA (Methane Sulphonic Acid), as secondary catalyst.

HEEF-405 and HEEF-25 are leading high speed commercial chromium plating catalysts, manufactured and marketed world wide by ATOTEC Co. (Summerset N.J. USA)

The working electrode speed of rotation varied between 0-3000 rpm. The experimental arrangement is presented in Figure 13.

A detailed literature search revealed **no** definitive information on efficiency of chromium anodic dissolution (deplating). It is mostly assumed to be about 100% and until introduction of Periodic Reverse Current (PRC) chromium deposition, it did not have too much practical significance. However, for PRC research it is important to establish dissolution rates under different deposition conditions in order to calculate exact anodic dissolution efficiencies.

For the study on anodic dissolution of chromium three different methods were used: weight difference resulting from anodic dissolution of chromium in Sargent Bath at three different current densities and temperatures; Quartz Crystal Microbalance (QCM) method with two temperatures using Sargent Bath; voltammetric study of chromium dissolution in chromic acid with and without sulphates and in the Sargent Bath with and without MSA addition.

II.4.1b. Experimental Equipment and Procedure

BAS (West Lafayette, Ind, USA) Potentiostat (Mod CV-27) coupled with BAS X-Y Recorder (Mod MF-9044) were used for Voltammetric experiments; Pine Instruments (Grove City, PA, USA) (Mod DDI) with variable speed (0-10.000) rotator (Model AS-R2) are used for RDE experiments. Plating cell was kept in a Precision Scientific Co (Chicago Ill. USA) constant temperature bath (Model 81) and thermostatically controlled (+/-1^0 C) with Protec (Mentor, Ohio, USA) temperature controller (Model DME 20). The working electrode was platinum wire embedded in glass rod with surface area of 0.033 cm^2 and, counter electrode was Alpha Product (Danvers, MA, USA) platinum wire, 2.0 mm in diameter (Mod 00900) and reference electrode was BAS (Mod MF-2063) Saturated Calomel Electrode (SCE) or Ag-AgCl reference electrode.

Also used were IBM Voltammetric analyser (Model EC/225) potentiostat/galvanostat coupled with X-Y plotter (Model 7424M) and Venking Potentiostat (Model 68TS3) capable of delivering up to 10 Amps, driven by Heath (Chicago, Ill. USA). pulse generator (Model 1277).

Before each consecutive experiment, the previously plated chromium deposit was stripped at +1.5 V and fresh chromium was deposited on the surface of the platinum working electrode. Before each experiment the cathode was mechanically polished with 240 and 600 paper, then with diamond powder to a finish of 1 μ. It was then rinsed with ethanol and doubly distilled water. Electrodeposition was carried out at the negative potential of -1.3 V for 10 sec. and then continued at -1.2 V for 3 minutes for particular catalysed solution under study.

The cyclic voltammograms (CV) were obtained between -1200 and +1500 mV at scan rates (v) between 10 to 142 mV/sec. CVs were repeated six times. Every voltammogram consisted of 8-10 cycles of polarisation before steady-state was reached.

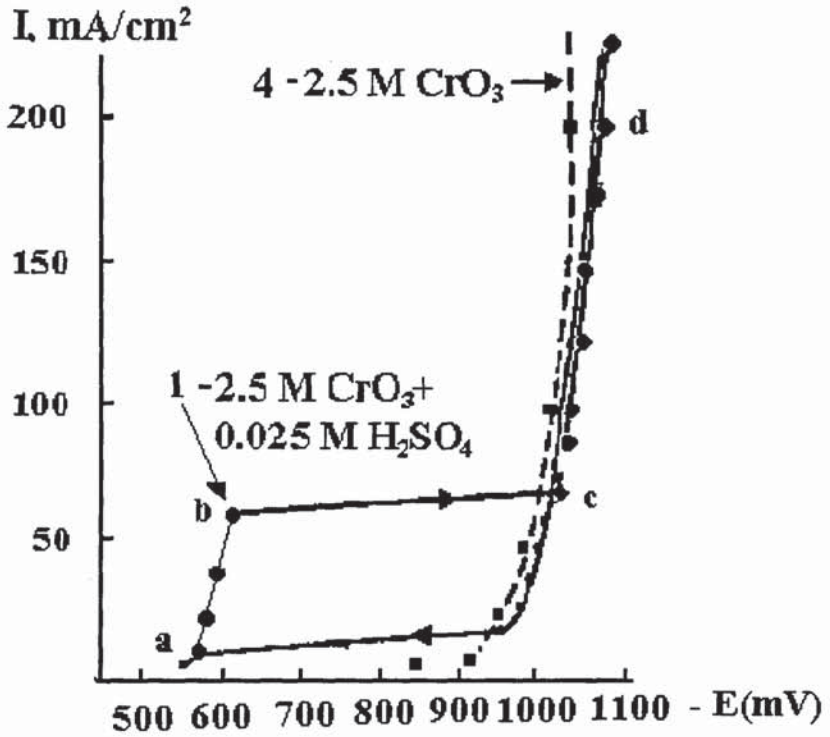

Figure 24. Galvanostatic current-potential response of the chromium electrode for 100:1 SB (lines 1 and 1') and for the solution of pure 2.5 M chromic acid (line 4) at 20^0 C.

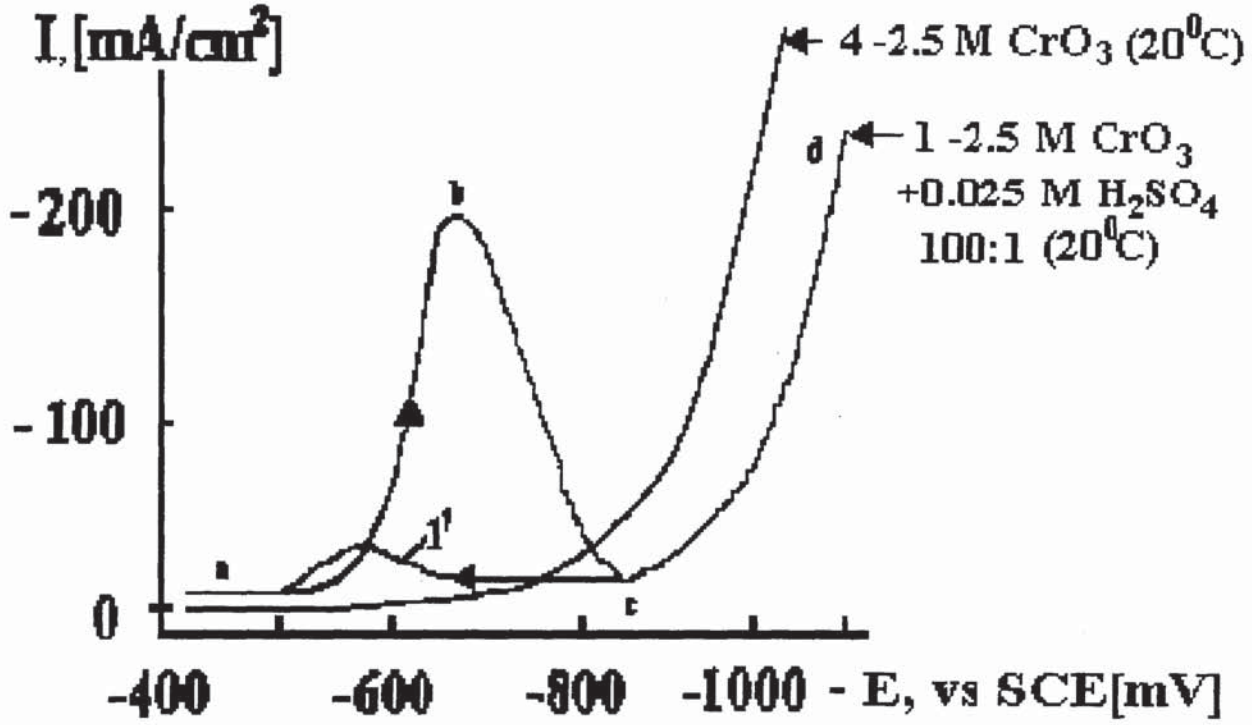

Figure 25. Potentiodynamic response of 2.5 M 100:1 Sargent bath (line 1) at 20° C and v = 142 mV/s., compared to pure 2.5 M CrO_3 (line 4)

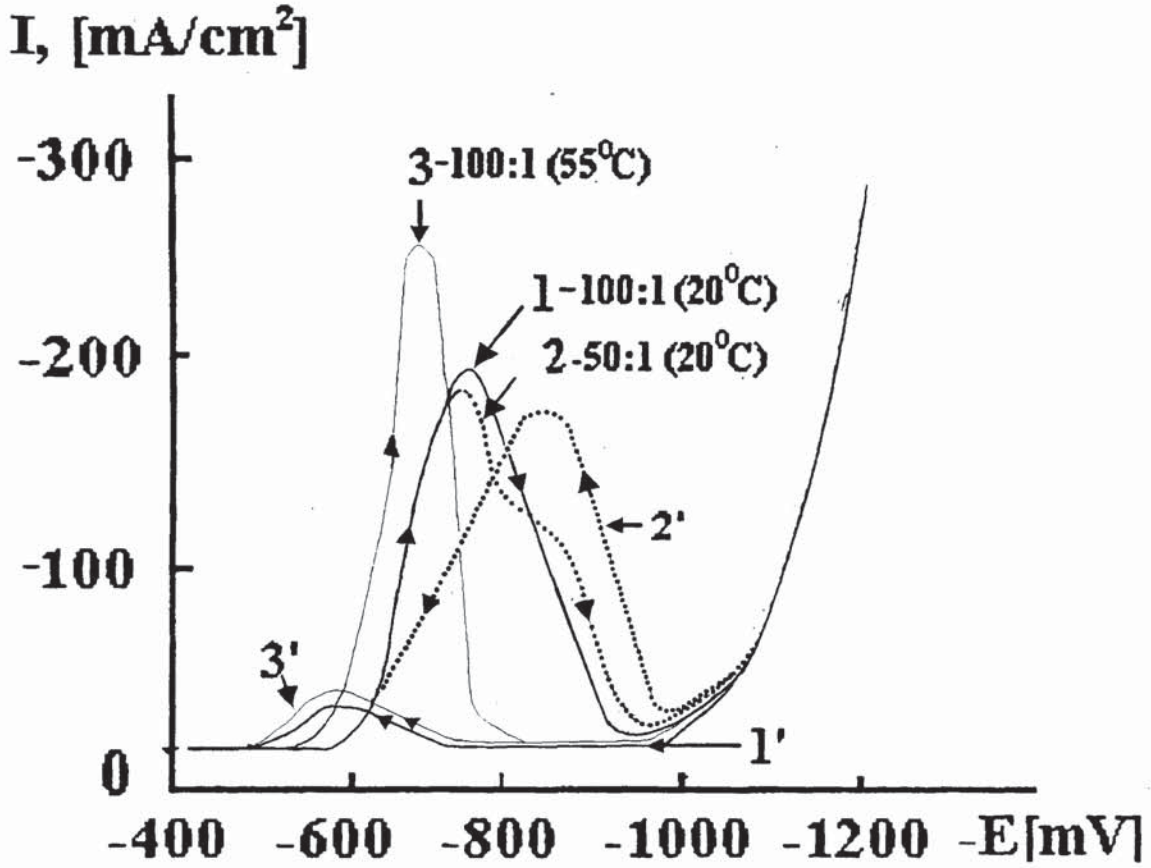

Figure 26. Linear Cyclic Polarization (LCP) Potential Scans for chromium cathode for Sargent Bath with 100:1 (1 - 1'), 50:1 (2 - 2') ratio at 20^0 C and for 50:1 (3 - 3') ratio at 55^0 C. v =142 m V/s.

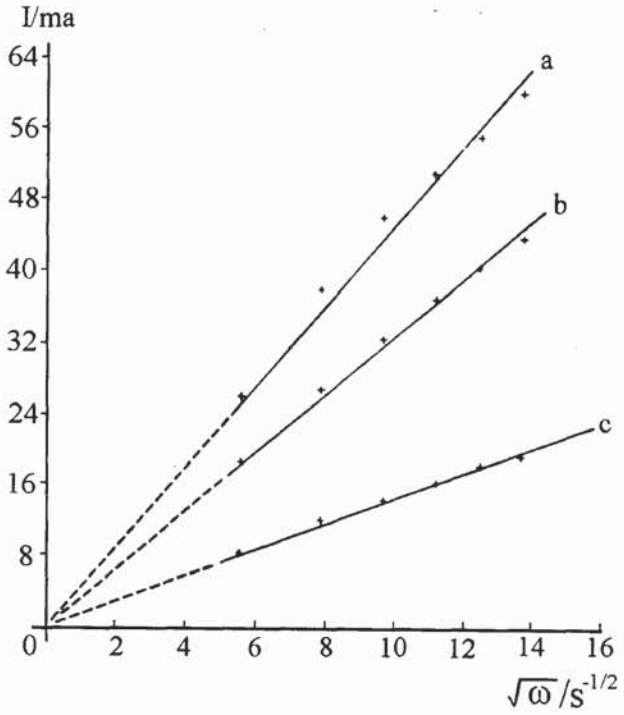

Figure 27. I vs. $\sqrt{\omega}$ for rotating Cr electrode in 2.0 M CrO_3 bath with **a**) 6 mM (33:1). **b**) 4 mM (50:1). **c**) 2 mM (100:1) H_2SO_4 (From Fletcher).[17]

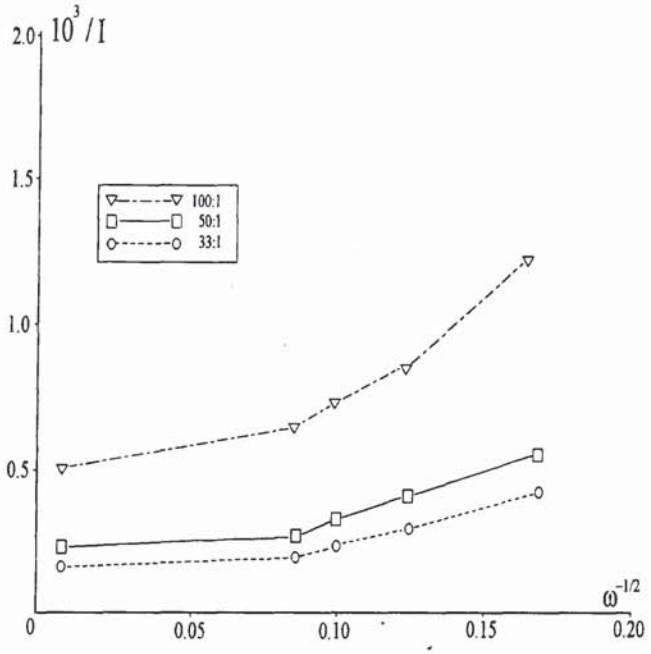

Figure 28. Inverse relationship 10^3 / I vs. $1/\omega^{1/2}$, reploted with data from Figure 27.

II.4.1d Deposition Mechanisms - Experimental Results

1. *SARGENT bath*

i. Description of the Linear and Cyclic Potential Polarisation Voltammograms

Figure 24 is current -potential response of a stationary chromium electrode plated galvanostatically in Sargent bath and in uncatalised 2.5 M CrO_3 solution. Figure 25 is potentiodynamic curve for 2.5 M (100:1) Sargent bath 20^0 C and stationary conditions. The scan rate is 142 mV/s. Figure 26 is potentiodynamic (v = 142 mV/s.) curve for 2.5 M Sargent bath where two different sulphate concentrations: 100:1 (lines 1,1') and 50:1 (lines 2,2') are compared at room temperature (20^0 C) with 100:1 ratio bath at 55^0 C (lines 3,3'). Figure 27 is I vs. $\omega^{1/2}$ reproduced from the paper by *Pletcher*[171]. Figure 28 is obtained from Figure 27 by taking the inverse values of I and $\omega^{1/2}$. Figure 29 is constructed by data from Table 41 and represents the inverse relationship between maximum current and rotation speed for 2.5 M (100:1) Sargent bath at 25 (a) and 50^0 C. (b) Figures 30 and 31 are preliminary cyclic voltammograms of stationary (Figure 30) and rotating (Figure 31) chromium electrode in a 100:1 Sargent bath (SB) without secondary catalyst. Voltammograms are presented for the Sargent bath (Figures 32-35) with four different additives under potentiodynamic conditions at a stationary electrode, (ω = 0), at scan rate v = 70 mV/s, as preliminary comparison of the influence of different catalysts under study. The scanning starts at a potential of -1200 mV and proceeds to +1500 mV, where a reverse scan begins.

Presented next is the influence of different scan rates at 20^0 C. At stationary electrode (ω = 0) , the effect of seven different scan rates (10, 20, 40, 58, 83, 100 and 142 mVs) is presented separately in Figures 36-42 and together in Figure 43. The effect of Sweep rate ($\sqrt{v}$) on the maximum cathode current, I, is also plotted in Figures 70 (compared to HEEF-25), 84 (compared to HEEF-25) and 98 (compared to SSA). In Figure 110 Sargent bath is compared with the other four additives under stationary conditions and for 5.0 g/l concentrations.

The influence of the hydrodynamic conditions resulting from the electrode rotation for five different speeds (ω = 500, 1000, 2000, 2500 and 3000 rpm) at v = 40 mV/s. is

presented separately in Figures 44-48 and together in Figure 49. At constant rotation speed (ω =2000 rpm) the influence of the three scan rates (v = 58, 83 and 100 mV/s.) is presented separately in Figures 50-52 and together in Figure 53. The maximum current response to rotation speed, I - $\sqrt{\omega}$, at v = 40 mV/s. is presented on Figure 54. The influence of hydrodynamic conditions on Sargent Bath alone and with four different additives at 5.0 g/l and v = 40 mV/s is presented in Figures 71, 87 and 101. In Figure 109 I vs. $\omega^{1/2}$ relationship is presented for SB in comparison with all additives under the investigation. The affect of higher temperature (55^0 C) is presented for stationary electrode at v = 56 mV/s on Figure 55.

ii Deposition Mechanisms - Discussion.

From the thermodynamic data presented in Table 1, it can be seen that hexavalent (poly) chromate ions can be reduced first to the trivalent state (+1.33 V) and then the hydrogen ($2H_3O+2e \rightarrow H_2 + H_2O$) at 0.00 V and chromium ions (-0.74 V) can be reduced to elementary state. The formation of chromous ions ($Cr^{3+} + e \rightarrow Cr^{2+}$) at -0.41 V and its reduction to metal ($Cr^{2+} + 2e \rightarrow Cr$) at -0.91 V is also possible and probable. However, its detection in such a strong oxidising medium as CrO_3 solution is difficult to quantify experimentally. In spite of the positive value of the reduction potential of the (poly) chromate ions to the trivalent state, the hydrogen evolution is the main cathode reaction on chromium cathode in the uncatalysed chromic acid solutions. From a comparison of the E-log I curves for electrolysis of chromium cathode in 0.3M H_2SO_4 (Figure 104) and chromium cathode in 2.5 M chromic acid solution (Figure 107), it is obvious that hydrogen reduction potential (E) is a linear function of log I in accordance to the Tafel equation which is the fundamental law of the kinetics of electrode processes ($E = a - b \log I$). It is also obvious that the hydrogen evolution overvoltage is higher in chromic acid than in sulphuric acid. At current density of log I = 1.0 mA/cm^2 the difference is about 80 mV. This retardation for hydrogen ion discharge is due to the formation of compact oxide film (C-film) on the electrode surface as already proven by a number of authors.

The oxidised cathode surface cannot be reduced either electrochemically or by atomic hydrogen. The oxide film on the surface interferes to some extent with the reduction of hydrogen ions, but the film acts as a very great obstacle to the reduction of (poly) chromate ion even when the cathode is polarised to very high potentials. This shows that the influence of the state of the cathode surface on metal ions reduction is much greater than the influence of cathode potential, which is an important electrochemical factor.

Although reduction of (poly) chromate ions is almost impossible at the chromium cathode (even at high negative potentials), the reduction is possible with small addition of certain catalytic ions (*e.g.*, SO_4^{2-}, F^-, Br^-, Cl^-) which will change the *nature* of electrochemical reaction which in turn will change its *rate*, expressed as current density.

Presented in Figure 25 is the potentiodynamic response (linear potential sweep) at v =142 mV/s of 2.5 M chromic acid without (line 4) and with (line 1) sulphuric acid. When line 4 is obtained galvanostatically (as presented in Figure 24, line 4) hydrogen evolution

curve , (in absence of sulphate) will change smoothly and hydrogen is evolved on the cathode at any current density.

The first section a-b has a gradual increase of the potential in either galvanostatic or potentiodynamic mode, corresponding to $Cr^{6+} \rightarrow Cr^{3+}$ reduction. For galvanostatic mode, transition from b to c is accompanied by a sharp horizontal jump; on the other hand, when the current density is reduced (curve 1' plotted in reverse direction), a characteristic hysteresis loop is obtained indicating that the film is formed during the increase of the potentials toward a more negative side and it is not removed when the potential is reduced on the return side. With the potentiodynamic method (Figure 25, line 1) the b-c transition is more gradual and forward and reverse curves are almost superimposed, except for the small hysteresis loop present between -600 and -700 mV under potentiodynamic conditions.

The important feature observed in this figure is that b-c transition in this case is *abnormal* in nature, since an increase in potential in section b-c, causes a decrease in current rather than usual increase. This idiosyncrasy shows that the *state* of electrode surface is changed in the potential range of the section b-c and that there is sharp difference in the energy conditions of the reactions occurring in section a-b ($Cr^{6+} \rightarrow Cr^{3+}$) and section b-c where three simultaneous reactions are occurring: (I) $Cr^{6+} \rightarrow Cr^{3+}$, (II) $Cr^{6+} \rightarrow Cr^{0}$ and (III) $2H^{+} \rightarrow H_2$. For reasons of clarity, reactions I, II, III are written in abbreviated form where Cr^{6+} represents the polychromate-bisulphate complex $[HCr_3O_{10}\ n\ HSO_4]^{n+1}$ and n is an integral number between 0 and 4.

By analysing chromic acid polarisation curves presented in Figure 25 with (line 1) and without (line 4) catalyst addition, it is obvious that the catalyst addition favours the electrode reaction in section a-b by shifting it to the left, toward less negative potentials, but that it also influences (by shifting toward right) the electrode reactions that are occurring in section b-c.

From this analysis, it is clear that the addition of catalyst actually increases the reduction potential of chromium metal deposition reaction, or in essence, passivates the cathode surface. However, this kind of passivation is different than the initial passivation of cathode (C-film) during its first contact with highly oxidising chromic acid solution, even before the current is applied, and it is due to the formation of a second film (L-film). This liquid film (called by the Russian researchers: "phase film") consists of products of electrochemical reactions that are proceeding on the cathode and considered to be mainly a

mixture of oxy-hydroxy chromium compounds in variable valence state and complexed with some amount of sulphates. This film retards some reactions while it facilitates others. Due to the presence of two films (C and L) the nature and the rates of electrode reactions are more influenced more by the state of the electrode surface, rather than the changes of state of the ions in the solution. This unique feature of chromium deposition, makes its deposition mechanisms substantially different compared to the deposition of other metals and up to this date makes chromium research torturous, puzzling, and extremely difficult albeit stimulating.

The current-transient studies,[171,225-230] on the other hand, did show that in the short, initial period (in the approximate range of one to a few seconds), the (poly) chromate ions can be reduced to metal state even in the pure chromic acid solutions, with current efficiency of approximately 1% and with the formation of "black" chromium. In this case, the cathode potential at the beginning shifted toward positive values which characterise a transition from one passive to active state of the cathode. Another support for this comes from the obvious fact that solid film cannot be formed on liquid electrodes. A number of polarographic investigations[231,232] have shown that chromate ions can be reduced on mercury drop in supporting electrolytes that contain no catalytic anions, *e.g.*, phosphates of alkalis and partial reduction of chromic acid can be observed at low current densities even in the absence of the catalyst. A similar effect is observed on the graphite cathodes[233,234] which are immune to chromic acid oxidation, all this indicates that in the special cases chromic acid can be reduced without a catalyst as long as the electrode is not covered by continuous oxide film (C-film). C-film formation is represented as Figures 25 and as a section a-b where current is increased. Once formed, under the influence of catalyst, the film starts to break down and the resistance is reduced. In the next section of polarisation curve (b-c), the second phase (L-film) starts to form as a consequence of accumulation of the products of incomplete chromium reduction reaction. While for the C-film it can be stated that it is just one of the unfortunate consequences of strong oxidising (passivating) properties of chromic acid solution, the L-film is probably helpful for two obvious and one less obvious reasons:

a) once formed it protects the cathode from the passivating effect of chromic acid.

b) provides the environment where Cr^{2+} ions can exist, being one of the steps of overall reduction mechanisms.

c) A less obvious reason is that continuous, partially adsorbed, continuously forming and dissolving , L-film is a genuine brightening agent. Chromium ellectrodeposition is the only major industrial deposition process where bright deposits are obtained without the addition of a brightener. It is well established that brightening is an adsorption/inhibition, diffusion controlled process that influences the crystallisation. The affect of brighteners arises from the fact that they or their reduction and decomposition products are adsorbed on the cathode surface in the form of a thin film. This adsorption may take place preferentially on the active or crystal growth points. Crystal growth in the sense of a repeatable steps is inhibited at these points and the metal ions are forced to deposit preferentially in depressions and at inactive cites.

Since at the steady state conditions during chromium deposition process, a thin liquid, partially adsorbed film is always present, conditions are met for production of bright deposits. This in a sense is a fortunate situation since the strong oxidising properties of CrO_3 would extremely limit the choice of suitable organic brightening additives.

On the other hand, L-film serves as a place where the products of a partial reduction of chromic acid are accumulated, where pH takes a value different from the bulk of the solution and, therefore, interferes with the partial chromium reduction reaction . It also is the place where the large, ponderous (poly) chromate-bisulphate complex has to travel in order to approach the cathode to be irreversibly adsorbed, partially decomposed and then finally reduced to metal.

One of the important features of the L-film is that it forms a continuous sheath, covering the electrode surface and if the current is decreased, the film swells, disintegrates and can be removed from the electrode in slices which will dissolve in electrolyte when the current is switched off [41,235] (in the presence of sulphate as a catalyst). In the presence of chloride as a catalyst L-film does not decompose when the current is switched off, and remains undissolved on the cathode, even after the cathode is removed from the solution. The composition of the film is *not* definitely established yet. According to some Russian research[42,43] it consists of Cr^{6+} , Cr^{3+} and SO_4^{2-} ions and concentration of the latter two is higher than their concentration in the bulk of the solution, while the concentration of the former is lower. (Other options on its composition are discussed in section I.2). Another important feature of the L-film is that it greatly inhibits the reduction of the number of ions

and that causes the shift of the cathodic potential up to the values of chromium metal deposition.

Kinetics of electrochemical reduction of chromic acid in 2.5 M Sargent bath is studied in a series of experiments on stationary and rotating chromium electrode The linear potential polarisation sweep plots are presented in Figure 25. These clearly indicate that the reduction process occurs in several sequences depending on the electrode potential. In the first sequence (a-b) of the reduction process, nearly 100% of the chromic acid is reduced to Cr^{3+} . Three cathodic processes taking place simultaneously as we move toward more negative potentials ($Cr^{6+} \rightarrow Cr^{3+}$, $2H^{+} = H_2$, $Cr^{6+} \rightarrow Cr^{0}$), making the mechanism of chromic acid reduction a complex problem. From the data presented and from the results of previous research, three major points of the sulphate role in the reduction process can be summarised:

a.) chromic acid can be cathodically reduced and metallic chromium deposited only in the presence of a catalytic anion, capable of forming complexes with Cr^{3+} (e.g. sulphates, fluorides, chlorides or even H_3BO_3.

b.) current, I, measured at the first maximum of polarisation curve (e.g. point b, Figure 26) and often called I_m (maximum current), is proportional to the concentration of sulphates or some other catalytic anion.

c.) Maximum current is directly affected by the hydrodynamic condition (stirring or in our case cathode rotation).

From this data it is obvious that the sulphate influence on the reduction process is complex. The main point is that the reduction rate on the cathode is dependent on the diffusion rate of sulphate migration toward the electrode.

Opinions of the role of the sulphate were changed considerably as the research on chromium progressed. At present, it can be safely stated that the layer formed at the cathode (L-film), where the products of incomplete reduction ($Cr^{6+} \rightarrow Cr^{3+}$) are accumulated, does indeed block the cathode surface. Cr^{3+} reacts with the sulphate ions forming soluble, metastable complexes that prevent the formation of extremely stable chromium aqua complexes: $[Cr\ (H_2O_6)]^{3+}$, which can obstruct the deposition process, through an oligomerasition process as detailed in section II.2. Sulphate complexes will eventually leave the L-film, travel toward the anode and decompose. Lead peroxide which

is always present[54] on the surface of a lead anode will reoxidise Cr^{3+} to Cr^{6+} and liberate the sulphates which will repeat complex formation again as presented in Figure 7. Since it is clear that the sulphate must be present in order to ensure the transfer of Cr^{6+} out of the bulk of the solution to the cathode, and to protect the cathode film from making the very stable Cr^{3+} aqua complexes and also move Cr^{3+} toward the anode for oxidation back to Cr^{6+} it is still insufficiently explained why the current is limited by diffusion of the sulphate ions. In order for such limitations to exist it is obvious that sulphates must be participants in total electrode process, not only by keeping the cathode film in liquid form but also by forming the electroactive complexes. Those complexes do not necessarily need to be extremely stable. It would be sufficient only that the average life time of these complexes have to be longer than the period of time that they spend in the diffusion layer. Since stable complexes of Cr^{3+} with sulphuric acid have been identified[236-240], this approach seems to be well founded. In order to provide more insight into the mechanisms and kinetics of chromic acid reduction it is necessary to more clearly determine the diffusion conditions involved.

A rotating disc electrode (RDE) is a fast, convenient and well established method of studying kinetics of this kind. Since Russians first introduced RDE for the study of electrode reactions, it is not surprising that the first RDE results for chromium deposition came from Russians too. *Matulis and Mitskus*[241] did it galvanostatically while *Kazakov and Shluger*[107], and *Vagramiyan and Usachev*[242] used a potentiostatic method. Much later *Hoare*[172] and *Pletcher*[171] used a potentiodynamic method, where the time component is present (by changing potential with time in a linear fashion). This method can give us a more complete understanding of the kinetics involved.

Figures 54, 71, 87, 101 and 109 are I-ω relationships for 2.5 M CrO_3 Sargent bath (100:1) alone with 4 different additives. By close examination of Figure 54, it appears that the relationship is not linear as one would expect if process is limited only by diffusion but rather more complicated (dashed line). At higher rotation speeds (> 600 rpm) a decrease in current is observed compared to the one that would satisfy a linear dependence, indicating that an additional limitation of the current is present and caused by an additional step that precedes the deposition process itself. For this step it can be safely postulated that it involves precipitatioin/dissolutioin reactions in the liquid film that exist on the cathode surface and formation of electroactive complexes. If this process is of a first order with respect to the concentration of the sulphate, then current can be calculated according to the

Frumkin-Tedoradse equation:

$$\frac{1}{I} = \frac{1}{I_d} + \frac{1}{I_K} = \frac{1}{I_K} + \frac{1}{B\omega^{1/2}} \qquad <117>$$

where I is measured (maximum) current, I_d is a current determined only by the diffusion rate and I_K, current determined by kinetics of the preceding reaction. Taking into account that according to *Levich*[148], I_d is proportional to ω, while I_K is independent of it, it then follows from <117> that 1/I must be a linear function of ω. Figure 27 is taken from the results by Pletcher[171] for rotating Cr electrode experiments. He used a similar, 2 M CrO_3 bath containing 6, 4 and 2 mM of H_2SO_4.

Although Pletcher extrapolated the lines a, b, and c to zero, a closer look reveals a small intercept on the I axis. After replotting this figure in $1/I - 1/\omega^{1/2}$ form, Figure 28 is obtained. By analysing Figure 28, it follows that a linear relationship exists, at least at high speeds. From the slope of this curve, I_d can be determined for $\omega = 1$, and I_K can be obtained from the intercept. In a separate calculation, not presented here, I_d for $\omega = 1$ and I_K are calculated and plotted vs. concentrations of H_2SO_4 (0.02, 0.04 and 0.06- M/l) in the manner previously described, using the values from Figure 28. Straight lines were obtained for I_d and I_K, indicating that *both* currents are proportional to the concentration of the sulphates.

Perhaps a significant consequence of the previous analysis is that if we substitute for diffusion coefficient D values of 1 to $3 \cdot 10^{-5}$ cm^2/s. in the Levich equation for diffusion current under laminar flow:

$$I_d = 0.62\ n\ F\ D^{2/3}\ \nu^{i/6}\ \omega^{1/2}\ C \qquad <118>$$

the values of n (the number of exchangeable electrons for one molecule of sulphuric acid) are between 12 and 24. However, only Cr^{6+} ions are participating in the reduction process and only 3 electrons are consumed per each molecule of CrO_3 ($Cr^{6+} + 3e \rightarrow Cr^{3+}$). It follows that an average 4 to 8 molecules of CrO_3 participate in the reduction process. Since new results[29,30,32] proved that in a plating strength solution (2 -3 M), Cr^{6+} exist mostly in the form of trichromate ion ($HCr_3O^-_{10}$) with some bichromates and tetrachromates present, it could be reasonably assumed that on average about two molecules of polychromates are reduced as one molecule of sulphuric acid interacts with the cathode layer.

The dependence of maximum current on temperature is presented in Figure 29 for 25 and 50^0 C for 2.5 M (100:1) Sargent bath. Those two temperatures are chosen since they represent the usual range of temperatures used in chromium plating practice: 25° C is common in decorative (bright) chromium plating and 50^0 C in hard (engineering) chromium plating.

The importance of this figure is that kinetic current (whose inverted value is equal to the intercept on the Y axis) does not significantly depend on the temperature, i.e., maximum current, I, is mainly influenced by diffusion limitations, as apparent from difference in the slopes of lines a) (25^0 C) and b) (50^0 C) in Figure 29. This diffusion limitation of the current shows that sulphate is, at least temporarily, "consumed" on the cathode surface, which in turn can happen if electroactive complexes are formed between reduction reaction products and sulphates. It is reasonable to postulate that the stability of these complexes must be sufficient enough not to decompose while they are present in the layer (L-film) which they will eventually leave, decompose and liberate sulphate from the complex again, this time complex as a complex with the Cr^{6+} ions from the polychromates ions from the bulk of the solution. In the matter of a few seconds a steady state will be reached.

On the other hand, at lower rotation speed (higher $1/\omega^{1/2}$ values), diffusion processes to and from the cathode are slowed down and Cr^{3+} complexes formed and present in the L-film may decompose even before they leave the diffusion layers. Sulphates released from the complex are available again to react with Cr^{3+} that is continuously forming at the cathode causing an increase in the demand for the current. The result of this is higher value of maximum current compared to those that would be expected from diffusion limitations only, indicating the influence of the kinetic limitations. This is demonstrated by the appearance of the deflection in low range and by higher values for the I_K (manifested as the intercept).

Influence of the sweep rate (ν) is presented in Figures 30 and 36-43 for the stationary conditions. As clearly demonstrated in Figures 30-42, as the ν is increased from 10 to 142 m V/s, the maximum current on reverse scans is increased from about 100 mA/cm^2 to about 220 mA/sm^2. This indicates that L-film at faster rates does not have time to be dissolved and that it remains on the cathode surface, resulting in an increase of the

current. On the forward scan with higher *v*, the maximum currents are higher, but potentials of the first rising branch on LPC scans the $Cr^{6+} \rightarrow Cr^{3+}$ reaction (e.g., denoted as region I in Figure 26 for line 1) starts as the more negative potential and reaches the maximum negative potential (~ -0.75 V) at 142 mV/s (Figure 42), compared to -0.65 V at 10 mV/s (Figure 36). The position of the second raising branch (region II) for the same reaction does not depend on the potential. The transition from the first to the second branch, where formation of L-film occurs, has a portion where current is unchanged, irrespective of the increase in the negative potential at low sweep rates (represented with double arrows in Figures 36 and 37). In the same transition area, there are minimum and maximum peaks, faintly recognisable in e.g. Figure 38 (single arrow), and more clearly in Figure 26 for line1.

Referring to Figure 43, it can be seen that for the low sweep rates (10 and 20 mV/s), not only the beginning of the first rising section of the polarisation curve it starts at considerably more positive potentials but also the maximum current peaks (beginning of L-film formation) are of the lower values and shifted toward less negative potentials.

At high sweep rates, or in other words, for short reaction periods, L-film is not completely removed and on the next sweep, more of the products of $Cr^{6+} \rightarrow Cr^{3+}$ incomplete reductions are accumulated, resulting in the elongation of the first raising sections on the voltammograms and the increase in the maximum current.

Considerable increase in the maximum current with the sweep rate indicates that *time* has a definite influence on the Cr^{6+} incomplete reduction, and also potential plays a role in the formation of the L-film. One of the arguments in favour of this is the increase the rate of *decrease* of the current with the shift of the potential toward a higher negative side (steeper slopes on the descending side of L-film formation region). The other argument is appearance of several maximums and minimums in the L-film region observed on some metals (e.g., gold[227,243,244] where oxide surface film is absent) where $Cr^{6+} \rightarrow Cr^{0}$ reduction begins at more positive potentials than with chromium and multiple peaks are a result of partial dissolution of the film as a result of its instability, caused in turn by the insufficiently negative potential. In the case of the chromium cathode, L-film instability and destruction causing formation of multiple peaks appears to depends on the sweep rate. It could be reasonably supposed that at the higher rates ($\upsilon > 142$ mV/s), film destruction

can be attributed to its insufficient quantity and at the low sweep rates (longer formation time) e.g., υ < 10 - 20 mV/s, increase in films quantity is more than offset with not enough negative potentials and film destruction (dissolution) is possible.

In the intermediate region of the negative potentials, a horizontal plateau is present where film is not removed and it is independent of the potential. The quasiequilibrium between potentials applied in this region and the time of the L-film formation exists.

The third argument that supports this reasoning about the L-film (in) stability and its partial destruction comes from observation that multiple maximums and minimums can be obtained, not only with the change of the sweep rate but also with the changes of the catalyst (e.g. H_2SO_4) concentration and the rotation speed. The influence of catalyst concentration and cathode rotation speed on L-film is going to be further analysed in section II.4.3.3

In Figures 36-43, the cyclic voltammograms for Sargent bath as a function of the scan rate (v) are presented. When scanning the potential of the Chromium electrode in the negative and reverse directions, the cathodic peaks on the voltammograms show that the I (or often denoted as I_m) the maximum rate of reduction of Cr^{6+} to Cr^{3+}) increases with the increase of scan rates and the rotation speed.

Figures 28, 29, 43, 49, 53, 54 (dashed line) and 108 show that maximum current I is not a linear function of the scan rate (v) and of the electrode rotation rate (ω) in all ranges under investigation. It is clear from these experiments and previous discussion that the electrochemical reaction: $Cr^{6+} \rightarrow Cr^{3+}$ is not only under diffusion control for the given set of experimental conditions as often claimed in the literature. It is known that the maximum cathodic peak on voltammograms characterises the reduction of Cr^{6+} to Cr^{3+} on the chromium electrode. However, neglecting to consider the chemical reaction within the cathode film and ignoring the presence of small but definite component of the kinetic current could lead to less complete understanding of this obviously complex phenomena.

Preliminary LPS cyclic voltammograms for four different catalysts are presented in Figures 30-35 under potentiodynamic conditions (v = 70 mV/s). When analysing them it can be seen that upon scanning the potential from -1200 mV to -900 mV, the current decreases sharply and only one distinct cathodic peak occurs at the potential of -750 mV corresponding to the reaction $Cr^{6+} \rightarrow Cr^{3+}$. With further decrease of the cathodic potentials

to 0.0 mV and at the anodic potentials, no additional peaks were observed. On the reverse scan from +125 mV to -1200 mV, the cathodic peak at the potential of -750 mV is absent, due to the chromium surface passivation after anodic dissolution of the L-film. The shape of voltammograms and the magnitude of the cathodic peaks, as shown in Figures 30-35 changes with the nature of additive. To obtain more insight on the cathodic processes , the additional, following experiments were done to investigate in more detail the influence of the different additives concentrations on the shape of voltammograms and the current peaks corresponding to the maximum cathodic current . The cyclic voltammograms were scanned at potentials between -200 and -1200 mV. The potential scanning starts at -200 mV.

Different additives will be discussed separately in more detail in the sections that follow .

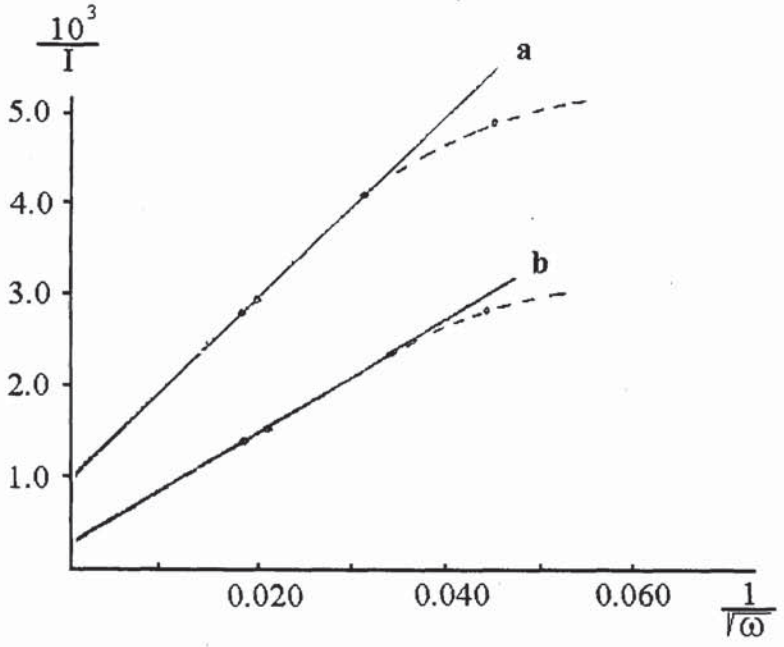

Figure 29. Relationship between maximum current and rotation speed for 2.5 M Sargent bath (100:1) at **a**) 25° C and **b**) 50° C. Data from Table 41.

Plating Bath	ω	$\omega^{-1/2}$	I	$10^3/I$	-E vs SCE (mV)
a) Sargent Bath 25° C	500	0.044	202	4.95	643
	1000	0.030	248	4.05	645
	2000	0.022	308	3.24	647
	2500	0.020	334	2.99	643
	3000	0.018	342	2.92	640
b) Sargent Bath 50° C	500	0.044	350	2.85	623
	1000	0.030	450	2.22	625
	2000	0.022	590	1.78	624
	2500	0.020	625	1.60	626
	3000	0.018	710	1.487	620

Table 41. Cathodic peak current density I (mA/cm^2) measured on Cr electrode and obtained from cyclic voltammograms at 25° and 50° C as a function of the rotation rate ω (rpm). Scan rate v = 40 mV/s.

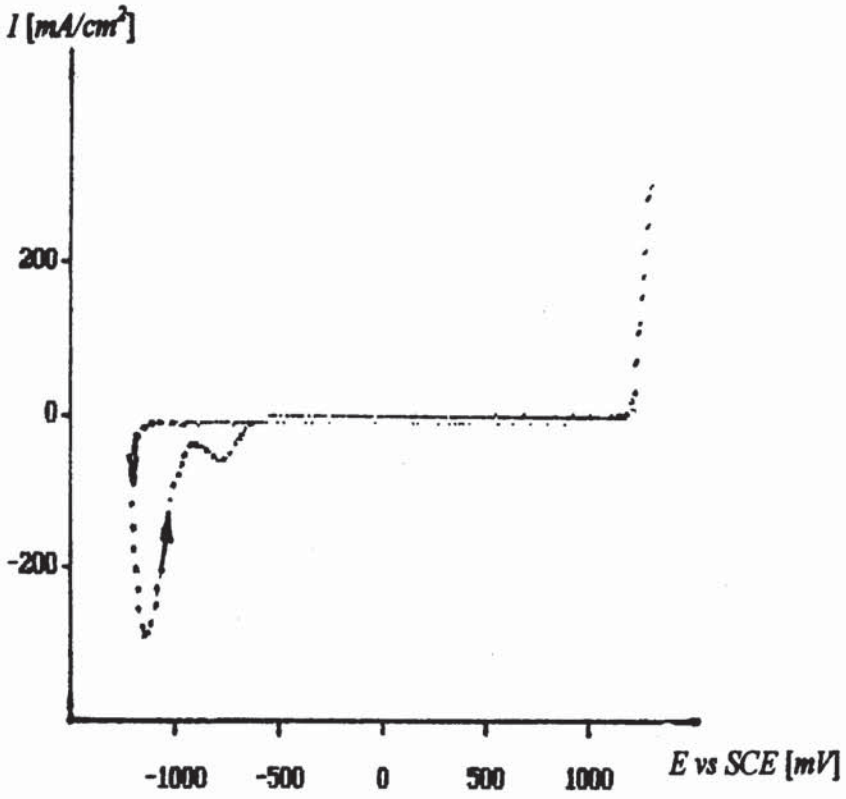

Figure 30. CrO_3 250 g/L; H_2SO_4 250 g/L; ω = 0 rpm; v = 70 mV/s.

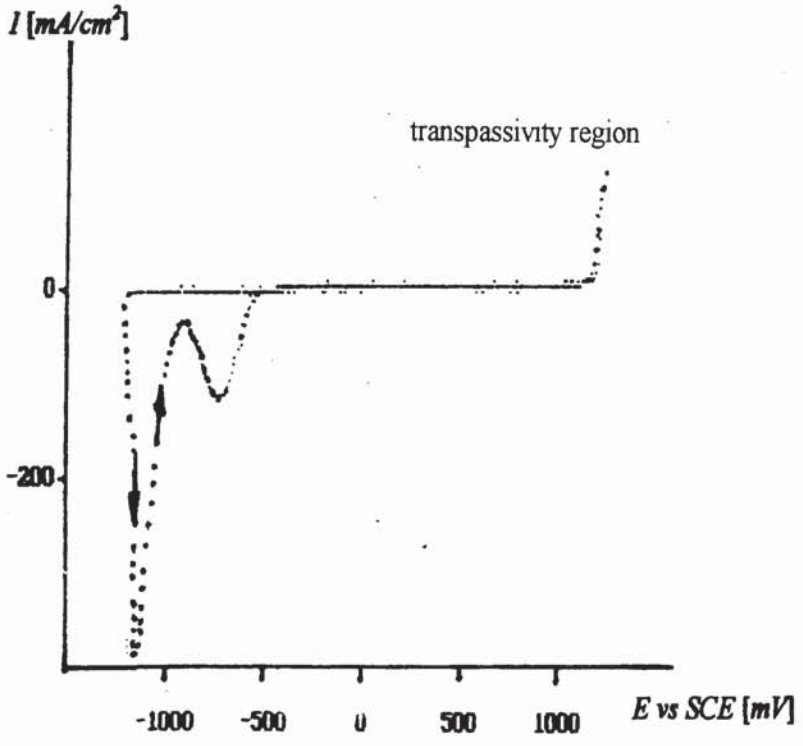

Figure 31. CrO_3 250 g/L; H_2SO_4 250 g/L; ω = 2000 rpm; v = 100 mV/s.

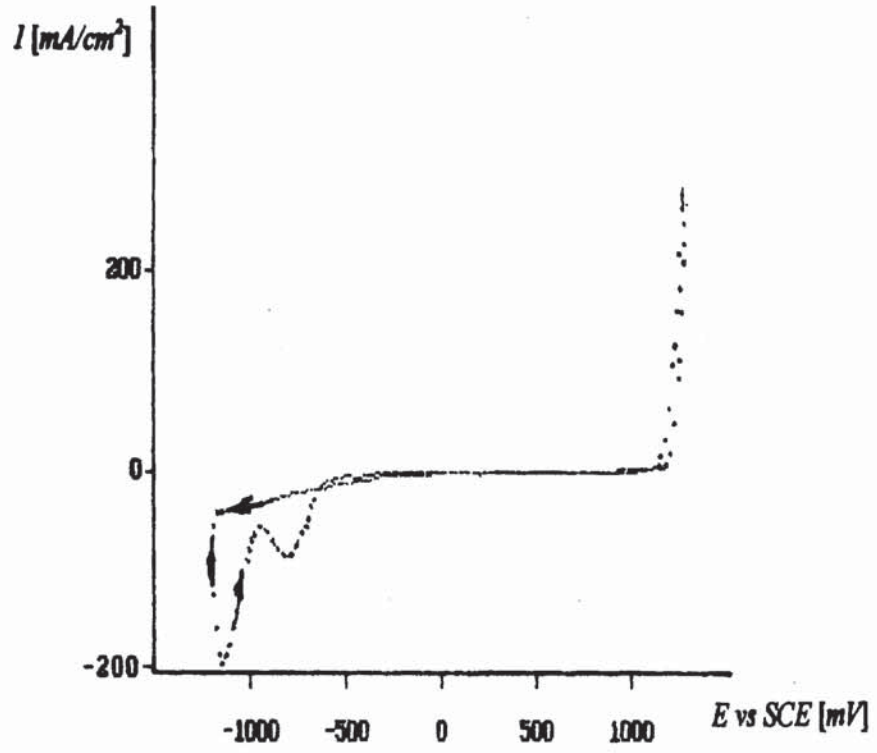

Figure 32. CrO_3 250 g/L; H_2SO_4 2.5 g/L; HEEF-405 5.0 g/L; v = 70 mV/s.

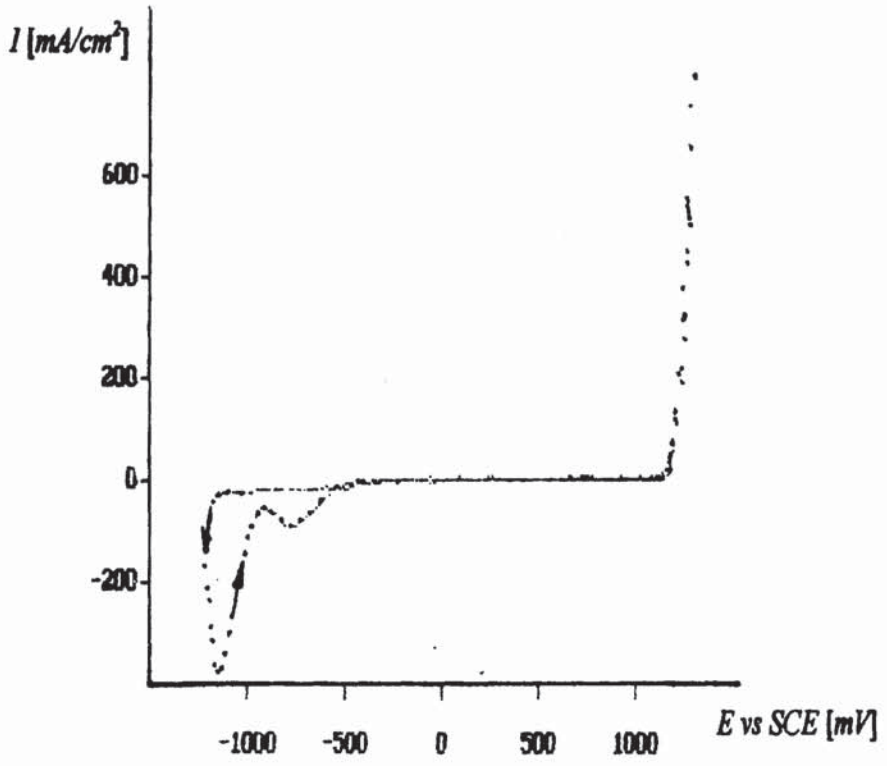

Figure 33. CrO_3 250 g/L; H_2SO_4 2.5 g/L; HEEF-25 5.0 g/L; v = 70 mV/s.

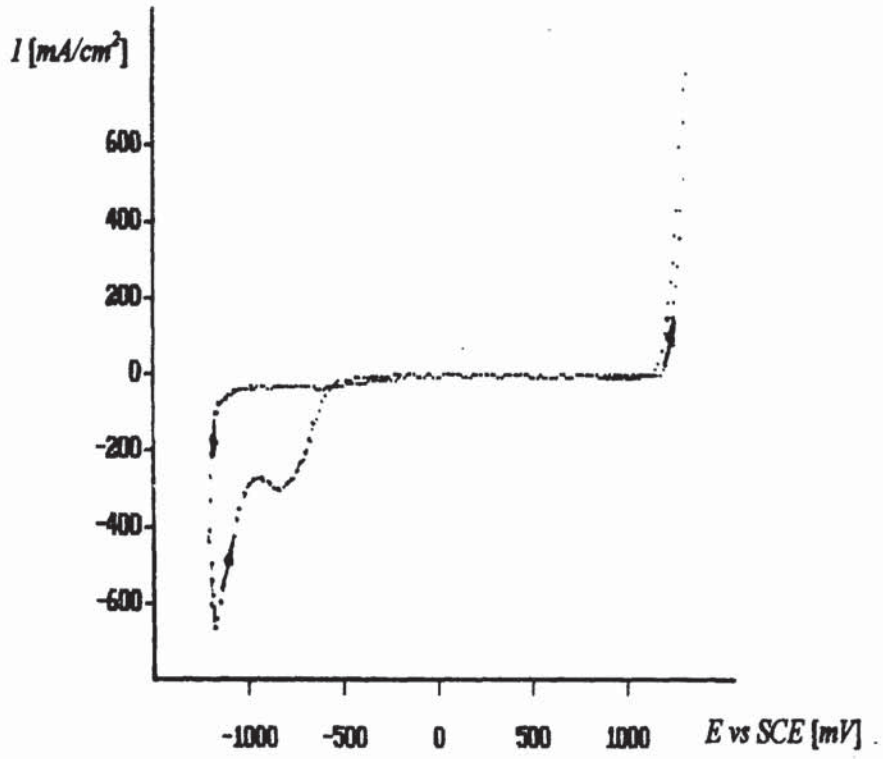

Figure 34. CrO_3 250 g/L; H_2SO_4 2.5 g/L; SSA 5.0 g/L; v = 70 mV/s

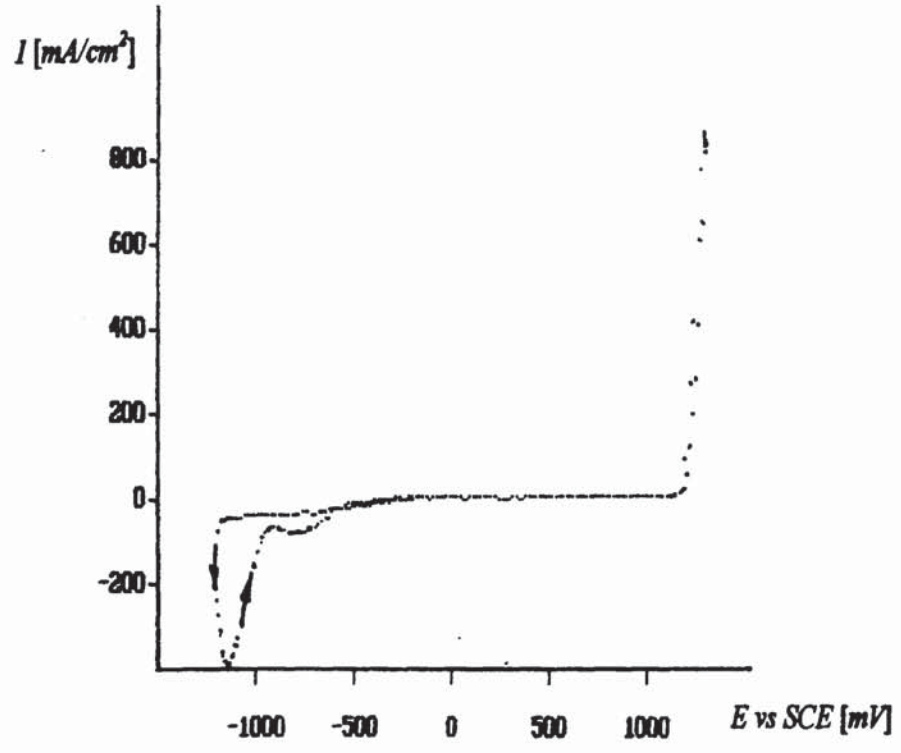

Figure 35. CrO_3 250 g/L; H_2SO_4 2.5 g/L; MSA 5.0 g/L; v = 70 mV/s.

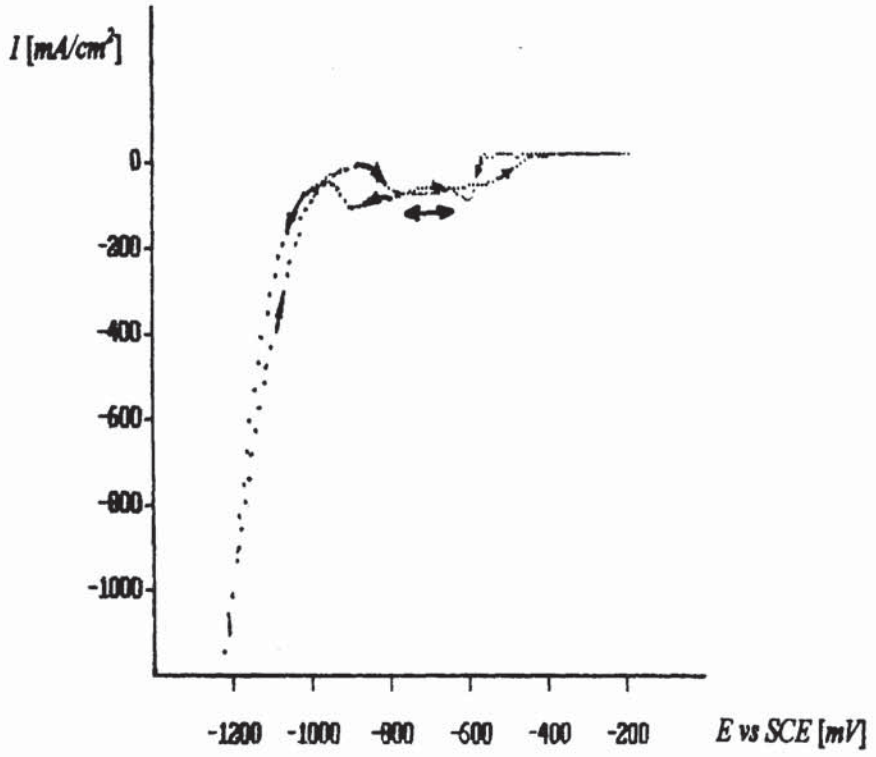

Figure 36. CrO_3 250 g/L; H_2SO_4 2.5 g/L; ω = 0 rpm; v = 10 mV/s.

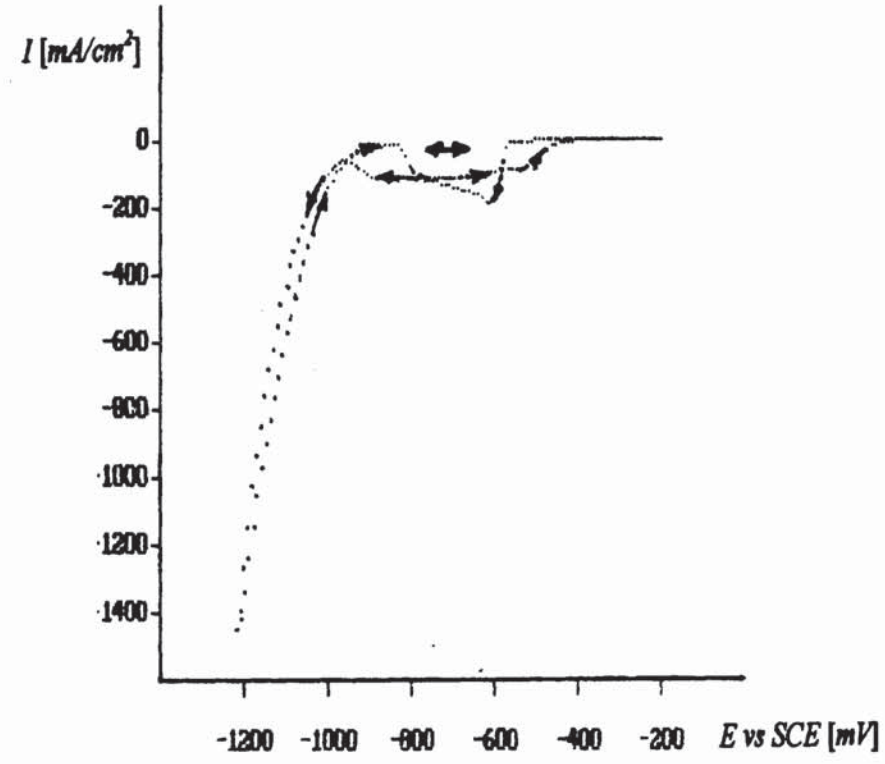

Figure 37. CrO_3 250 g/L; H_2SO_4 2.5 g/L; ω = 0 rpm; v = 20 mV/s.

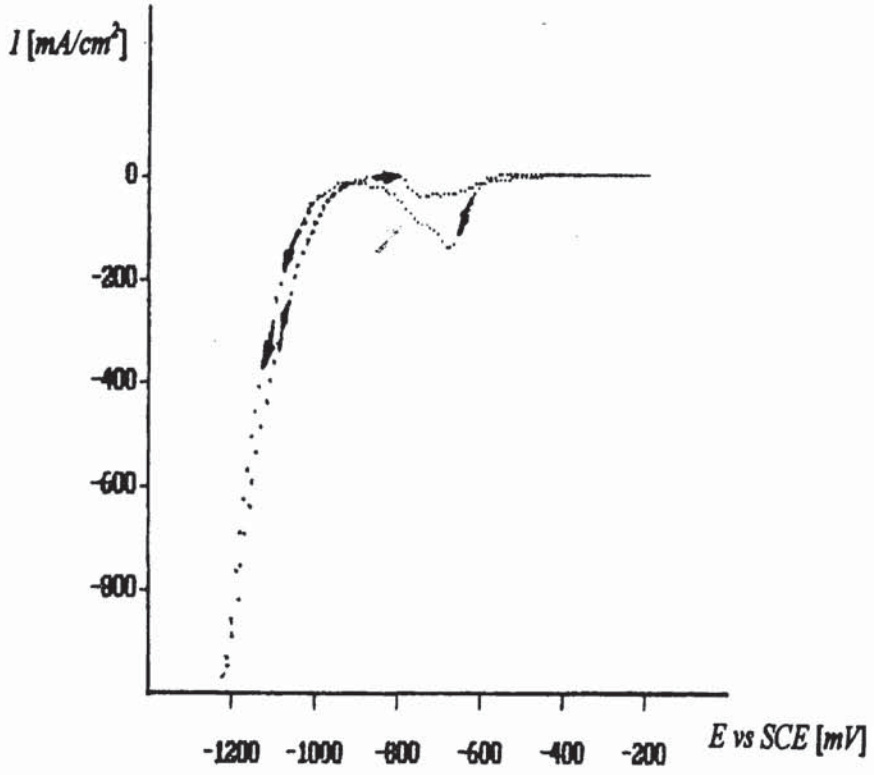

Figure 38. CrO_3 250 g/L; H_2SO_4 2.5 g/L; ω = 0 rpm; v = 40 mV/s.

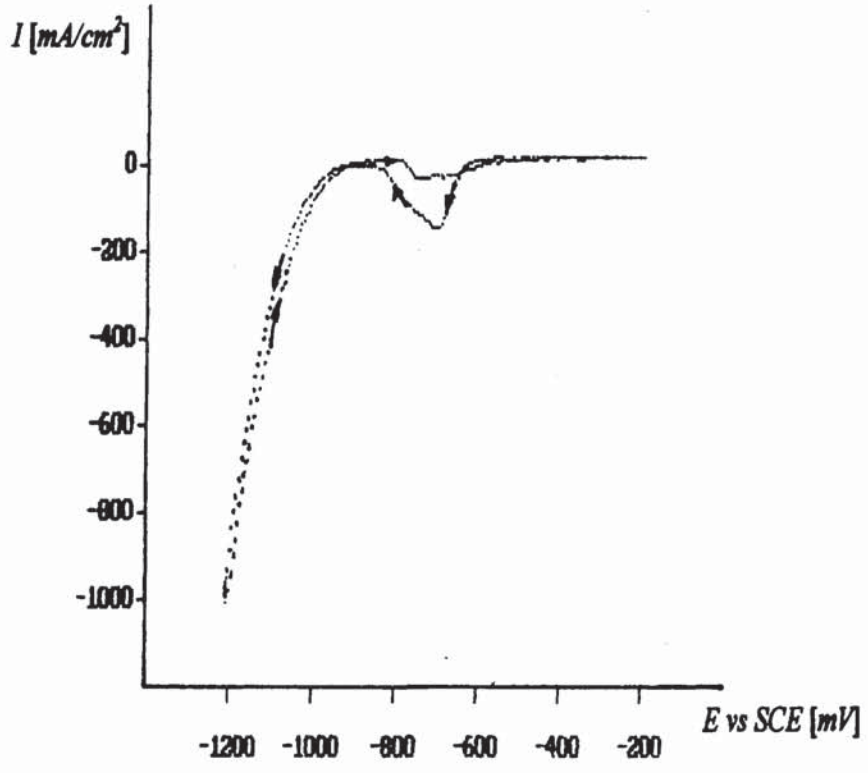

Figure 39. CrO_3 250 g/L; H_2SO_4 2.5 g/L; ω = 0 rpm; v = 58 mV/s.

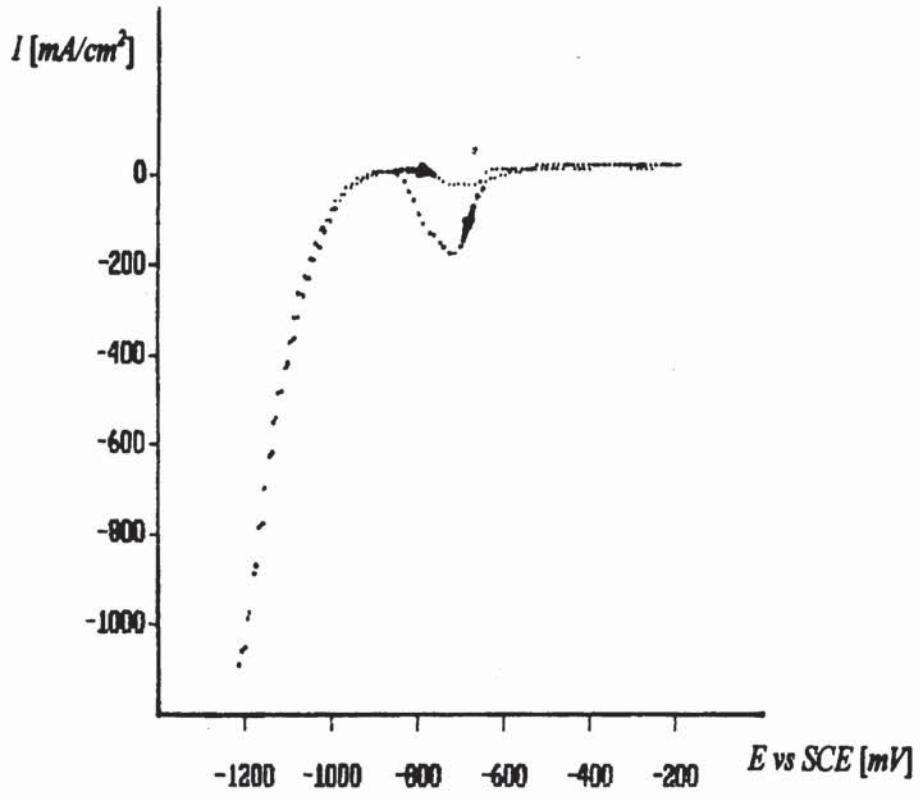

Figure 40. CrO_3 250 g/L; H_2SO_4 2.5 g/L; ω = 0 rpm; v = 83 mV/s.

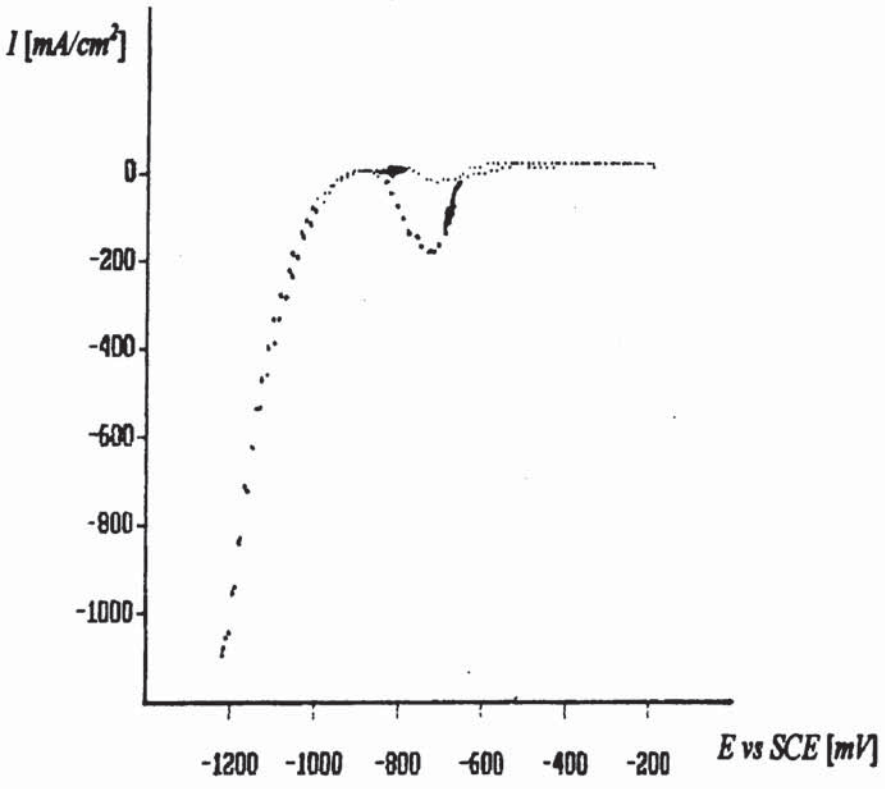

Figure 41. CrO_3 250 g/L; H_2SO_4 2.5 g/L; ω = 0 rpm; v = 100 mV/s.

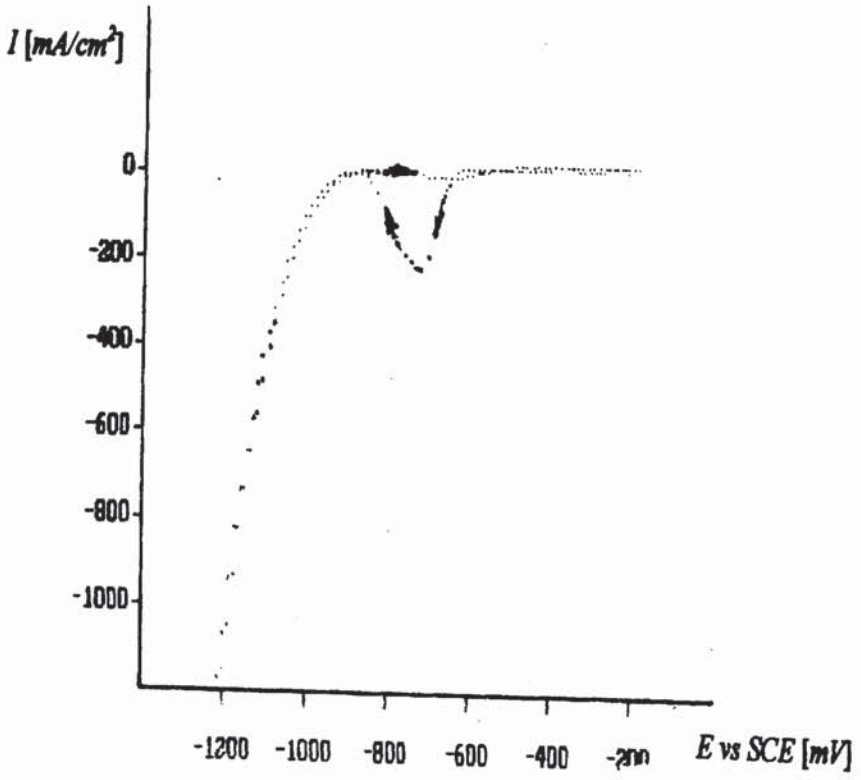

Figure 42. CrO_3 250 g/L; H_2SO_4 2.5 g/L; ω = 0 rpm; ν = 142 mV/s.

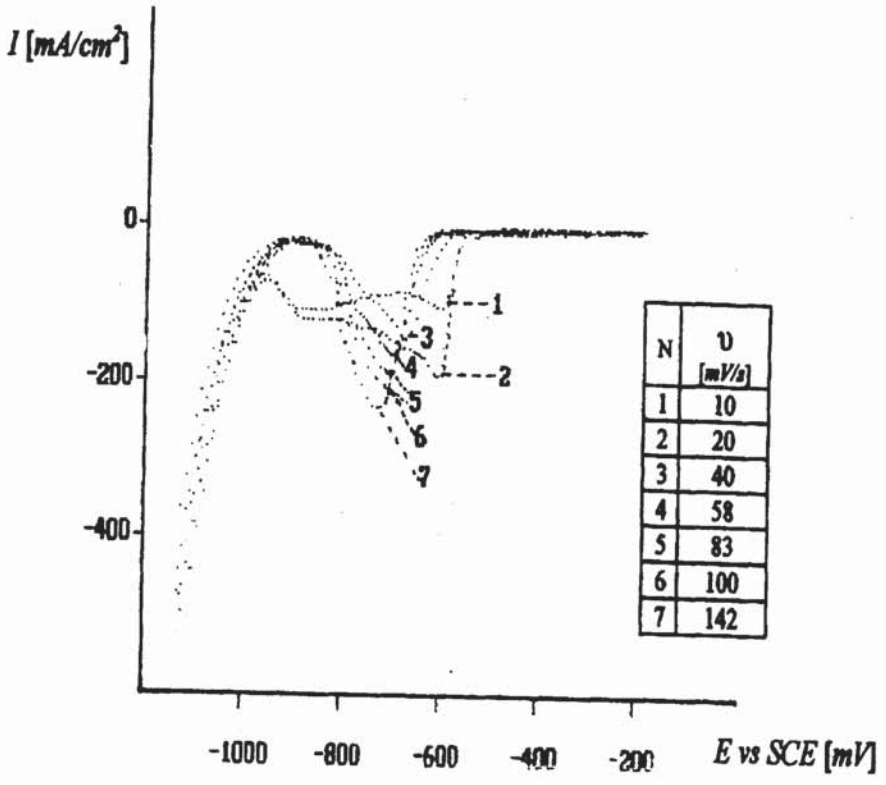

Figure 43. CrO_3 250 g/L; H_2SO_4 2.5 g/L; direction from -200 mV/s to -1200 mV/s.

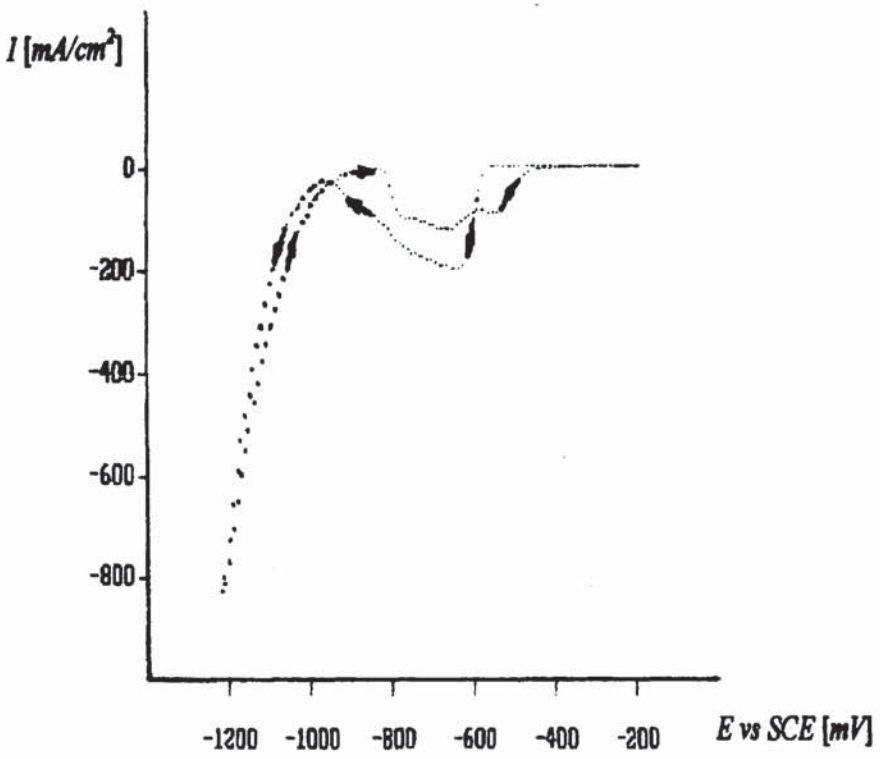

Figure 44. CrO_3 250 g/L; H_2SO_4 2.5 g/L; ω = 500 rpm; v = 40 mV/s.

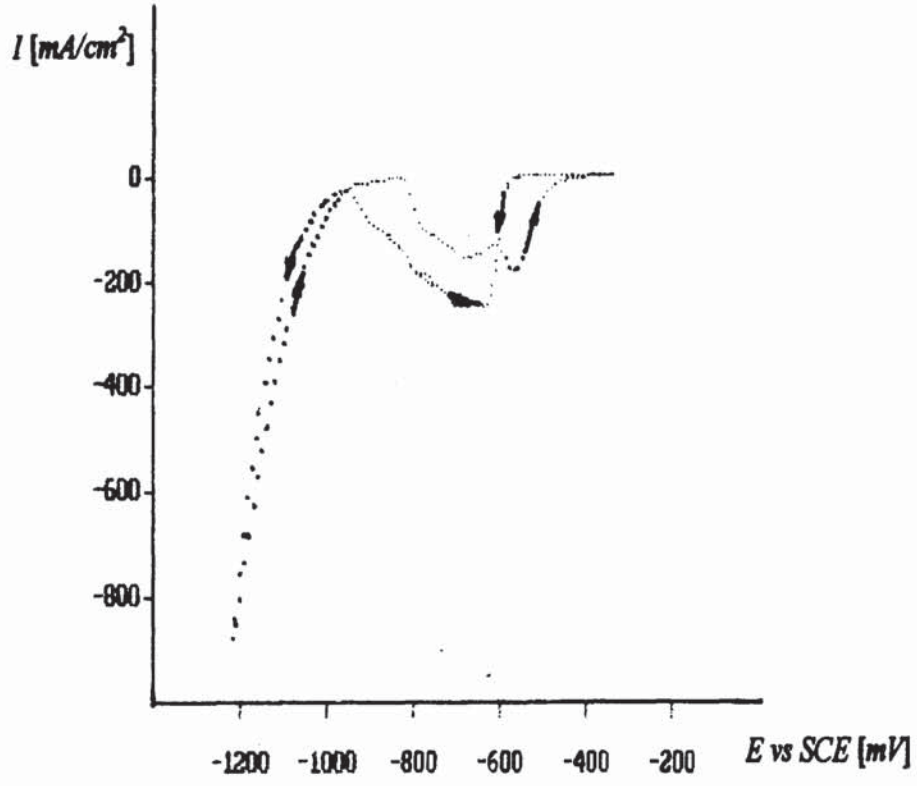

Figure 45. CrO_3 250 g/L; H_2SO_4 2.5 g/L; ω = 1000 rpm; v = 40 mV/s.

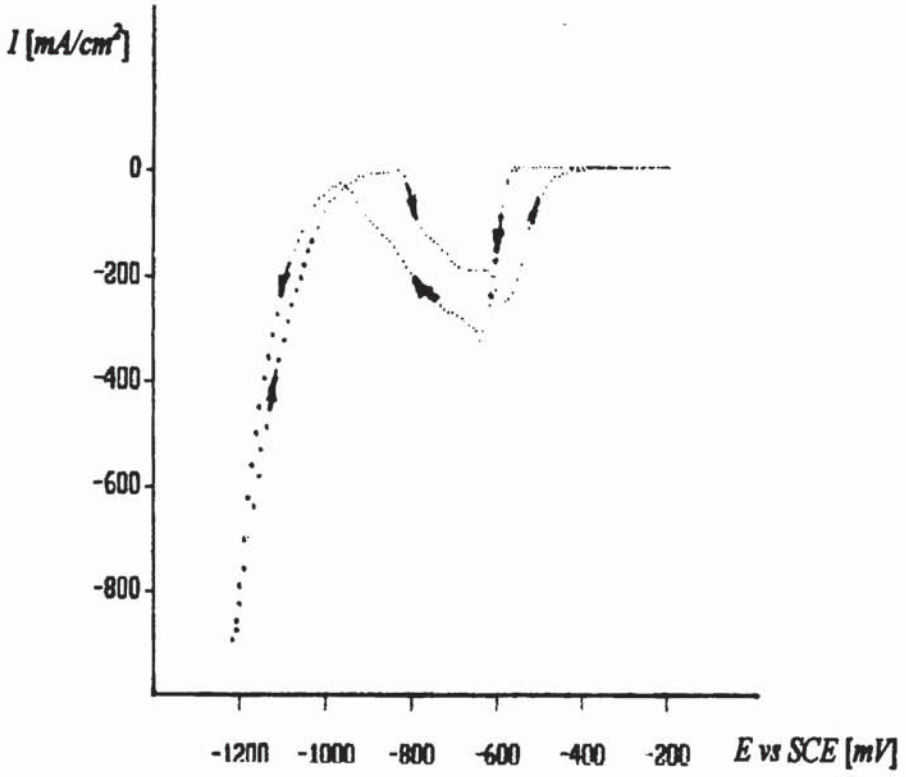

Figure 46. CrO_3 250 g/L; H_2SO_4 2.5 g/L; ω = 2000 rpm; ν = 40 mV/s.

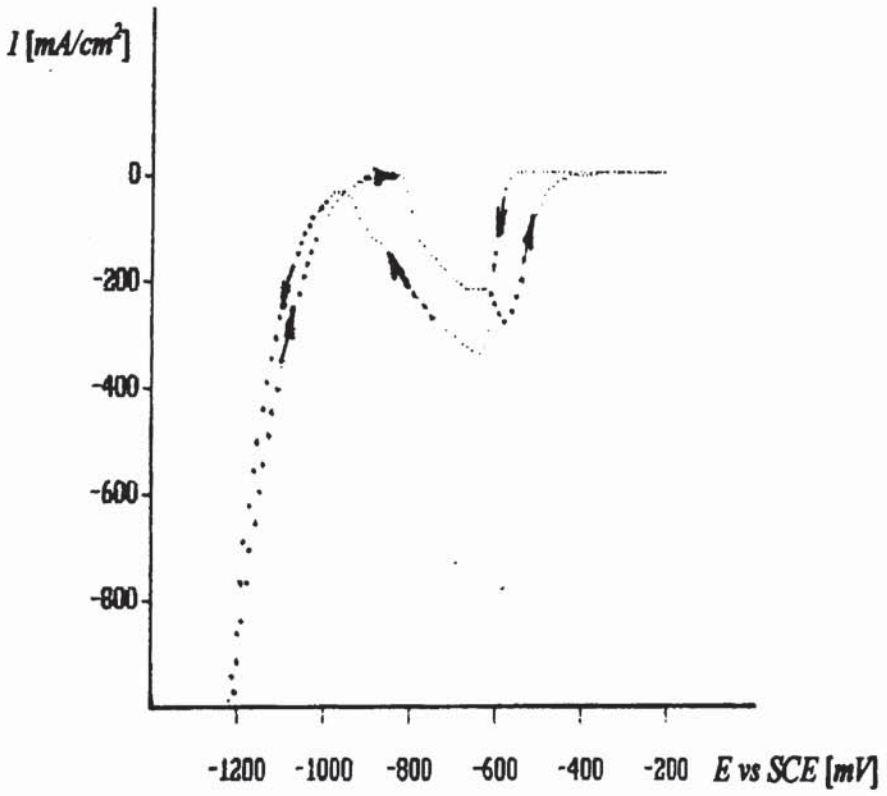

Figure 47. CrO_3 250 g/L; H_2SO_4 2.5 g/L; ω = 2500 rpm; ν = 40 mV/s.

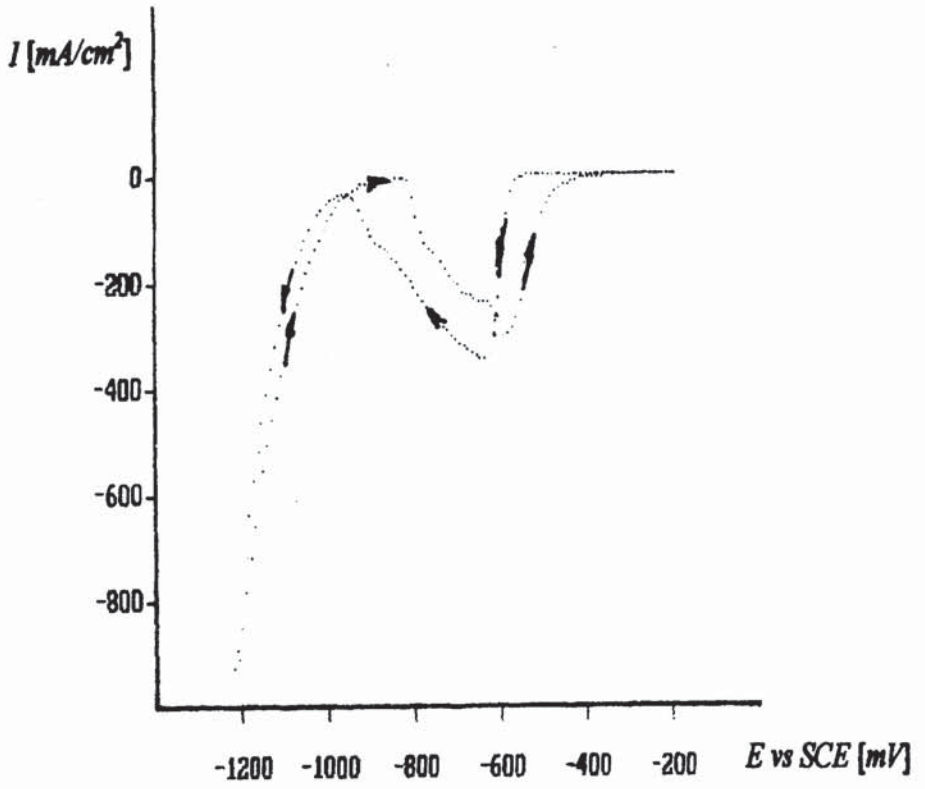

Figure 48. CrO_3 250 g/L; H_2SO_4 2.5 g/L; ω = 3000 rpm; v = 40 mV/s.

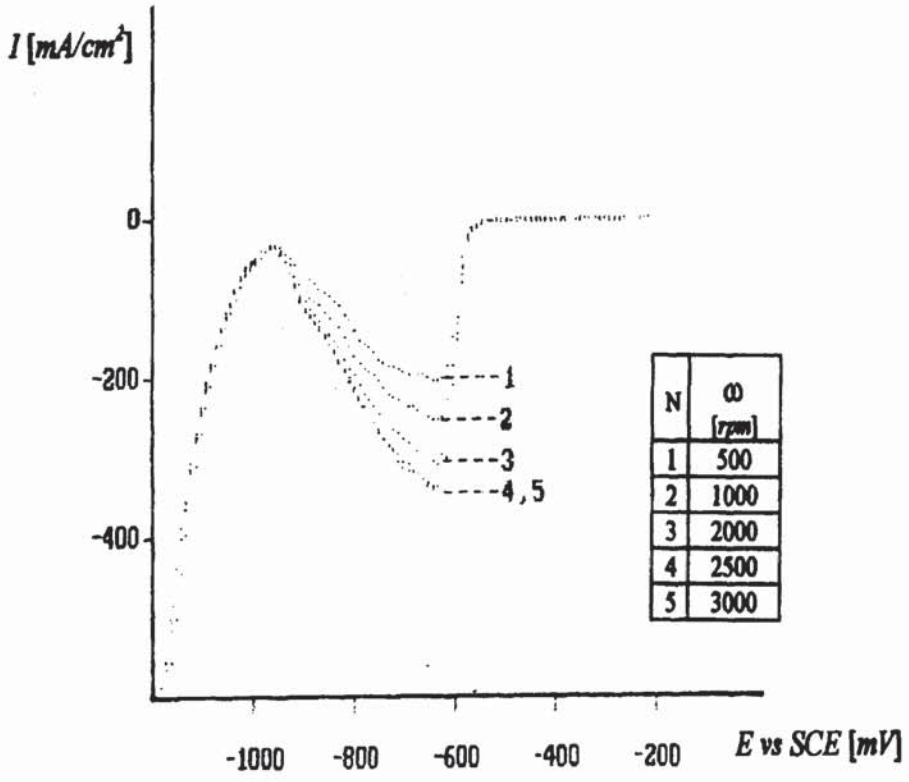

Figure 49. CrO_3 250 g/L; H_2SO_4 2.5 g/L; v = 40 mV/s; from -200 mV to-1200 mV.

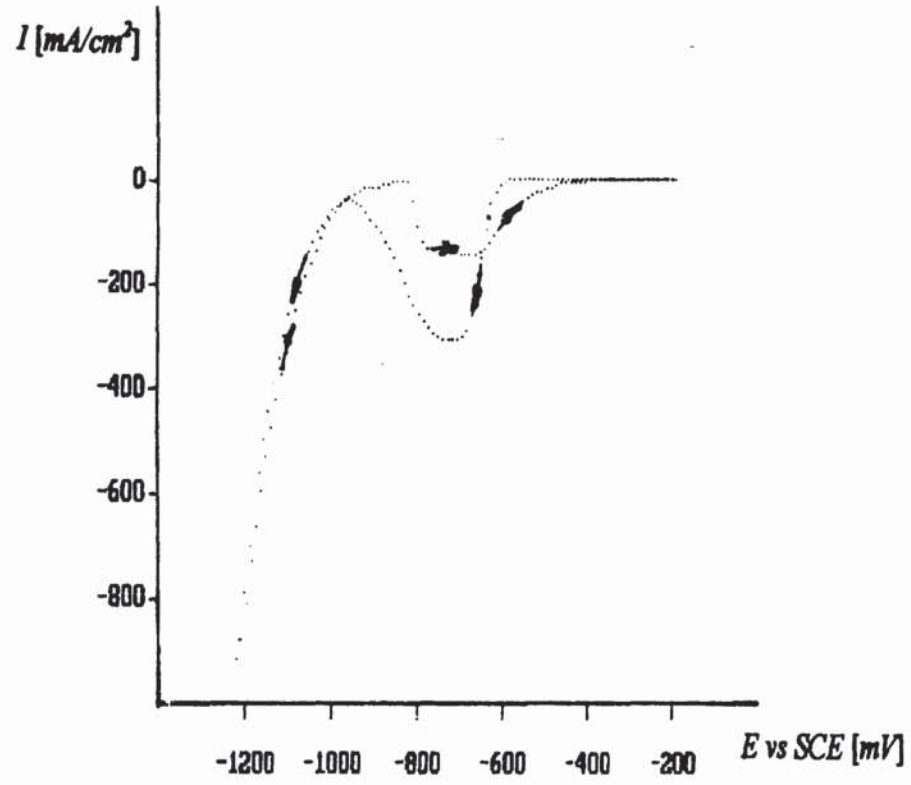

Figure 50. CrO_3 250 g/L; H_2SO_4 2.5 g/L; ω = 2000 rpm; ν = 58 mV/s.

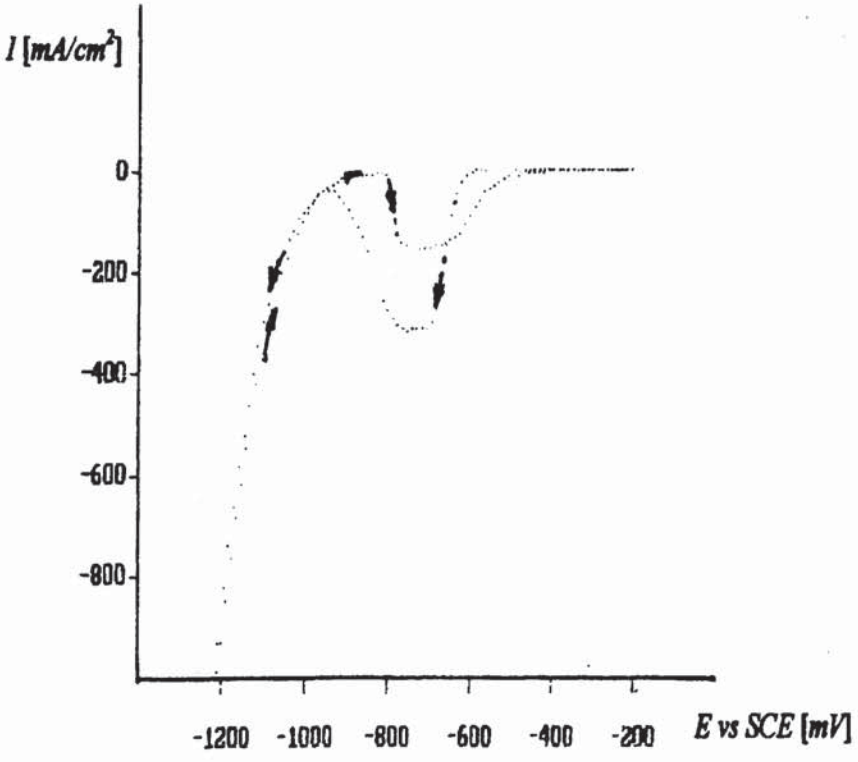

Figure 51. CrO_3 250 g/L; H_2SO_4 2.5 g/L; ω = 2000 rpm; ν = 83 mV/s.

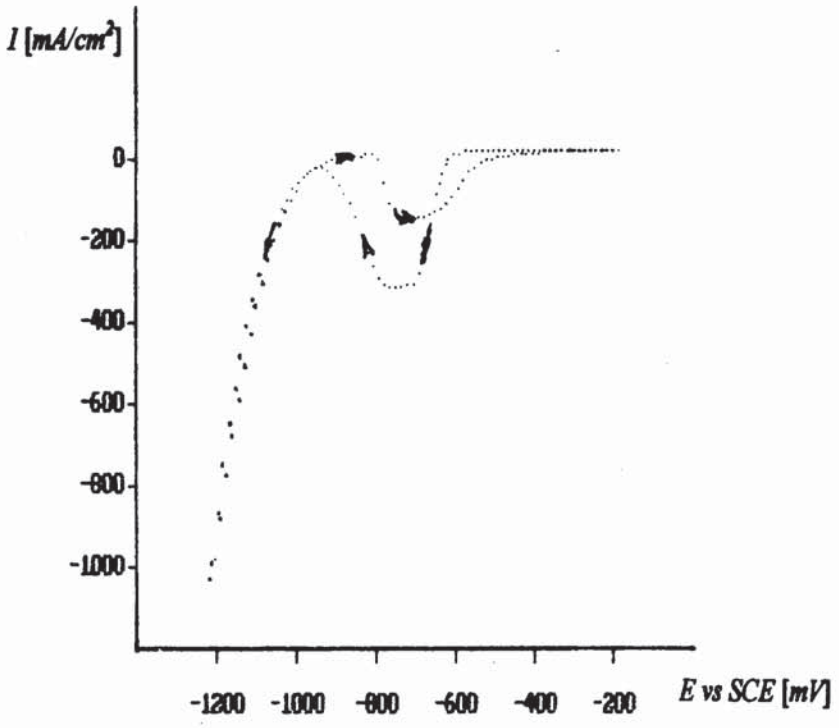

Figure 52. CrO_3 250 g/L; H_2SO_4 2.5 g/L; = 2000 rpm; v = 100 mV/s.

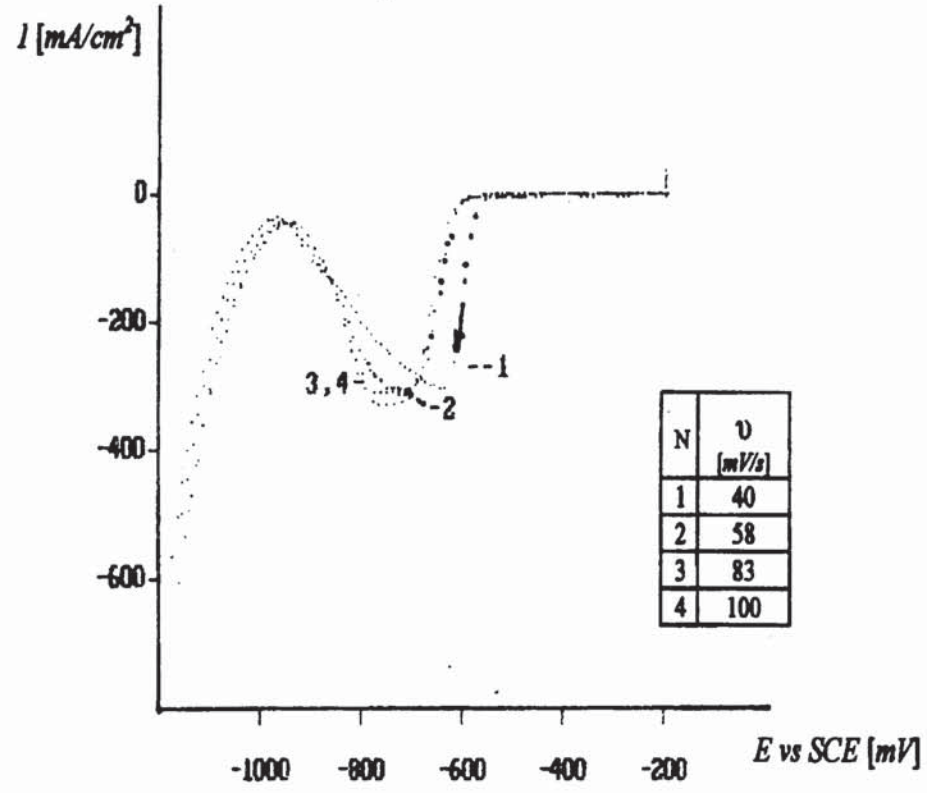

Figure 53. CrO_4 250 g/L; H_2SO_4 2.5 g/L; ω = 2000 from -200 mV to -1200 mV.

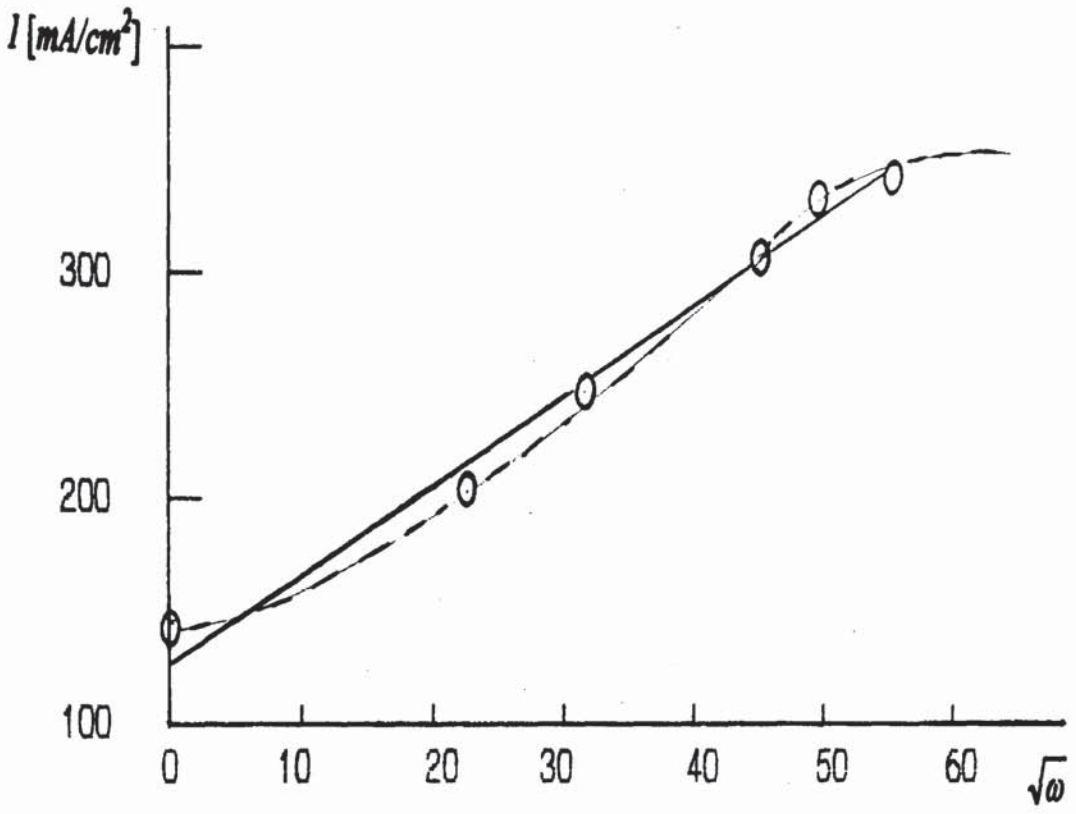

Figure 54. I as a function of $\sqrt{\omega}$ for Sargent Bath. at v = 40 mV/s. Data from Table 9.

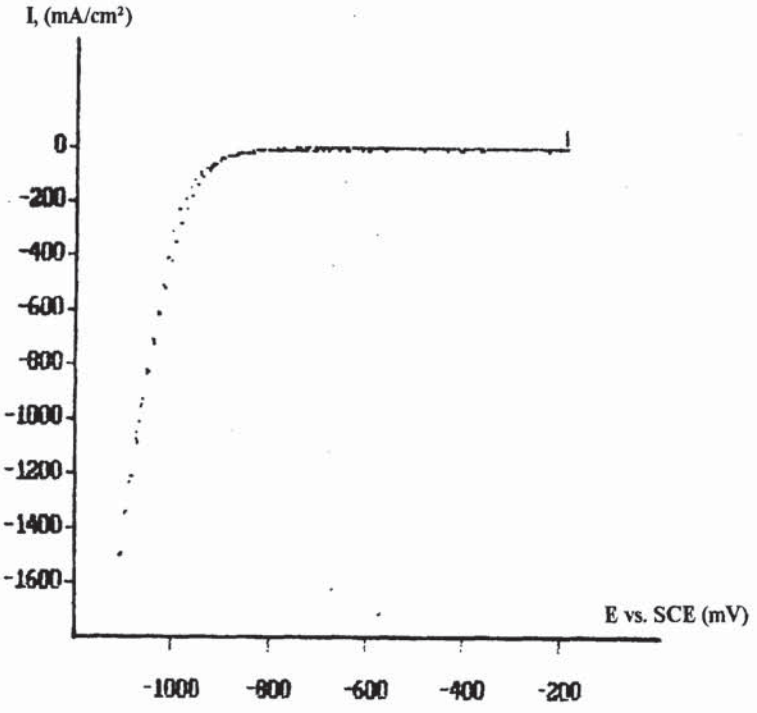

Figure 55. CrO_3, 250 g/L; H_2SO_4, 2.5 g/L; ω = 0 rpm; v = 56 mV/s.; T = 55° C.

2. *HEEF-405 bath*

i. Peculiarity of dissolution:

During the addition to Sargent Bath, the HEEF-405 additive forms at first black clots and then black powder. Spot test analysis indicated presence of iodine compound. The black powder immediately dissolves in the hot Sargent bath, turning it dark. It is clear that the colour transformation of the HEEF-405 may be a result of a redox process during iodine dissolution in the bath. A Raman Laser Spectrographic analysis is presented in Appendix V, displays a peak at 808 cm^{-1} which is the identifying characteristic for IO^{-}_{3} ion. This confirmed that HEEF-405 contains iodine compound.

ii. *The Description of the Linear and Cyclic Linear Potential Polarisation Plots.*

Unlike Sargent Bath, the cathodic wave appears only during scanning of the potential in the negative direction; on the reverse scan, no current is observed (Figures 61 and 70). The cathodic peak decreases with an increase of HEEF-405 concentration.

HEEF-405 as secondary catalyst at 5.0 g/ℓ and 20^0 C is presented in Figures 56-60 for stationary conditions. Four scan rates were investigated (v = 10, 20, 40 and 58 mV/s.) and presented separately in Figures 56-59 and together in Figure 60.

In Figure 61 the influence of increased temperature (20 vs. 55^0 C) is presented for the stationary electrode for two different scan rates (56 and 100 mV/s.). The influence of lower concentration (2.5 g/ℓ.) is presented in Figures 62-63 and together in Figure 64 for v = 10, 40 and 142 mV/s.

For 1.25 g/ℓ two scan rates (v = 10 and 142 mV/s.) are presented separately in Figures 65-66 and together in Figure 67. The effect of scan rate ($v^{1/2}$) on a cathodic peak for all three different concentrations (1.25, 2.5 and 5.0 g/ℓ)are presented in Figure 70 and compared with Sargent Bath, whereas in Figure 108 all four additives are compared at 5.0 g/ℓ..

Figures 68 and 69 are LPP voltammograms representing the hydrodynamic influence of different rotation speeds at v = 40 and 100 mV/s. Figure 71 shows the relationship of rotation rate ($\omega^{1/2}$) and the cathodic peak at v = 40 and 100 mV/s. for this additive as compared with Sargent Bath at v = 40 mV/s.

iii. Discussion.

The drastic increase of the cathodic Current Efficiency in the bath with HEEF-405, resulted from the composite effect of one, two or three parallel reactions occurring on the chromium electrode. Cyclic voltammograms presented, characterise the influence of this additive only on the first reaction: $Cr^{6+} \rightarrow Cr^{3+}$ (the cathodic peak at -750 mV). It is impossible to draw definite conclusions of the additive influence on the other two reactions ($2H^+ + 2e = H_2$ and $Cr^{6+} \rightarrow Cr^0$) that occur during the chromium electrodeposition at the steady state by using only the Voltammetry. Therefore, additional methods have to be applied for investigating the influence of this additive on the other two reactions that follow.

The I - $v^{1/2}$ curve for different concentrations of HEEF-405 has a complex shape (Figure 70). It contains two linear sections for 2.5 and 5.0 g/L. The cathodic current was constant at sweep rates ranging from 10 to 40 mV/s, and then increased as the scan rate increased from 40 to 142 mV/s. Figures 57, 58 and 60 show that I- $v^{1/2}$ curves have a different slope at v = 40 mV/s and at v = 142 mV/s. Thus at v = 40 mV/s , I is a linear function of $v^{1/2}$ between 500 -2000 rpm but decreases with an increase in rotation from 2000 to 3000 rpm indicating an influence of kinetic control. At v = 142 mV/s, I is a linear function of v as in the case of Sargent bath.

Since the peak current I in the HEEF-405 bath is not always a linear function of v and of ω, it follows that the diffusion process in the electrolyte is complicated by the formation of the cathode film of a rather complex nature, (L-film) on the electrode surface between 750 and 950 mV. The L-film consists of products of the incomplete reduction of Cr^{6+} to Cr^{3+} that are accumulating on the electrode surface (as explained in detail in section I.2). In chromium plating baths containing catalysts, in general, during scanning of the potential in both directions the cathodic peak at -750 mV is usually observed. When scanning the potential from -1200 mV to -900 mV, the L-film dissolves and the reaction $Cr^{6+} \rightarrow Cr^{3+}$ starts at -750 mV on the chromium electrode surface.

It will be seen later that in the presence of MSA, when scanning the potential in the reverse direction from -1200 mV to -200 mV, the reaction $Cr^{6+} \rightarrow Cr^{3+}$ is also absent. The reason for it is the stability of the L-film, which does not dissolve at these potentials. This phenomena may be explained by the structure, adsorptive properties and density of the L-film. The film "blocks" the electrode surface and hinders the reaction: $Cr^{6+} \rightarrow Cr^{3+}$ from occurring. Similar phenomenon, absence of the cathodic wave, takes place in the bath with HEEF-25 as additive, indicating indirectly that this additive contains an alkyl-sulphonic

acid. Raman laser spectroscopy confirmed the presence of Hydroxy-ethane sulphonic acid (trade name Isothionic acid) as an ingredient in HEEF-405, The analytical results are presented in Appendix V.

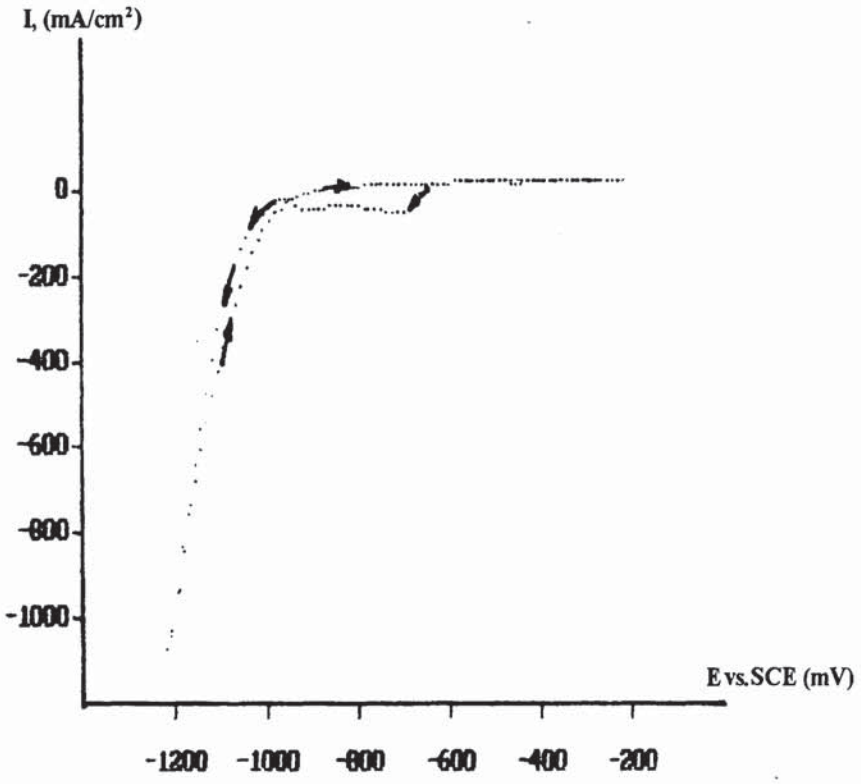

Figure 56. CrO_3 250 g/L; H_2SO_4 2.5 g/L; HEEF-405 5 g/L; ω = 0 rpm; v = 10 mV/s.

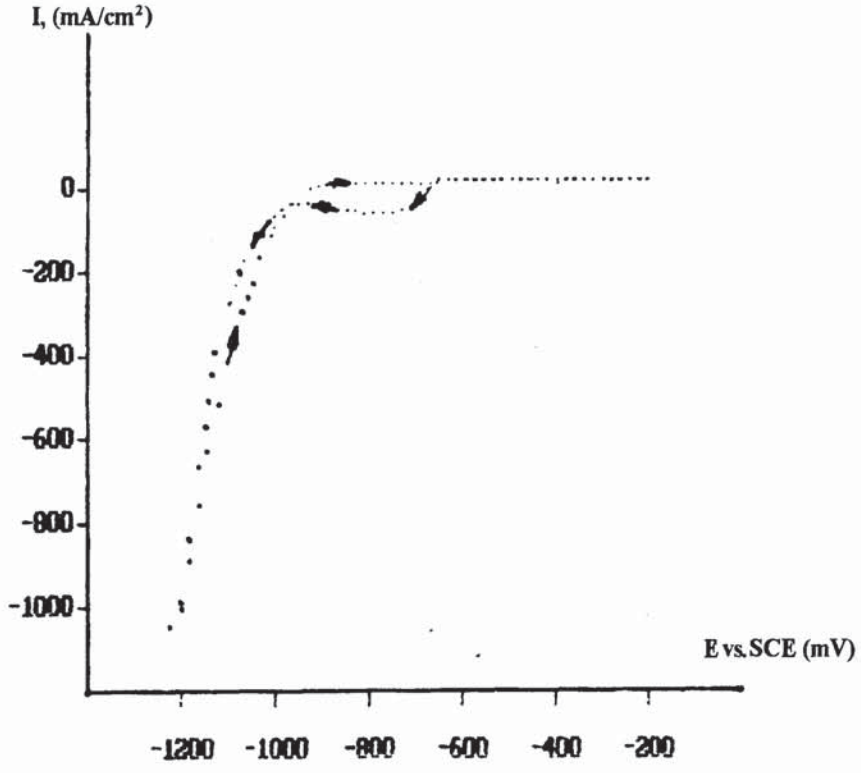

Figure 57. CrO_3 250 g/L; H_2SO_4 2.5 g/L; HEEF-405 5 g/L; ω = 0 rpm; v = 20 mV/s.

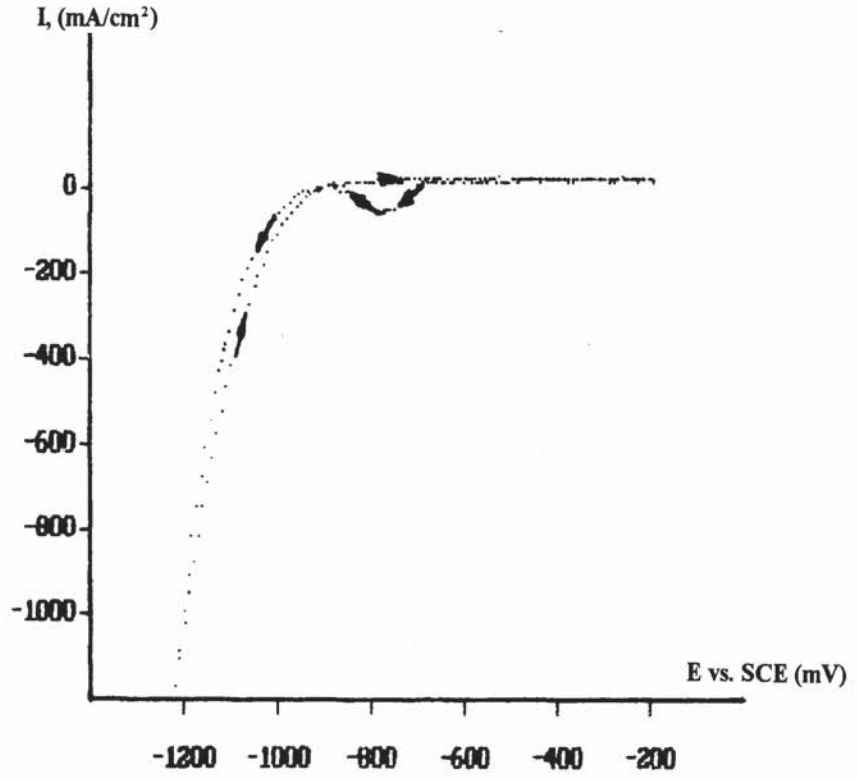

Figure 58. CrO_3 250 g/L; H_2SO_4 2.5 g/L; HEEF-405 5.0 g/L; ω = 0 rpm; ν = 40 mV/s.

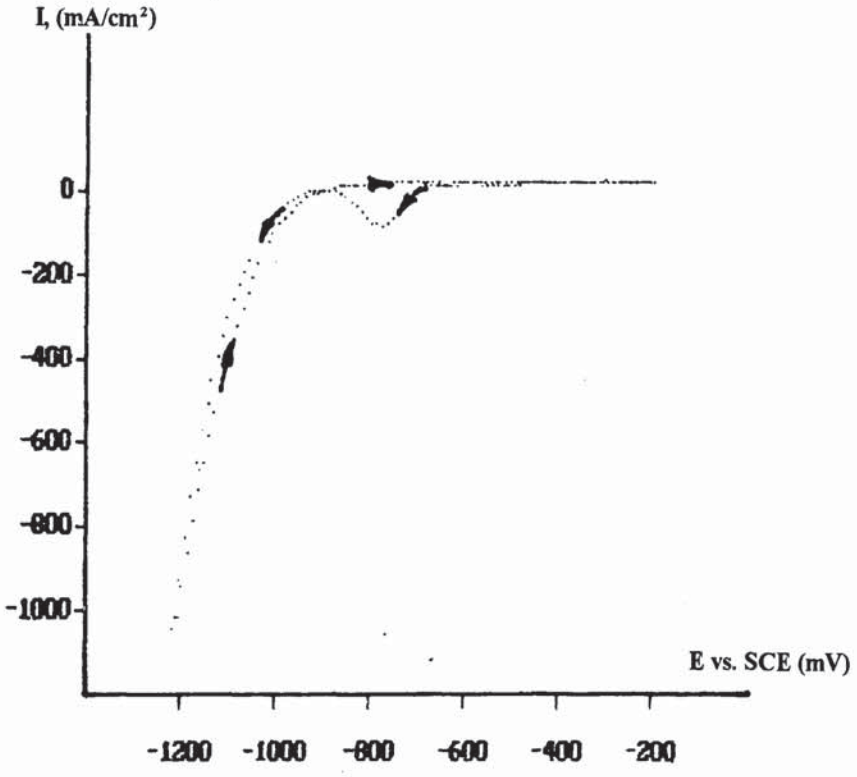

Figure 59. CrO_3 250 g/L; H_2SO_4 2.5 g/L; HEEF-405 5 g/L; ω = 0 rpm; ν = 58 mV/s.

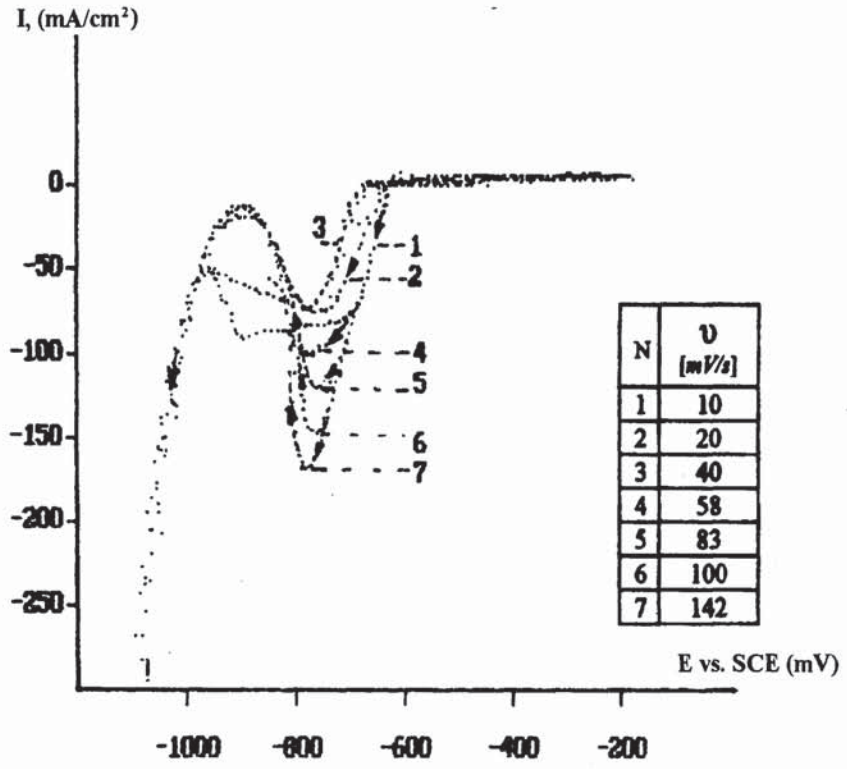

Figure 60. CrO_3, 250 g/L; H_2SO_4, 2.5 g/L; HEEF-405, 5.0 g/L; ω = 0 rpm; from - 0.2 V to -1.2V.

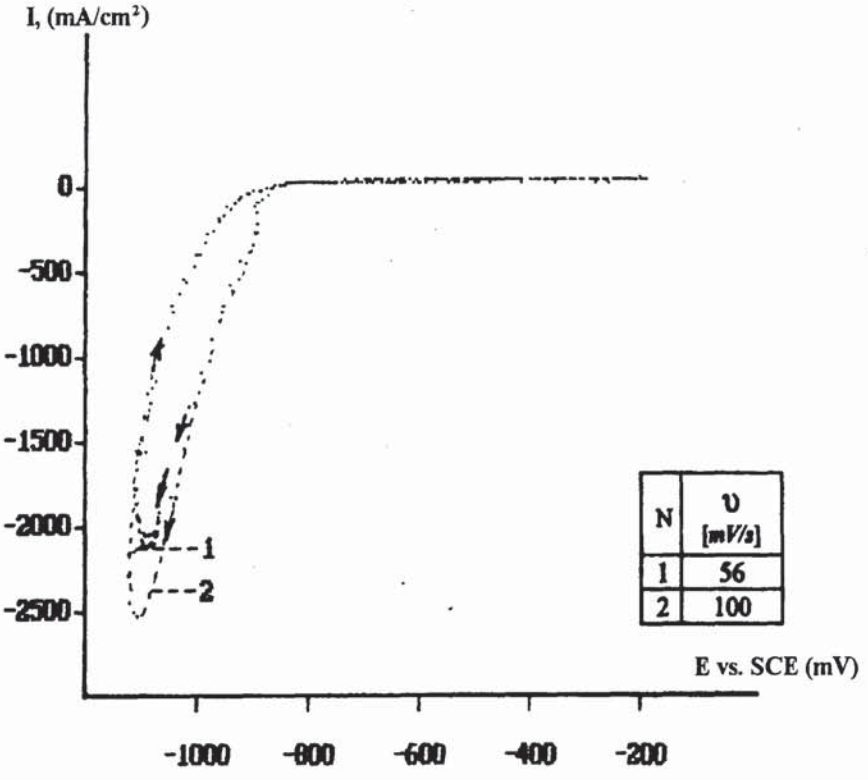

Figure 61. CrO_3, 250 g/L; H_2SO_4, 2.5 g/L; HEEF-405 5.0 g/L; ω = 0 rpm; T = 55^0 C.

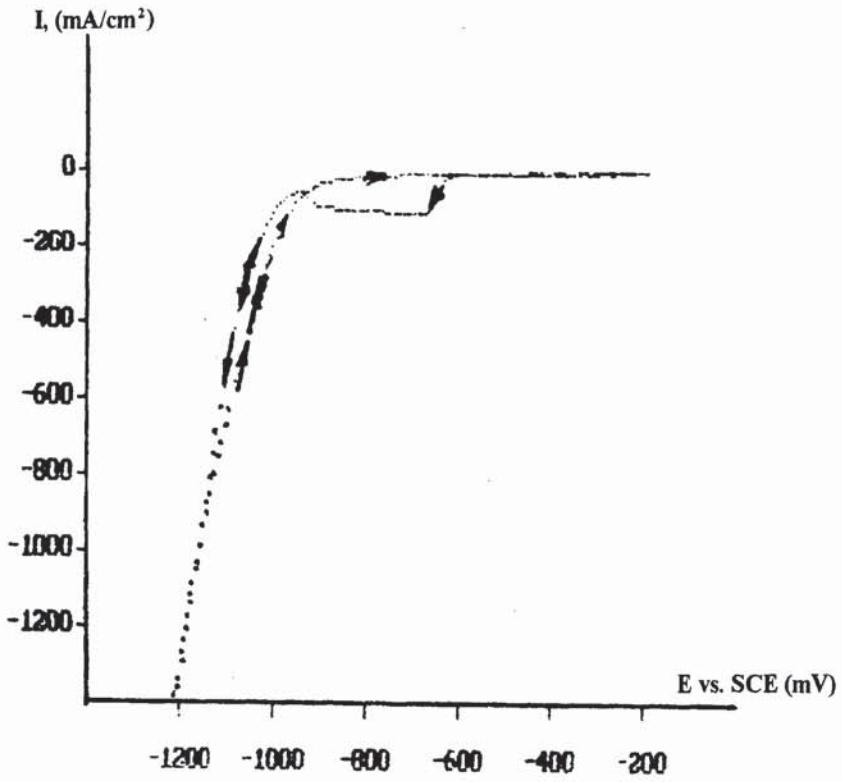

Figure 62. CrO_3,250 g/L; H_2SO_4, 2.5 g/L; HEEF-405, 2.5 g/L; ω = 0 rpm; v = 10 mV/

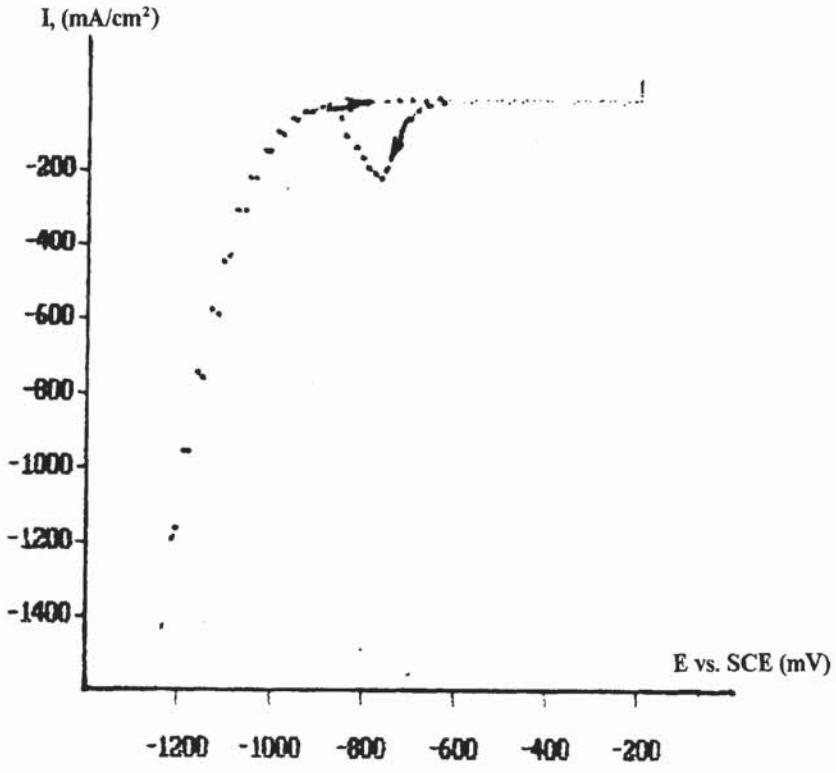

Figure 63. CrO_3, 250 g/L; H_2SO_4, 2.5 g/L; HEEF-405, 2.5 g/L; ω = 0 rpm; v = 142 mV/s.

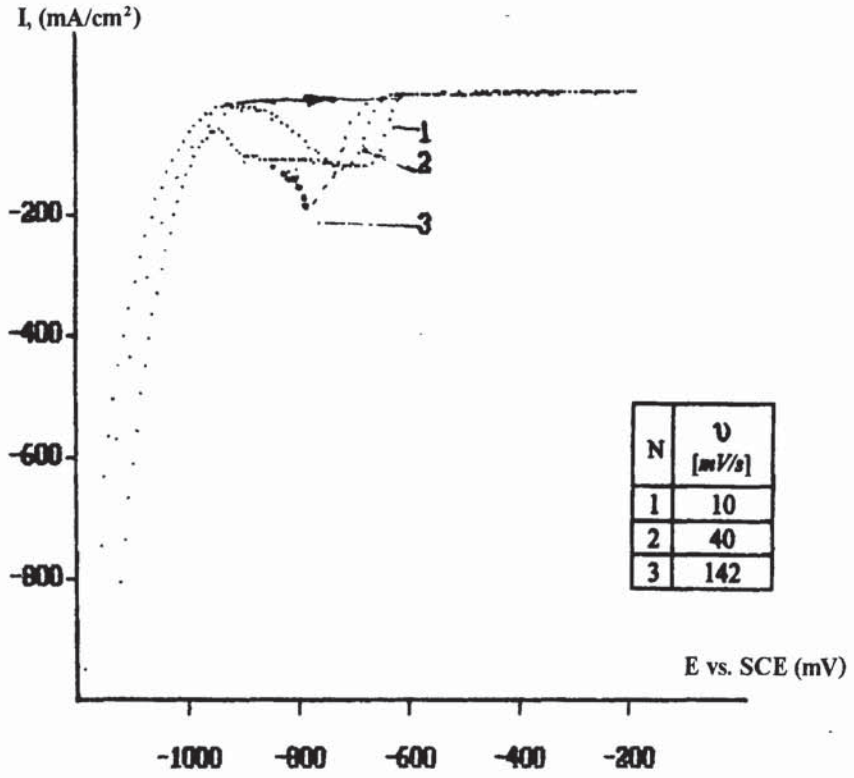

Figure 64. CrO_3, 250 g/L; H_2SO_4, 2.5 g/L; HEEF-405, 2.5 g/L; ω = 0 rpm.

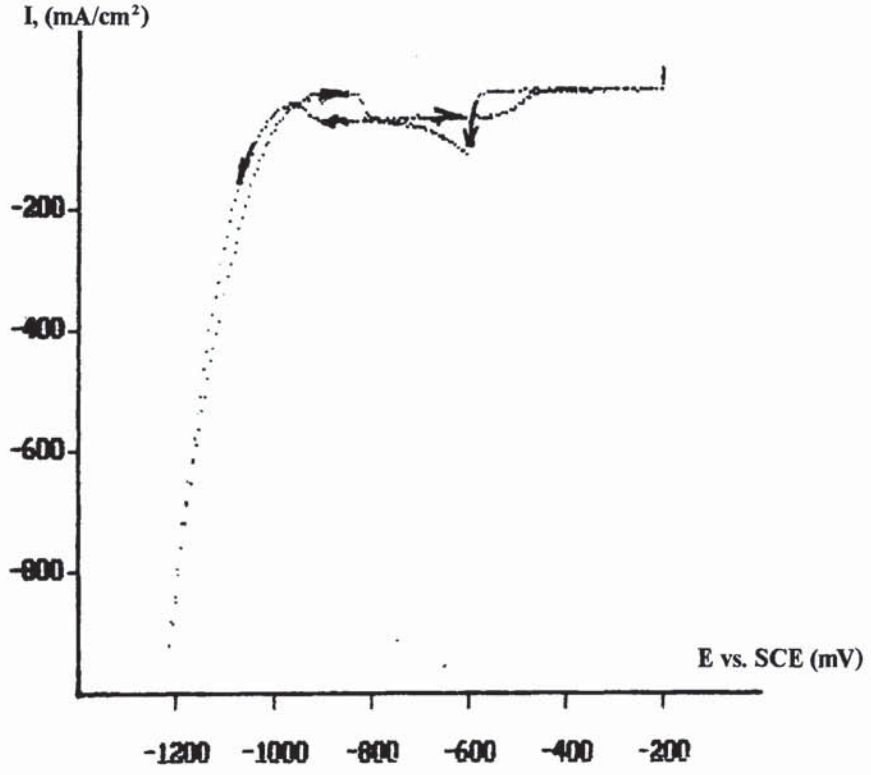

Figure 65. CrO_3, 250 g/L; H_2SO_4, 2.5 g/L; HEEF-405, 1.25 g/L; ω = 0 rpm; ν = 10 mV/s.

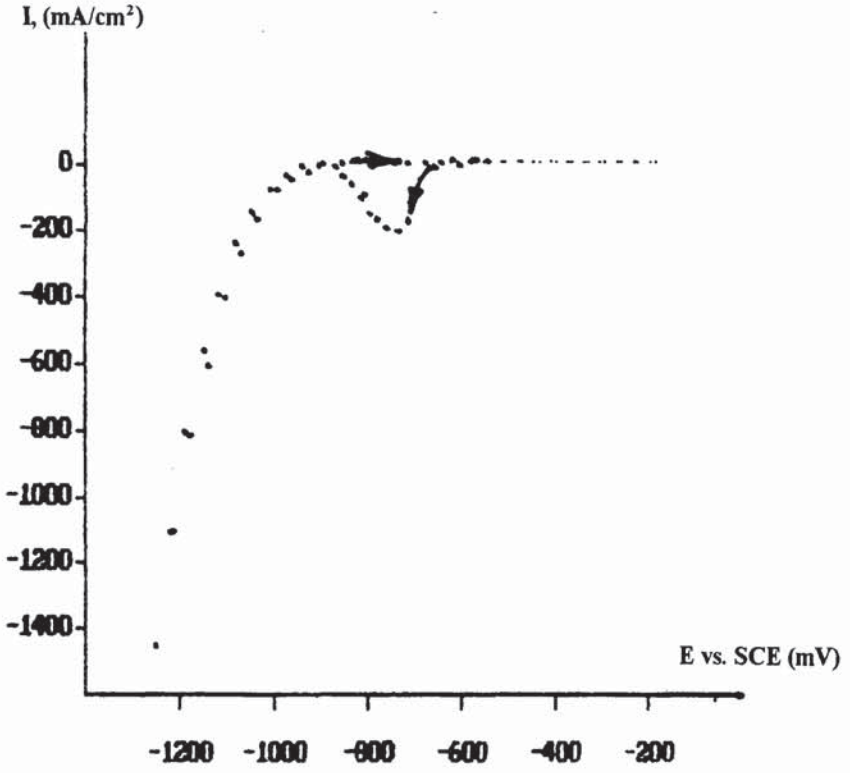

Figure 66. CrO_3, 250 g/L; H_2SO_4, 2.5 g/L; HEEF-405, 1.25 g/L; ω = 0 rpm; ν = 142 mV/s.

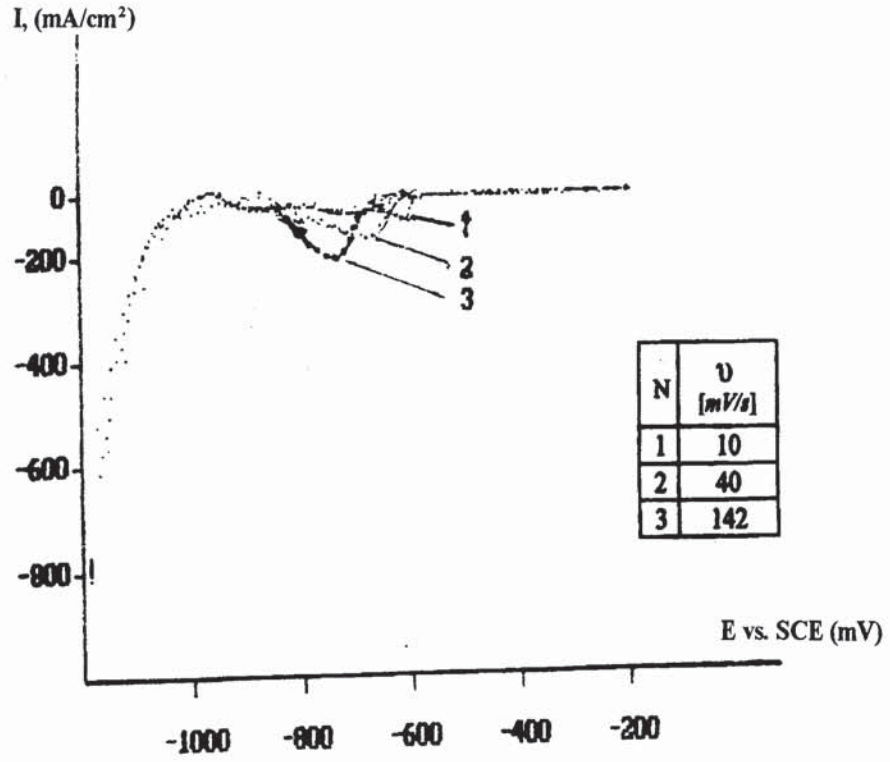

Figure 67. CrO_3, , 250 g/L; H_2SO_4, 2.5 g/L; HEEF-405, 1.25 g/L; ω = 0 rpm;scanning from -200 mV to -1200 mV.

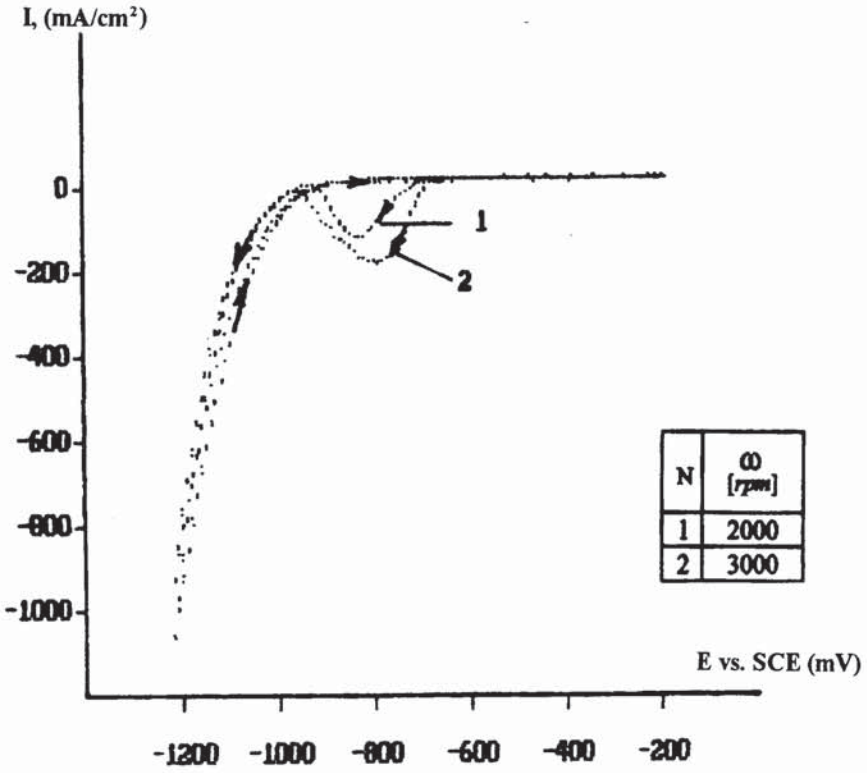

Figure 68. CrO_3, 250 g/L; H_2SO_4, 2.5 g/L; HEEF-405, 5.0 g/L; $v = 40$ mV/s.

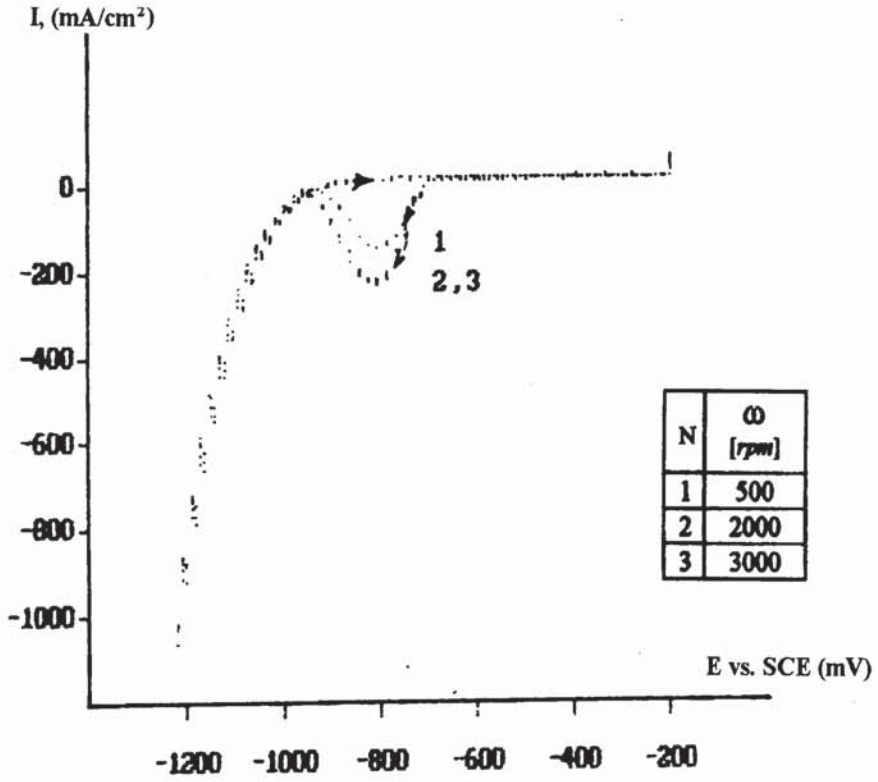

Figure 69. CrO_3, 250 g/L; H_2SO_4, 2.5 g/L; HEEF-405, 5.0 g/L; $v = 100$ mV/s.

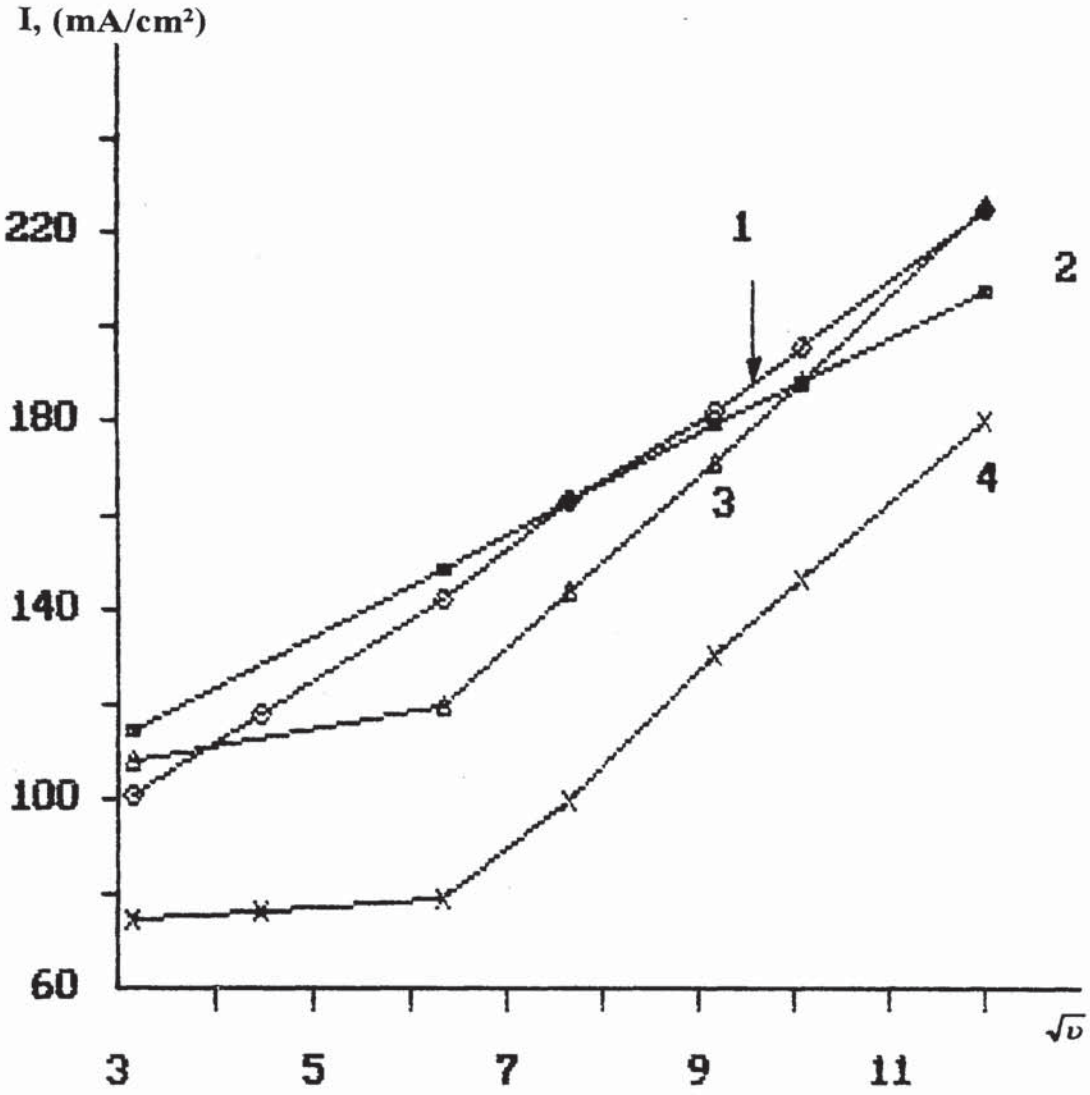

Figure 70. The Effect of the Scan Rate on the Cathodic Peak for HEEF-405 at 3 different concentrations. Data from Table 42.

1) Sargent bath.
2) HEEF-405 (1.25 g/L).
3) HEEF-405 (2.5 g/L).
4) HEEF-405 (5.0 g/L).

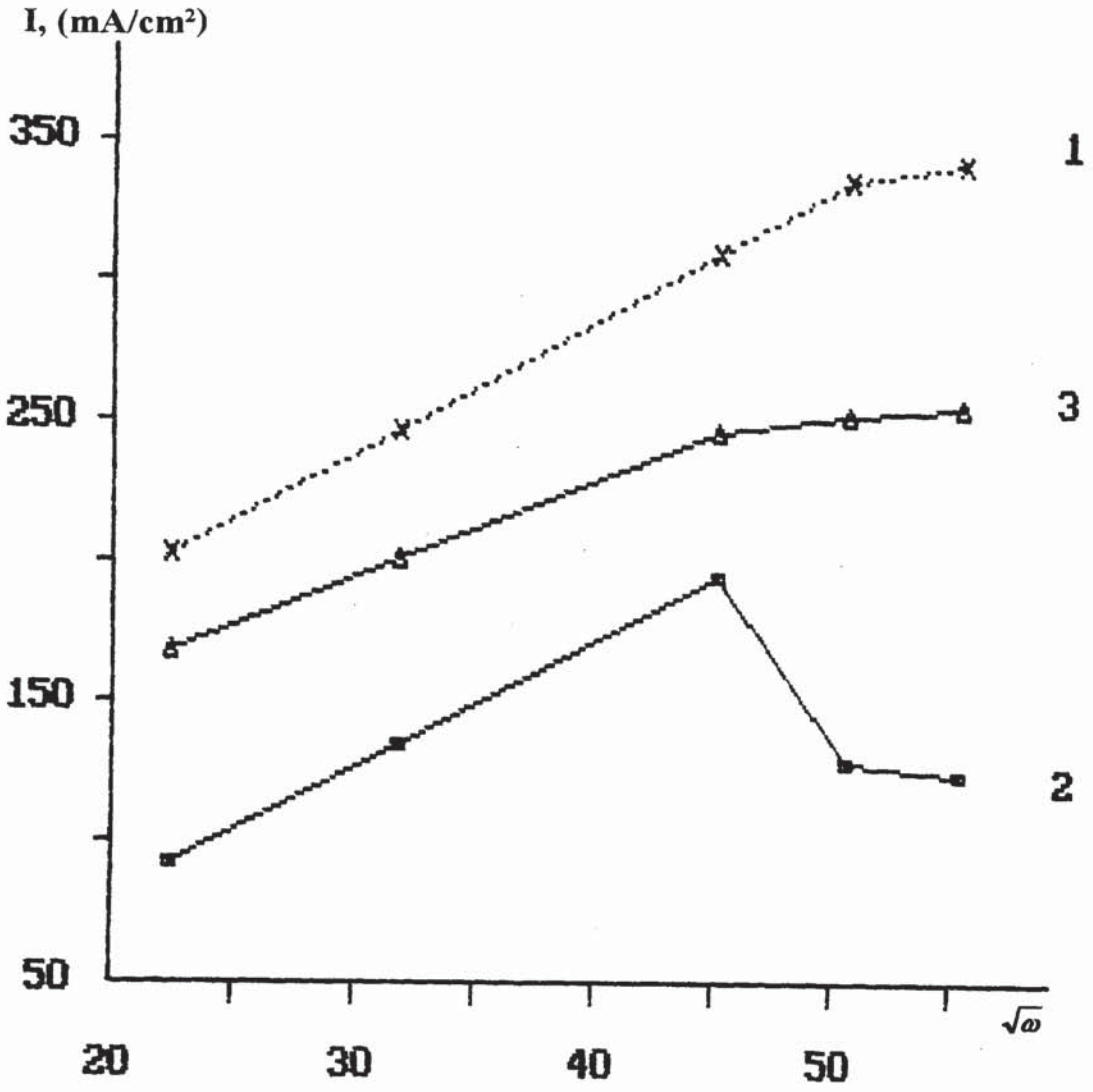

Figure 71. The Cathodic Peak *I* as a Function of the Electrode Rotation Rate ($\sqrt{\omega}$).
Data from Table 45.

1) Sargent bath; 40 mV/s.
2) HEEF-405, 5.0 g/L; 40 mV/s.
3) HEEF- 405, 5.0 g/L; 100 mV/s.

Sweep rate (mV/s)	Concentration	I (mA/cm^2)	-E vs. SCE (mV)
10	1.25	114	609
40	1.25	154	680
58	1.25	164	708
83	1.25	169	715
100	1.25	189	728
142	1.25	207	731
10	2.5	108	685
40	2.5	120	725
58	2.5	135	735
83	2.5	172	735
100	2.5	188	735
142	2.5	225	738
10	5.0	75	694
20	5.0	77	702
40	5.0	79	780
58	5.0	100	775
83	5.0	126	765
100	5.0	155	762
142	5.0	180	763

Table 42. Cathode peak current density (I) obtained from cyclic voltammograms for the Sargent bath with HEEF-405 additive as a function of scan rate, *v*.

3. *HEEF-25 bath*

i. Description of Linear Potential Polarisation Cyclic Voltammograms.

HEEF-25 as secondary catalyst at 5.0 g/ℓ at stationary electrode ($\omega = 0$) is presented separately in Figures 72-76 for v = 10, 20, 58, 83 and 142 mV/s and together at Figure 77.

At 2.5 g/ℓ ($\omega = 0$), the influence of two scan rates v = 10 and 142 mV/s are presented separately in Figures 78 and 79 and also together in Figure 80 for v = 10, 58 and 142 mV/s.

At 1.5 g/ℓ ($\omega = 0$), the influence of two scan rates v = 10 and 142 mV/s is presented separately in Figures 80 and 81 and also for v = 10, 40 and 142 mV/s in Figure 83.

Dependence of I on $\sqrt{v}$ at 1.25, 2.5 and 5.0 g/ℓ is presented in Figure 84 and in Figure 108 for 5.0 g/ℓ in comparison with the other four baths.

The influence of rotation speed (ω) at 5.0 g/ℓ and 20^0 C on cathodic peak I (maximum current) at scan rate v = 40 mV/s is presented in Figure 85 for 500 rpm and in Figure 86 for 3000 rpm.

Figure 87 is the relationship I - $\sqrt{v}$ for 5.0 g/ℓ bath at scan rate v = 40 mV/s. as compared with Sargent Bath, for 20^0 C. The influence of higher temperature (55^0 C) for a stationary electrode at v = 56 mV/s is presented in Figure 88 for 5.0 g/ℓ bath.

ii. Discussion.

HEEF-25 behaviour is somewhat similar to that of pure Sargent bath and cathodic peaks are observed upon scanning the potential in positive and negative directions (Figures 72-83). It could be seen in that, I increases slightly (Figures 72-76) at concentrations of 5.0 g/L, but the lower concentrations (1.25 and 2.50 g/ℓ) had no influence on I. It is clear from these experiments that HEEF-25 is a weak catalyst for the reaction $Cr^{6+} \rightarrow Cr^{3+}$. The cathodic peak I increases with the increase of the scan rate and with the electrode rotation rate and is a linear function of $\sqrt{\nu}$ and of $\sqrt{\omega}$; therefore, in the HEEF-25 bath, $Cr^{6+} \rightarrow Cr^{3+}$ reaction is diffusion controlled at least at the rpm range investigated.

The clearly established increase in the cathode current efficiencies, presented in Figures 22 and 23 are obviously related to the influence of HEEF-25 on the reactions other than $Cr^{6+} \rightarrow Cr^{3+}$.

It is quite obvious that DMSA, found to be the ingredient of HEEF-25 catalyst, is influencing the L-film formation and its physico-chemical properties.

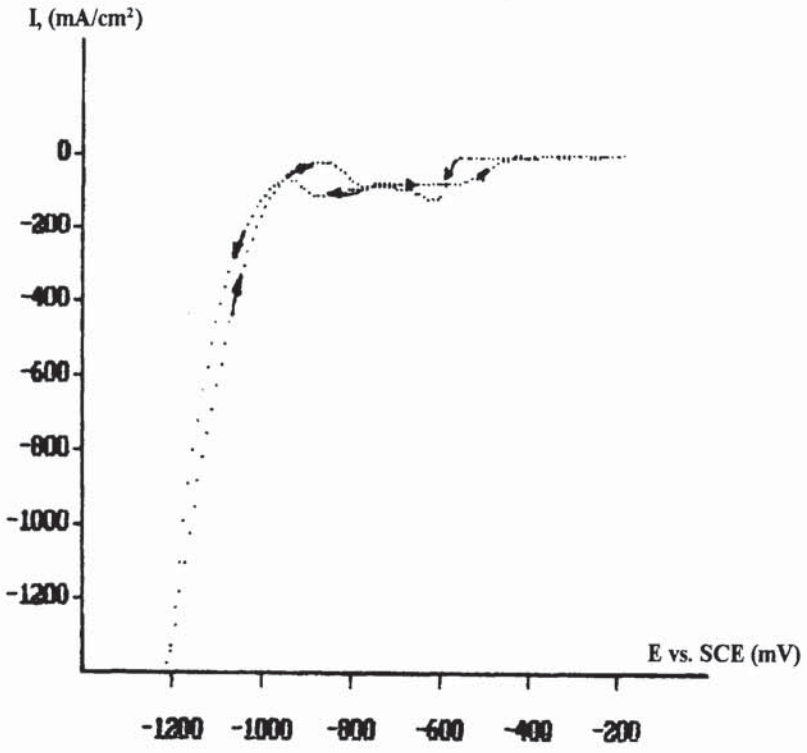

Figure 72. CrO_3, 250 g/L; H_2SO_4, 2.5 g/L; HEEF-25, 5.0 g/L; $\omega = 0$ rpm; $\nu = 10$ mV/s.

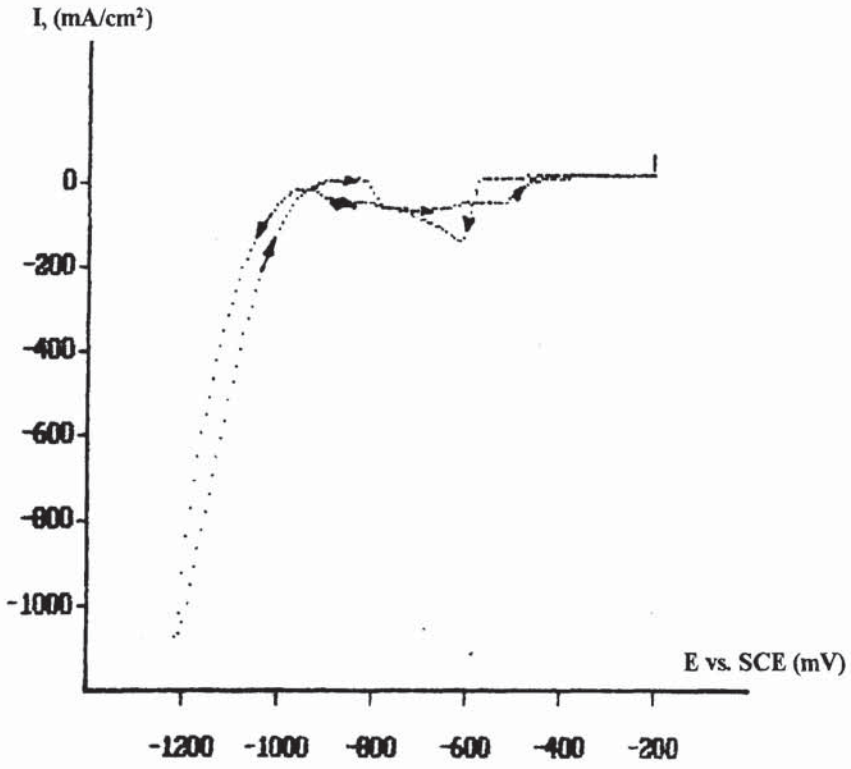

Figure 73. CrO_3, 250 g/L; H_2SO_4, 2.5 g/L; HEEF-25, 5.0 g/L; $\omega = 0$ rpm; $\nu = 20$ mV/s.

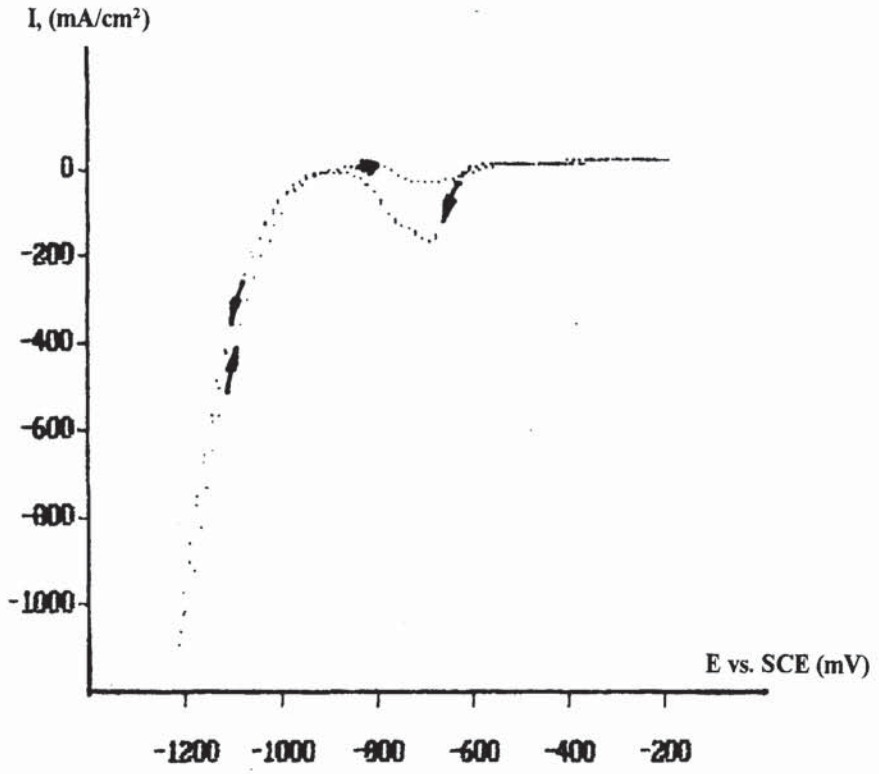

Figure 74. CrO_3, 250 g/L; H_2SO_4, 2.5 g/L; HEEF-25, 5.0 g/L; $\omega = 0$ rpm; $\nu = 58$ mV/s.

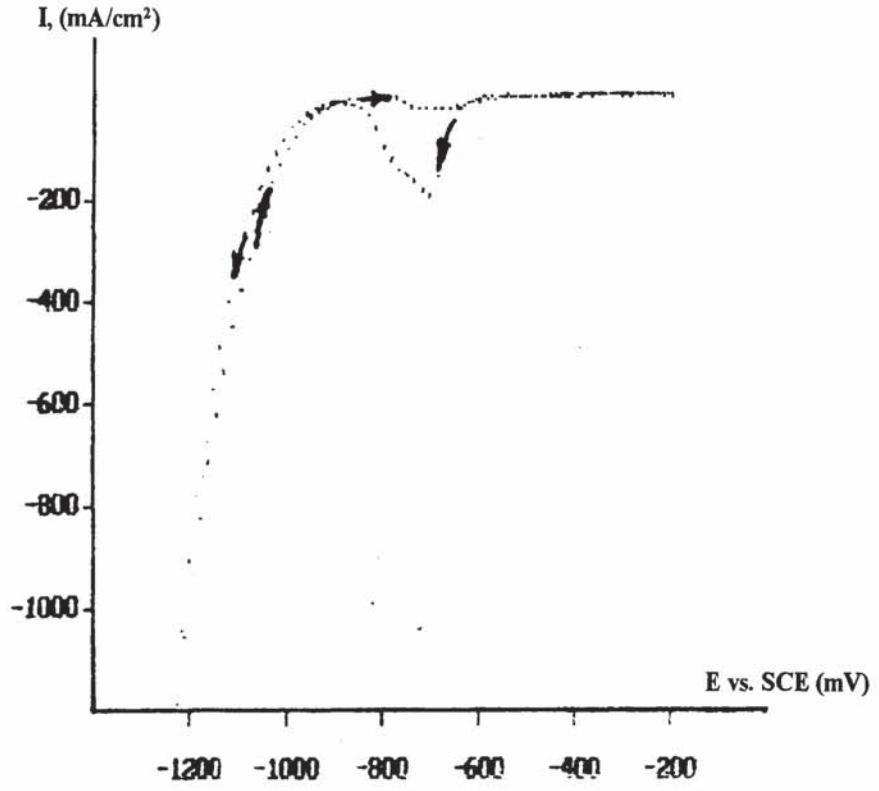

Figure 75. CrO_3, 250 g/L; H_2SO_4, 2.5 g/L; HEEF-25, 5.0 g/L; $\omega = 0$ rpm; $\nu = 83$ mV/s.

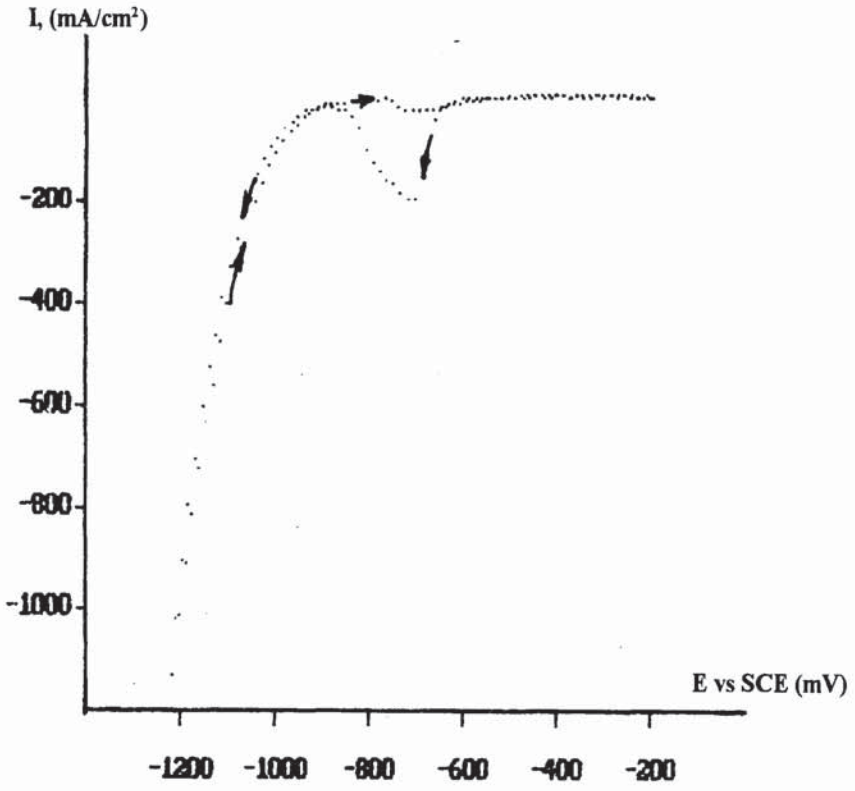

Figure 76. CrO_3, 250 g/L; H_2SO_4, 2.5 g/L; HEEF-25, 5.0 g/L; ω = 0 rpm; v = 100 mV/s.

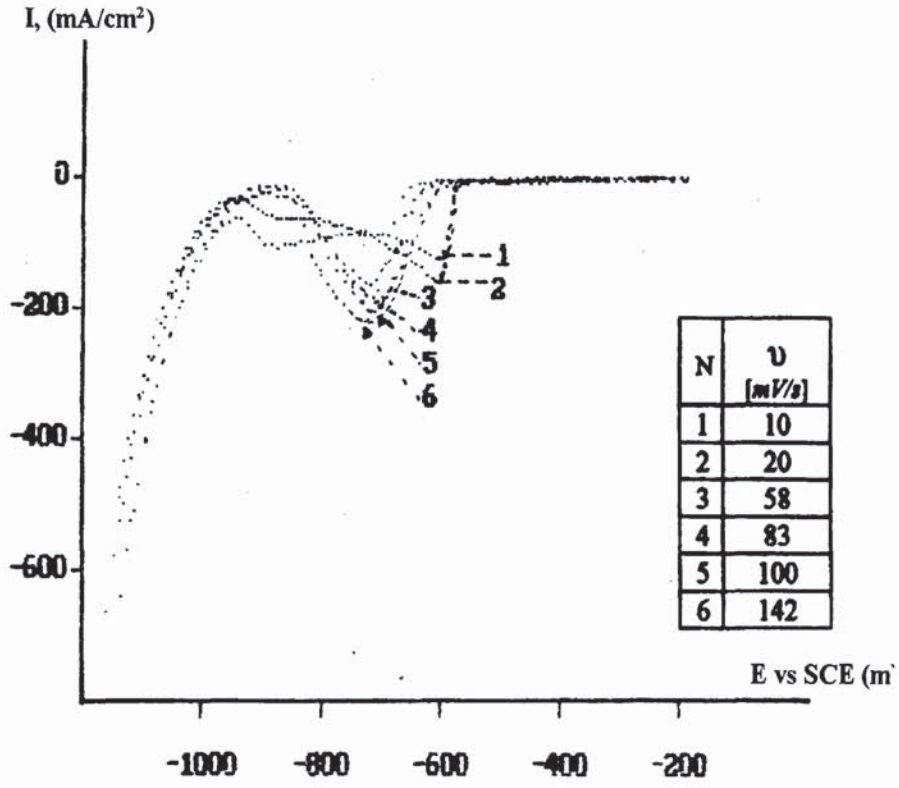

Figure 77. CrO_3, 250 g/L; H_2SO_4, 2.5 g/L; HEEF-25, 5.0 g/L; ω = 0 rpm; from -200 mV/s. to -1200 mV/s.

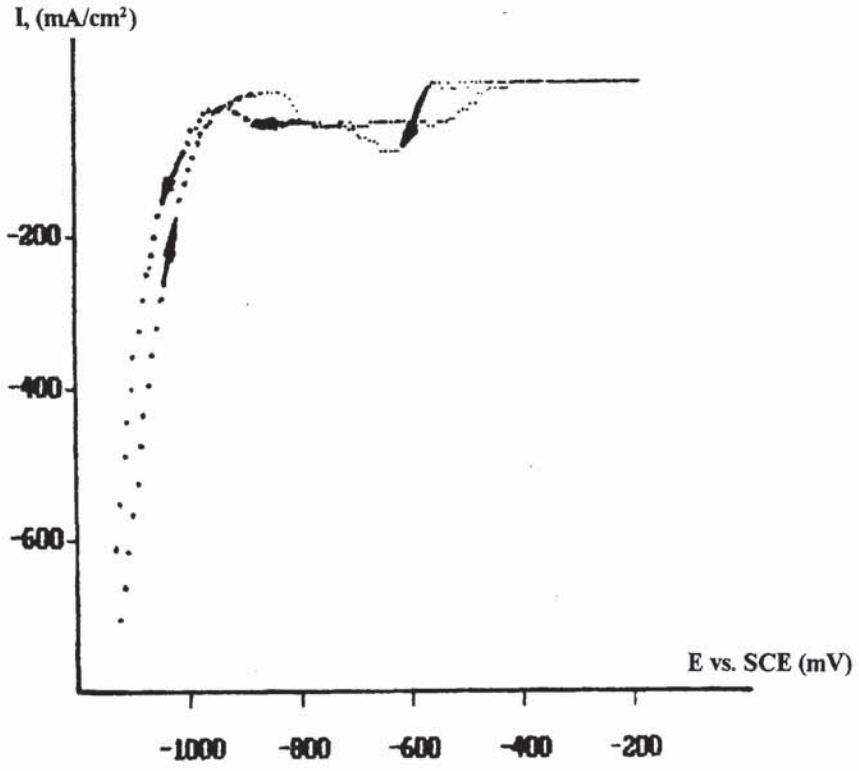

Figure 78. CrO_3, 250 g/L; H_2SO_4, 2.5 g/L; HEEF-25, 2.5 g/L; ω = 0 rpm; v = 10 mV/s.

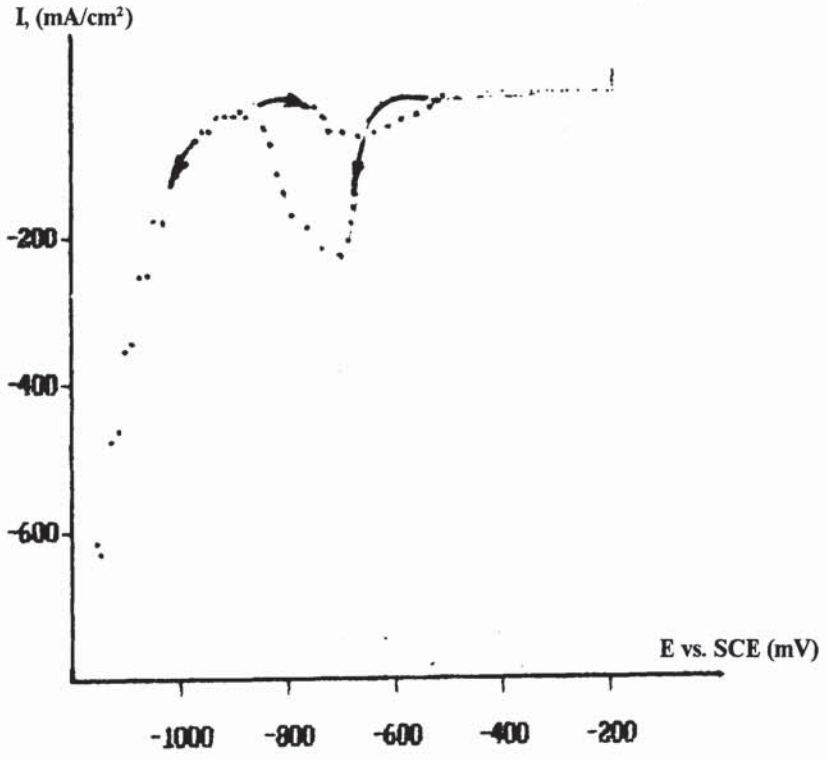

Figure 79. CrO_3, 250 g/L; H_2SO_4, 2.5 g/L; HEEF-25, 2.5 g/L; ω = 0 rpm; v = 140 mV/s.

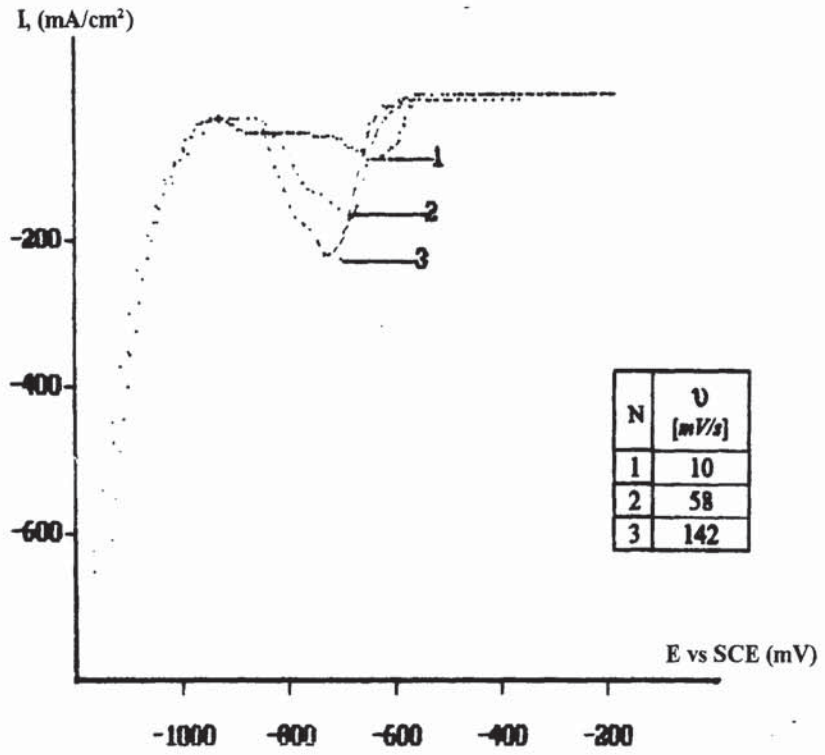

Figure 80. CrO_3, 250 g/L; H_2SO_4, 2.5 g/L; HEEF-25, 2.5 g/L; $\omega = 0$ rpm. The reverse scans are not shown.

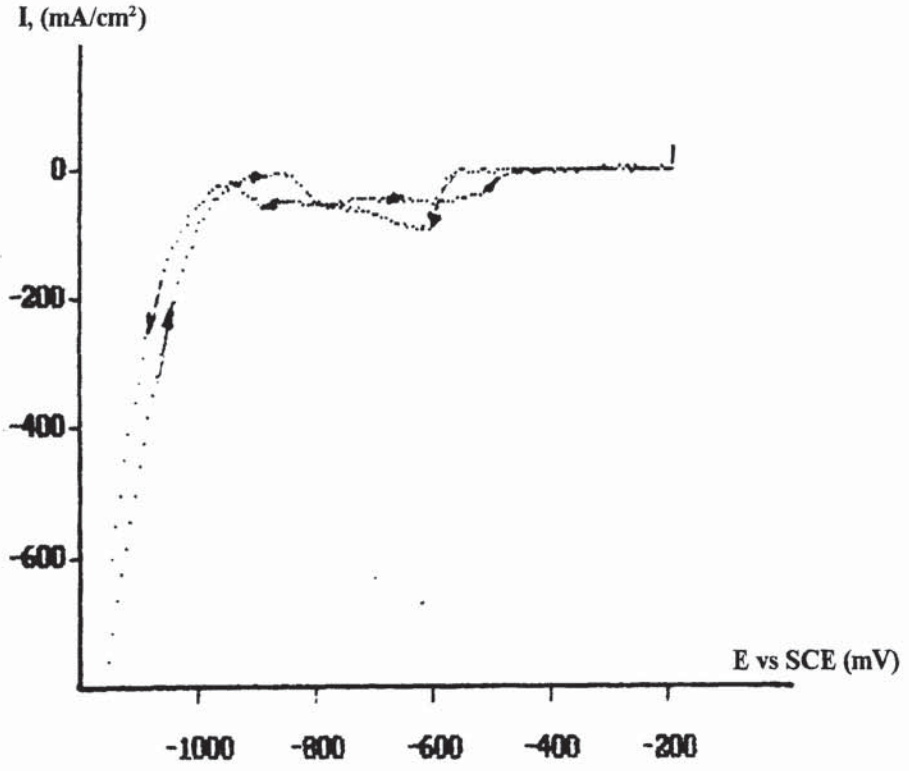

Figure 81. CrO_3, 250 g/L; H_2SO_4, 2.5 g/L; HEEF-25, 1.25g/L $\omega = 0$ rpm; $v = 10$ mV/s.

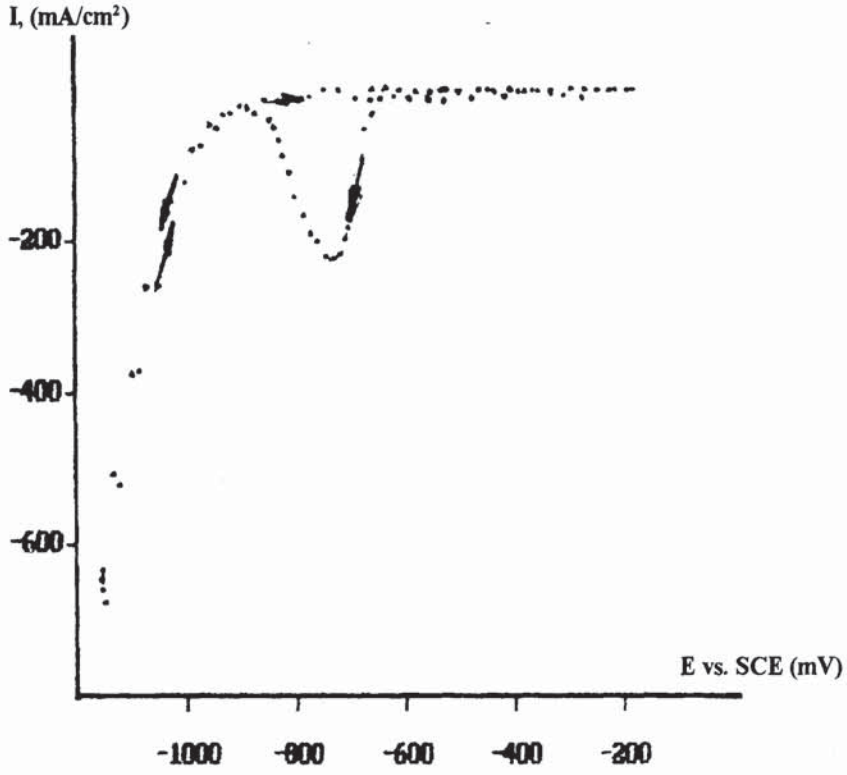

Figure 82. CrO_3, 250 g/L; H_2SO_4, 2.5 g/L; HEEF-25, 1.25 g/L; ω = 0 rpm; v = 142 mV/s.

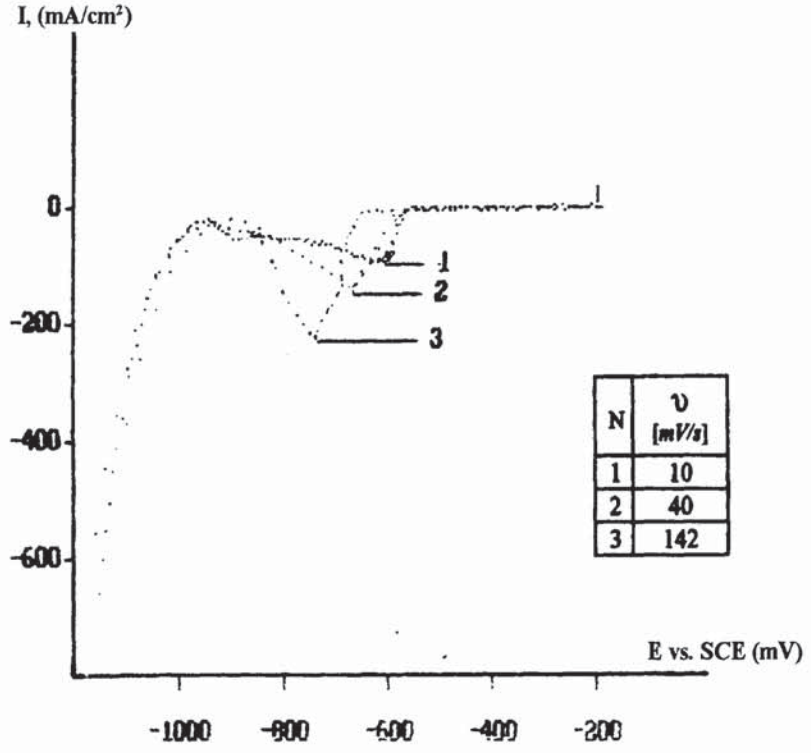

Figure 83. CrO_3, 250 g/L; H_2SO_4, 2.5 g/L; HEEF-25, 1.25 g/L; ω = 0 rpm.
The reverse scans are not shown..

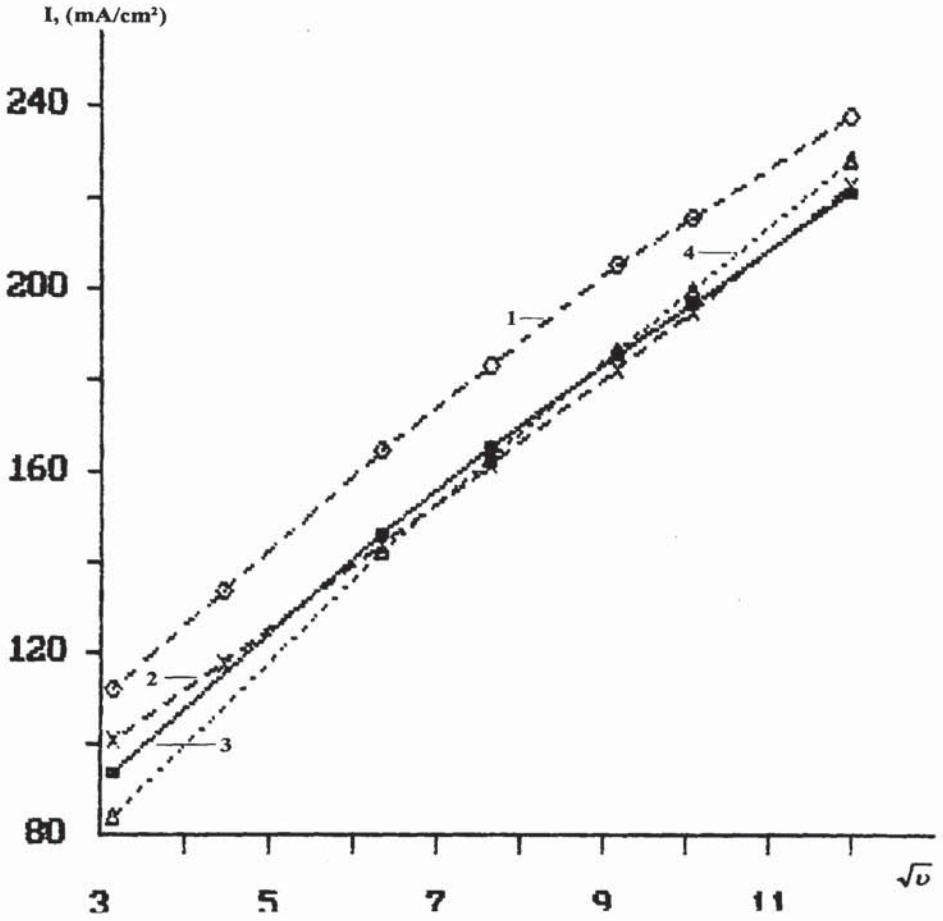

Figure 84. The Effect of the Scan Rate on the Cathodic Peak. Data from Table 43.

1- Sargent Bath (SB). (O)
2- HEEF-25 (1.25 g/L) (X)
3- HEEF-25 (2.5 g/L). (◊)
4- HEEF-25 (5.0 g/L). (Δ)

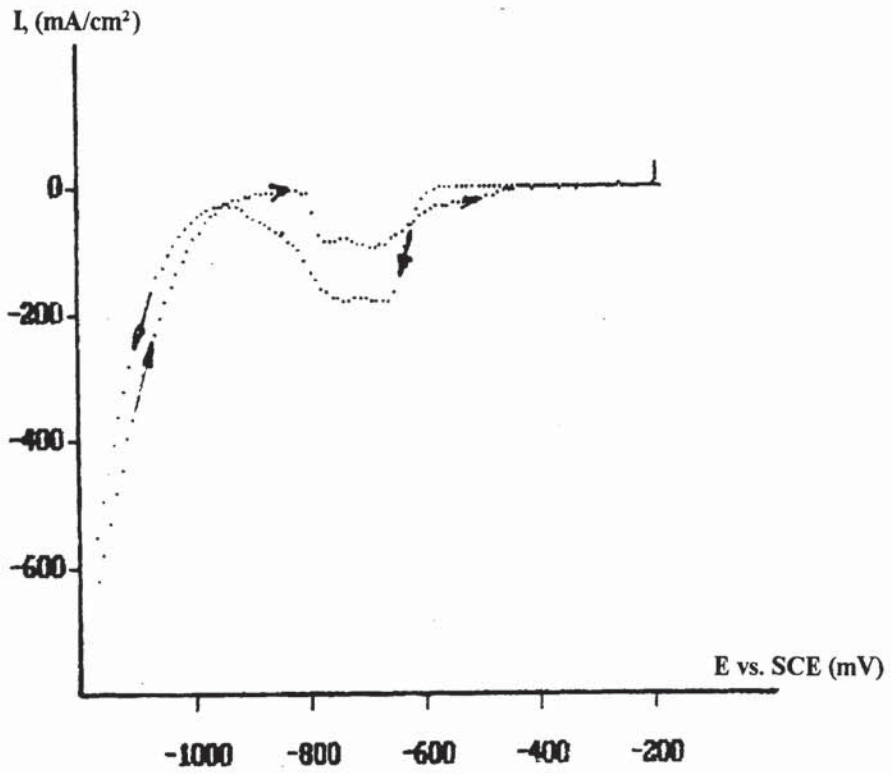

Figure 85. CrO_3, 250 g/L; H_2SO_4, 2.5 g/L; HEEF-25, 5.0 g/L; ω = 500 rpm; ν = 40 mV/s.

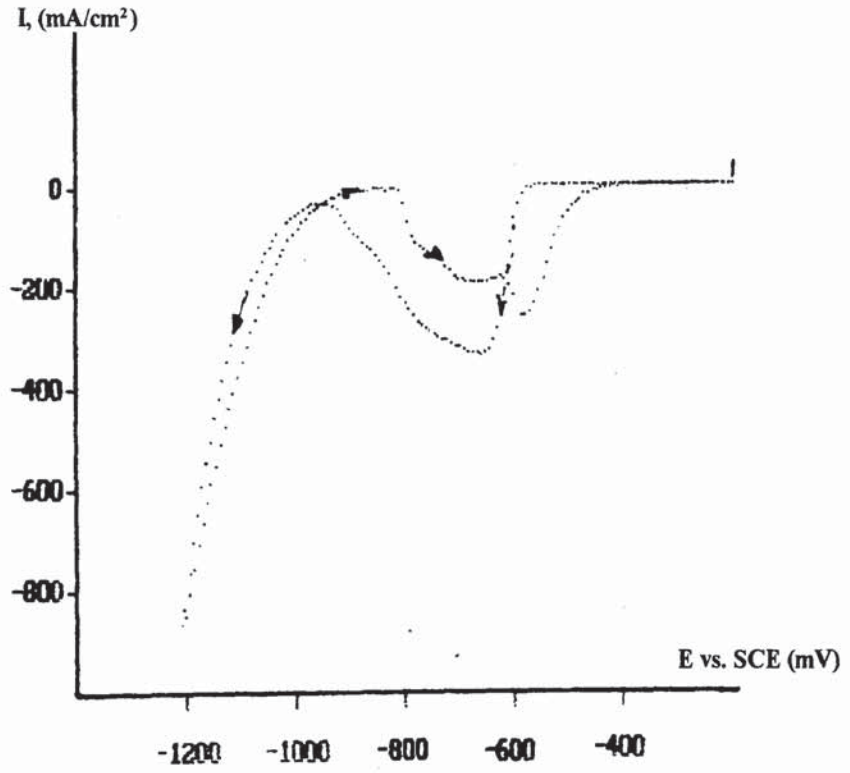

Figure 86. CrO_3, 250 g/L; H_2SO_4, 2.5 g/L; HEEF-25, 5.0 g/L; ω = 3000 rpm; ν = 40 mV/s.

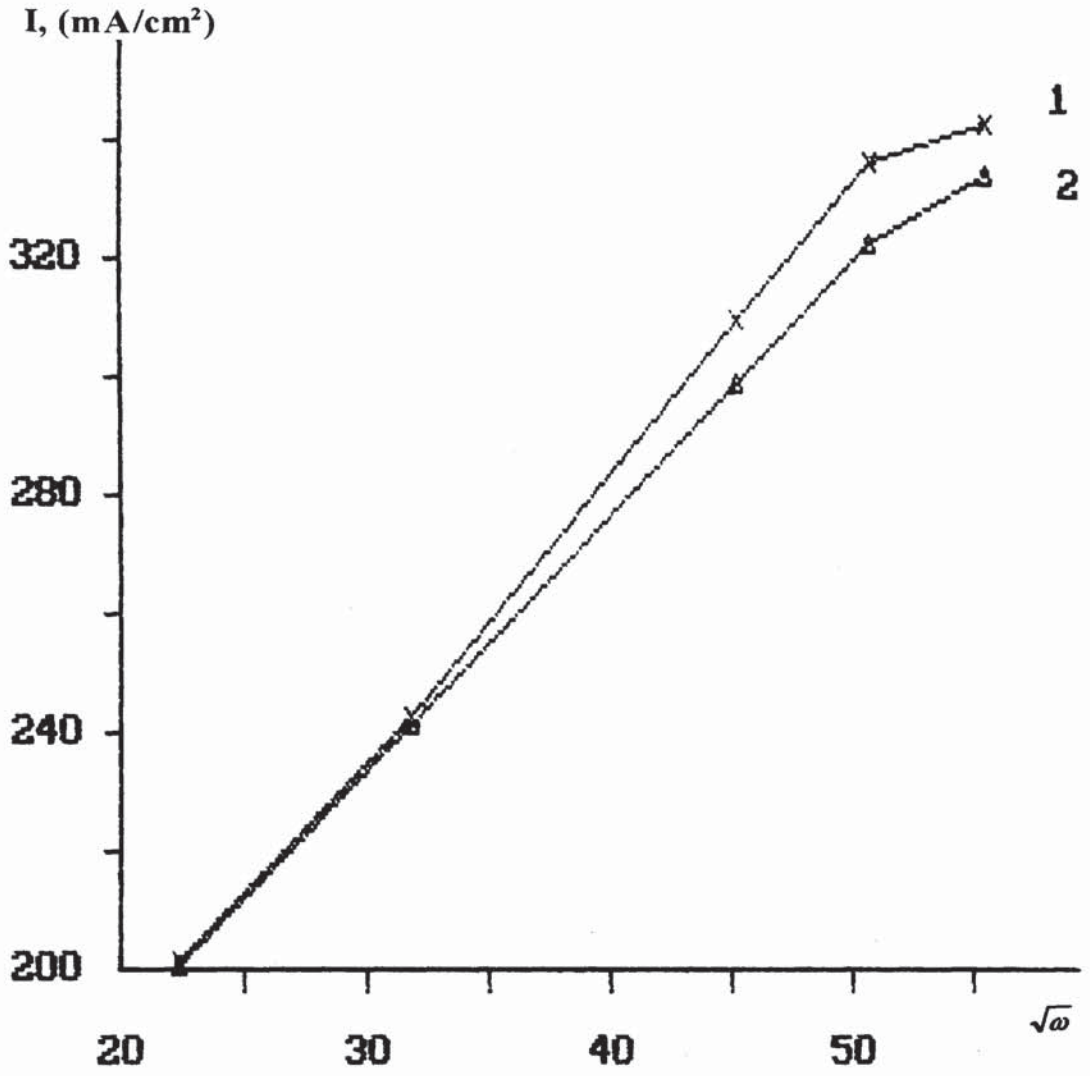

Figure 87. The Cathodic Peak (*I*) as a Function of the Electrode Rotation Rate ($\sqrt{\omega}$).
Data from Table 45.
1. Sargent Bath (SB); 40 mV/s.
2. SB + HEEF-25 5.0 g/L; 40 mV/s.

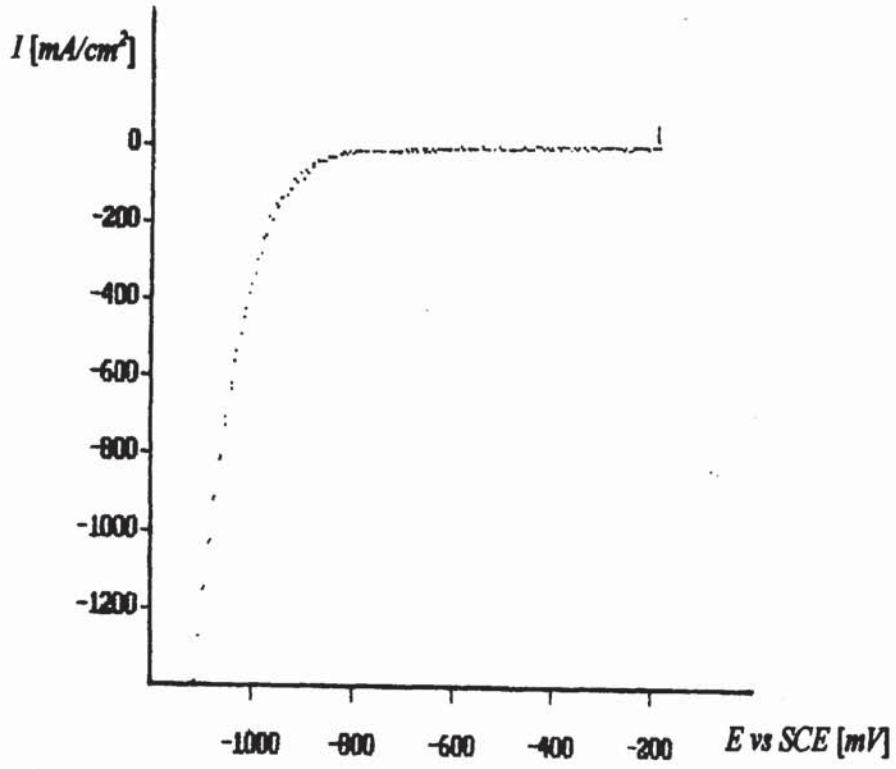

Figure 88. CrO_3, 250 g/L; H_2SO_4, 2.5 g/L; HEEF-25, 5.0 g/L; ω = 0 rpm; v = 56 mV/s. T = 55^0 C.

v (mV/s.)	Concentration (g/l)	I (mA/cm^2)	-E vs. SCE (mV)
10	1.25	94	615
40	1.25	152	668
58	1.25	171	675
83	1.25	186	712
100	1.25	194	724
142	1.25	222	735
10	2.5	85	625
40	2.5	144	665
58	2.5	174	691
83	2.5	194	705
100	2.5	199	724
142	2.5	229	735
10	5.0	119	605
20	5.0	134	610
40	5.0	165	670
58	5.0	179	692
83	5.0	200	705
100	5.0	219	707

Table 43. Maximum current (I) obtained from cyclic voltammogram by cathodic-going sweep for the Sargent Bath with HEEF-25 additive as a function of scan rate v.

4. *SSA bath*

i. Description of Linear Polarisation Cyclic Voltammograms.

SSA (Sulphosalycilic Acid) as secondary catalyst at 5.0 g/ℓ (20^0 C) at stationary electrode (ω = 0) is presented in Figures 89 and 90 for scan rates v = 10 and 20 mV/s and in Figure 91 for v = 10, 20, 40, 83 and 142 mV/s.

At 2.5 g/ℓ at stationary electrode, separate voltammograms are presented for scan rates v = 10 mV/s. (Figure 92) and 142 mV/s. (Figure 83) and composite LPP scan for 10, 40 and 142 mV/s. (Figure 94).

Figures 95-97 are of the same fashion but for 1.5 g/ℓ.

Figure 98 depicts the influence of on cathodic peak for 1.5, 2.5 and 5.0 g/ℓ at 20^0 C and also shows the comparison with Sargent bath without additive.

Influence of the rotation rate, for Sargent and SSA baths (5.0 g/ℓ at 20^0 C) at v = 40 mV/s. are presented in Figures 89 and 100 for 500 and 3000 rpm, and I - $\sqrt{\omega}$ relationship in Figure 101. The influence of higher temperature (55^0 C) for a stationary electrode at v = 56 mV/s. is presented in Figure 102.

ii. *Discussion.*

The cathodic wave is observed on voltammograms when scanning potential in the negative and in the reverse direction (Figures 89-100). It is obvious that SSA additive is a strong catalyst: maximum current, I, increases significantly with increased SSA concentration and, I is not a linear function of scan rate as seen from Figure 98. In this case the diffusion process is complicated by accumulation of the phase products on the electrode surface (Figure 95). The reaction rate: $Cr^{6+} \rightarrow Cr^{3+}$ in the SSA bath is very high, indicating an increase in the liquid phase products formation in the L-film. I is a linear function of the rotation rate over the range between 500-2500 rpm. (Figure 101). At 2500-3000 rpm, I becomes a constant due to the reaching of the limiting diffusion current. Obviously, at the higher rotation rates deposition becomes kinetically controlled.

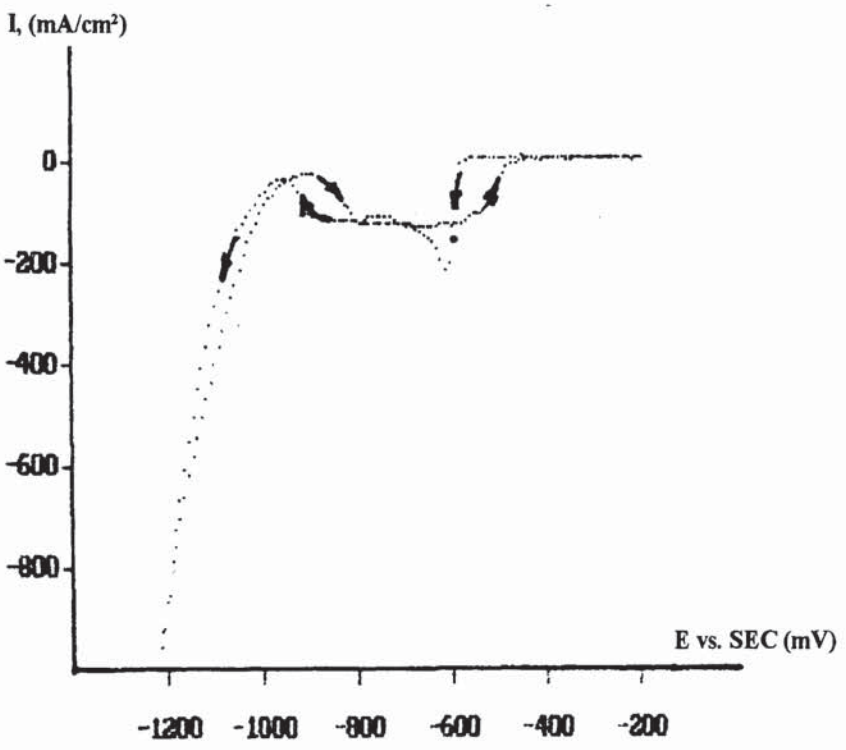

Figure 89. CrO_3. 250 g/L; H_2SO_4, 2.5 g/L; SSA, 5.0 g/L $\omega = 0$ rpm; $\nu = 10$ mV/s.

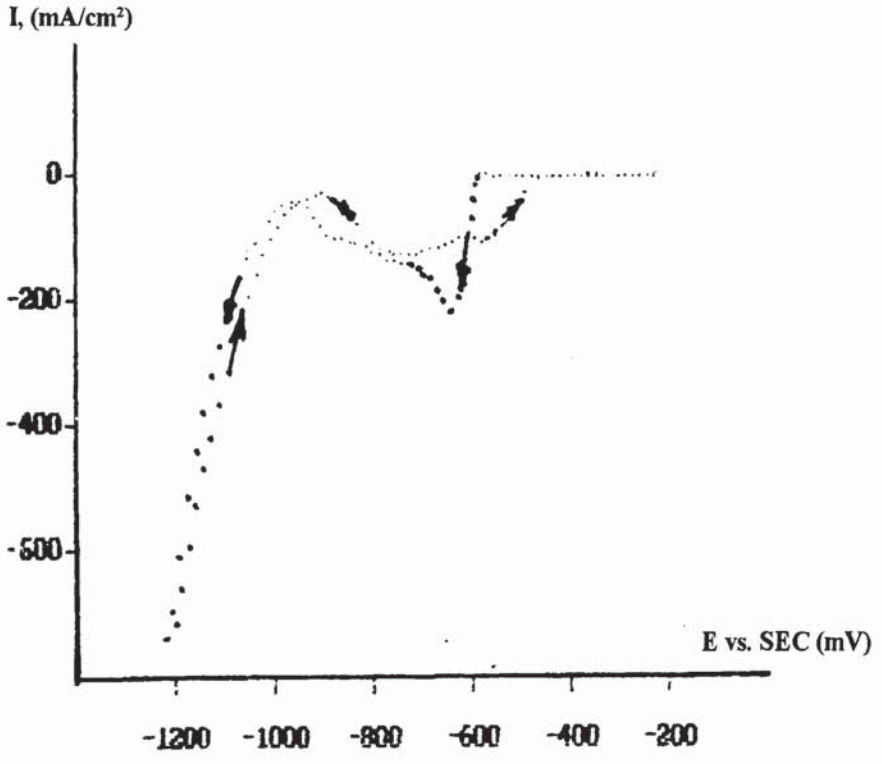

Figure 90. CrO_3, 250 g/L; H_2SO_4, 2.5 g/L; SSA, 5.0 g/L $\omega = 0$ rpm; $\nu = 20$ mV/s.

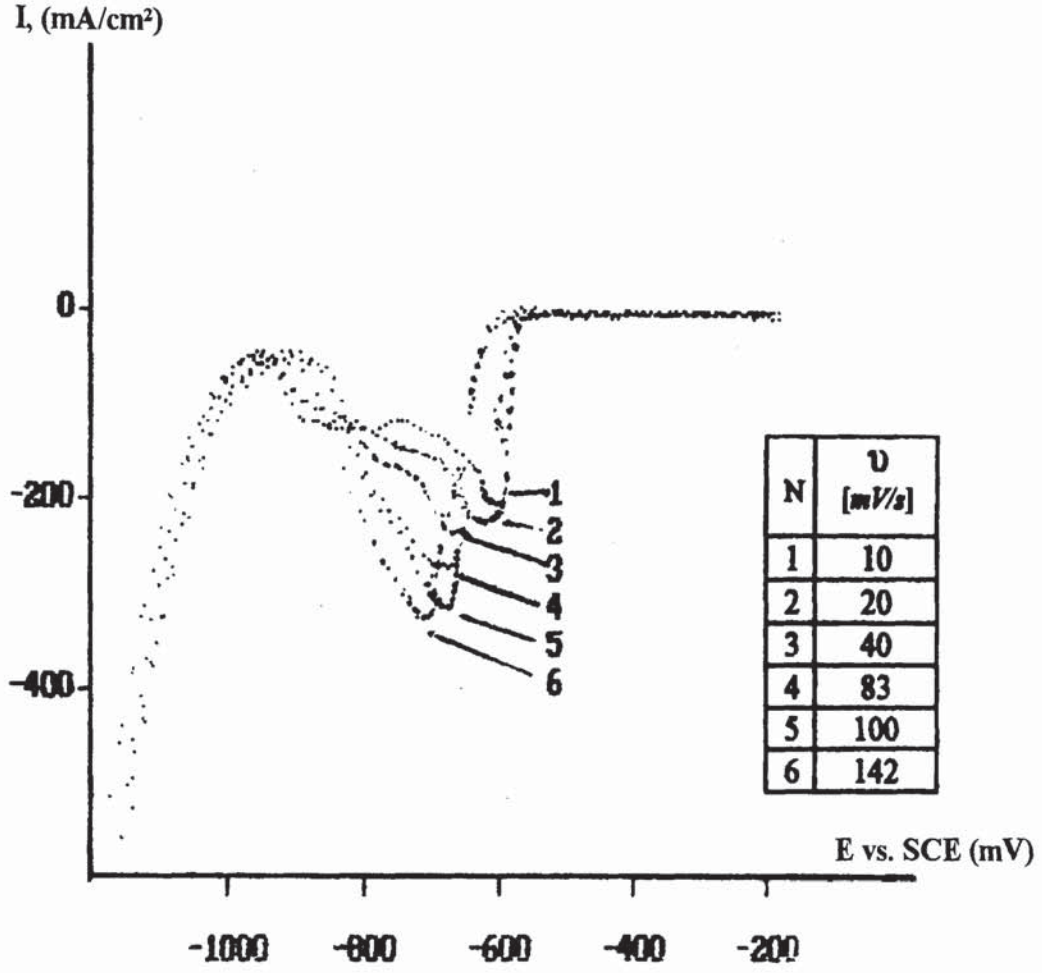

Figure 91. CrO_3, 250 g/L; H_2SO_4, 2.5 g/L; SSA, 5.0 g/L; ω = 0 rpm; potential range from -200 mV/s. to -1200 mV/s.

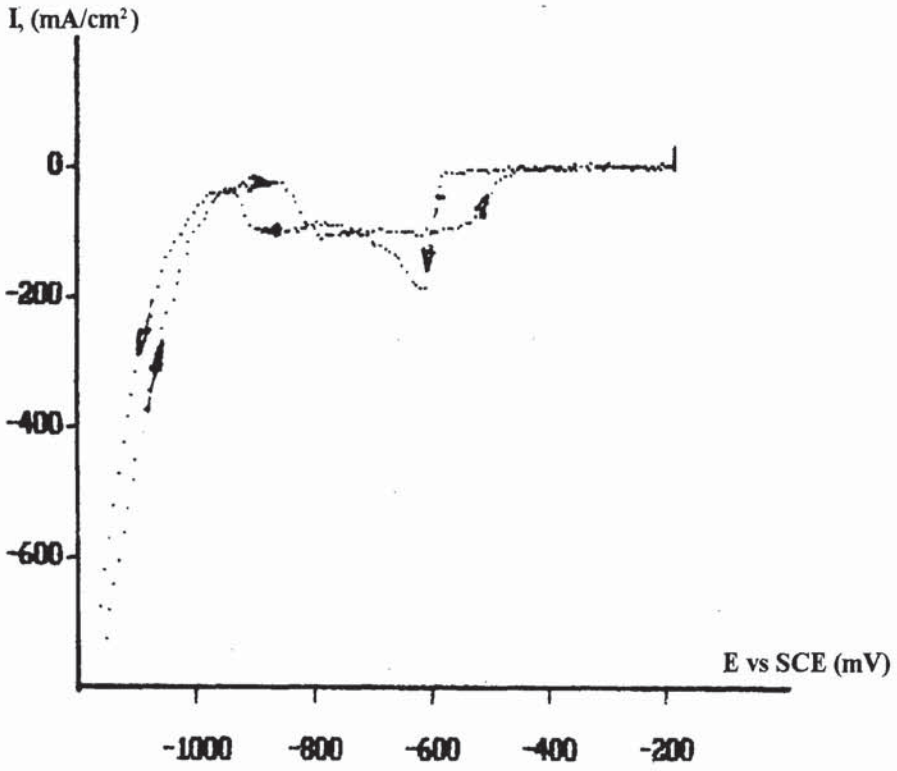

Figure 92. CrO_3, 250 g/L; H_2SO_4, 2.5 g/L; SSA, 2.5 g/L; ω = 0 rpm; v =10 mV/s.

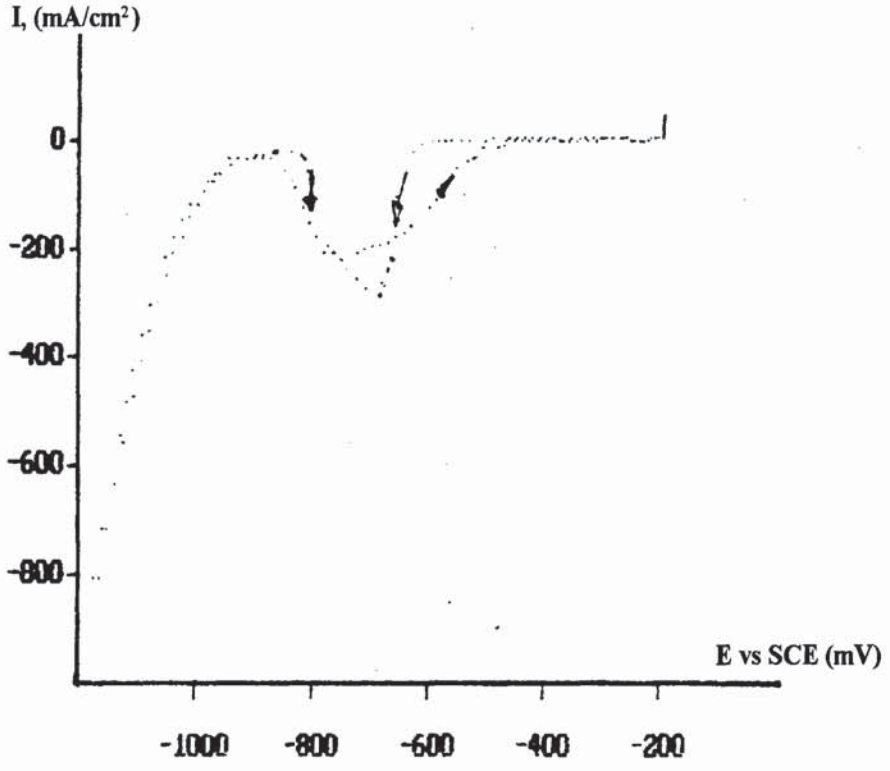

Figure 93. CrO_3, 250 g/L; H_2SO_4,, 2.5 g/L; SSA, 2.5 g/L; ω = 0 rpm; v =142 mV/s.

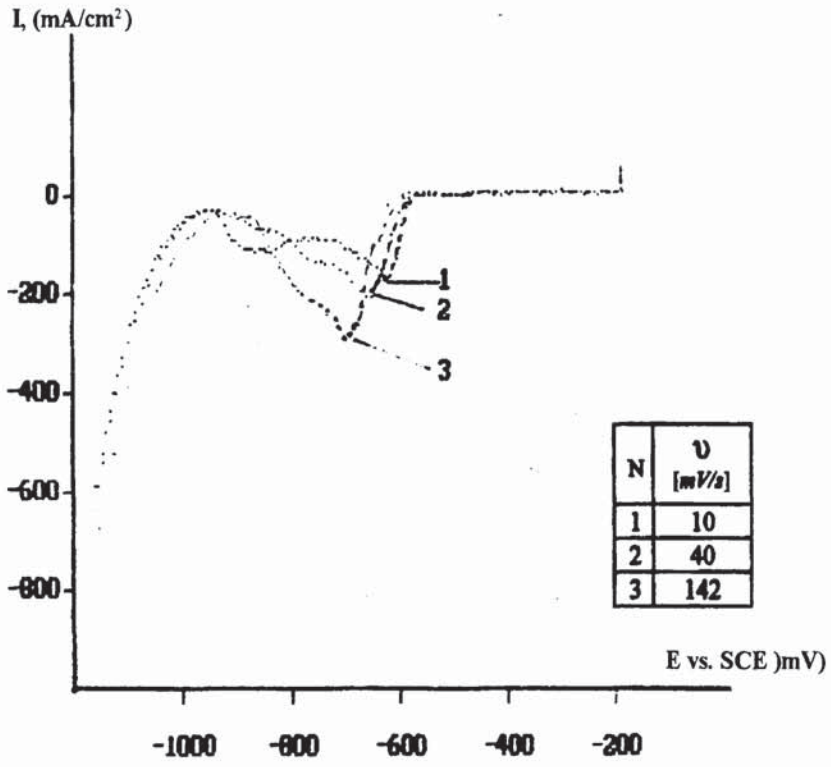

Figure 94. CrO_3, 250 g/L; H_2SO_4, 2.5 g/L; SSA, 2.5 g/L; $\omega = 0$ rpm. The reverse scans are not shown..

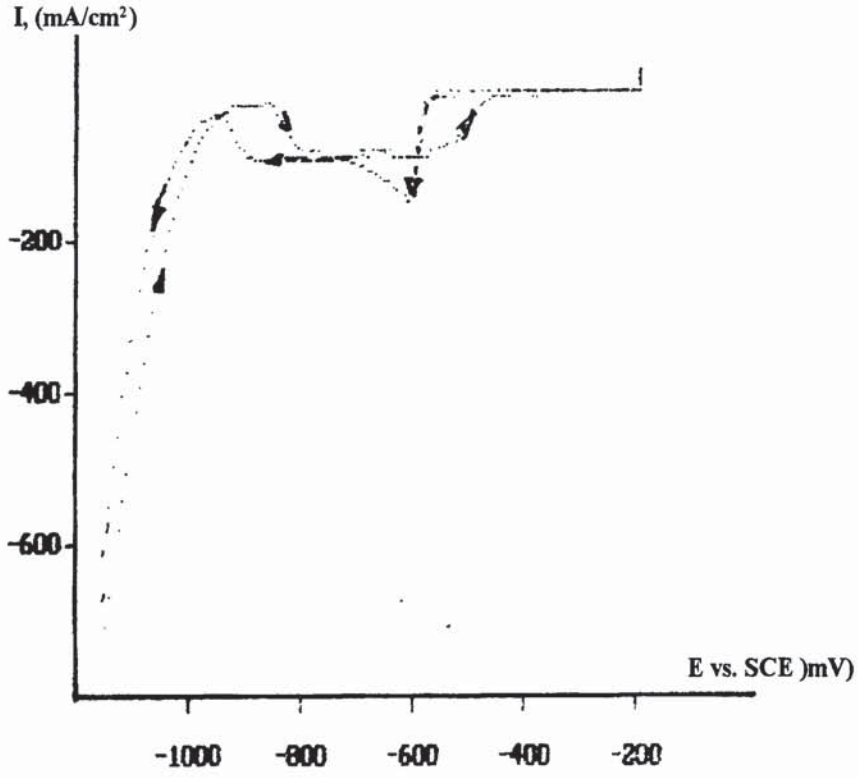

Figure 95. CrO_3, 250 g/L; H_2SO_4, 2.5 g/L; SSA, 1.25 g/L; $\omega = 0$ rpm; 10 mV/s.

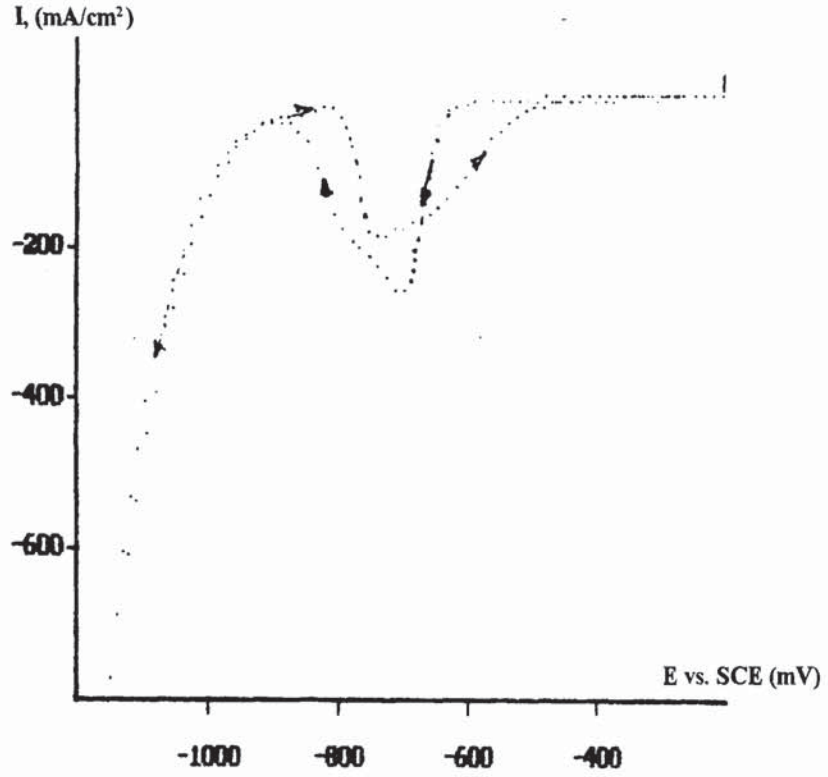

Figure 96. CrO_3, 250 g/L; H_2SO_4, 2.5 g/L; SSA, 1.25 g/L; ω = 0 rpm; 142 mV/s.

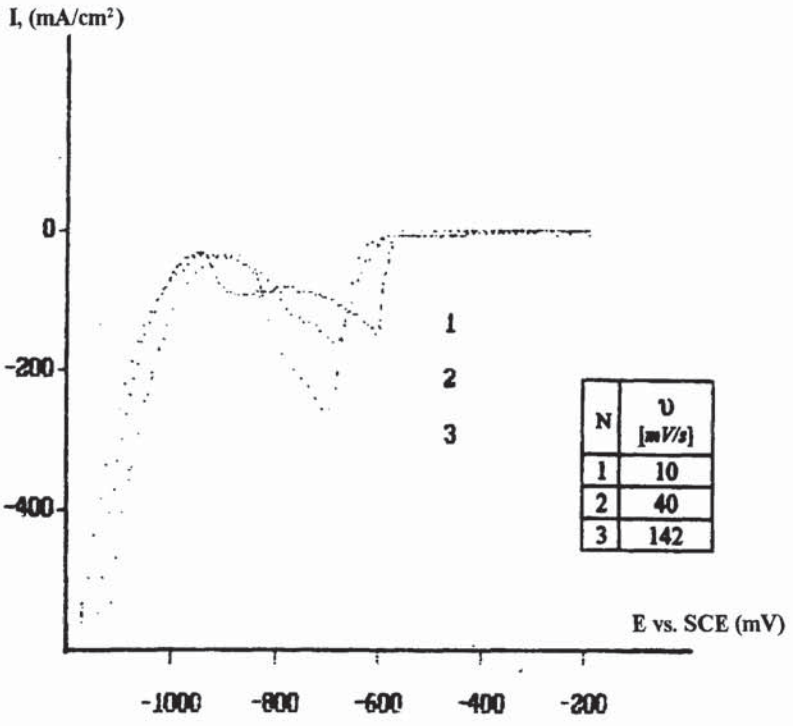

Figure 97. CrO_3, 250 g/L; H_2SO_4, 2.5 g/L; SSA, 1.25 g/L; ω = 0 rpm.
The reverse scans are not shown.

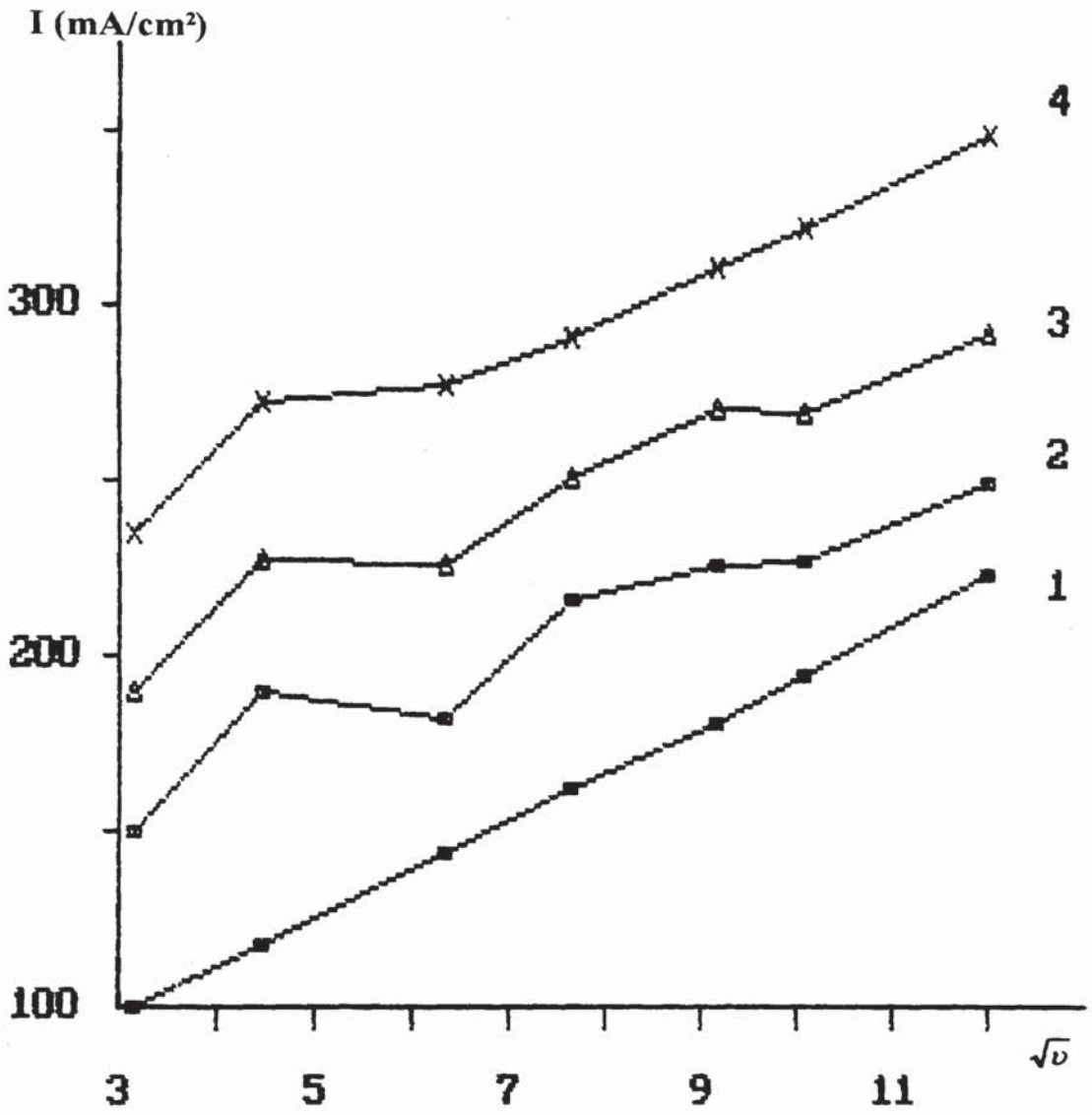

Figure 98. The effect of the scan rate on the cathodic maximum current (ω = 0 rpm). Data from Table 44.

1) Sargent Bath (SB).
2) SSA (1.25 g/L).
3) SSA (2.5 g/L).
4) SSA (5.0 g/L).

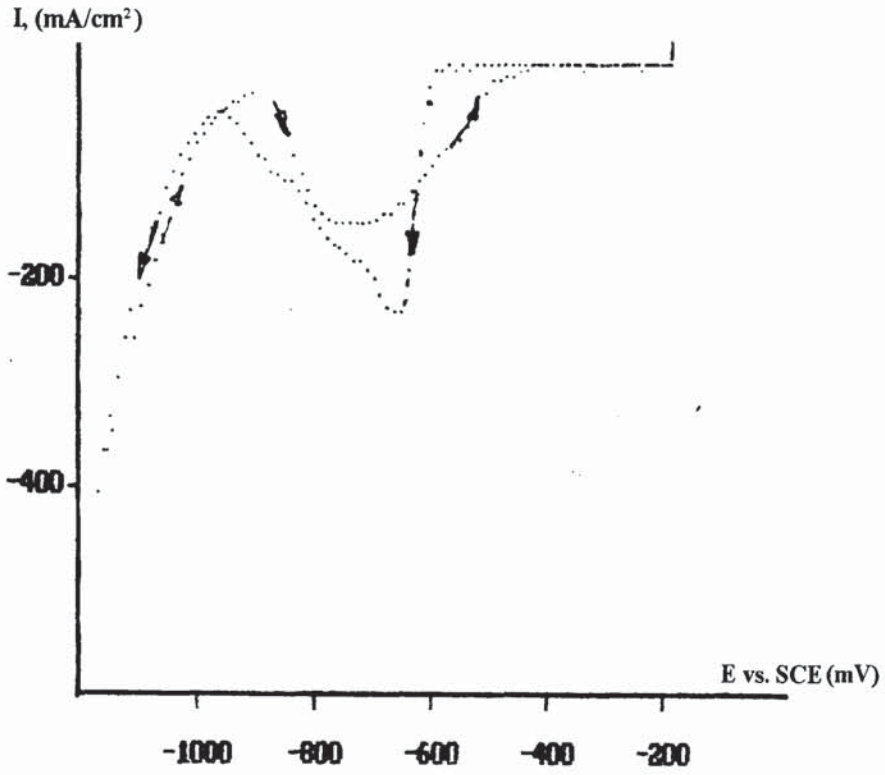

Figure 99. CrO_3, 250 g/L; H_2SO_4, 2.5 g/L; SSA, 5.0 g/L; ω = 500 rpm; 40 mV/s.

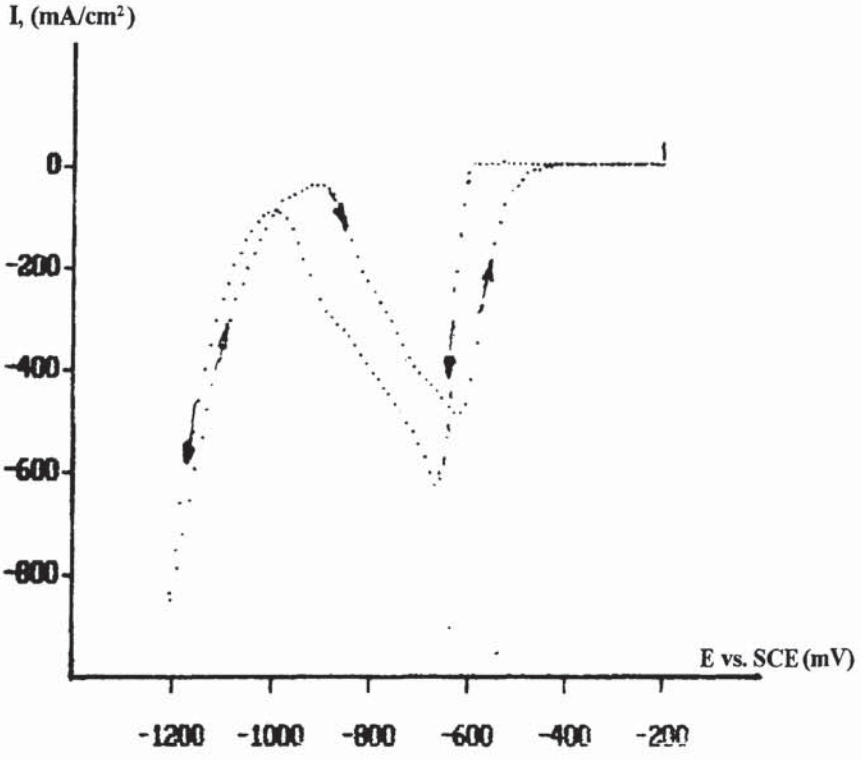

Figure 100. CrO_3, 250 g/L; H_2SO_4, 2.5 g/L; SSA, 5.0 g/L; ω = 3000 rpm; 40 mV/s.

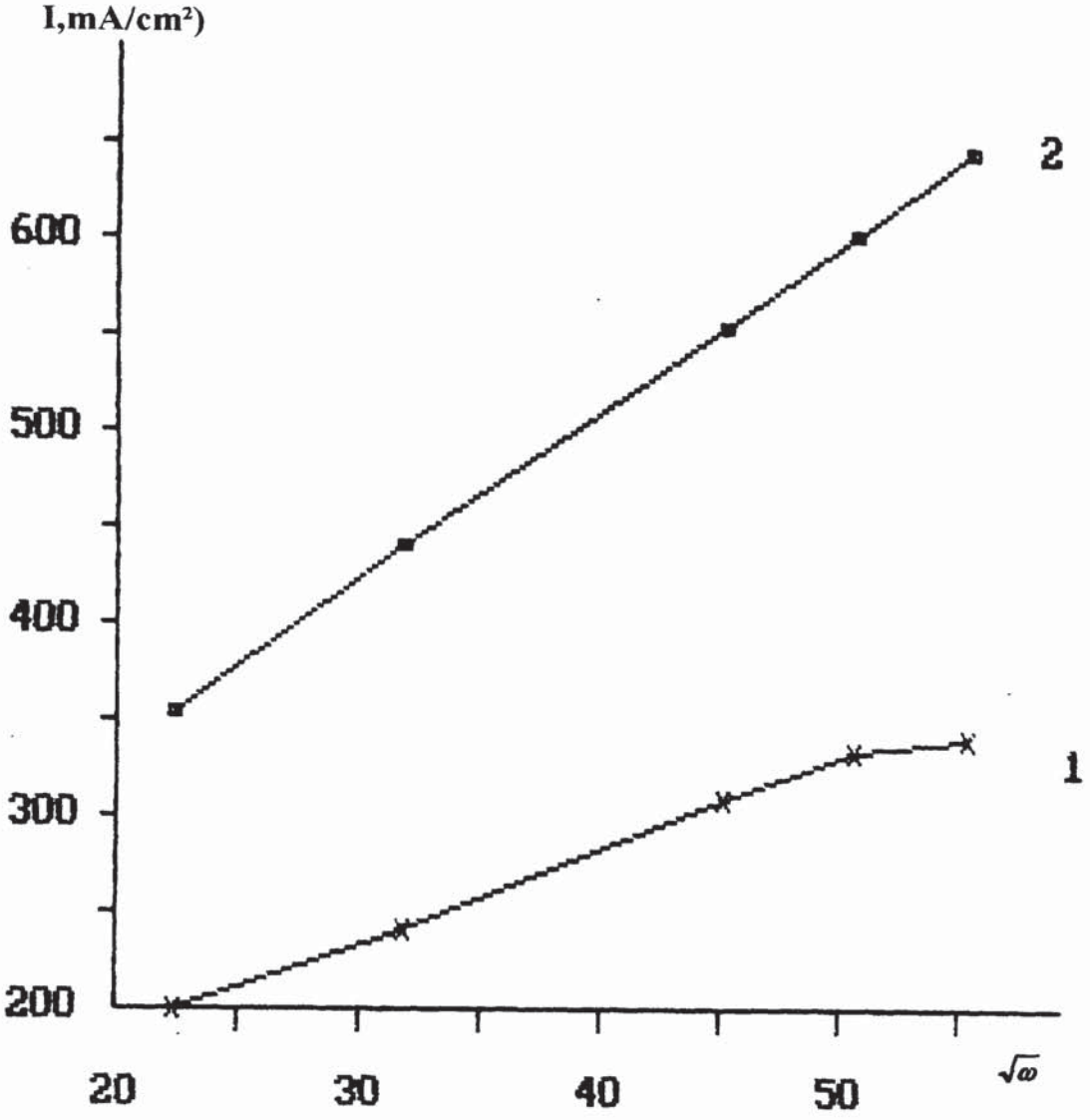

Figure 101. The cathodic peak as a function of the electrode rate ($\sqrt{\omega}$).
Data from Table 45.

1) Sargent Bath (SB); ν = 40 mV/s.
2) SB + SSA (5.0 g/L); ν = 40 mV/s.

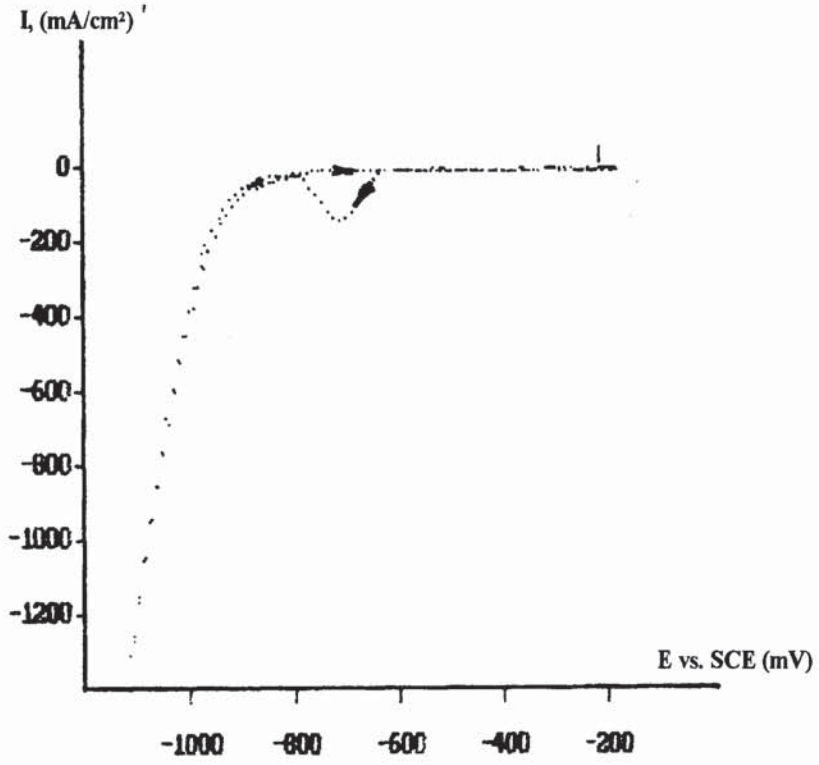

Figure 102. CrO_3, 250 g/L; H_2SO_4, 2.5 g/L; SSA, 5.0 g/L; $\omega = 0$ rpm; $v = 56$ mV/s; $T = 55^0$ C.

υ, mV/s	Concentration , g/l	I, mA/cm^2	E vs. SCE (mV)
10	1.25	150	609
20	1.25	190	612
40	1.25	183	653
58	1.25	217	670
83	1.25	227	685
100	1.25	228	686
142	1.25	250	709
10	2.5	190	615
20	2.5	228	620
40	2.5	227	655
58	2.5	252	674
83	2.5	272	685
100	2.5	270	690
142	2.5	293	705
10	5.0	235	607
20	5.0	273	613
40	5.0	278	653
58	5.0	292	665
83	5.0	307	680
100	5.0	323	692
142	5.0	349	707

Table 44. Maximum current (I), on Cr Electrode obtained from LPP cyclic voltammograms by cathodic-going sweep for the Sargent bath with SSA additive (1.25, 2.5 and 5.0 g/l) as a function of scan rate , *v*.

5. MSA Bath

i. Description of Linear Potential Polarisations and Cyclic Voltammagrams.

MSA (Methane Sulphonic Acid) at 5.0 g/ℓ as secondary catalyst is presented under the potentiodynamic condition in Figure 103 for scan rate v = 10 mV/s. and in Figure 104 for v = 100 mV/s. Figure 105 represents the influence of four scan rates (v = 10, 20, 58, 83 and 142 mV/s) plotted on one graph for 20^0 C.

The influence of higher temperature (55^0 C) for a stationary electrode at v = 56 mV/s. is presented in Figure 106.

Figure 107 shows the effect of electrode rotation rate on cathodic peak at 5.0 g/ℓ (20^0 C) and v = 56 mV/s and Figure 108 represents I - $\sqrt{\omega}$ relationship at 40 mV/s. for MSA catalyst and in the comparison with Sargent Bath. Figure 109 represents the same relationship for all five baths.

Lower concentrations (2.5 and 1.25 g/ℓ) did not change the cathodic peak, I, and corresponding voltammograms are not shown .

Figure 110 represents the relationship for I- $\sqrt{v}$ for all five plating baths.

ii. Discussion.

Figures 109 and 110 show that in the MSA bath the voltammograms have the same shape as in HEEF-25; no current is observed on the reverse scan. Unlike HEEF-405 additions (as evident in Figure 70) increase in MSA concentration did not change the cathodic peak I, and therefore, the cyclic voltammograms for MSA baths at 1.25 and 2.5 g/ℓ are not shown. The relationship of I- $v^{1/2}$ has a linear character at scan rates between 10-144 mV/s and almost coincides with those for Sargent bath plot. A closer look at the relationship of I-$\omega^{1/2}$ exhibits a curvature similar to Sargent bath as in Figure 54, indicating the presence of the kinetic component of the current. This is more noticeable at rotation speeds higher than 2500 rpm ($\omega^{1/2} = 50$) as clearly evident in Figure 108.

Since later results presented in Section II.3.4 are clearly indicating that MSA drastically improves cathodic current efficiency (CCE), it can be concluded that the increase in CCE is not due to the influence of MSA to the partial reduction reaction ($Cr^{6+} \rightarrow Cr^{6+}$), but rather to the state of the L-film.

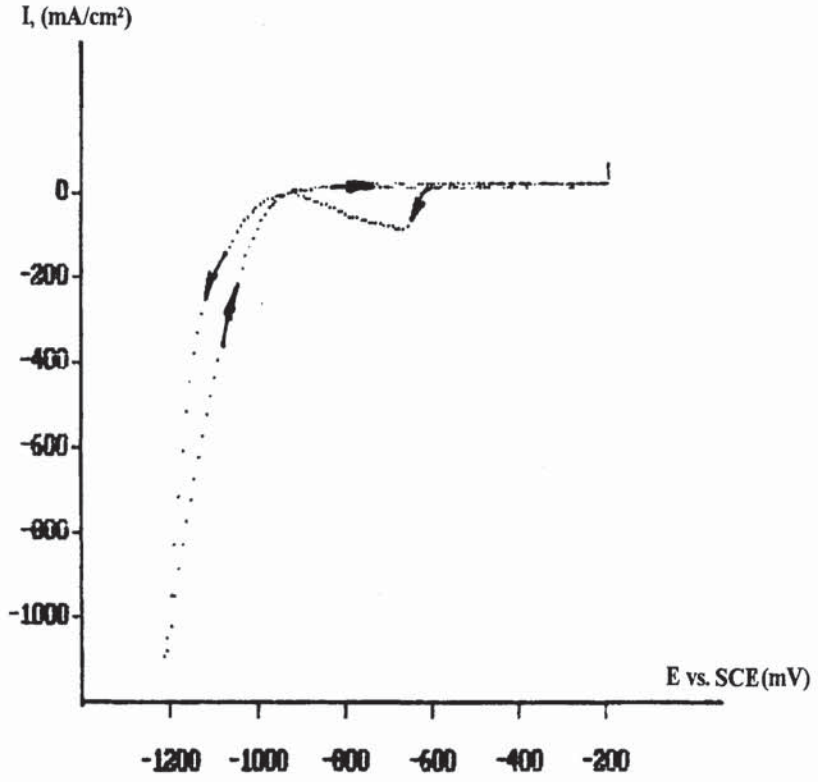

Figure 103. CrO_3, 250 g/L; H_2SO_4, 2.5 g/L; MSA, 5.0 g/L; $\omega = 0$ rpm; $\nu = 10$ mV/s.

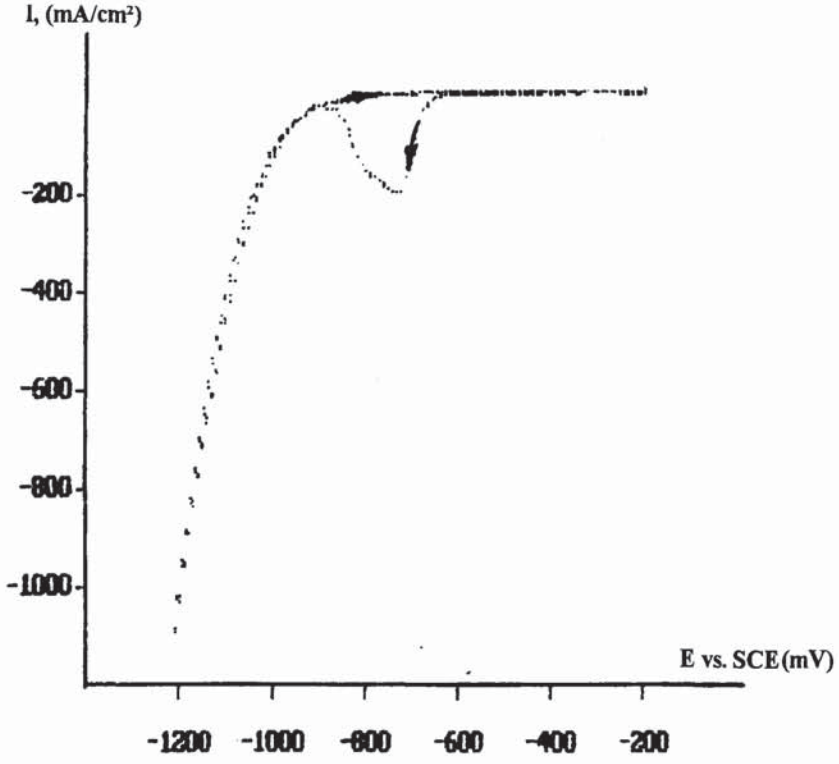

Figure 104. CrO_3, 250 g/L; H_2SO_4, 2.5 g/L; MSA, 5.0 g/L; $\omega = 0$ rpm; $\nu = 100$ mV/s.

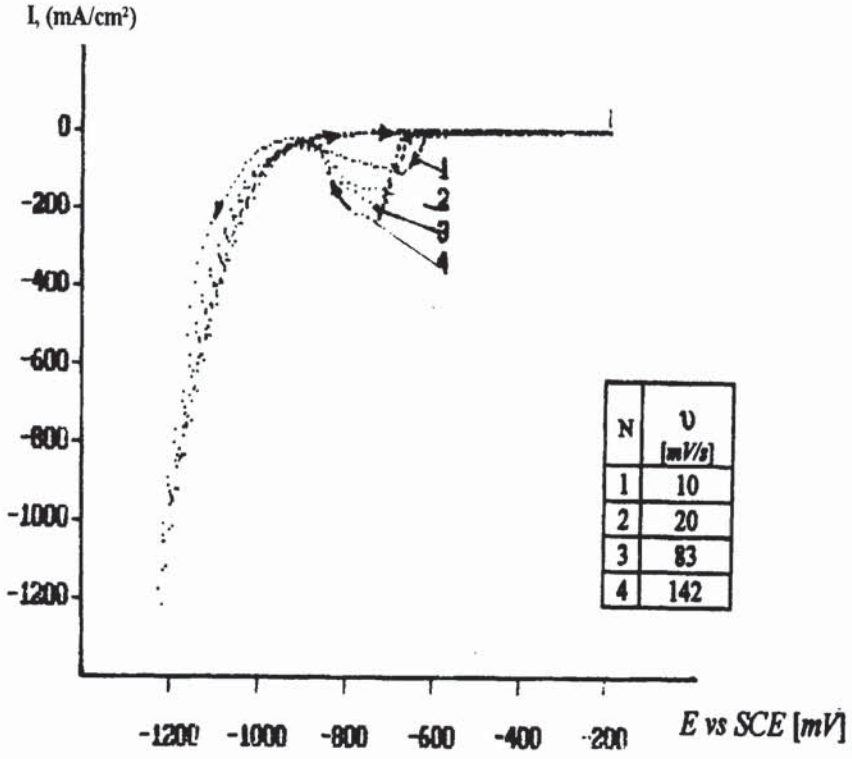

Figure 105. CrO_3, 250 g/L; H_2SO_4, 2.5 g/L; MSA, 5.0 g/L; $\omega = 0$ rpm.

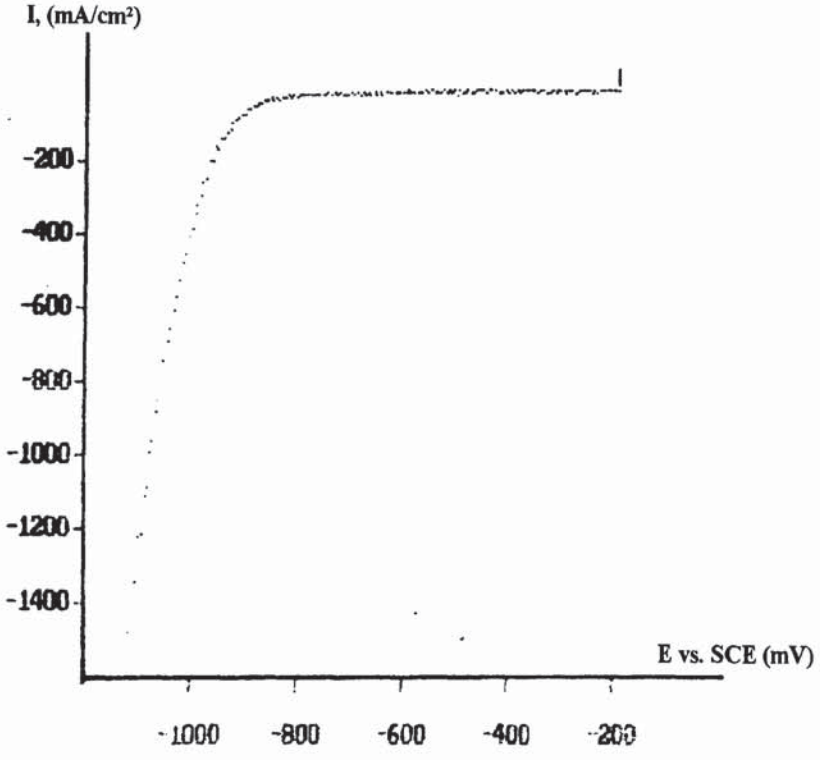

Figure 106. CrO_3, 250 g/L; H_2SO_4, 2.5 g/L; MSA, 5.0 g/L $\omega = 0$ rpm.
$v = 56$ mV/s.; T = 55° C.

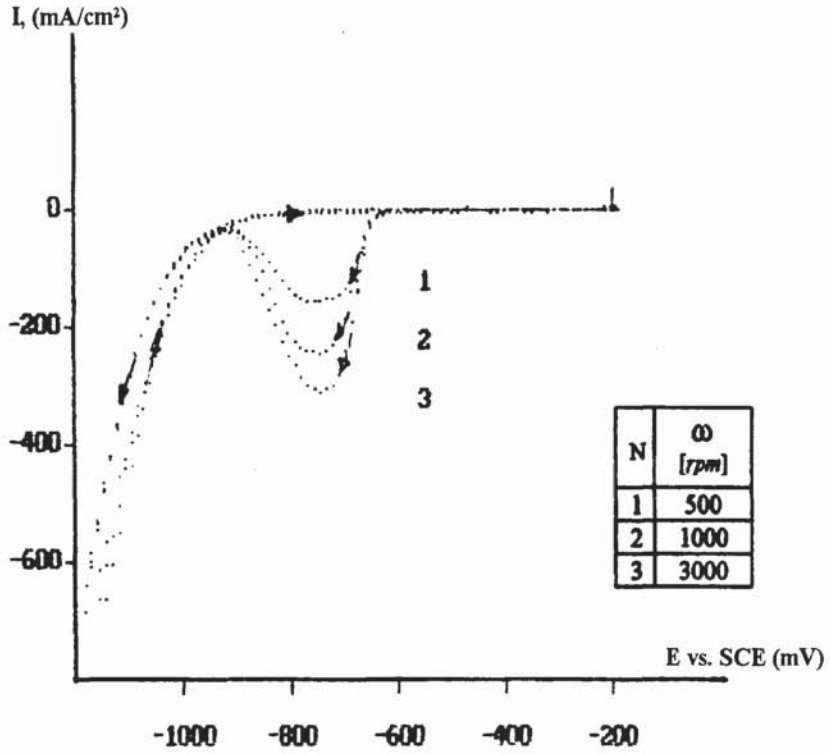

Figure 107. CrO_3, 250 g/L; H_2SO_4, 2.5 g/L; MSA, 5.0 g/L; v = 56 mV/s.

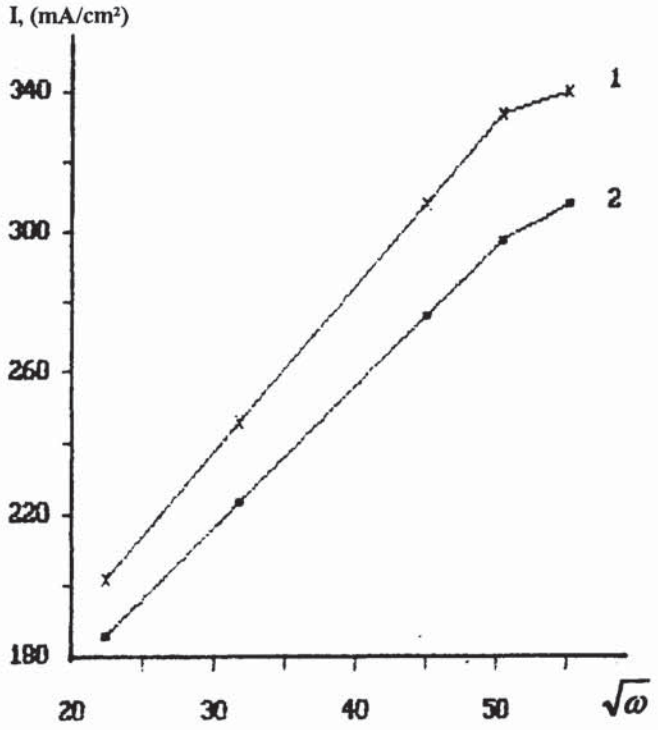

Figure 108 The Maximum Current I as a function of the electrode rotation rate ($\sqrt{\omega}$)
Data from Table 45.

1. Sargent Bath (SB); 40 mV/s.
2. SB + MSA 5.0 g/L; 40 mV/s.

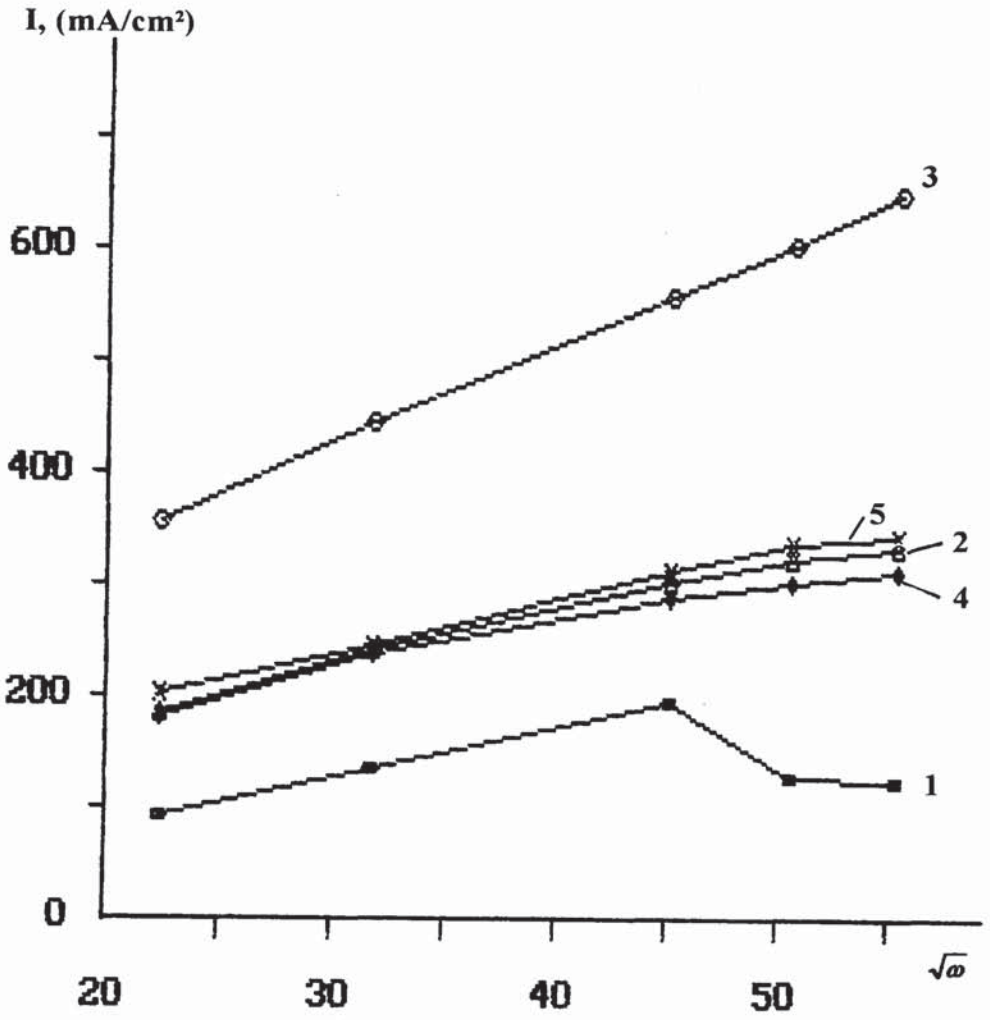

Figure 109. The Maximum Current *I* as a function of the electrode rotation rate ($\sqrt{\omega}$).
Data from Table 45.

1) HEEF-405 (5.0 g/ℓ); v = 40 mV/s.
2) HEEF-25 (5.0 g/ℓ); v = 40 mV/s.
3) SSA (5.0 g/ℓ); v = 40 mV/s.
4) MSA (5.0 g/ℓ); v = 40 mV/s.
5) Sargent Bath (SB).

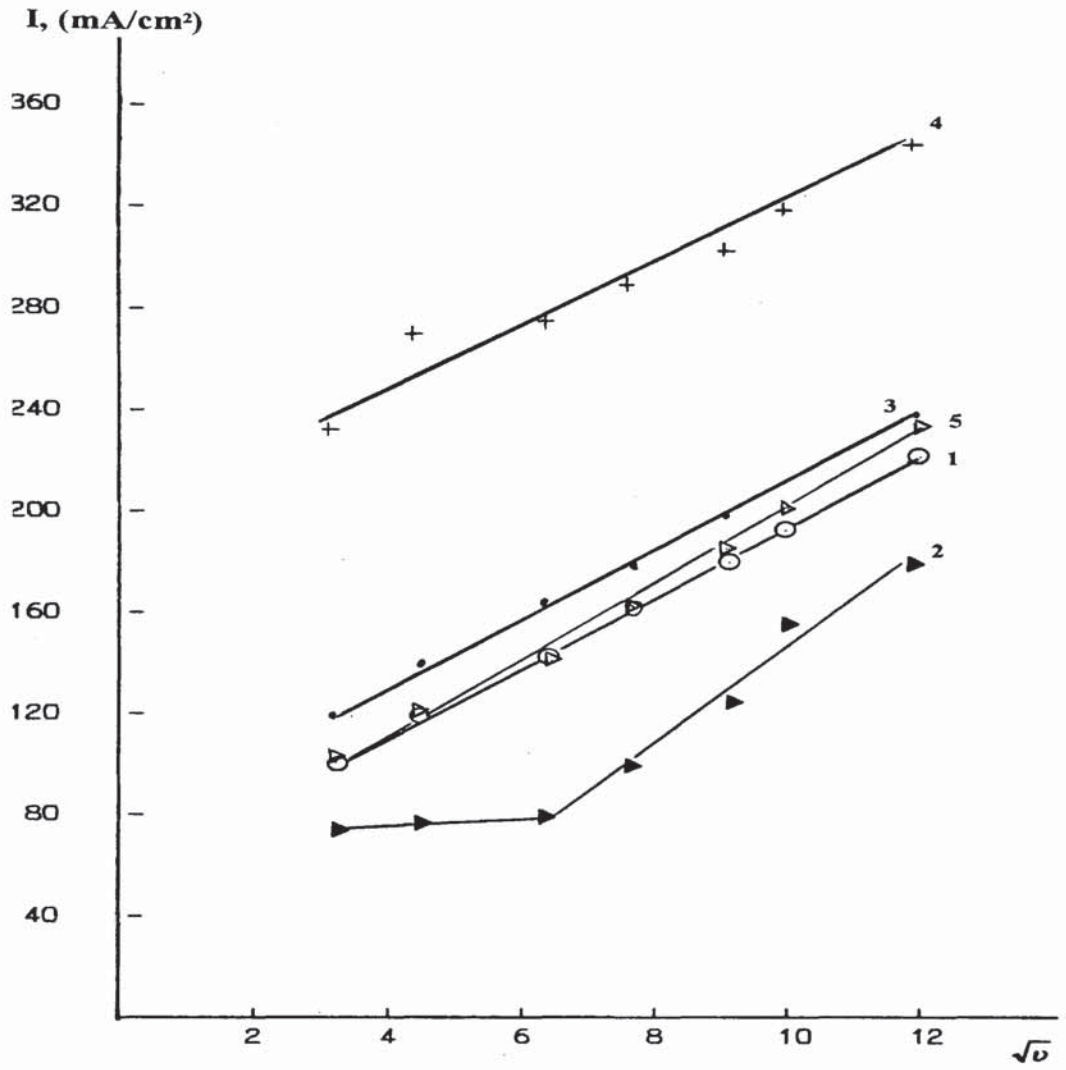

Figure 110. The Cathodic Peak I as a function of $\sqrt{v}$. Data from Table 46.

1) Sargent Bath.
2) HEEF-405 Bath. (5.0 g/l)
3) HEEF-25 Bath. (5.0 g/l)
4) SSA Bath. (5.0 g/l)
5) MSA Bath. (5.0 g/l)

ω, rpm	SB		SB +HEEF -405		SB+ HEEF-25		SB + SSA		SB +MSA	
	I	-E	I	-E	I	-E	I	-E	I	-E
500	202	643	92	790	185	605	353	654	179	736
1000	248	645	162	790	241	665	392	654	236	747
2000	308	647	194	790	298	660	560	654	286	736
2500	334	643	128	820	321	650	597	656	299	740
3000	342	640	124	830	332	656	642	656	308	747

Table 45. Maximum current, I, (mA/cm^2), on Cr electrode for four different solutions with four additives (5.0 g/l) as a function of ω. Scan rate $v = 40$ mV/s E vs. SCE (mV).

Plating Bath	n, (mV/s)	I, (mA/cm^2)	-E vs. SCE (mV)
Sargent Bath (SB)	10	102	601
	20	121	615
	40	142	676
	58	163	695
	83	182	715
	100	195	720
SB + HEEF-405	10	75	694
	20	77	702
	40	79	780
	58	100	775
	83	126	765
	100	155	762
SB + HEEF-25	10	119	605
	20	134	610
	40	165	670
	58	179	692
	83	200	705
	100	219	707
SB + SSD	10	235	607
	20	273	613
	40	278	653
	58	292	665
	83	307	680
	100	323	692
SB + MSD	10	104	665
	40	142	717
	58	165	720
	83	188	731
	100	204	731

Table 46. Cathodic maximum current. (I) , for the Sargent bath alone and with four [illegible] as a function of scan rate, . (20^0 C)

6. *SYNTHETIC ADDITIVE*

From observations and data on behaviour of the Sargent bath catalysed with HEEF-25 and HEEF-405, new additive is prepared and designated as "synthetic." Additive is prepared from 5 g/L of methane sulphonic acid and 7.0 g/L of potassium iodide (KI). When dissolved in chromic acid, KI behaved similarly to HEEF-405 catalyst and produced a familiar colour change. It is known that iodide can be transformed into iodate or periodate by the reaction with a strong oxidising agent, in our case, by CrO_3. The reaction proceeds with formation of the intermediate substance: iodine (I_2). It was previously observed that during dissolution of HEEF-405 in Sargent bath, the black powder formed is probably elementary iodine . Voltammograms of the synthetic catalyst have a shape somewhat similar to the HEEF-405 bath. It is reasonably possible that HEEF-405 catalyst can consist of iodide and an alkyl sulphonic acid or their salts. However, later analysis by Raman laser spectroscopy (RLS) proved that sulphonic acid involved is isothionic acid (hydroxy-ethane sulphonic acid). It is truly unfortunate that isothionic acid is unstable in the presence of strong, hot chromic acid. It is used in household detergent formulations and therefore being inexpensive and readily available. Analytical results were obtained by an outside laboratory with the use of a Raman Laser Spectrograph, (Model U-1000 by Instruments S.A), The wavelengths used for the argon laser were 514 and 532 nm. The photo multyplier detector with photon counting used was Model C31034. RLS results are presented in Appendix V

7. THE EFFECT OF HIGHER TEMPERATURE (55^0 C)

The cathodic wave disappears at higher temperatures (except for HEEF-405) probably due to the passivation of the chromium surface. However, the SSA bath shows strong, *apparent* catalytic activity. *Actual* catalytic activity, however, is due to the action of the sulphates from original H_2SO_4 content and additional sulphate ions from SSA . SSA has been transformed (broken down) due to the redox reaction with chromic acid, which attacks the SSA molecule and supplies additional sulphate ions as products of its decomposition and this influences the L-film, formation and its character. The affect of temperature will be detailed in Section II.4.2.

II.4.1.e Summary - Deposition Mechanisms

From the previous separate discussions and from the results presented in Figures 109 and 110, the role of additives can be summarised in order of their influence on the reaction rate $Cr^{6+} \rightarrow Cr^{3+}$:

MSA. (methane sulphonic acid) has no influence on this reaction; severely attacks Pb anodes; CCE is increased.

HEEF-25. (methane disulphonic acid) is a week catalyst. CCE is increased .

SSA. (salycil sulphonic acid) is a strong but unstable catalyst.

HEEF-405. (isothionic acid with KIO_3) inhibits the reaction, greatly increases CCE but has an unacceptable adhesion problem.

The electrochemical aspect of the mechanisms were discussed in detail under separate headings for each of the catalysts, and in general in section II.4.1.c

II. 4.2 ELECTROCHEMICAL KINETICS OF CHROMIUM DEPOSITION IN THE PRESENCE OF MSA AND DMSA.

II. 4.2.1 **Experimental Details**

Experimental procedures and equipment used is similar to that described in II.3.1a. Scanning rates are purposely kept low (2 mV/s.) in order to be close to steady state conditions.

II. 4.2.2 **Experimental Results**

1. INFLUENCE OF TEMPERATURE ON THE SULPHATE, MSA AND DMSA CATALYSED BATHS .

a) *Description of the experiments*

i. Sulphate catalysed baths:

The influence of temperature on potentiodynamic curve is presented in Figure 111 for low concentration (1.0 M,), a very low ratio (40:1), high sulphuric content chromium plating bath for 20, 40, 50, and 68^0 C. In Figure 112 peak currents are plotted vs. temperatures for the same bath. Figure 113 is a similar potentiodynamic curve for less diluted (1.6 M CrO_3) a still low ratio (64:1) bath. Figure 114 represents the influence of temperature on maximum current for standard Sargent bath. Figure 115 is a potentiodynamic curve presenting the influence of different low sulphate ratios on maximum current for low concentrations (0.5, 1.0 and 1.6 M) chromium plating baths.

ii . MSA catalysed baths:

Figures 116-120 are potentiodynamic curves for (100:1) standard Sargent bath with the addition of 1% MSA as secondary catalyst for five different temperatures (25, 30, 40, 50 and 60^0 C), are plotted separately. They are also plotted together in figure 121. For purposes of clarity, the three most important temperatures (30, 40 and 50^0 C) are presented in Figure 122.

Low concentration (0.5 M, 50 g/ℓ), low ratio (20:1), high sulphuric acid content, chromium plating bath is presented in Figure 123 for 20, 40, 50, and 70^0 C. Figure 124 represents the influence of different temperatures on maximum currents for standard [illegible] addition.

iii. DMSA catalysed bath.

In the same fashion, potentiodynamic curves for 2.5 M (250g/l CrO_3) standard Sargent bath (100:1) with 1% DMSA addition is presented separately in Figures 125-129 for 25, 30, 40, 50 and 60^0 C. Figure 130 represents magnitudes of maximum current for all five different bath temperatures. Figure 131 is potentiodynamic response of the Sargent bath with sulphate catalyst alone. Figure 132 represents 1% of MSA and DMSA additions as secondary catalysts at 30^0 C.

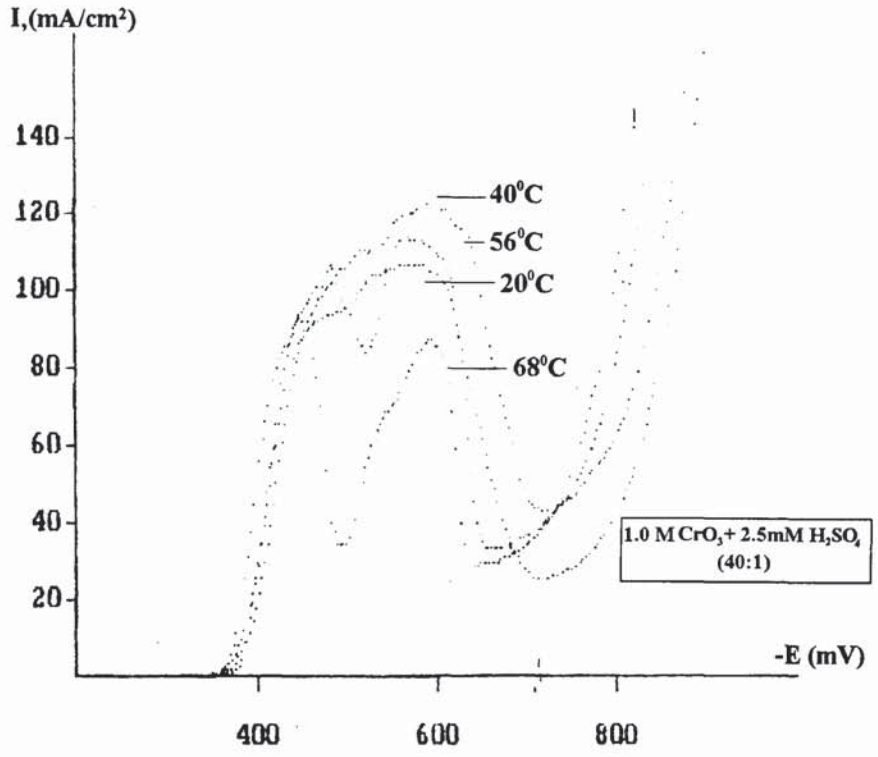

Figure 111. Potentiodynamic scans for 1.0 M CrO_3 +2.5 mM H_2SO_4 (40:1) plating bath at 20, 40, 56 and 68^0 C.

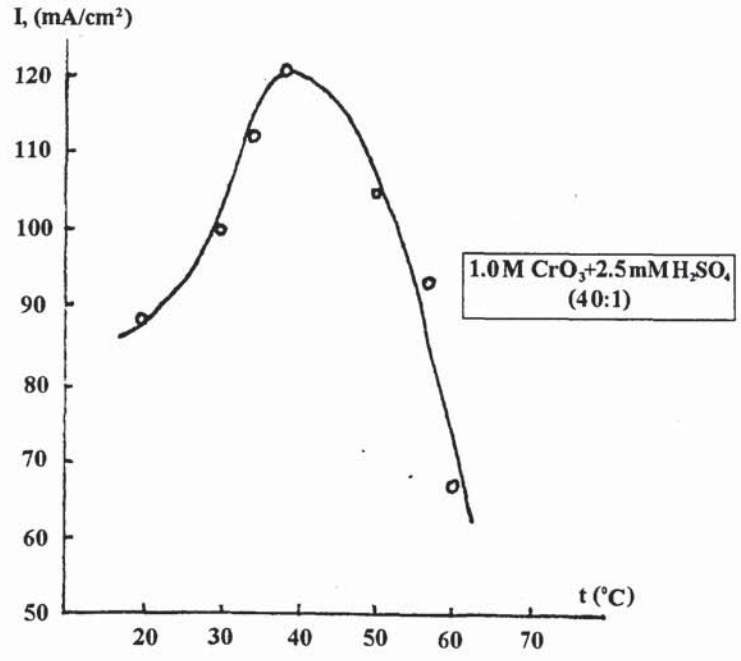

Figure 112. Influence of temperature on maximum current for 1.0 M (40:1) plating bath.

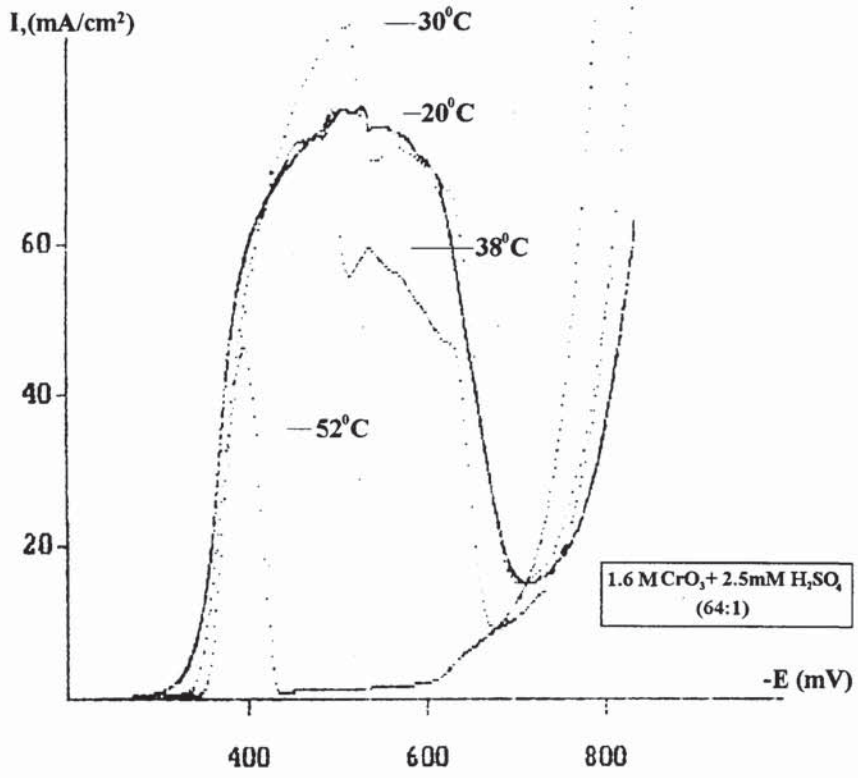

Figure 113. Potentiodynamic scans for 1.6 M CrO_3 +2.5 mM H_2SO_4 (64:1) at 20, 30, 38 and 52° C.

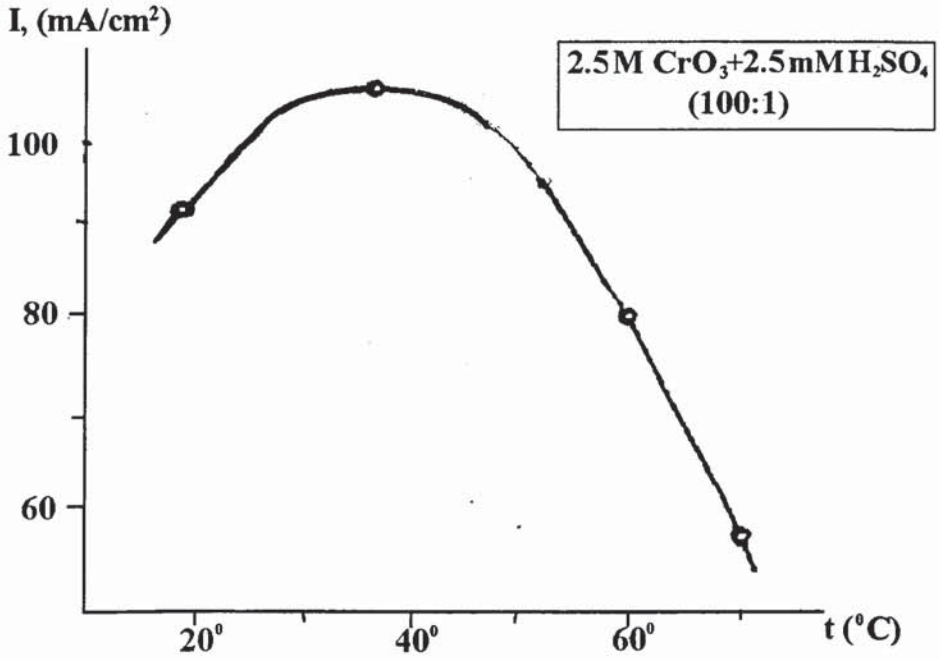

Figure 114. Influence of temperature on maximum current for (100:1) Sargent bath.

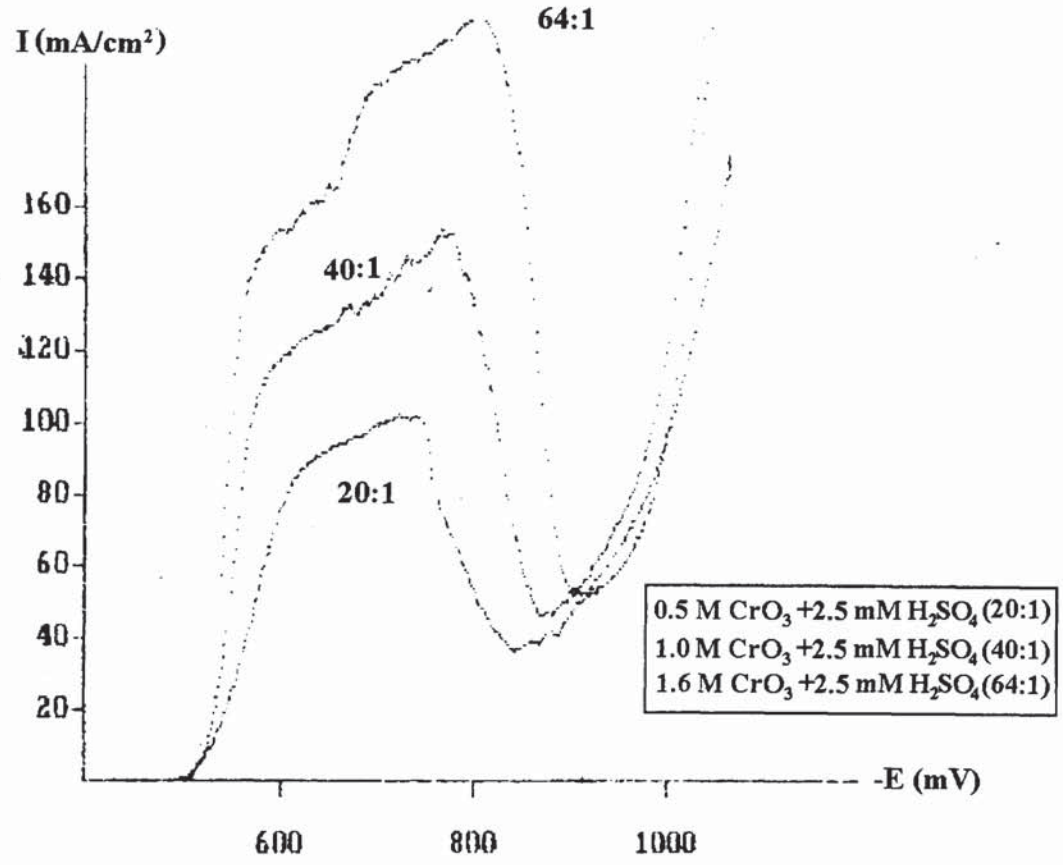

Figure 115. Influence of different CrO_3 concentrations and sulphate ratios on maximum current at 30^0 C.

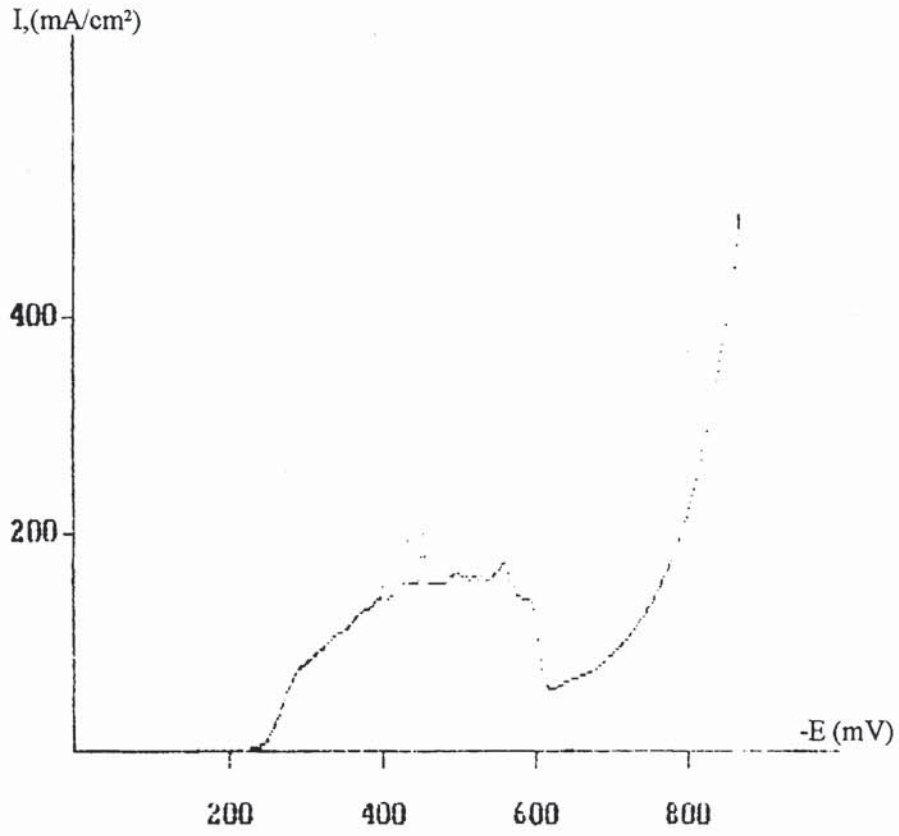

Figure 116. Potentiodynamic scan for Sargent Bath (100:1) + 1% MSA at 25^0 C.

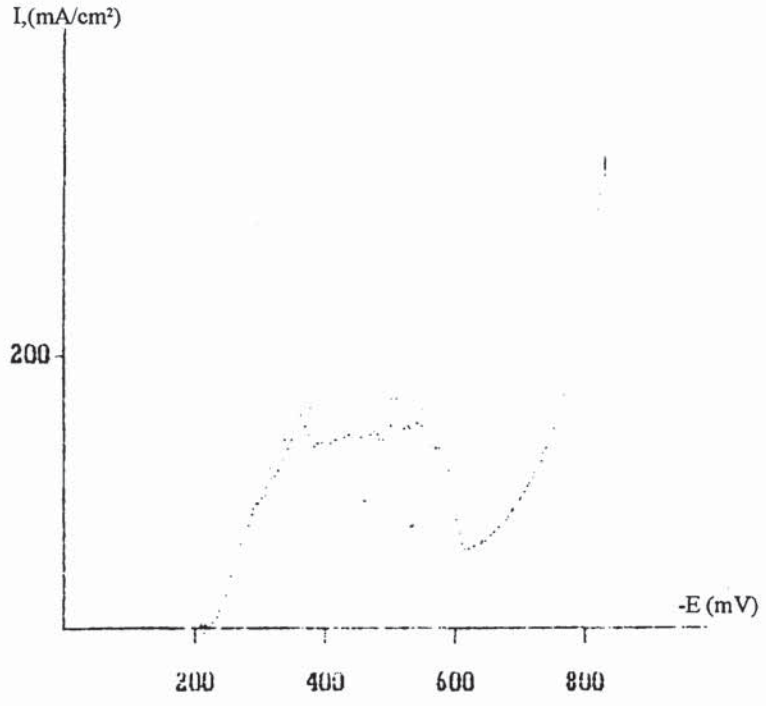

Figure 117. Potentiodynamic scan for Sargent Bath (100:1) + 1% MSA at 30^0 C.

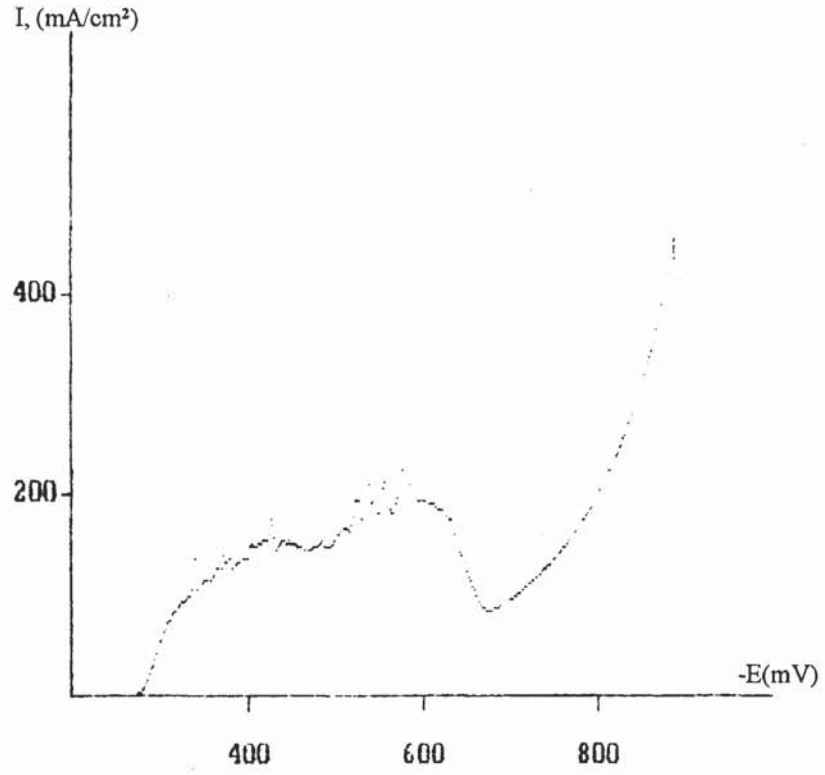

Figure 118. Potentiodynamic scan for Sargent Bath (100:1) + 1% MSA at 40^0 C

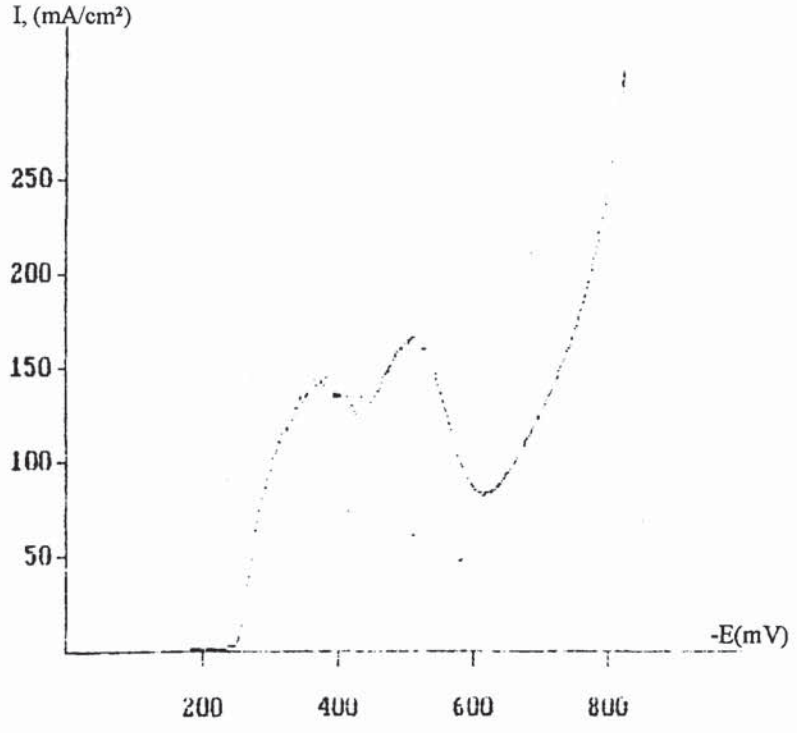

Figure 119. Potentiodynamic scan for Sargent Bath (100:1) + 1% MSA at 50^0 C.

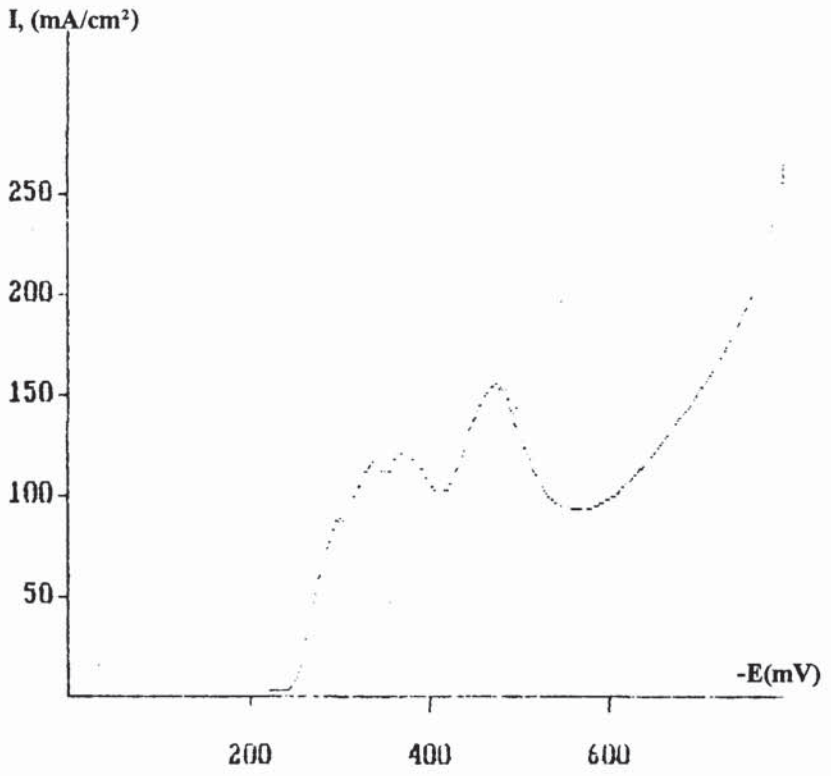

Figure 120. Potentiodynamic scan for 2.5 M Sargent Bath (100:1) + 1% MSA at 60^0 C.

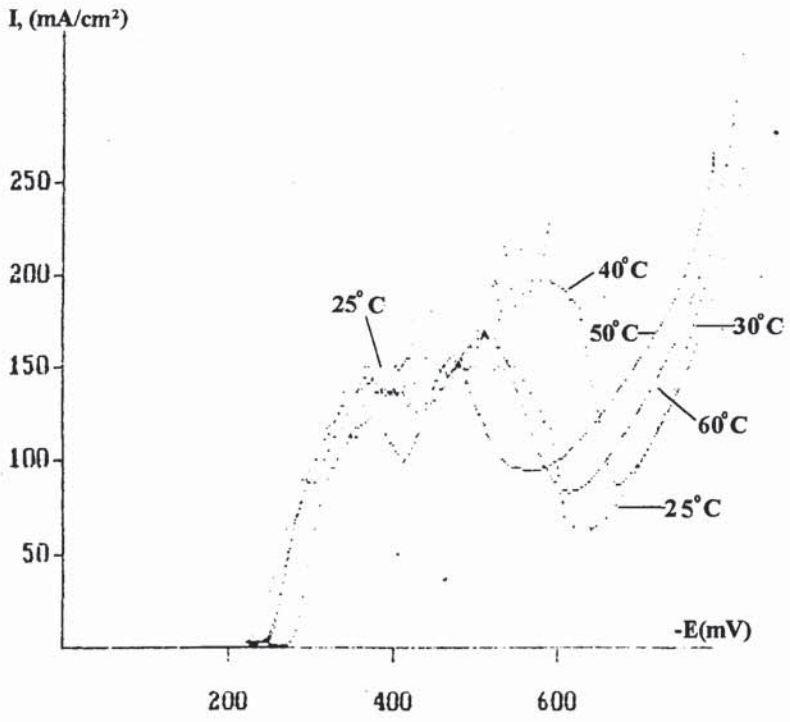

Figure 121. Potentiodynamic scans from for 2.5 M SB + 1% MSA bath (Figures 116-120) plotted together.

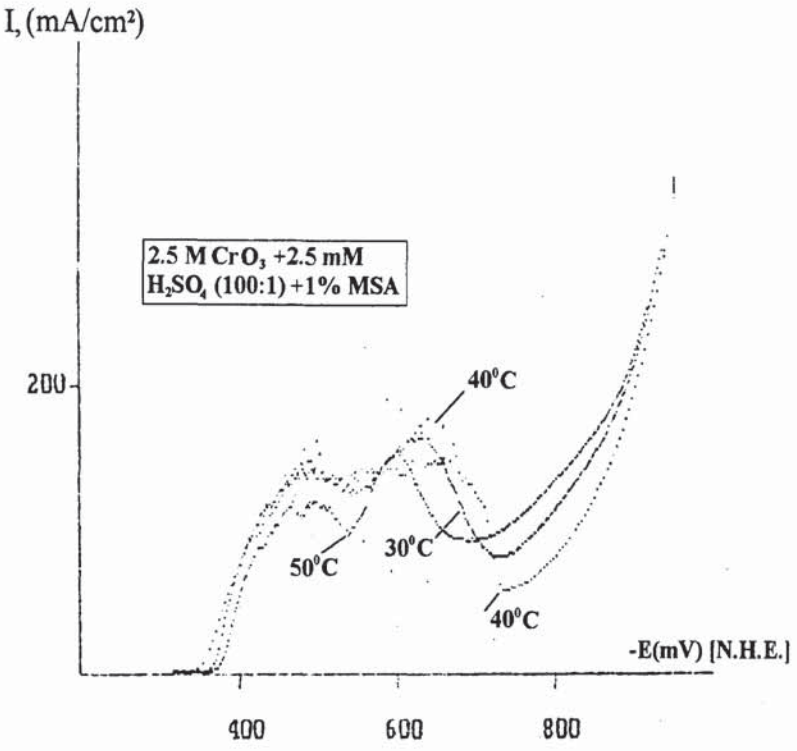

Figure 122. Potentiodynamic scan for SB (100:1) + 1% MSA bath at 30, 40 and 50° C.

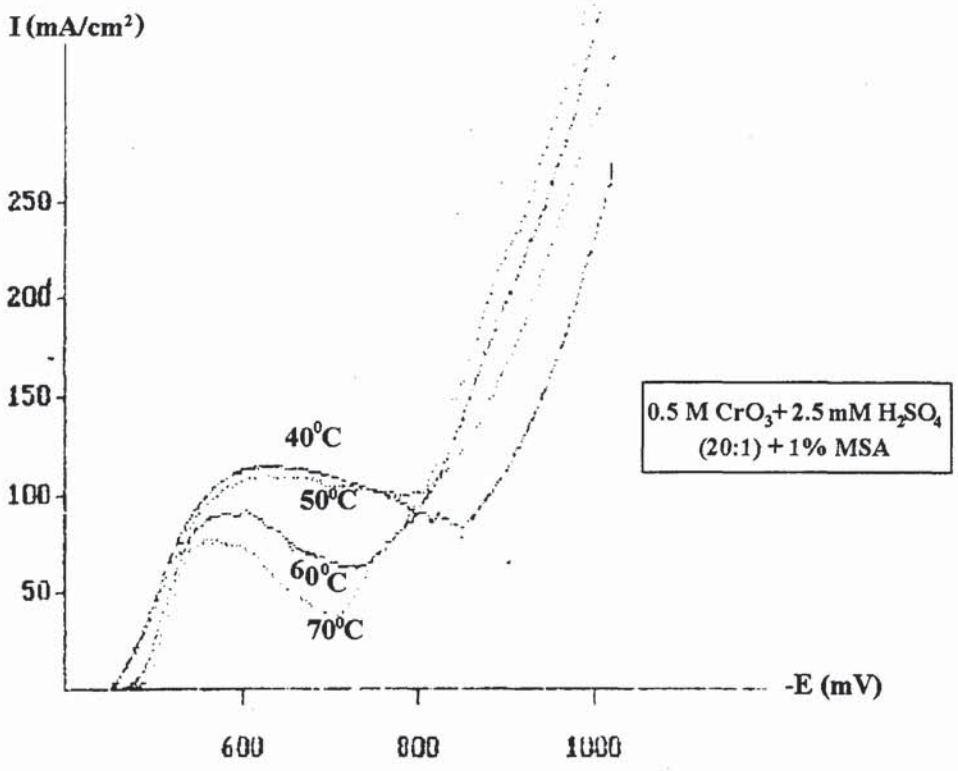

Figure 123 Potentiodynamic scans for SB (20:1) + 1% MSA bath at 40, 50, 60 and 70° C.

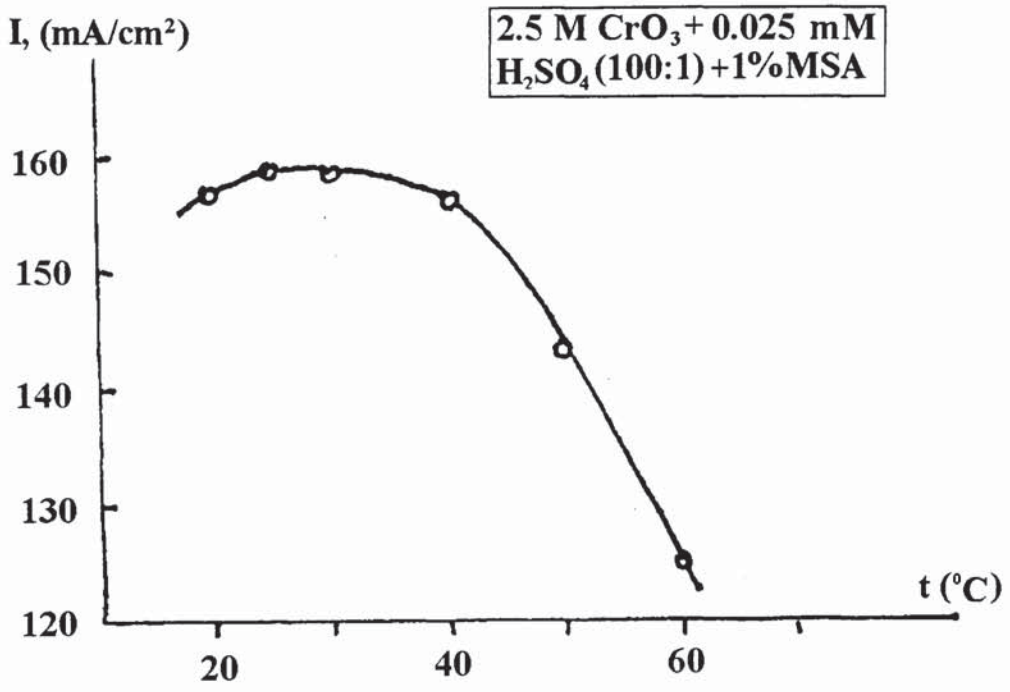

Figure 124. Influence of temperature on maximum current for SB + 1% MSA bath.

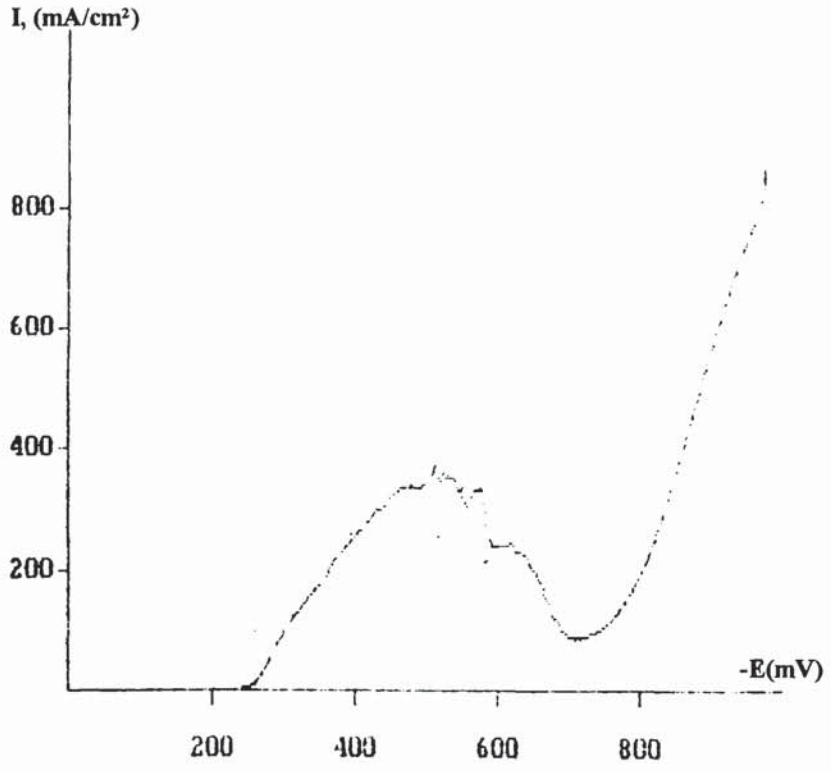

Figure 125 Potentiodynamic scan for Sargent Bath (100:1) + 1% DMSA at 25^0 C.

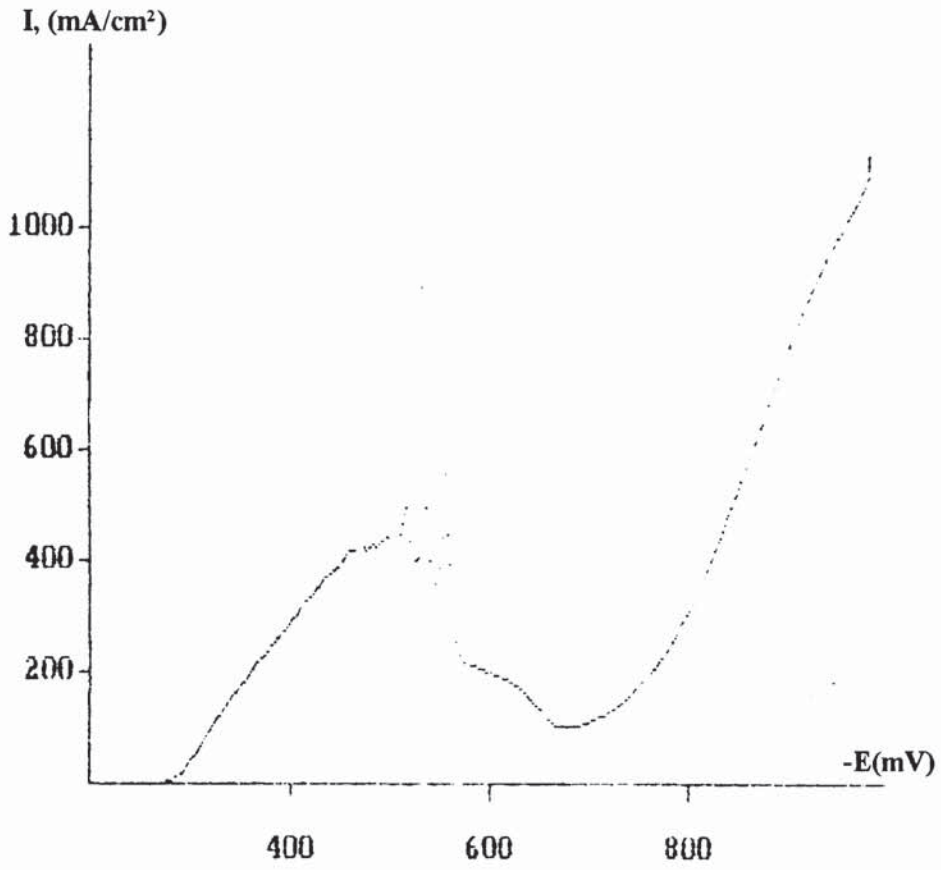

Figure 126. Potentiodynamic scan for Sargent Bath (100:1) + 1% DMSA at 30^0 C.

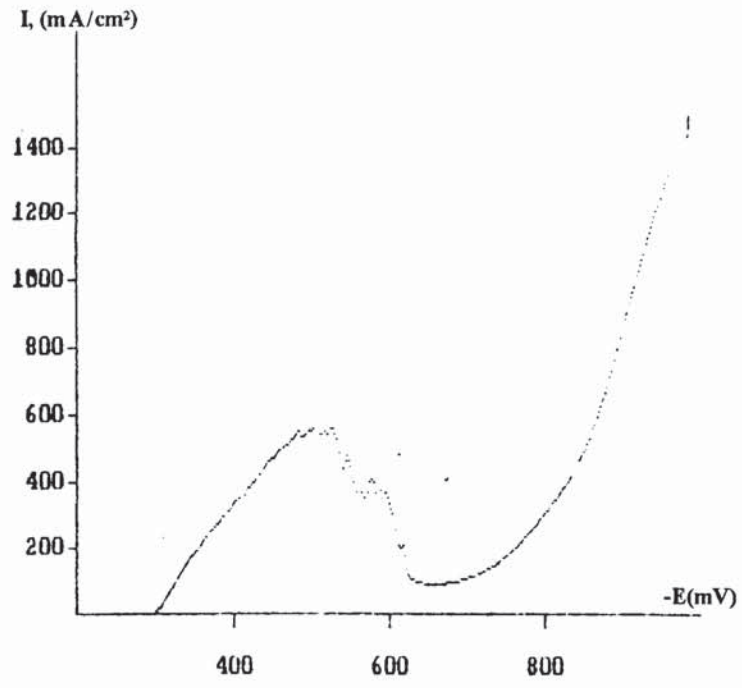

Figure 127. Potentiodynamic scan for Sargent Bath (100:1) + 1% DMSA at 40^0 C.

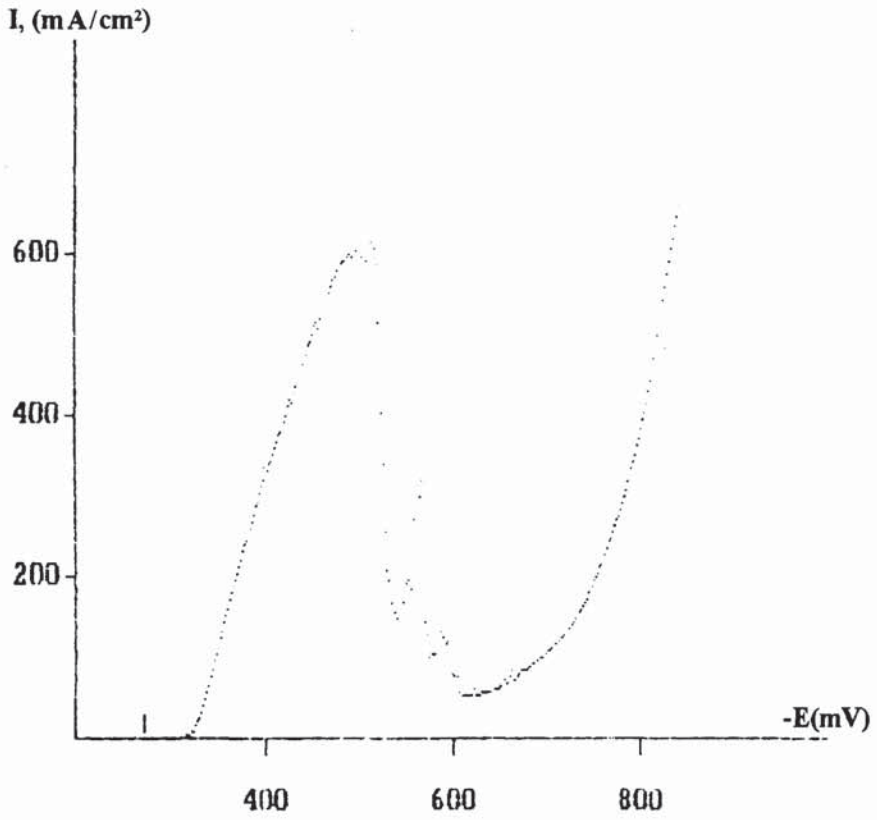

Figure 128. Potentiodynamic scan for Sargent Bath (100:1) + 1% DMSA at 50^0 C.

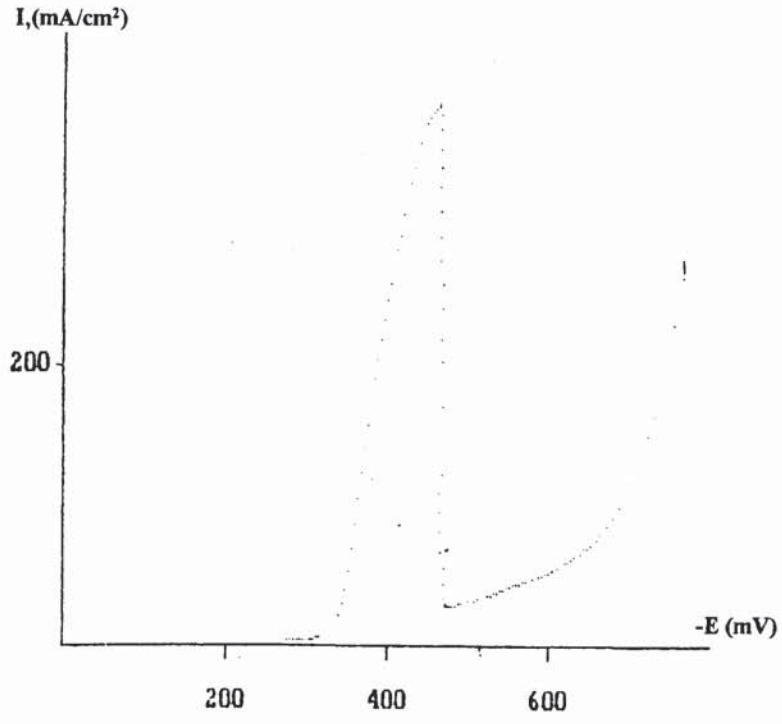

Figure 129. Potentiodynamic scan for Sargent bath (100:1) + 1% DMSA at 60^0 C.

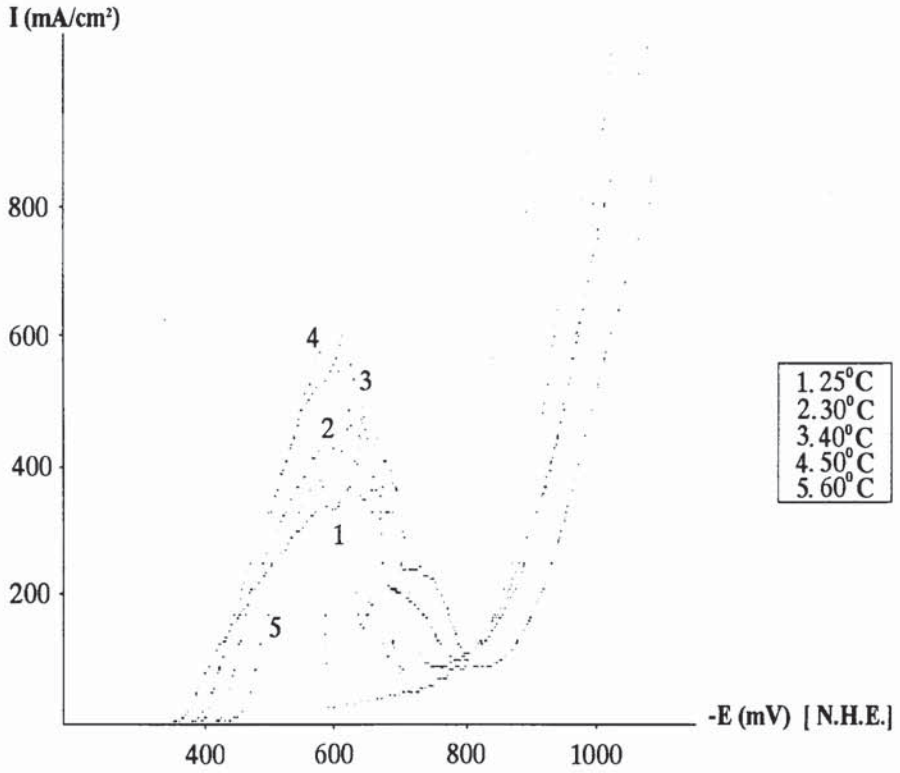

Figure 130. Figures 125-129 plotted together. [SB (100:1) + 1% DMSA bath.].

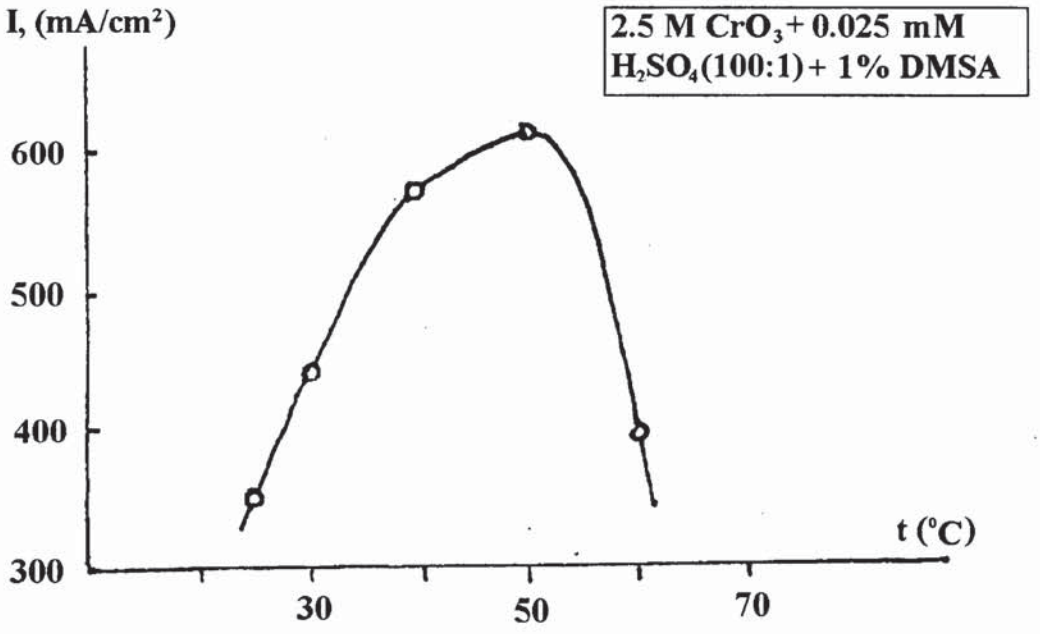

Figure 131. Influence of temperature on maximum current for Sargent bath + 1% DMSA.

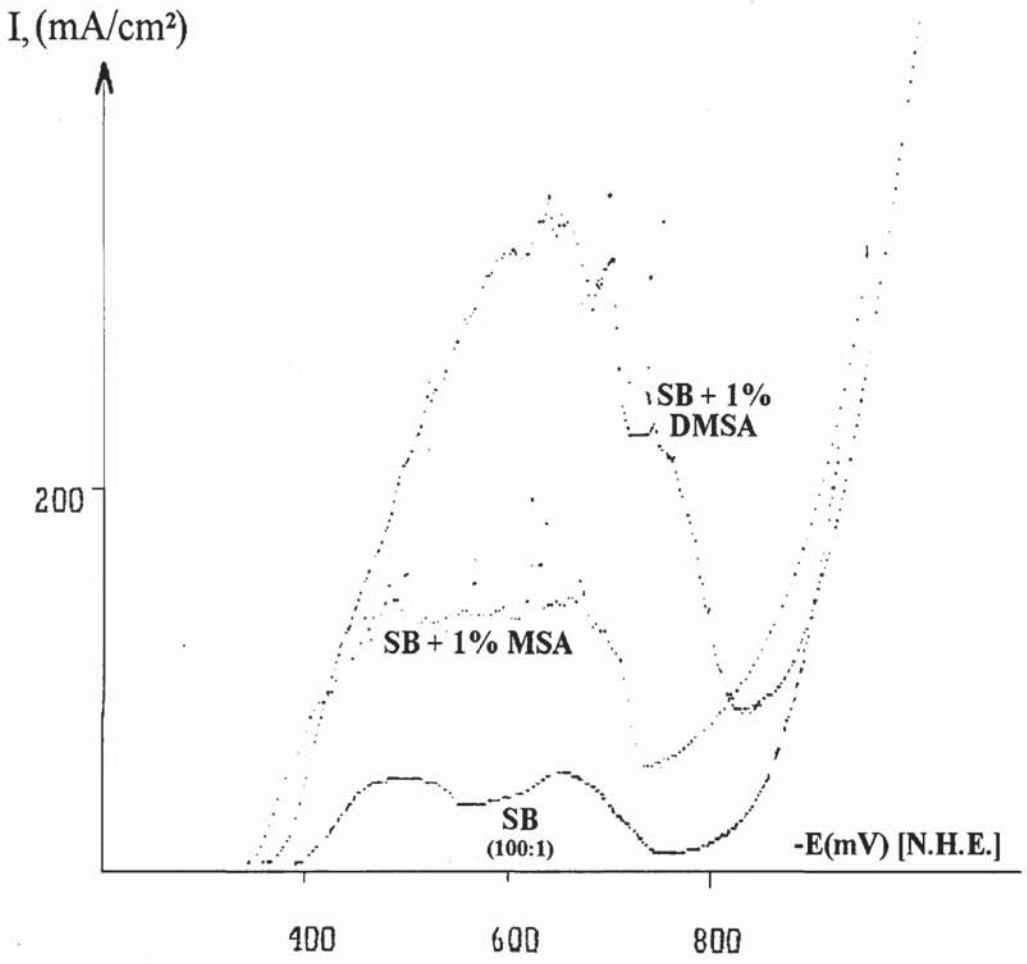

Figure 132. Comparison of MSA and DMSA additions to 2.5 M (100:1) SB at 30^0 C.

b. *Discussion*

The deposition mechanism of chromium is complex due to the apparent complications that, under a given set of conditions, a fraction of Cr^{6+} ions is reduced directly to metal (complete reduction, $Cr^{6+} \rightarrow Cr^{0}$) while another fraction is reduced to trivalent state only (incomplete reduction, $Cr^{6+} \rightarrow Cr^{3+}$). At the same time, the third coupled reaction, hydrogen evolution, $2H^{+} \rightarrow H_2$ (expressed as the fraction of the total current) is proceeding simultaneously.

If we assume for a moment that these reactions have different mechanisms, the rates of complete and incomplete Cr reductions should be governed by its own rules. A study of those two reactions as a function of sulphate catalyst concentration by *Soloveva and Petrova*[245] indeed proved that those reactions are governed by its own rules. Due to its importance Figure 132-1 is reproduced from this classical paper. On the left side of Figure 131-1, influence of temperature is presented for total current density of I = 250 mA/cm^2 and three different temperatures for all three coupled reactions and also compared to I = 650 mA/cm^2 (right side). In absence of the catalyst (H_2SO_4), virtually all current is consumed for liberation of hydrogen. When small portion of H_2SO_4 (0.5 g/l) is introduced (500:1 ratio), deposit on the cathode becomes metallic and the proportion of the current for complete reduction rises sharply to 18.5% (line 1 - 20^0 C). The rate of $2H^{+} \rightarrow H_2$ reaction falls considerably and the proportion of current consumed for intermediate reduction is about 3%. The rate of complete reduction (Cr metal deposition) continues to accelerate with increased catalyst concentration up to 2.5 g/l (100:1 ratio) and then slows down; at high sulphuric acid concentrations, it ceases entirely. At higher temperatures (40^0 C - line 2 and 60^0 C - line 3), lines 2 and 3 have a same general shape: complete reduction passes through maximum, incomplete reduction continuously increases and hydrogen evolution falls with the increase of H_2SO_4 concentration.

However, with the increase of the temperature, absolute values of reaction rates are changing (redistributed) differently. While complete chromium reduction rates are reduced, the other two reduction rates are changing differently. At lower concentrations of sulphuric acid incomplete reduction is somewhat increased while $2H^{+} \rightarrow H_2$ reaction is increased; at higher concentrations of sulphuric acid, incomplete reduction rises sharply with increase in temperature while hydrogen evolution reaction falls.

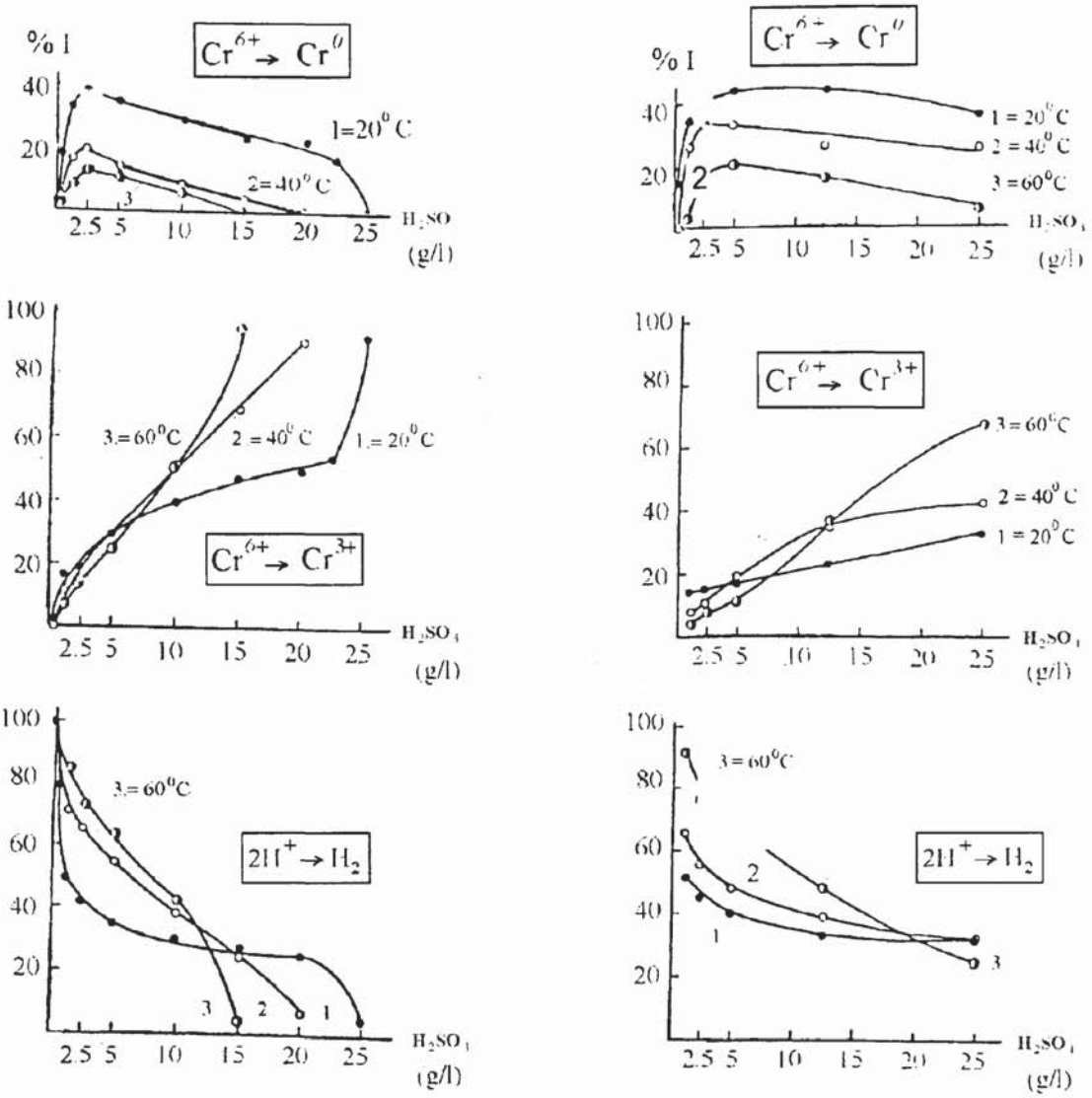

Figure 132-1. Partial currents (% I) for coupled Cr deposition reactions vs. H_2SO_4 conc. at 20(1), 40(2) and 60°C (3). Total currents: I=250 mA/cm²(left) and I=650mA/cm² (right).

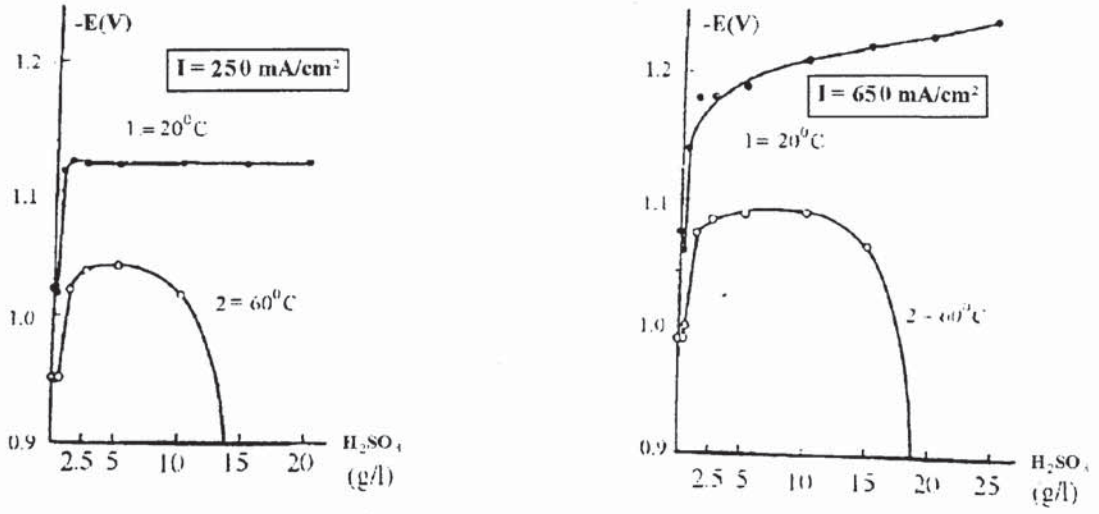

Figure 132-2. Potential vs. H_2SO_4 concentration for 20°C (1) and 60°C (2). Total currents: 250 mA/cm² and 650 mA/cm².

At higher current densities (650 mA/cm^2), the relationship between reaction rates for all three coupled reactions and sulphuric acid concentration do not alter the general character, only they become less pronounced, especially in the case of complete reduction, $Cr^{6+} \rightarrow Cr^0$. Comparison of the left and right side of the Figure 132-1 clearly shows that increase in current density (C.D.) increased the rate of metal deposition but decreased rates of incomplete reduction and hydrogen evolution. The chromium is the only major electrodeposited metal (together with the Ni and low C.D.) that increases in C.D. increase the cathode current efficiency. An unfortunate consequence of this is exceptionally poor throwing power and lack of levelling.

Figure 132-2 is a variation of cathode potential (E) with H_2SO_4 concentration and temperature. It could be seen that introduction of enough sulphuric acid to induce the beginning of electrodeposition (0.5 g/l, 500:1 ratio), shifts the cathode potential sharply into negative direction by about 100 mV. With the further increase of H_2SO_4 concentration change of E depends on C.D. and temperature: the lower the C.D. and higher the temperature, the lower the H_2SO_4 concentration at which the sharp change of the cathode potential occurs.

Important consequences of above analysis is the relationship between the temperature and L-film properties. Since L-film dissolution is increased with increase in the temperature, potentials are shifted toward more positive directions where more favourable reactions will proceed ($Cr^{6+} \rightarrow Cr^{3+}$) at the expense of the deposition reaction. This is clearly indicated for potentiodynamic conditions as presented in Figure 26 for 55^0 C (line 3) vs. 20^0 C (line 1).

However, it should be always kept in mind that voltammograms usually presented in most of the electrochemical studies are actually representing the composite of all three reactions that are concurrently proceeding. This fact, together with the presence of liquid cathode film makes analysis rather complicated. The often-neglected hydrogen evolution reaction should be considered from two aspects: change of the pH of the L-film and it increases with the temperature.

The formation of the L-film is apparently essential but not a sufficient condition for chromium deposition at any appreciable rate. Its presence shifts the $Cr^{6+} \rightarrow Cr^0$ reaction (thermodynamically most difficult) toward the more negative directions which favours this reaction while accumulation of Cr^{3+} within the film can retard the $Cr^{6+} \rightarrow Cr^{3+}$ reaction.

In most of the electrochemical studies of Cr, chemical reactions within L-film are either neglected or barely mentioned.

At the present, there is no abundance in the literature of *prima facie* evidence about the existence of chromate-complexes and olation and related processes, but rather scattered bits and pieces. Still, we think those reactions are recognised enough to be taken into serious consideration due to the possible role in the overall deposition mechanism, especially on their influence on the second polarisation branch.

In both cases, due to the sulphate complexation and Cr^{3+} olation, oxolation and probable polymerisation, chemical reactions within the L-film can influence the electrochemical reaction. Often mentioned presence and detection of chromium hydroxide $Cr(OH)_3 \bullet H_2O$ as a component of the L-film can also be interpreted from the coordination chemistry point of view as the presence of a tridimensional olated complex.

Auger[133] and ESCA[49,244,246,247] data that identifies the presence of Cr hydroxide and/or oxy-hydroxies in the L-film can also be interpreted as a presence of dehydrated olated complex. There is an apparent congruity with the undisputed fact that current efficiency of chromium deposition decreases with an increase in the temperature, Cr^{3+}, CrO_3 concentration and pH, the exact factors that promote olation. A further complication is the role of divalent chromium which according to *Hoare*[34] definitely participates in the final step of Cr electrodeposition, but at the same time promotes olation and the related processes. The role of Cr^{2+} is also recognised in electrochemical studies of trivalent chromium plating. Due to the interweaving relation between Cr^{3+} as a product of incomplete reduction during electrodeposition from sixvalent baths and Cr^{3+} from trivalent baths, knowledge of the former can compliment knowledge of the latter and visa versa. In trivalent baths it is somewhat easier, but not easy to identify Cr^{2+} due to the less oxidising environment.

Furthermore, looking at this from the diffusional aspects alone, the increase of the temperature increases diffusivity of accumulated Cr^{3+} products away from the outside of the cathode towards the bulk of the solution. This increase in the rate of removal of the products of Chromium incomplete reduction in turn increases the rate of incomplete reduction. All of this together makes interpretation of the mechanism quite difficult, almost intuitive.

Going back to analyse the influence of MSA and DMSA on Sargent bath, we can compare Figures 121 (MSA) and 130 (DMSA) where different temperatures are plotted together during potentiodynamic scanning at low sweep rate (4 mV/s). It is clearly evident that optimum situation is when temperature is in 40-50^0 C range. Taking also into account Figures 114 (SB), 124 (MSA) and 131 (DMSA) where peak currents are plated vs. temperatures, it is obvious the best operating range for electrodeposition is shifted toward higher temperature compared to Sargent bath. Also, the first sections of the polarisation curves are somewhat steeper, indicating the faster rates of incomplete reduction; peak currents are also higher. An important feature is the steeper slopes in the region after current maximum (L-film formation is faster).

Finally, it is also apparent that in this higher (but optimum) temperature range, the potential of complete reduction (Cr deposition range) is shifted toward more negative potentials which are favouring the thermodynamically most difficult reaction ($Cr^{6+} \rightarrow Cr^0$). Currents at the minimum of the E-I curves (corresponding to the end of the L-film formation and beginning the deposition) are higher, indicating the faster deposition.

At Figure 132, where potentiodynamic curves for SB, MSA and DMSA are plotted together, this analysis is more obvious. The obvious question arises: why are the MSA and DMSA influencing the C.E.'s ?

No definite answer is possible at this point due to all the complexities involved, except that they influence the L-film formation and properties. One possibility is that MSA and DMSA are promoting the Cr^{3+} - sulphate complexation, olation and related processes, causing faster formation of L-film. Since olated products are of higher molecular weight, their removal from the outside of the L-film toward the bulk is slowed down, shifting the equilibrium due to high Cr^{3+} concentration present in L-film and subsequently slowing down incomplete reduction. The presence of more compact L-film causes the polarisation to move in the direction of more negative potentials that are favouring the complete reduction. At certain, high enough temperature, diffusion probably takes over by faster removal of olated product toward the bulk and chemical equilibrium is shifted again toward increased Cr^{3+} production.

Increasing the rotation speed above a certain, high level can influence the L-film in a way similar to the temperature: it can, by faster removal of the Cr^{3+} ions from the L-film, shift the equilibrium toward increased production of Cr^{3+} and offset the advantage of faster

replenishing of the cathode layer of depleted Cr^{6+} ions, needed for the main reaction. This change of chemical equilibrium can be the cause of the presence of the kinetic component and that becomes more apparent at higher rotation speeds.

While during plating from trivalent baths, olation is unwanted due to its influence on the main reaction ($Cr^{3+} \rightarrow Cr^{0}$) which requires the fastest possible removal of Cr^{3+} ions and much less negative potentials; in the case of plating from sixvalent baths, the opposite possibly can be true. Nevertheless, understanding of coordination chemistry of chromium and electrochemistry of an heterogeneous system where chemical step (solid and liquid film formation) precedes electrochemical step is equally important in both cases.

2. DETERMINATION OF CHARGE TRANSFER COEFFICIENT α_C FOR PARTIAL CHROMIUM REDUCTION REACTION: $Cr^{6+} \rightarrow Cr^{3+}$

Chromium is reduced on the cathode through multistep process: $Cr^{6+} \rightarrow Cr^{3+} \rightarrow Cr^{2-} \rightarrow Cr^{0}$ (+ simultaneous H_2 evolution), with probable involvement of intermediate oxidation states of Cr^{4+} and Cr^{5+}. The first step ($Cr^{6+} \rightarrow Cr^{3+}$) is probably the most important and the main focus in many published papers is based on this reaction.

The set of Figures 133-136, are obtained from Figures 117-121 by measuring the values of the potential and the current in the region of the first rising branch of LPS curves ($Cr^{6+} \rightarrow Cr^{3+}$ - incomplete reduction). This method is based on the following principle:

When diffusion does not affect kinetically controlled current (*i.e*, $I_{lim} >> I$), it can then be written that: $I_{lim} = I$ where I is measured current density.

But at conditions of mixed kinetics, the role of diffusion has also to be taken into account:

$$\frac{1}{I} = \frac{1}{I_{Kin}} + \frac{1}{I_{\lim}} \qquad <96>$$

or it can also be expressed in the form of Frumkin - Tedoratse equation:

$$\frac{1}{I} = \frac{1}{I_{\lim}} + \frac{1}{B' \omega^{\frac{1}{2}}} \qquad <97>$$

Equations <96>, <97> and <98> allow one to evaluate relative importance of kinetic and mass transport controlled steps of the cathodic processes where I_{lim} is limiting diffusion current, ω is rotation speed, D is diffusion coefficient, v is sweep rate and B' is the constant which for a rotating disc electrode is equal to $0.62\, n F D^{\frac{2}{3}} \nu^{\frac{1}{6}} C_o$

From equation <96> , after rearranging, we have:

$$\frac{1}{I_{kin}} = \frac{1}{I} - \frac{1}{I_{\lim}} = \frac{I_{\lim} - I}{I_{\lim} \bullet I} \qquad <98>$$

After further rearranging of <98> it follows that:

$$I_{kin} = \frac{I_{\lim} \bullet I}{I_{\lim} - I} \qquad <99>$$

From equation <106> after taking the log of both sides, we have:

$$\log I_{kin} = \underbrace{\log K + p \log C}_{A} \underbrace{- \alpha_c \frac{nF}{RT} E}_{B} = A - B \bullet E \qquad <100>$$

By substituting <99> into <100>, we now obtain:

$$\log \frac{I_{lim} \bullet I}{I_{lim} - I} = A - B \bullet E \qquad <101>$$

Equation <101> represents a straight line. It is know from theory of the kinetics electrode processes that the constant B depends on the mechanism of reaction and it is equal to $\alpha_c \frac{nF}{RT}$ only for the case of simultaneous transfer of n electrons. For the slow transfer of the first electron: $B = \alpha_c \frac{F}{RT}$, for the second electron $B = (1 + \alpha_c) \frac{F}{RT}$, third electron $B = (2 + \alpha_c) \frac{F}{RT}$, etc.

Consequently, we can obtain information on electrochemical mechanism by measuring the slope B (usually we measure b = 1/B, in millivolts), and calculating the α_c .

From Figures 133-136 [for 100:1 Sargent bath + 1% MSA] it is determined that the slopes are 75 mV for 30^0 C, 85 mV for 40^0 C, 70 mV at 50^0 C and 60 mV for 60^0 C. This gives us values for the transfer coefficient α_c 0.80; 0.78; 0.91 and 1.10, respectively.

Obtained values for slope b and α_c indicate that there is probably a slow transfer of the first *and* second electrons with the electrochemical rates close to each other. Coefficient b is always smaller than 120 mV when addition of second or third electron are slow or when I_{kin} is present (for reaction orders $p \geq 1$).

It has to be added that those calculations are rather approximate, for two reasons:

(a) It is difficult to accurately measure the true value for limiting (maximum) current for the process of incomplete reduction $Cr^{6+} \rightarrow Cr^{3+}$ from experimental curves due to the oscillation of the current and decreasing the current after maximum is reached; also this "limiting" current is not truly diffusion controlled since the true diffusion limiting current always increases with temperature. In our case I_{lim} increases only up to the $40\text{-}50^0$ C region and then falls. Consequently, the results for 30 and 40^0 C should be considered more accurate.

(b) An attempt is made to use initial (Tafel) parts of the voltammograms (where the influence of the diffusion is negligibly small ($I << I_{lim}$) for less concentrated solutions (Figure 111,113 and 115). However, the slopes in this region, are unusually small (results

are presented in Figure137). Similar diminishing of the slope can be observed from the initial parts of the Figures 134-136 in the regions where I is small; *i.e.*, at more positive potentials (dashed line). The slopes of 10-20 mV are relatively small for the usual electrochemistry. The probable reason for such small values is the formation of the cathodic surface film and/or the strong influence of adsorption. It is obvious that there is only a narrow region of potentials and temperatures available to construct the Figures 133-136.

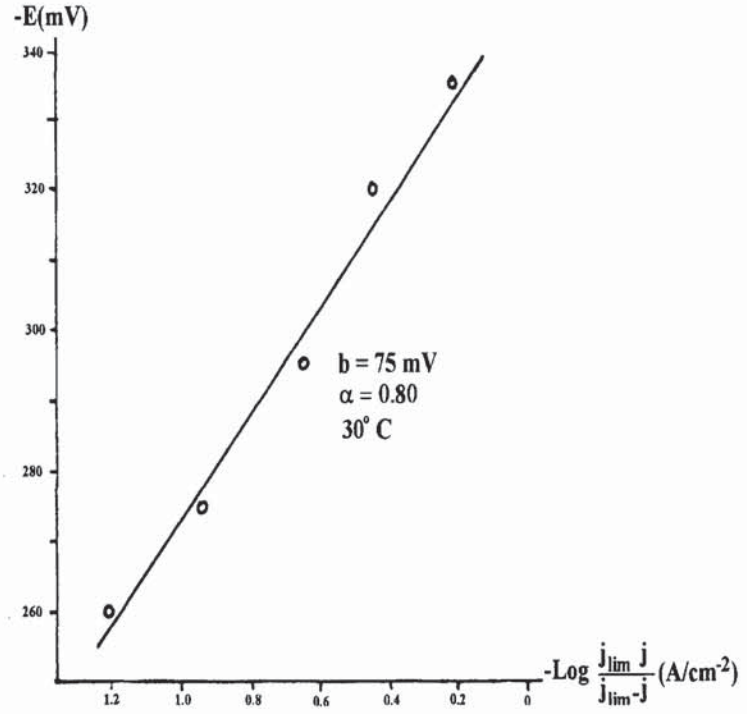

Figure 133. Tafel plot for $Cr^{6+} \rightarrow Cr^{3+}$ reduction in Sargent bath (100:1) + 1% MSA at 30°

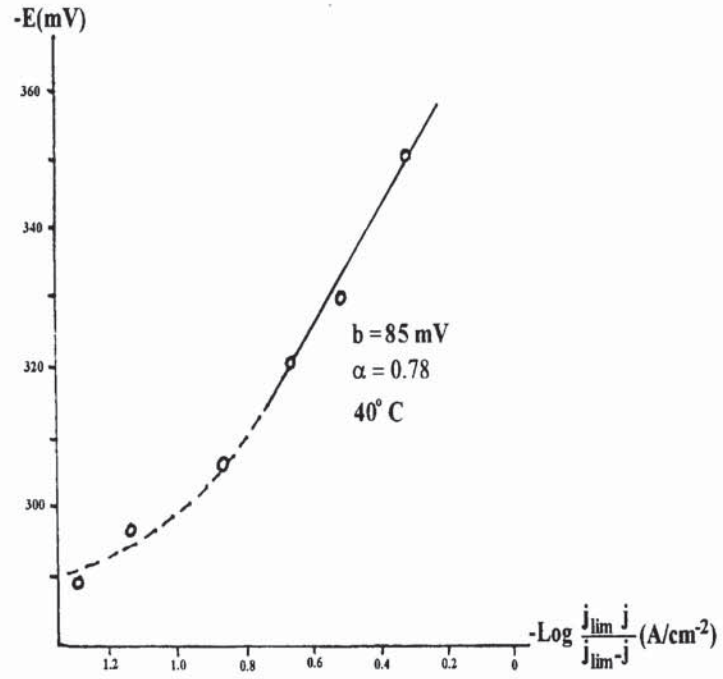

Figure 134. Tafel plot for $Cr^{6+} \rightarrow Cr^{3+}$ reduction in SB (100:1) + 1% MSA at 40° C.

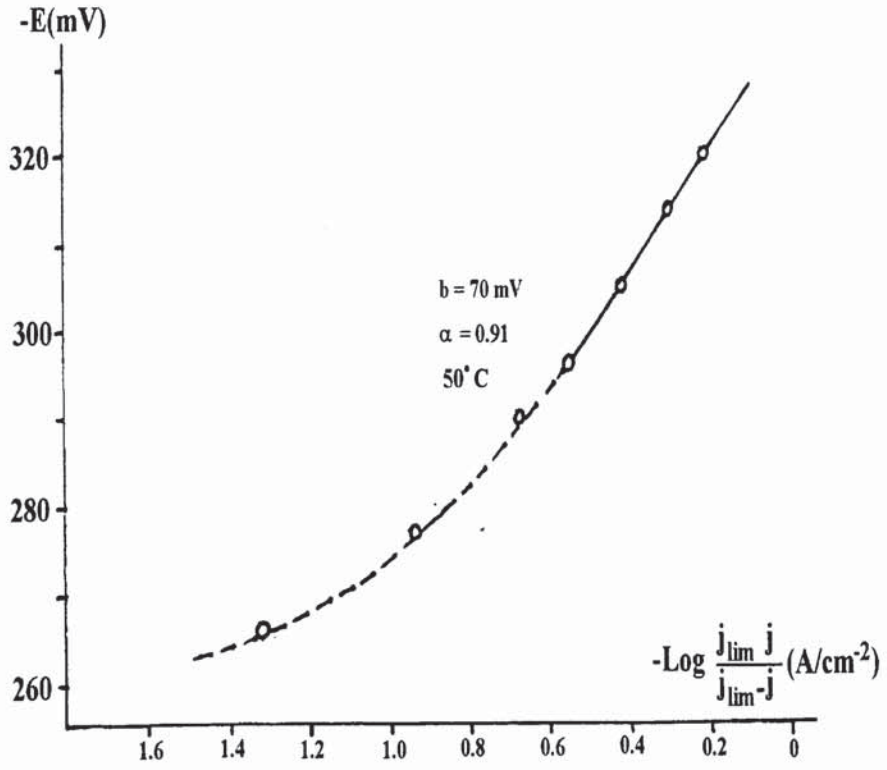

Figure 135. Tafel plot for $Cr^{6+} \rightarrow Cr^{3+}$ reduction in SB (100:1) + 1% MSA at 50° C.

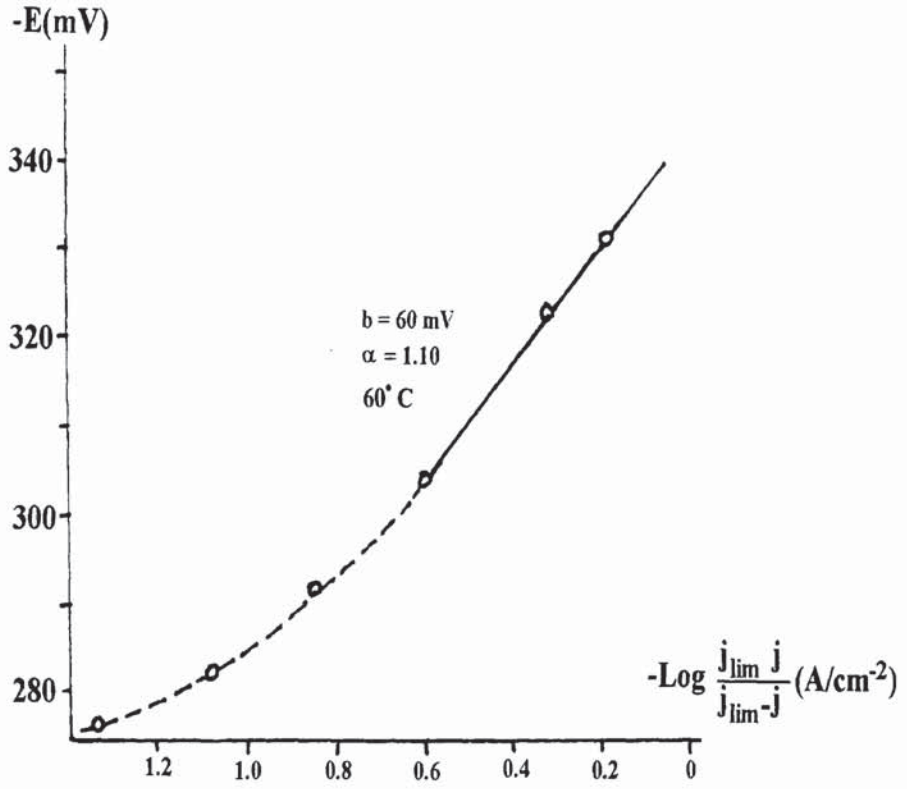

Figure 136. Tafel plot for $Cr^{6+} \rightarrow Cr^{3+}$ reduction in Sargent bath (100:1) + 1% MSA at 60°.

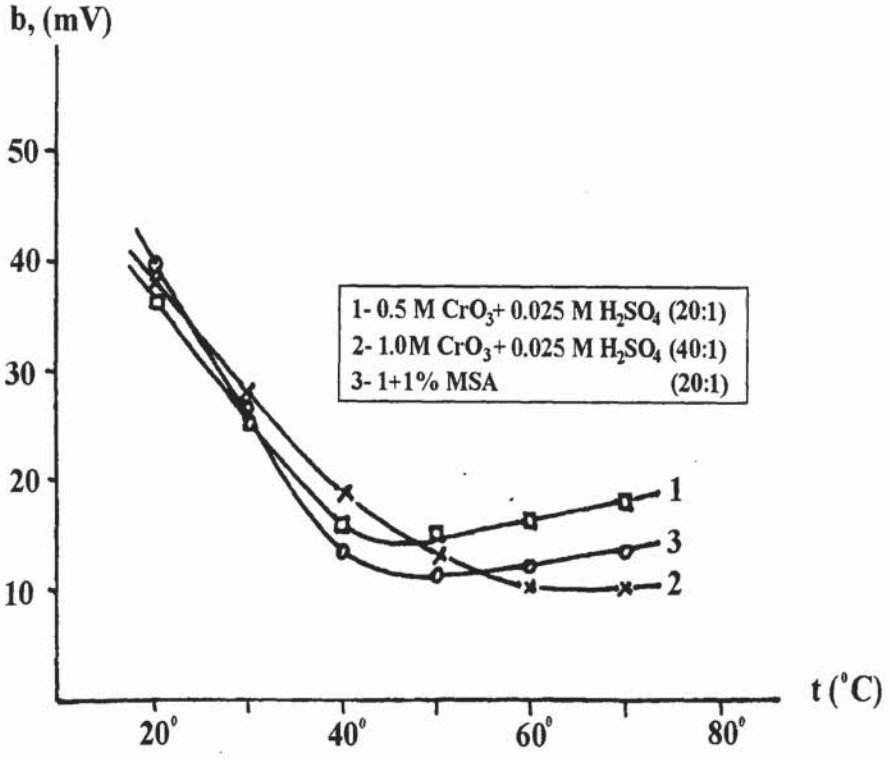

Figure 137. Influence of temperature on Tafel slope for three different plating solutions.

3. DETERMINATION OF ELECTROCHEMICAL REACTION ORDER (p) FOR PARTIAL REDUCTION REACTION $Cr^{6+} \rightarrow Cr^{3+}$

a) *The Order of an Electrodic Reaction - definition*

In the kinetics of chemical reactions, the order of a reaction is a straight-forward concept. One simply observes the exponents of the concentration terms in the expression for the reaction rate, e.g.,

$$-\frac{dc_A}{dt} = Kc_A^a c_B^b \ldots c_N^n \qquad <102>$$

Each exponent is termed the order of reaction in respect to the species concerned, while the sum of the exponents of the concentration terms defines the overall order of a reaction.

Individual reaction orders are often expressed as derivatives of the log of the rate in respect to the log of concentrations of all the other species, for it follows from <102> that in a general case as[248],

$$\left(\frac{\partial \log J}{\partial \log c_i}\right)_{C_{j\neq i}} = p_i \qquad <103>$$

In electrodics, the reaction rate is expressed in terms of current density I.

Thus, one would expect, by analogy, the electrochemical order of the reaction to be given by an expression similar to <103> which should result from the Butler - Volmer expression:[248]

$$I = n\ (I_a - I_c)\ \left(K C_A^a C_B^b \cdot \cdot \cdot e^{\frac{\alpha_c F}{RT} E} - K C_{A'}^{a'} C_{B'}^{b'} \cdot \cdot \cdot e^{\frac{\alpha_c F}{RT} E}\right) \qquad <104>$$

where A', B', . . . are the products of charge -transfer reactions involving A, B, respectively. The exponents a, b, . . . and a' , b' , . . . in <104> which relates the rate of reaction (current density) to the concentration of various species, are termed the electrochemical - reaction orders. It is stressed here that these electrochemical - reaction orders can only be related to equations such as <102> when E is constant and, hence, constant E becomes an essential part of the definition of electrochemical - reaction orders as given above <103>.

At potentials sufficiently cathodic to neglect the anode reaction, the electrochemical - reaction orders a' and b' are defined in general form for cathodic reaction:

$$\left(\frac{\partial \log I}{\partial \log c_i}\right)_{c_{i\neq j},E} = p_{i,c} \qquad <105>$$

The potential E must be chosen sufficiently far from the reversible potential E_e so that the exponential law applies even at the highest concentrations used or the given species in de-electrodonation reactions and the lowest concentrations in the electrodonation reactions. It is assumed that change of concentrations of the species whose reaction order was determined does not affect the potential distribution in the double layer, i.e., that E = constant. This is true only if the concentration of ions in the double layer remains high and unchanged with varying concentrations of the ionic species investigated. This condition can be closely approximated if the ionic strength of the solution is kept high and constant by the addition of foreign ions, i.e., of a supporting electrolyte which does not participate in the reaction.

Experimentally determined reaction orders belong to the most important mechanism - indicating criteria. They may confirm or eliminate an assumed mechanism, depending on whether the rate equation corresponding to the latter postulates the same or different values of p_i as those experimentally established.

b) *Determination of reaction order*

Figure 138 is presented in order to calculate the electrochemical reaction order p. The method for determining the p is based on the fundamental electrochemical equation for the current density that depends on charge transfer or chemical reaction, derived from <104> and written in a form :

$$I_{Kin} = \mathrm{K}\, C^p \left(-\alpha_C \frac{nF}{RT} E\right) \qquad <106>$$

where K is the rate constant, p is electrochemical reaction order, - α_c is cathodic transfer coefficient ($0 < \alpha_c < 1$), n is the number of electrons transferred, C is concentration of reacting ions and E, R and T have general meaning.

From <106>, at E = Constant and after taking the log of both sides and rearranging, we can write:

$$\log I_{Kin} = \log \mathrm{K} - \frac{\alpha_c nFE}{RT} + p \log C = \text{Const.} + p \log C \qquad <107>$$

In order to determine reaction order with respect to chromium we used 0.5, 1.0. 1.6 and 2.5 M CrO_3 solution at constant sulphuric acid concentration (0.025 M). From current density data for $Cr^{6+} \rightarrow Cr^0$ reaction that are obtained at the potential of metal deposition (E = -1.12 V), Figure 138 is constructed; the plot log I - log C is linear and the slope is $p \approx 1$. For the processes limited by the electron addition, log I - log C plot should be a straight line and the reaction order can be determined from the slope[86]. From Figure 138 it follows that the chromium deposition is a first order reaction in respect to CrO_3.

c. *Discussion*

In a recent paper *Efimov*[249] by the same method as above obtained the reaction order of $p = 1.05$. He used a stronger CrO_3 solution (1.5, 2.0, 2.5 and 3.5 M; $v = 4$ mV/s., E = -1.1 V). In this and an other more recent paper[250] he obtained from E - log C plots, the values of b = 120 mV and $\alpha_c = 0.5$, for 2.5 M Sargent bath. From this data he concluded that the process of complete reduction is limited by slow addition of the first electron to the electroactive chromium atom (one out of three chromium atoms in the trichromate anion, in accordance with the mechanism by Hoare[74]) since, for the addition of second and subsequent electrons, b should be smaller than 120 mV (60 mV for the first order reaction). For the mechanism of incomplete reduction, *Efimov et al.*[251] obtained the values of b = 150 mV and $\alpha_c = 0.5$ for graphite electrodes and 2.5 M (100:1) Sargent bath. He also referred to another Russian paper where *Danilov and Ben - Ali* [252] had determined the values for b = 150 mV, and $\alpha_c = 0.4$ for $p = 0.89$. They also used graphite as a electrode and unusually low CrO_3 concentration (0.05, 0.1 and 0.2 M at 25^0 C and $v = 5$ mV/s). Since graphite electrodes do not form soluble oxide films like Cr electrodes and in view of the low concentrations used,[252] the conclusion made by Efimov that incomplete reduction is under mixed control and limited by the slow steps of addition of the first electron and the slow diffusion of electroactive ion, seems less possible. Therefore, part of his conclusions that incomplete reduction involved anion containing one chromium atom ($HCrO^-_4$) is questionable Raman spectroscopy data[31] proved that $HCrO^-_4$ anion does not exist in acidic solution of sixvalent chromium.

Therefore, it appears that our mechanism, based on results by using a chromium electrode and 0.5, 1.0, 1.6 and 2.5 M solution seems more probable and that limiting step is

the addition of the first and second electron. It is hard to understand that the addition of MSA can cause such a drastic change in the mechanism. The results presented in section II.4.1c and discussion on page 208 shows that SB + MSA bath has very little influence on incomplete reduction but rather has influence on the L-film. The question of the nature of the anion involved is open at this point.

From the above data and analysis it can be concluded that complete and incomplete reductions are two parallel electrochemical processes that are proceeding with two different electoactive anions and at two different potentials.

The obtained kinetic results do not change, but rather support the basic approach on the role of L-film. The role of the film has to be considered from the point of chemical and electrochemical steps that are proceeding within.

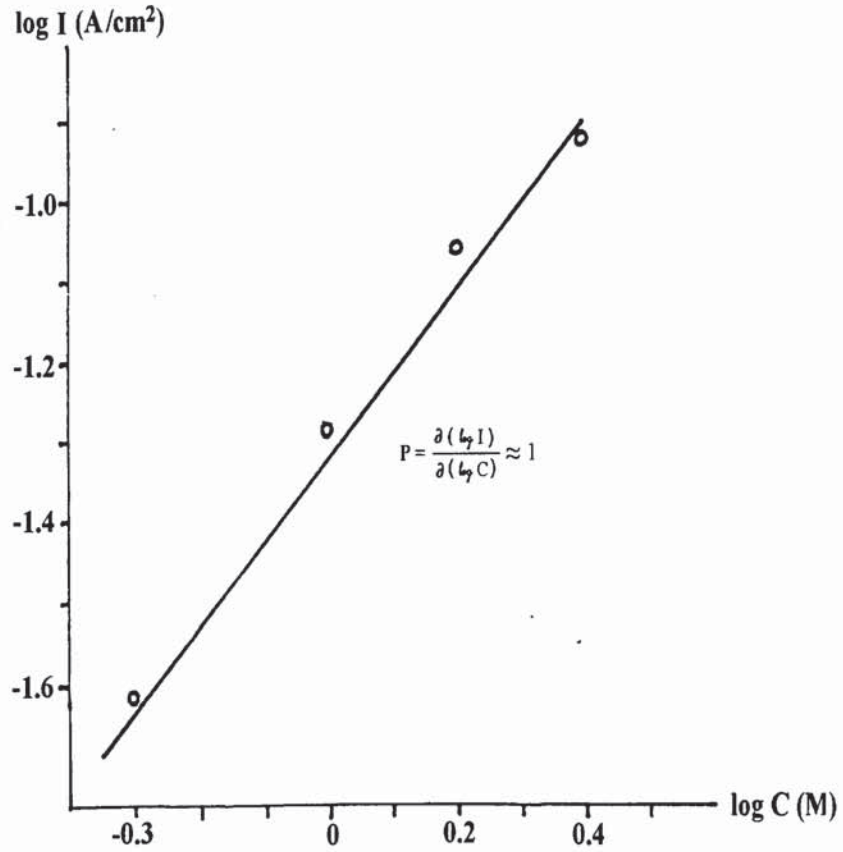

Figure 138. Reaction rate order (p) determined from CrO_3 vs. log I plot for 0.5, 1.0, 1.6 and 2.5 M CrO_3 ; H_2SO_4 = 0.025 M. 30^0 C. ν = 2mV/s. E = -1.12 V.

II.4.3. ON THE HYDROGEN EVOLUTION

For investigation of the MSA influence on the hydrogen evolution rate, three solutions: 0.3M H_2SO_4, 250 g/ℓ CrO_3 and 250 g/ℓ CrO_3 + 5 g/ℓ MSA were used. Current -potential response for these solutions are presented in Table 47. The potential and current values from Table 47 were taken from cyclic voltammograms (Figures 139, 142 and 145) which were also presented in E - log I form in Figures 140, 141, 143, 144, 149 and 150.

a. *Sulphuric Acid:* The results of experiments for 0.3 M H_2SO_4 solution (Figures 139-141) indicated that in this solutions the steady-state voltammograms are not obtained. As shown in Figure 139, active Cr dissolution with oxide formation proceeds at the potential between -500 and -600 mV as indicated by the high value of "b" (Figure 140). The Tafel slope for the first linear section of the first cycle is 0.032 V and for the last cycle "b" increases to 0.126 V (Figure 141). The Tafel slope for the second linear section of the last cycle increases to 0.312 V. Also the "b" value increases with the electrode rotation rate (Figure 148).

b. *Chromic Acid:* During the repeated scanning in CrO_3 bath with and without sulphuric acid the steady-state voltammogram is not obtained. In the chromic acid bath, the H_2 evolution after the second and the consequent cycles takes place on the oxidised Cr surface. The products of reduction reaction $Cr^{6+} \rightarrow Cr^{3+}$ constantly form on the Cr surface causing the high hydrogen overpotential on Chromium cathode. During the first cycle on the fresh Cr surface, the products of reaction $Cr^{6+} \rightarrow Cr^{3+}$ are not present. The Tafel slope for the first linear section of the first cycle in CrO_3 solution with or without H_2SO_4 is 0.054 V. The values for slope "b" for the second cycle of voltammogram increases to 0.2-0.3 V. The increase in electrode rotation rate (Figure 151) and temperature (Figure 155), increases the Tafel slope.

c. *Chromic Acid with MSA*: In all three solutions only during the first cycle of voltammograms the hydrogen evolution does not influence secondary reactions and in all three solutions the reaction $2\ H^+ + 2e \rightarrow H_2$ occurs. The Tafel slope "b" is the potential change when the current changes ten times. The Tafel slope of the first linear sections in H_2SO_4, CrO_3 and CrO_3 + MSA solutions are equal to 0.032, 0.054 and 0.054V respectively. In H_2SO_4 solution the active Cr dissolution with oxide formation proceeds in the second and following cycles while in the other two solutions in the second and following cycles the

oxidation of Cr surface takes place as a consequence of the reaction $Cr^{6+} \rightarrow Cr^{3-}$. This reaction has a very small rate, but is present and the Tafel slope "b" of the last cycle increases to 0.3 V. The "b" increases with temperature (Figure 145) and electrode rotation rate, ω (Figure 154) Apparently increased temperature and ω are responsible for increased passivation of the Cr surface resulting in the very high hydrogen overpotential on the surface of the chromium electrode.

The above results and discussion indicates that it is difficult to make any definitive conclusion about the mechanism of hydrogen evolution in chromium plating solutions at this point. As a consequence of the same Tafel slope for CrO_3 with and without MSA we can conclude that MSA does not influence the hydrogen evolution mechanism. Since we already established that MSA is a week catalyst for the $Cr^{6+} \rightarrow Cr^{3+}$ reaction, it follows that an increase in cathode current efficiency in MSA co-catyalysed solutions are due to MSA influence on the state and physico-chemical properties of L-film and the reactions that are proceeding within the film.

Cycle No.	0.3 M H_2SO_4		2.5 M CrO_3		2.5 M CrO_3 + MSA (5g/)	
	- E, (m V)	I, (mA/cm^2)	- E, (m V)	I, (mA/cm^2)	- E, (m V)	I, (mA/cm^2)
1	921	149	924	20	924	40
	1100	936	1100	40	1100	40
	1192	1319	1195	139	1195	229
	1210	1809	1210	279	1210	428
2	924	408	924	100	924	149
	1197	2007	1195	2351	-	-
	1210	2121	1212	2820	1200	3252

Table 47. Current -Potential relationship for H_2SO_4, CrO_3 , CrO_3 + MSA solutions.

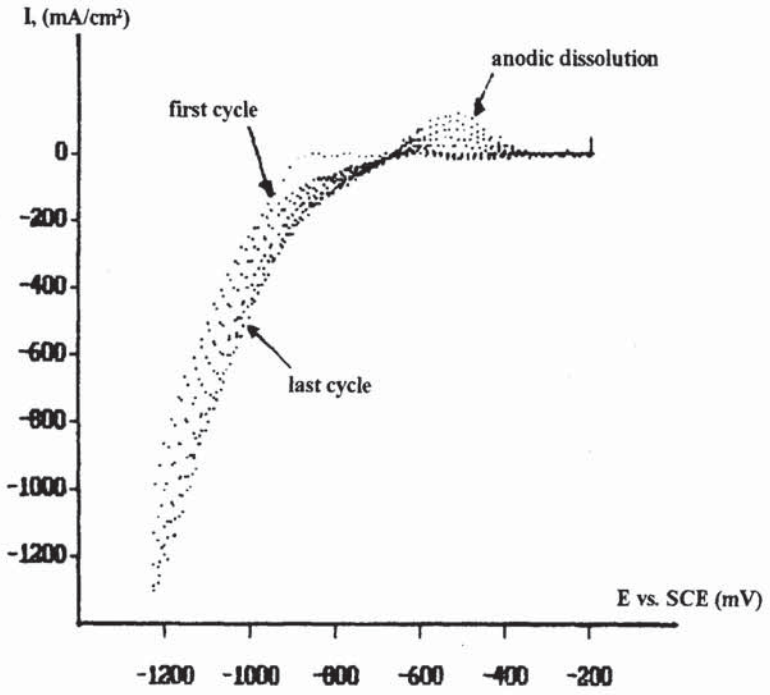

Figure 139. The cyclic voltammograms on Cr electrode in 0.3 M H_2SO_4. The scans start at -200 to -1200 mV; ν = 83 mV/s.

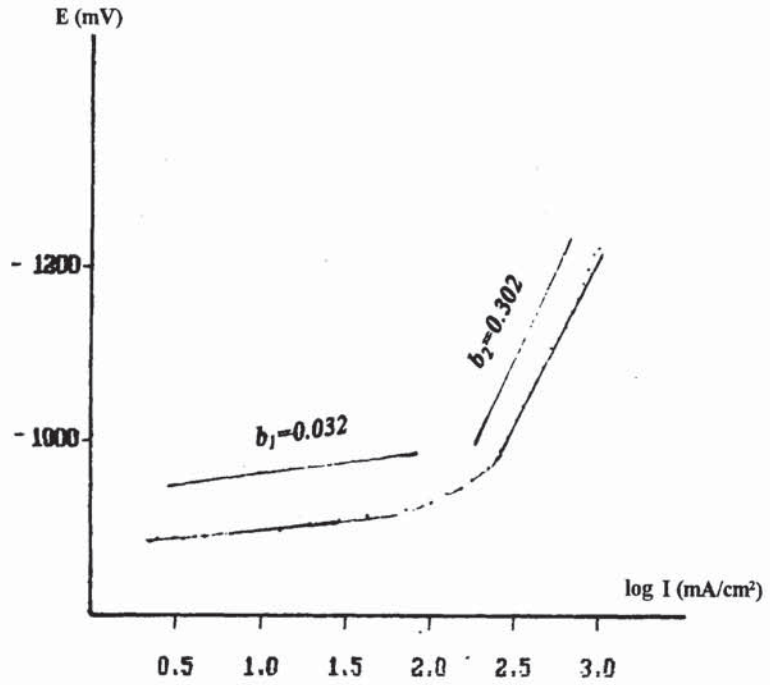

Figure 140. E - log *I* curve for the first cycle (Figure 139) on Cr in 0.3M H_2SO_4.

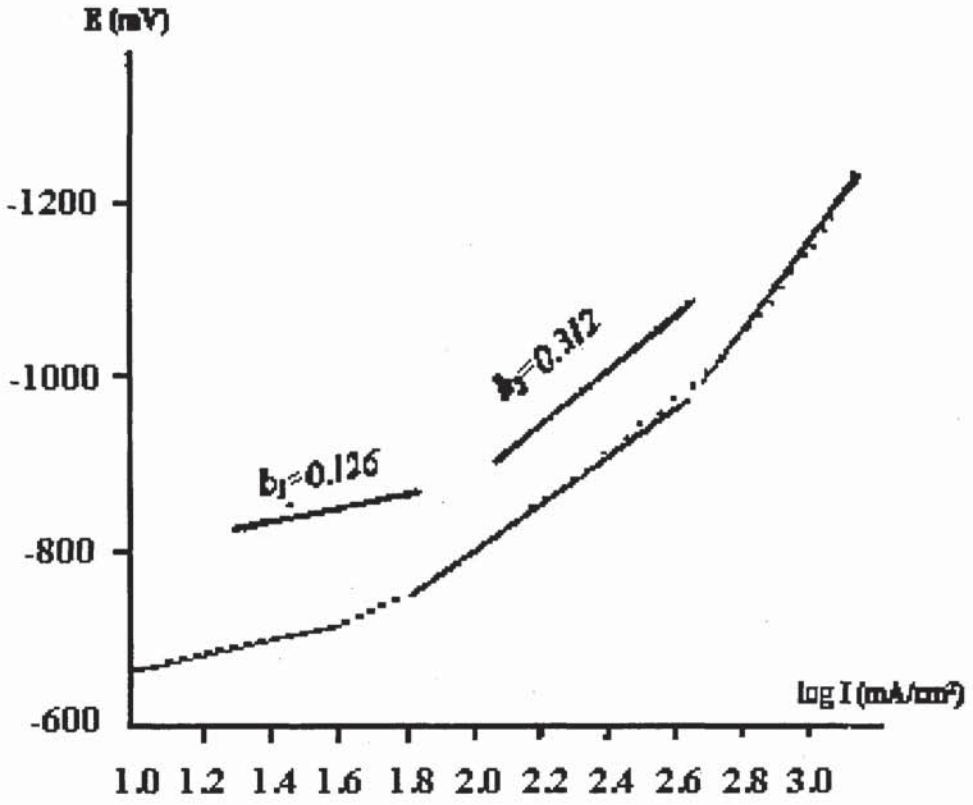

Figure 141. E - log *I* curve for the last cycle (Figure 139) on Cr in 0.3M H_2SO_4.

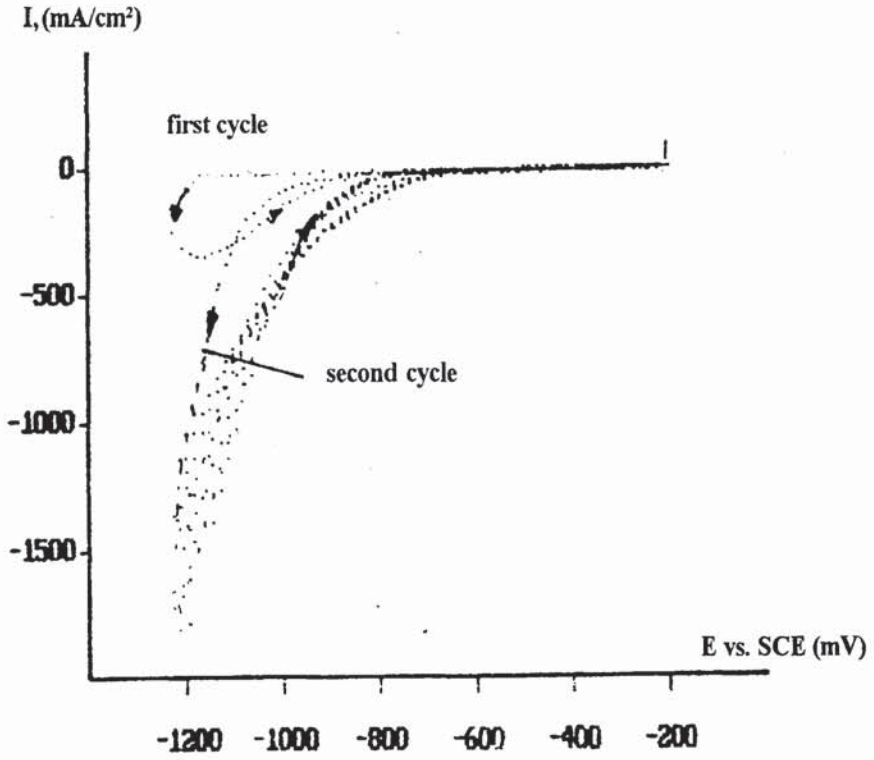

Figure 142. The cyclic voltammograms obtained on Cr in CrO_3 (250 g/L) solution.

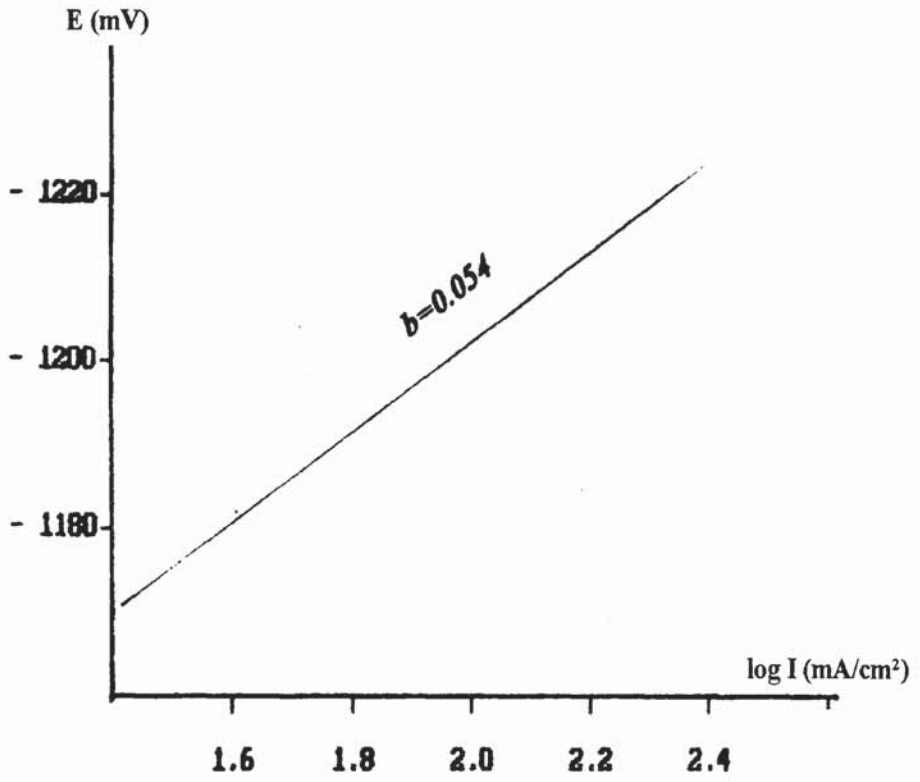

Figure 143. E - log *I* curve for the first cycle of Figure 142 for Cr in CrO_3 solution.

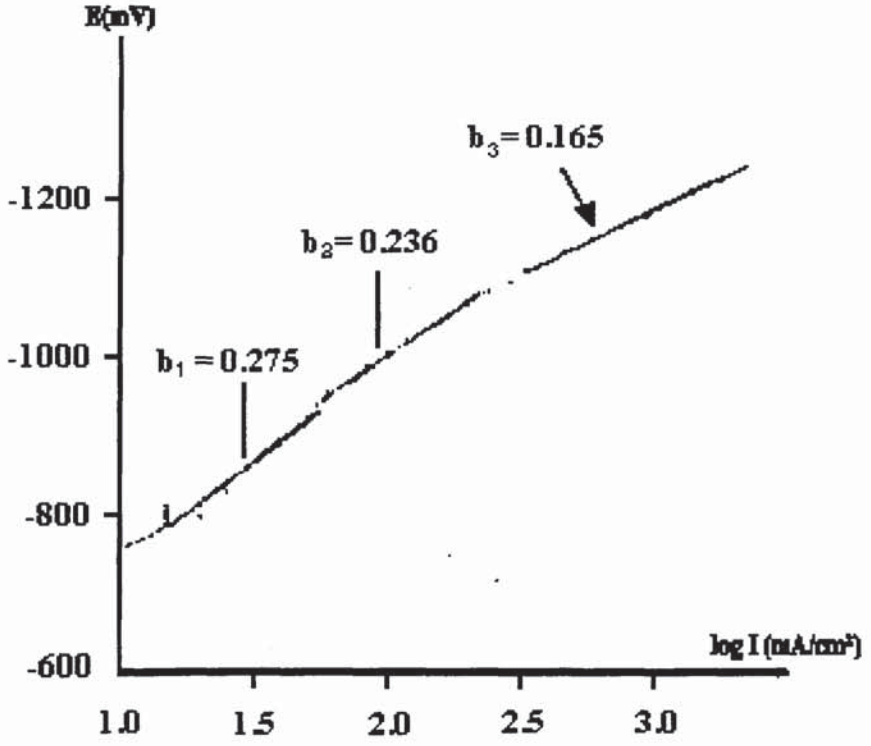

Figure 144. E - log *I* curve for the second cycle of Figure 142 on Cr in CrO_3 solution.

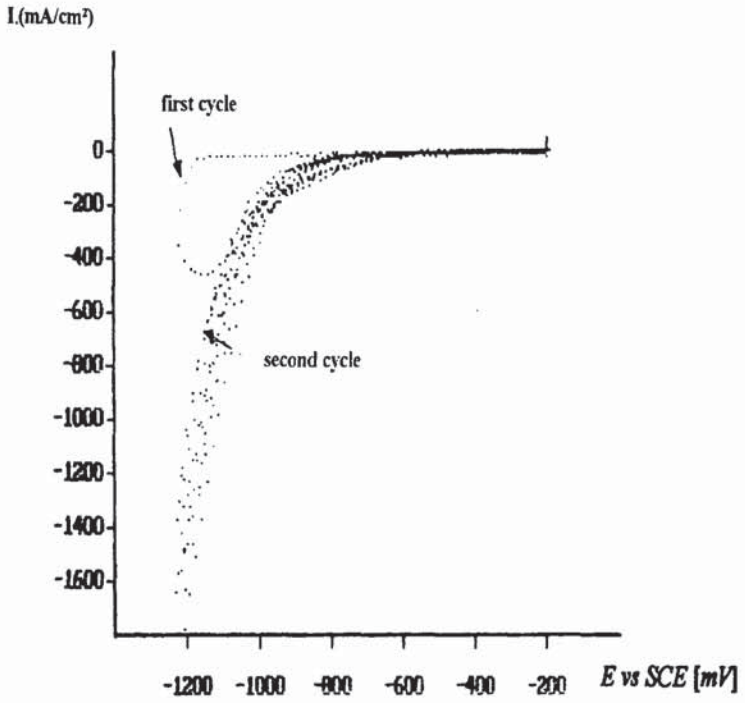

Figure 145. The cyclic voltammograms on Cr electrode in CrO_3 (250 g/L) + MSA (5.0 g/) bath: v = 83 mV/s. (T = 55^0 C).

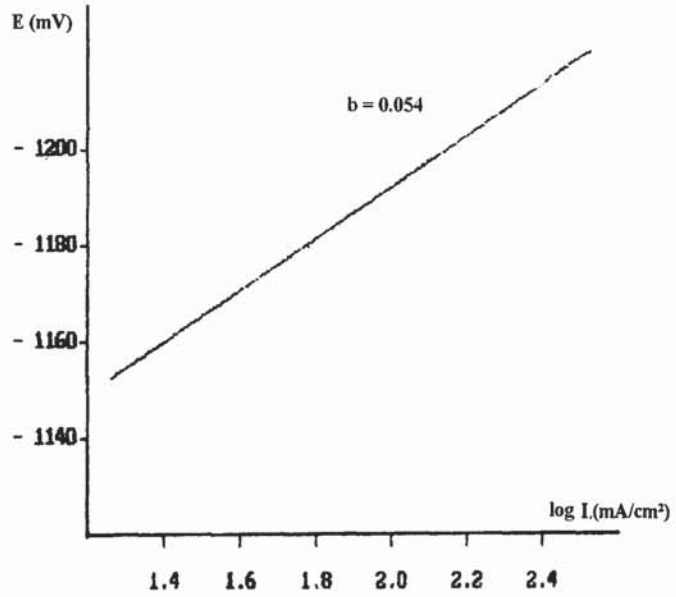

Figure 146. E - log I curve for the first cycle (Figure 145) on Cr electrode in CrO_3 (250 g/L) + MSA (5.0 g/L) bath: v = 83 mV/s.

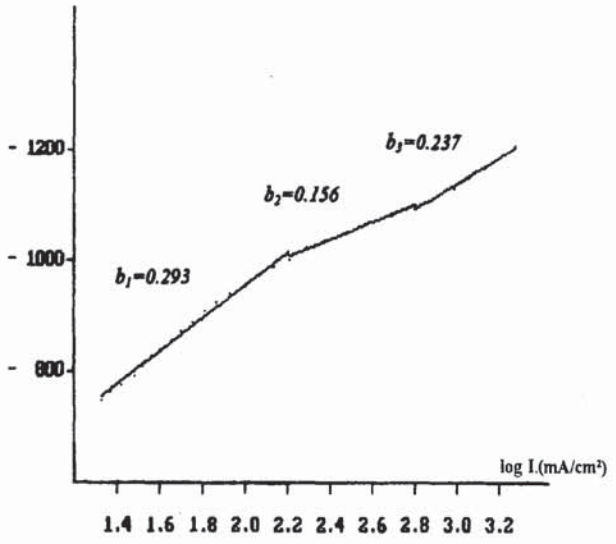

Figure 147. E - log *I* curve for the second cycle (Figure 145) on Cr electrode in CrO_3 (250 g/L) + MSA (5.0 g/L) bath.

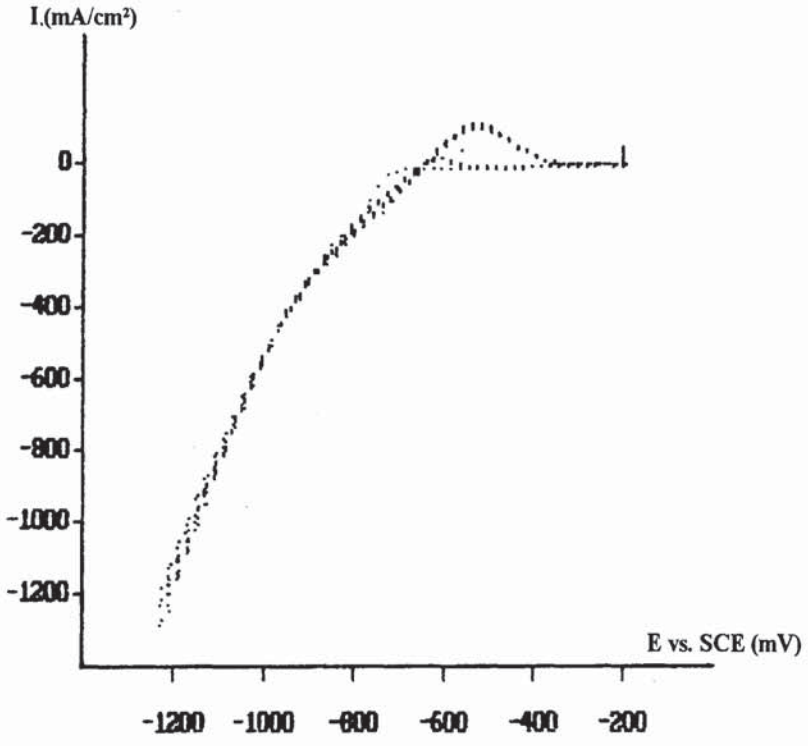

Figure 148. The cyclic voltammograms on Cr electrode on rotating chromium 0.3M ω = 2000 rpm; v = 83 mV/s.

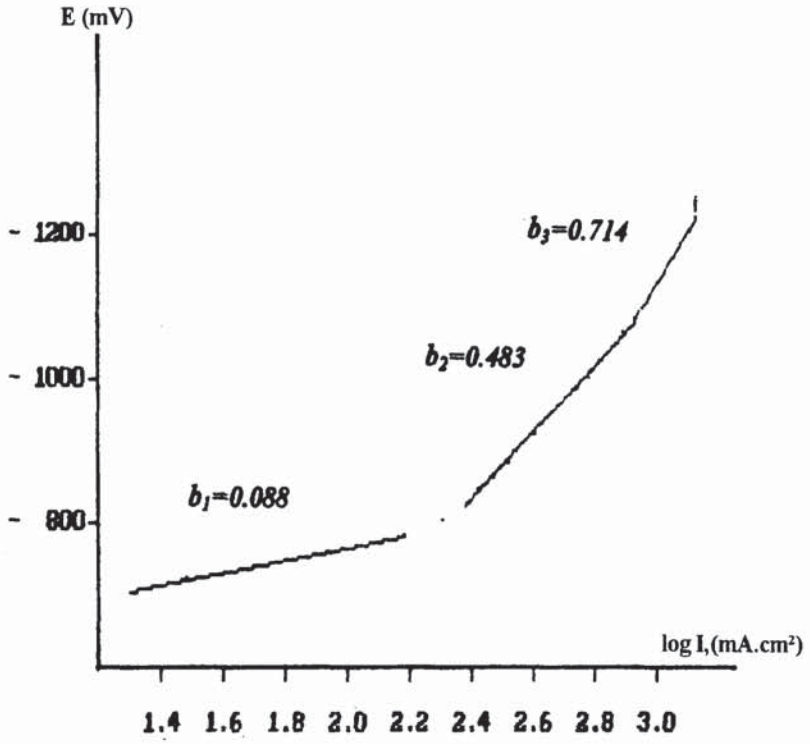

Figure 149. E - log *I* curve for the first cycle on Figure 148 on Cr in 0.3M H_2SO_4.

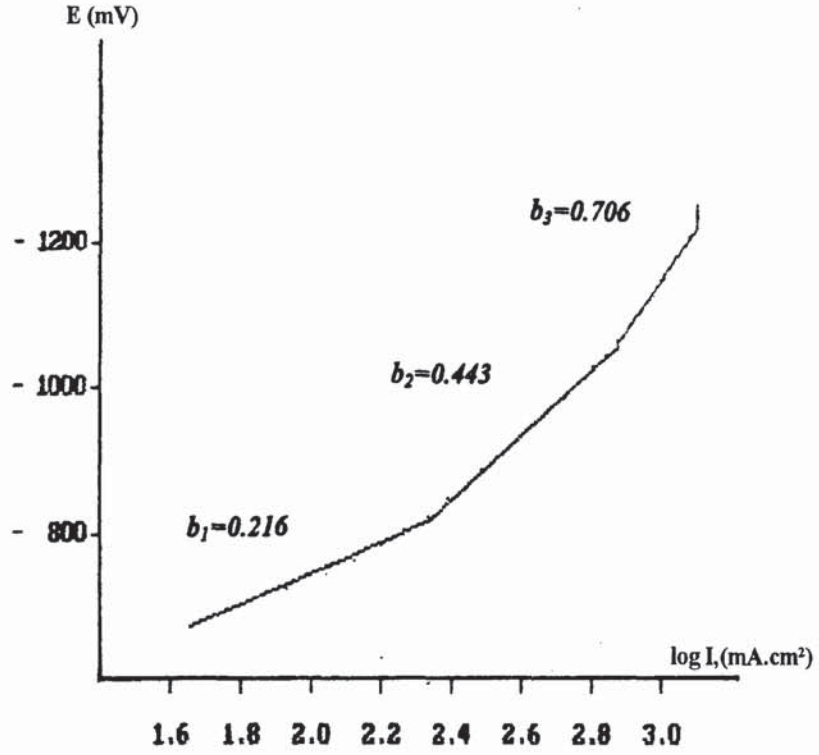

Figure 150. E - log *I* curve for the second cycle on Figure 148 on Cr in 0.3M H_2SO_4.

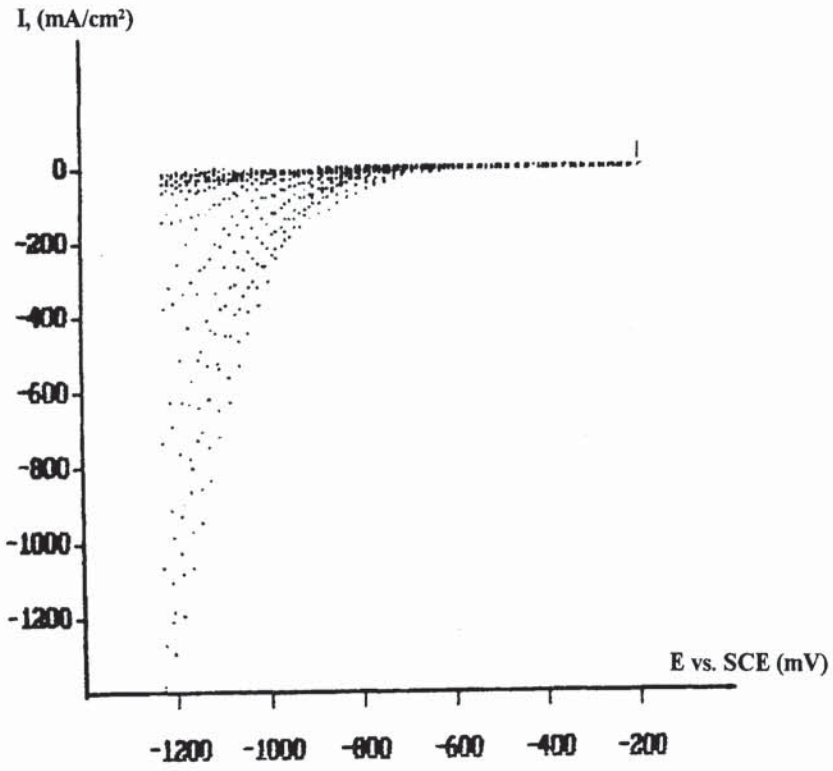

Figure 151. The cyclic voltammograms on rotating chromium electrode in 250 g/L CrO_3 solution. ω = 2000 rpm; v = 83 mV/s.

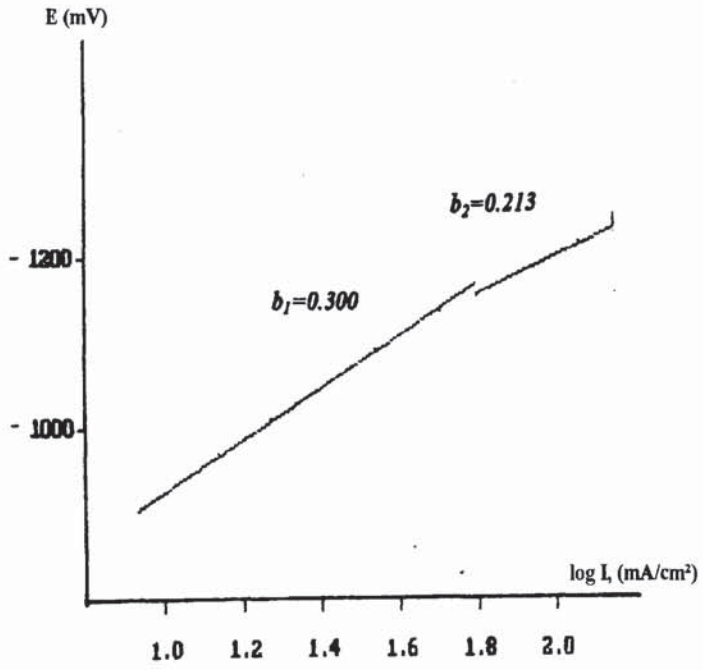

Figure 152. E - log *I* curve for the third cycle on Figure 151 on Cr in CrO_3 solution.

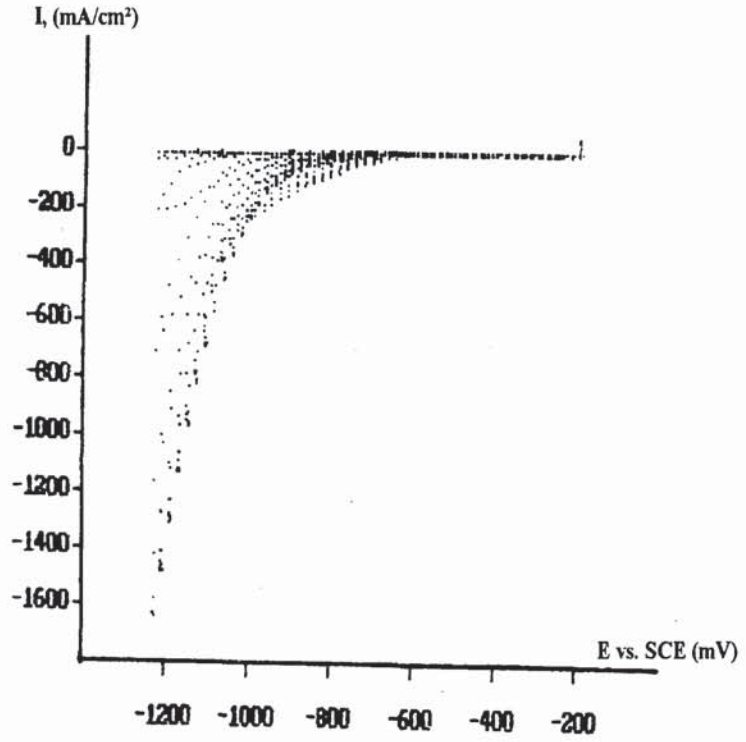

Figure 153. The cyclic voltammograms on rotating chromium electrode in CrO_3 (250 g/L) + MSA (5.0 g/L) bath; ω = 2000 rpm: ν = 83 mV/s.

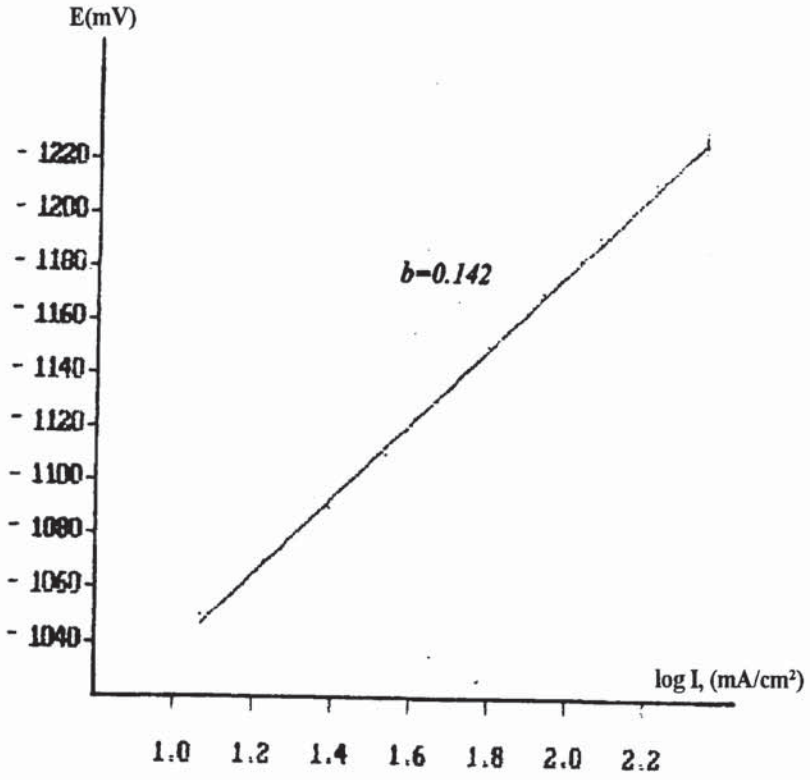

Figure 154. E - log *I* curve for the third cycle of Figure 116 on rotating chromium electrode in CrO_3 (250 g/L) + MSA (5.0 g/L) bath.

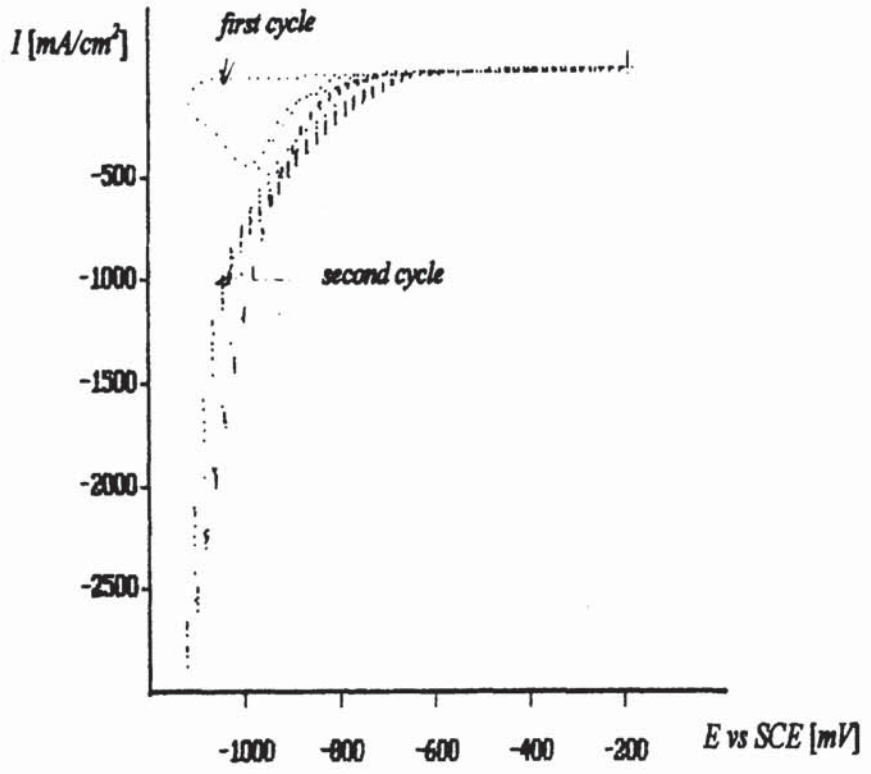

Figure 155. The cyclic voltammograms on electrode in uncatalysed CrO_3 (250 g/L). The scanning starts on -0.2 to -1.1V v = 81 mV/s.; T = 55^0 C.

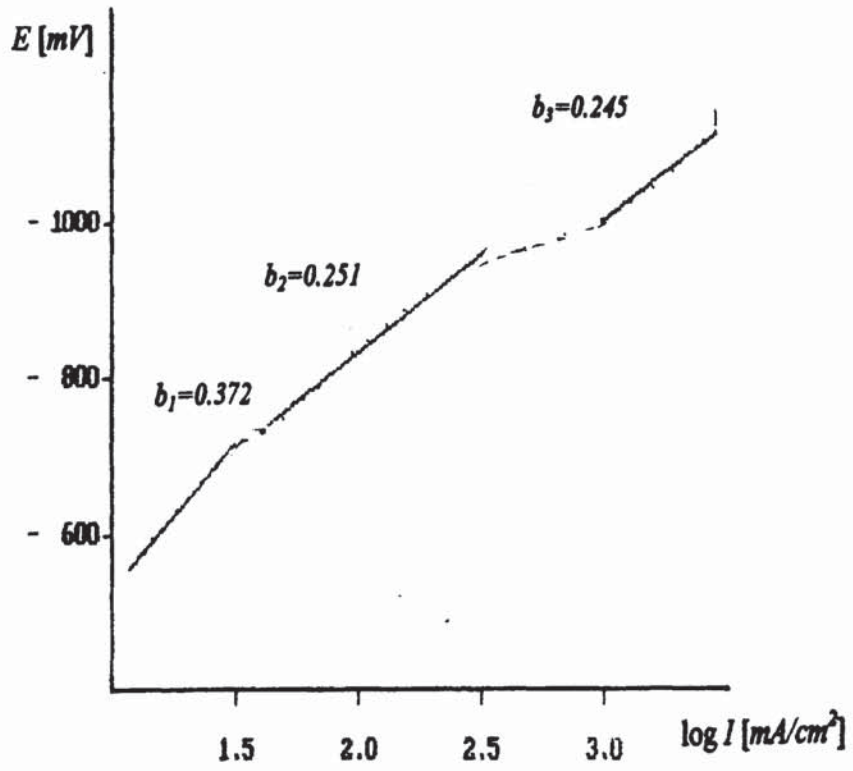

Figure 156. E - log I curve for the second cycle at Figure 155. on rotating chromium electrode in uncatalysed CrO_3 (250 g/L); T = 55^0 C.

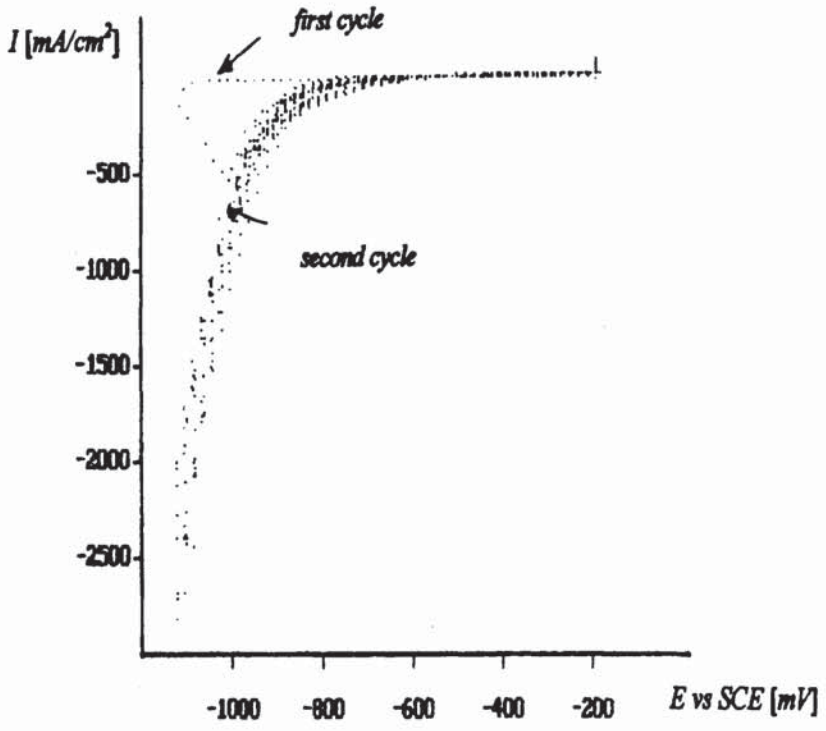

Figure 157. The cyclic voltammograms on Cr electrode in CrO_3 (250 g/L) + MSA (5.0 g/L) solution; v = 81 mV/s.; T = 55^0 C.

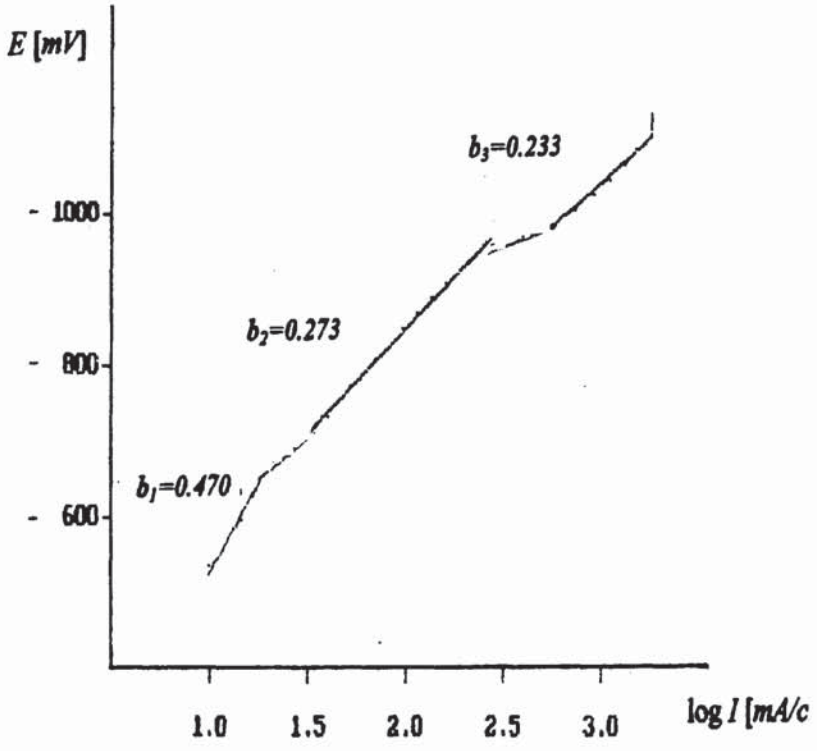

Figure 158. E - log I curve for the second cycle of Figure 157 on Cr electrode in uncatalysed CrO_3 (250 g/L) solution; T = 55^0 C.

II.4.4 DISSOLUTION CHROMIUM MECHANISMS

Chromium anodic reactions are studied by a few methods: Anodic linear polarisation, Dissolution efficiency, Weight difference experiments, Quartz Crystal Microbalance and by Gravimetry.

II.4.4a **Anodic Polarisation During Chromium Dissolution.**

An attempt was made to study the process of anodic dissolution of chromium in Sargent bath (with and without MSA) by potentiodynamic method. The reference electrode was SCE. Measurements were conducted on the chromium plated micro electrode (2 10^{-2} dm^2) within the potential range from 0.5 to 1.2 V and potential sweep rate v = 70 m V/s.

It was found (Figure 159) that in the Sargent bath (SB) chromium dissolves only under positive potential (> + 1.0 V), that is in the passive region. No peaks are observed corresponding to the active chromium dissolution as it was already observed by many investigators, for the case of the chromium dissolution in H_2SO_4 solution. We can assume at this point that the chromium dissolves mainly as Cr^{6+} .

The increase of temperature from 20 to 55^0 C did not show appreciable influence (Figures 150 and 159) on the dissolution of chromium in sulphuric acid.

The E - I curves for the SB with MSA baths (Figures 161 and 166) have the same shape as in the Figures 159 and 164: the current at the start of the chromium dissolution commences at potential of +1.15 V. There is no current in the negative (active) region of potential, unlike that for the chromium dissolution in H_2SO_4 solution (-0.5 to -0.3 V).

The increase in the first part of the anodic dissolution E - I curves (Figures 159 and 163) with the increase in the rate of chromium dissolution in this electrolyte (SB + MSA) can be seen, but the effect is small.

In half-logarithmic coordinates (Figures 160, 162, 165 and 167) there are two linear parts on the E-log I curve with b_1 = 0.58 and 0.064 and b_2 = 0.120 and 0.185 for SB and SB + MSA solutions, respectively. A preliminary attempt was made to use a platinum ring disk electrode to detect Cr^{2+} as an intermediate stage but without success due to the suspected rapid oxidation of any Cr^{2+} present by Cr^{6+} according to the reaction below :

$$Cr^{3+} + Cr^{6+} = 2Cr^{3+}.$$

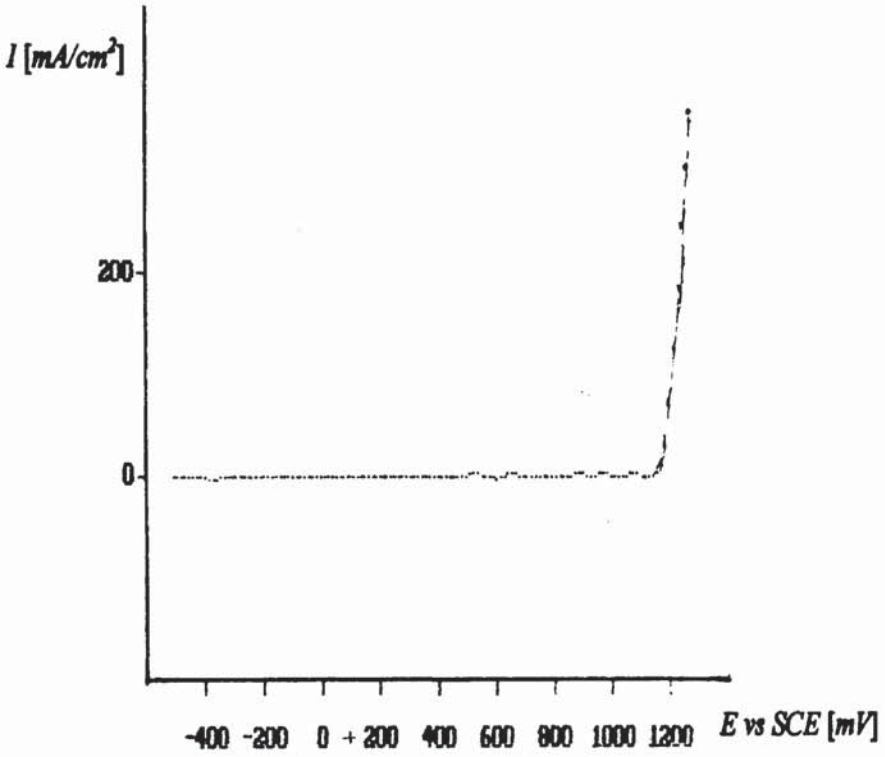

Figure 159. Anodic LPP scan for CrO_3 250 g/L; H_2SO_4 2.5 g/L bath; ω = 0 rpm; v = 70 mV/s.; T = 20^0 C.

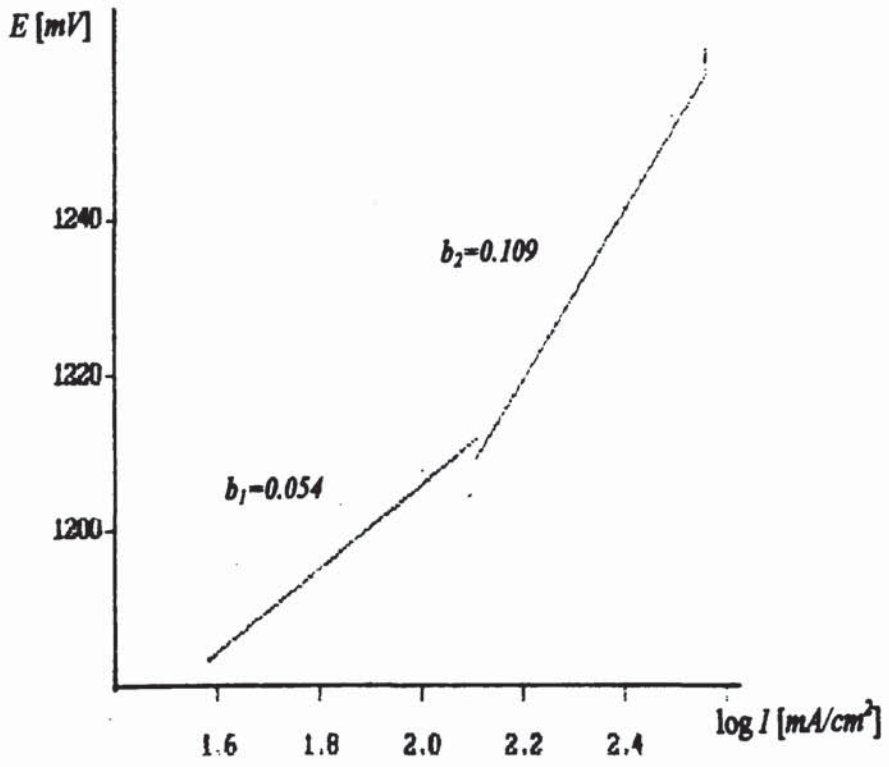

Figure 160. E - log I plot for curve on Figure 159.

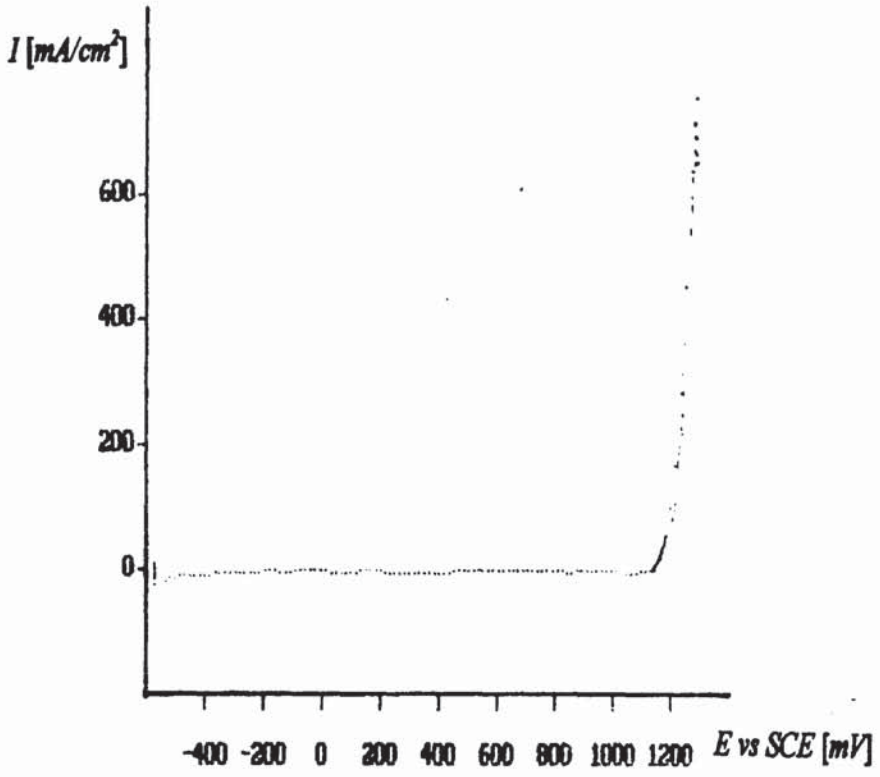

Figure 161. Anodic LPP scan for CrO_3 250 g/L, H_2SO_4 2.5 g/L, MSA, 5.0 g/L, bath; ω = 0 rpm; ν = 70 mV/s.; T = 20^0 C.

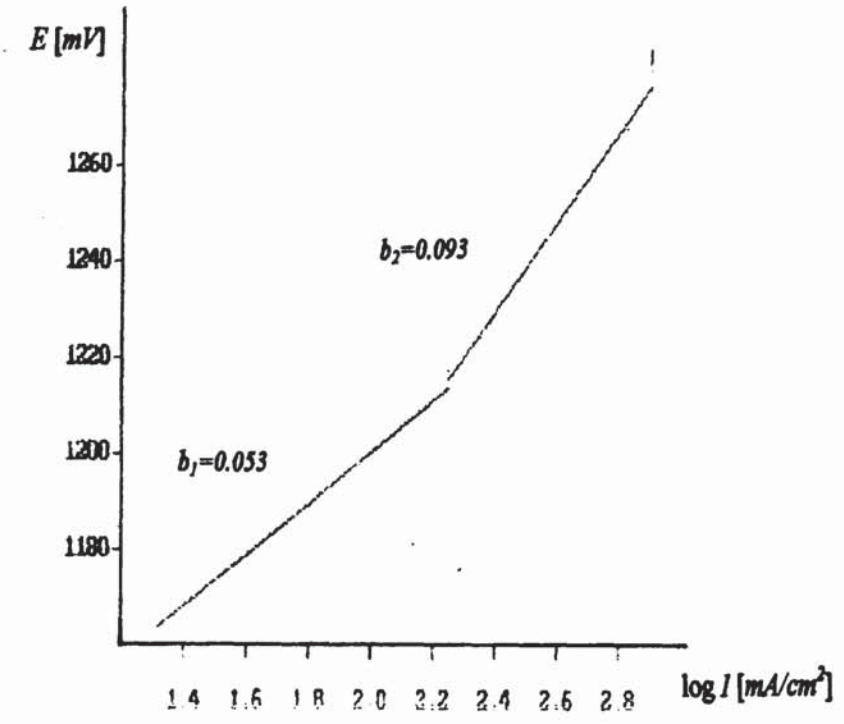

Figure 162. E - log I plot for curve on Figure 161.

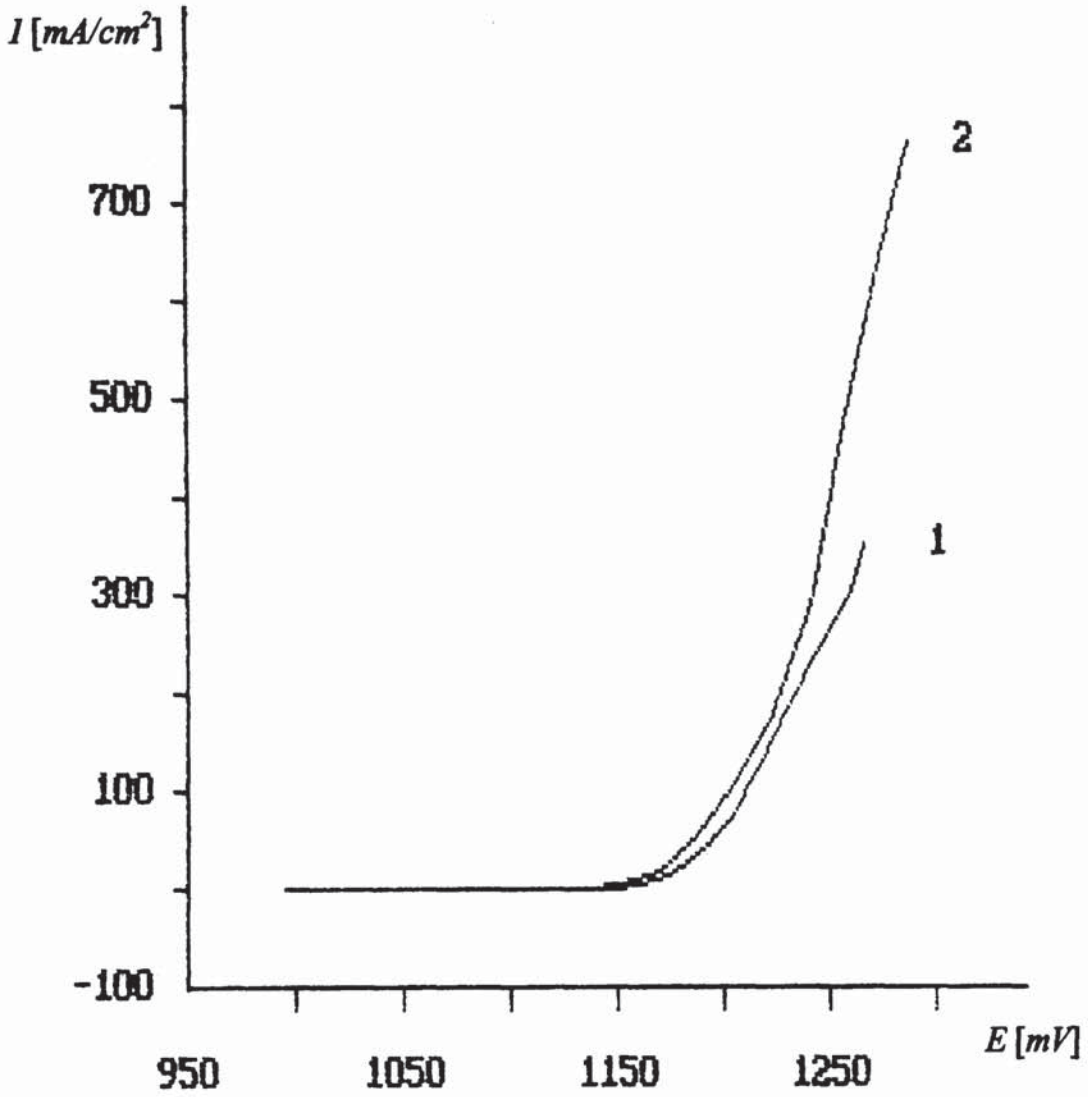

Figure 163. Anodic LPP scans on Cr electrode; v = 40 mV/s.; T = 20^0 C.
1) CrO_3 250 g/L; H_2SO_4 2.5 g/L bath.
2) CrO_3 250 g/L; H_2SO_4 2.5 g/L; + MSA; 5.0 g/L bath.

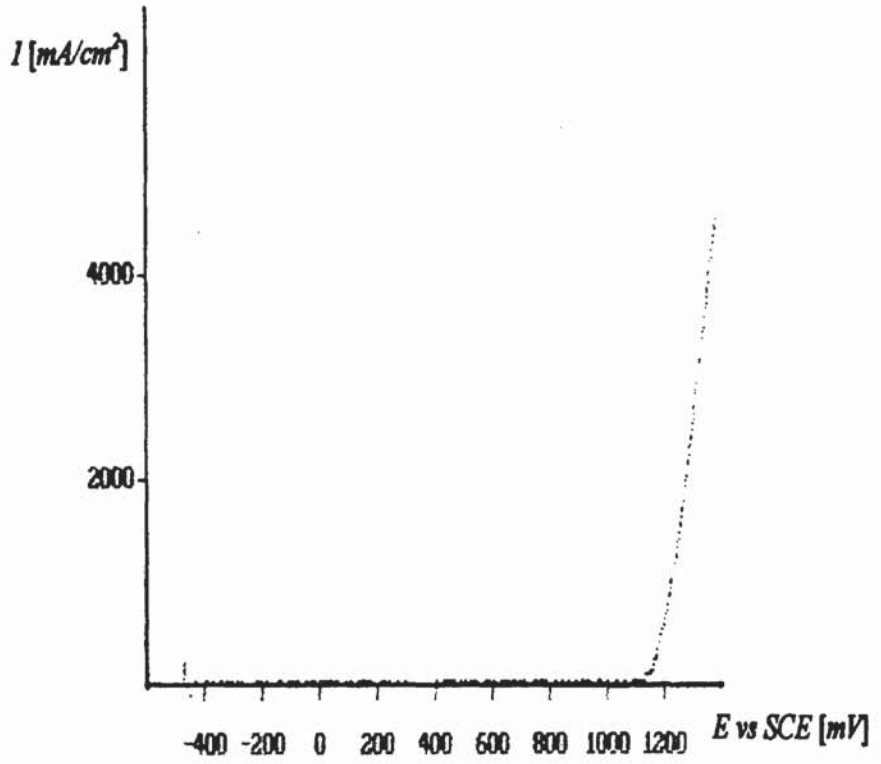

Figure 164. CrO_3 250 g/L; H_2SO_4 2.5 g/L; $\omega = 0$ rpm; $\nu = 70$ mV/s.; T = 20° C.

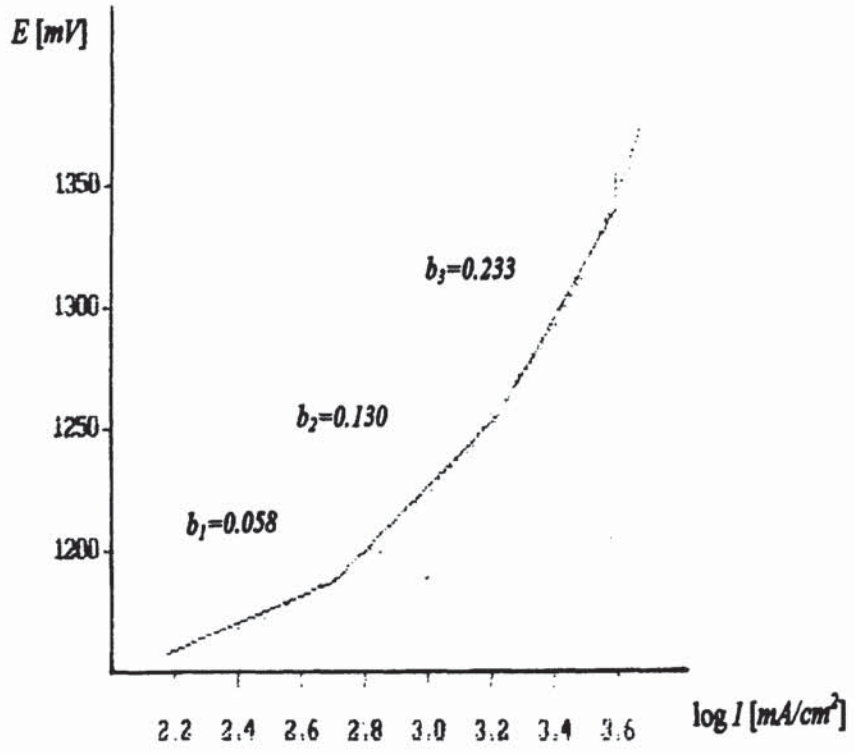

Figure 165. E log I plot from the scan from Figure 164.

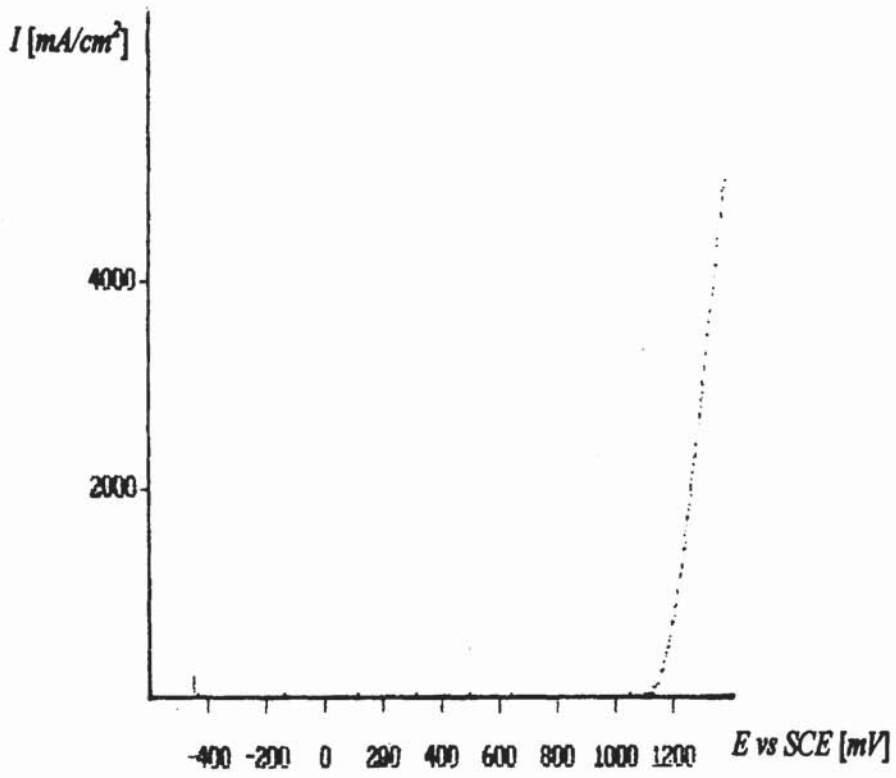

Figure 166. CrO_3 250 g/L; H_2SO_4 2.5 g/L; MSA 5.0 g/L; T = 55^0 C.

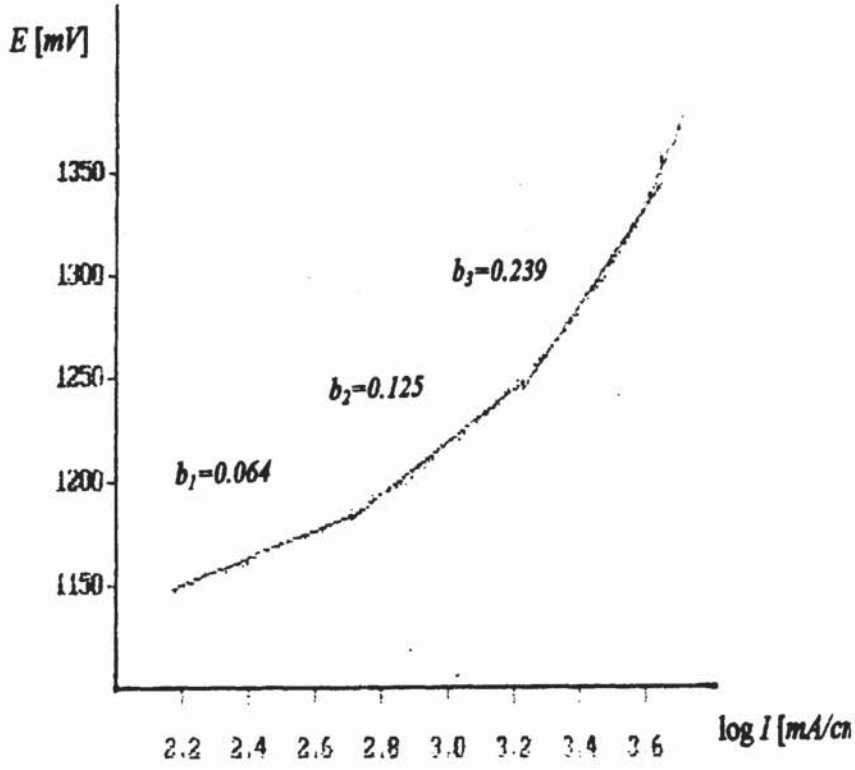

Figure 167. E - log I plot for curve on Figure 166.

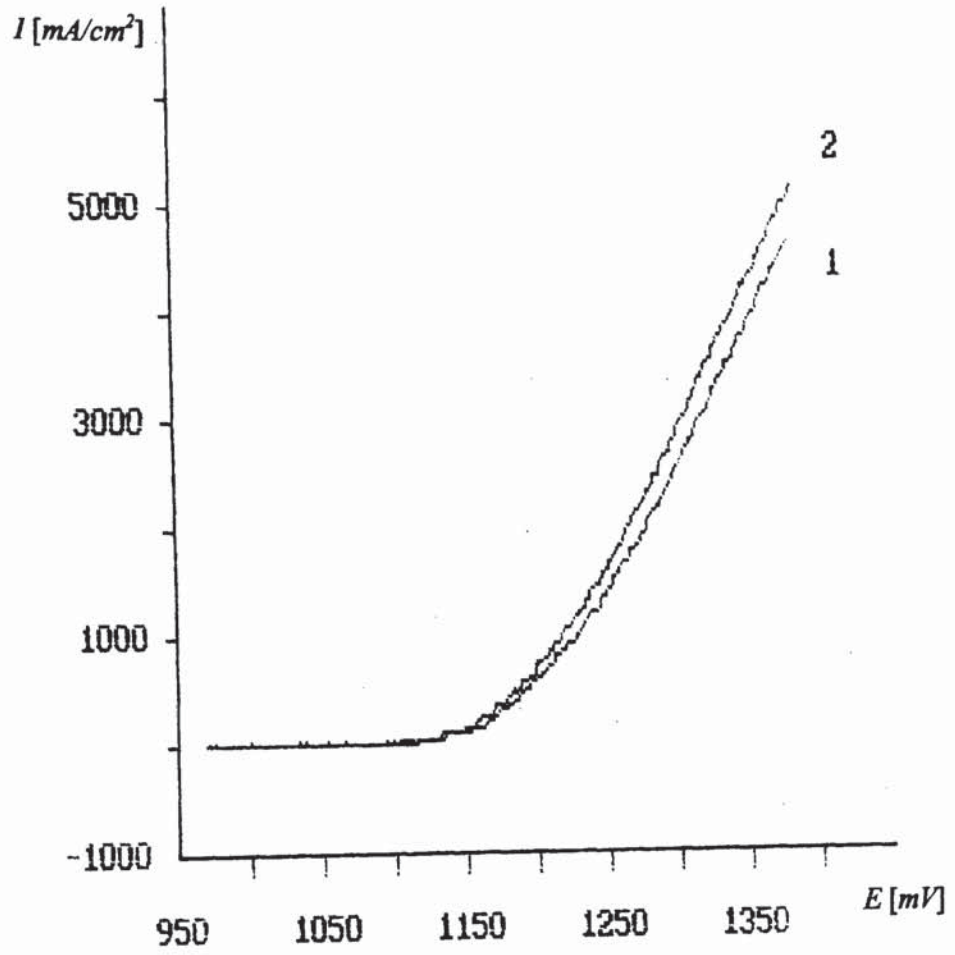

Figure 168. Anodic LPP scans for Cr electrode; v = 10 mV/s.; T = 55^0 C; ω = 0
1) CrO_3 250 g/L; H_2SO_4 2.5 g/L.
2) CrO_3 250 g/L; H_2SO_4 2.5 g/L; + MSA; 5.0 g/L.

II.4.4.b **Dissolution Efficiency from Weight Difference Experiments**

1. **Introduction:**

The detailed literature search in Section I.5 revealed **no** definitive information on the efficiency of chromium anodic dissolution (deplating). It is mostly assumed to be about 100 % and until introduction of Periodic Reverse Current chromium deposition it did not seam to have much practical significance.

However, for PRC research it is important to establish dissolution rates under different deposition conditions in order to calculate exact current deposition efficiencies and study electrodeposition mechanisms.

Dissolution rates were determined by plating first the thick chromium deposit and then anodically dissolving chromium at successive time periods. Three current densities (20, 30 and 40 Adm^{-2} were used as well as three different bath temperatures: 47, 53 and 58^0 C, (117, 127 and 136^0 F).

Faraday's Law is used to calculate anodic current (dissolution) efficiency in the same way as used for calculating deposition cathodic current efficiency. The same electrochemical equivalent equal to 0.3234 g/A·h was tentatively used, assuming for this moment that dissolution reaction goes as: $Cr^0 - 6e = Cr^{6+}$.

2. Preliminary Experiments Anodic Current Efficiency at 20 Adm^{-2}

Solution: 240 g/ℓ Sargent Bath, 100:1 ratio; 53^0 C. Time: 3, 10, 23 and 60 min.

Exp. no.	Temp. ^0F / ^0C	i_c Adm^{-2}	i_a Adm^{-2}	t_a min	t_c s	Dep. Wt gr/hr	Q_a / Q_c x 1000	CCE %	Note:
323-2	127 / 53	0	20	3	0	0.270	-	119.3	
321-1	127 / 53	0	20	10	0	0.830	-	110.0	
321-2	127 / 53	0	20	23	0	2.010	-	115.8	
322	127 / 53	0	20	60	0	4.977	-	109.9	

Table 48: Anodic Current Efficiency of Chromium at 20 Adm^{-2}.

It is obvious from the results in Table 48 and Figure 169 that dissolution of chromium is not fully linear with time. However, almost straight line has been drawn in Figure 169. The slight deviation is probably due to chromium deposition on the cathode. Therefore, the next set of experiments is performed to establish the behaviour of chromium during stripping at predetermined times: 1, 2, 5, 10 and 15 minutes for a given temperature at three different current densities. Results are presented in Tables 49 and 50.

3. Chromium Stripping Rate at 20, 30 and 40 Adm^{-2} (53^0 C)

Exp. no.	Temp. ^0F / ^0C	i_c Adm^{-2}	i_a Adm^{-2}	t_a s	t_c s	Dep. Wt gr.	Q_a / Q_c x 1000	CCE %	Note:
323-a	127 / 53	0	**20**	1	0	0.093	-	123.2	
323-b	127 / 53	0	20	2	0	0.180	-	119.3	
323-c	125 / 52	0	20	5	0	0.430	-	114.0	
323-d	127 / 53	0	20	10	0	0.865	-	114.6	
324-a	127 / 53	0	**30**	1	0	0.132	-	114.6	
324-a	127 / 53	0	30	1	0	0.129	-	116.6	
324-b	127 / 53	0	30	5	0	0.623	-	114.0	
324-c	127 / 53	0	30	10	0	1.362	-	110.0	
324-d	127 / 53	0	30	15	0	1.857	-	109.4	
346-a	127 / 53	0	**40**	1	0	0.180	-	119.3	
346-b	127 / 53	0	40	1	0	0.179	-	108.6	
346-d	127 / 53	0	40	10	0	1.830	-	121.2	
346-e	127 / 53	0	40	17	0	2.871	-	111.9	

Table 49: Chromium Anodic Current Efficiency at 20, 30 and 40 Adm^{-2} vs. Time

It follows from Table 49 and Figure 169, that at the beginning, chromium is anodically dissolving slightly faster at all three current densities explored or, in other words, it is *time dependent*. However, it is also *CD dependent*, having a maximum value at 20 Adm^{-2}. (123.2 %) Results are graphically depicted in Figure 169.

4. Anodic Current Efficiency-Time Dependence at 47, 53 and 58^0 C (40 Adm^{-2})

Fresh Solution is used. Sargent Bath, 240 g/l CrO_3 100:1 ratio.

Exp. no.	Temp. ^0F / ^0C	i_c Adm^{-2}	i_a Adm^{-2}	t_a min	t_c s	Dep. Wt g	Dep. Wt g/h	CCE %	Note:
363-a	**117** / 47	0	40	1	0	0.183	10.98	121.2	
363-b	117 / 47	0	40	2	0	0.337	10.11	116.6	
363-c	117 / 47	0	40	5	0	0.830	9.96	110.0	
363-d	117 / 47	0	40	15	0	1.635	9.81	108.3	
363-e	117 / 47	0	40	10	0	2.461	9.84	108.6	
346-a	**137** / 58	0	40	1	0	0.172	10.32	113.9	
346-b	137 / 58	0	40	1	0	0.324	9.72	107.3	
346-c	137 / 58	0	40	5	0	0.864	10.32	114.5	
346-d	137 / 58	0	40	10	0	1.661	9.96	110.0	
346-e	137 / 58	0	40	15	0	2.573	10.92	109.2	
346-a	**127** / 53	0	40	1	0	0.180	10.80	119.3	From Table 17
346-b	127 / 53	0	40	1	0	0.179	10.74	108.6	
346-c	127 / 53	0	40	10	0	1.830	10.98	121.2	(!)
346-d	127 / 53	0	40	17	0	2.871	10.43	111.9	

Table 50: Anodic Current Efficiency vs. Temperature at 40 Adm^{-2}.

It follows from Table 50 that temperature does have some influence on chromium dissolution rate and that it is higher at lower temperature for short time periods, similar to deposition efficiency.

This dependence is graphically presented in Figure 170.

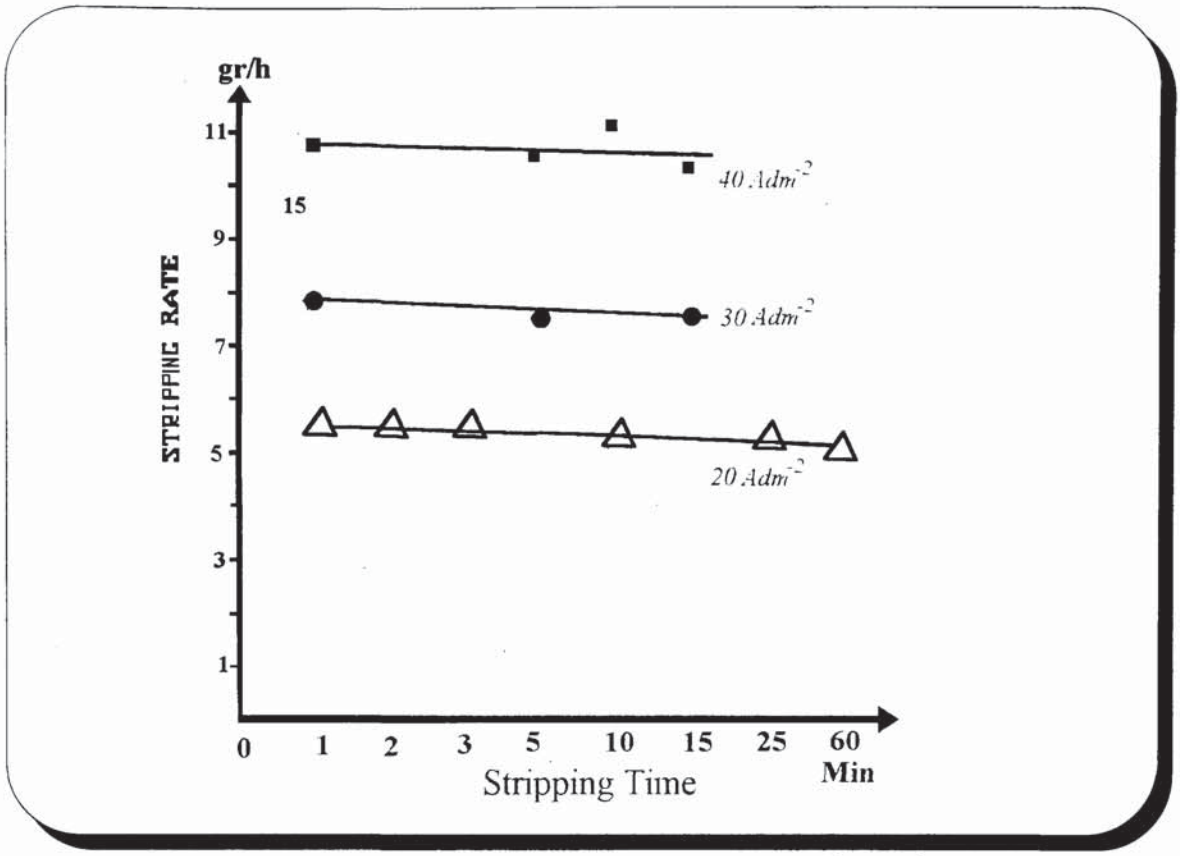

Figure 169. Chromium Stripping Rate at 20, 30, and 40 Adm^{-2}; (53^0 C).

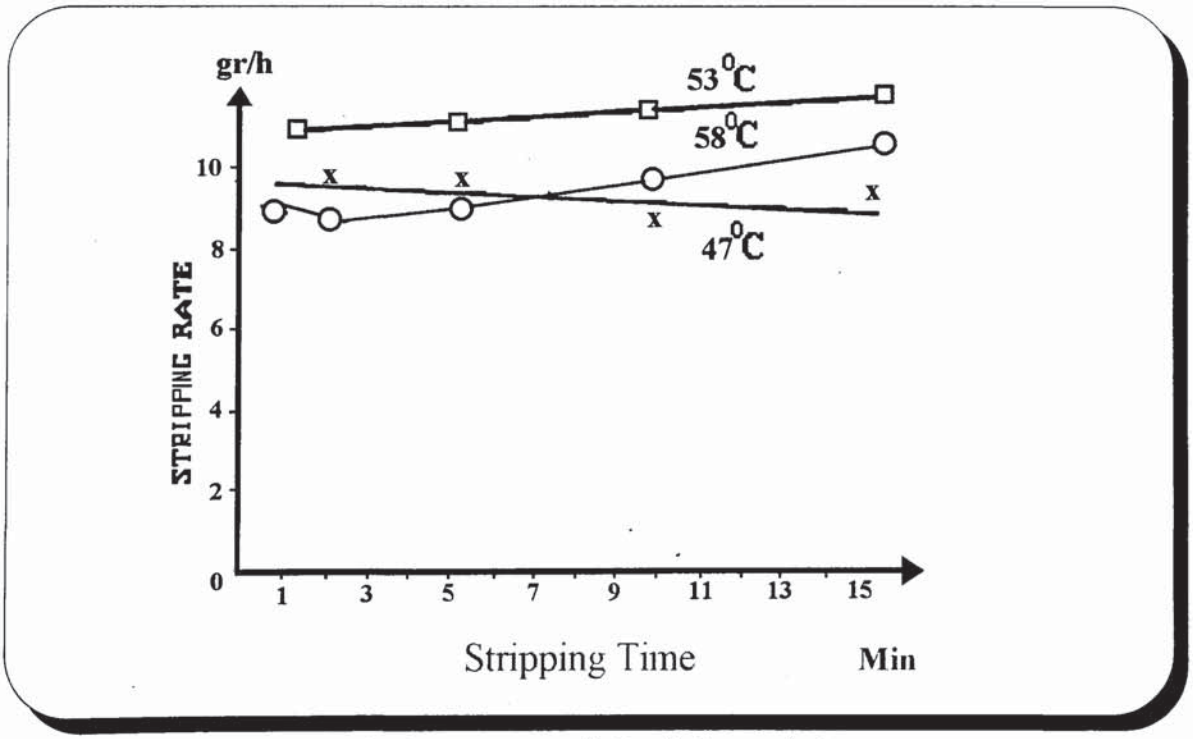

Figure 170. Chromium Stripping Rate at 47^0 C, 53^0 C and 58^0 C (40 Adm^{-2}).

II.4.4.c **Gravimetric Determination of Anodic Dissolution of Chromium**

i. *Equipment*

Same experimental arrangements as in II.2.1.

ii. *Experimental results*:

Anodic behavior and anodic current efficiencies of the electrolytically deposited chromium were investigated in the solution of chromic acid alone and with Sulphuric acid and/or MSA as additives. Iron working electrode (area = $2 \cdot 10^{-3}$ cm^2) was previously plated in Sargent or MSA catalysed baths at 55^0 C and C.D. = 50 Adm^{-2} in all dissolution experiments except one with C.D. = 30 Adm^{-2} at 70^0 C. Chromium thickness was about 50 - 80 microns. After dissolving the chromium deposited at the cathode in 1:1 HCl, gavimetric method was used for the determination of anodic chromium current efficiency assuming that chromium dissolves as Cr^{6+} in the positive region of potentials. (+1.2V)

From results given in Table 51 it can be seen that chromium dissolves with anodic current efficiency (ACE) in 102 - 109% range (calculated as Cr^{6+}) and that is practically independent of the MSA addition during deposition (105.2 vs. 105.1%) or dissolution (105.2 vs. 106.2%). Dissolution current density has only a slight influence (105.2 vs. 106.0%). ACE decreases to 103.6% for chromium plating at higher temperature (70^0 C) and at 30 Adm^{-2}. This could be arguably attributed to the well known fact that Chromium has fewer cracks when plated at a higher temperature and lower CCD's. According to early Russian research[126,127], due to lower *actual* current density, generation of Cr^{3+} is favoured in the cracks.

It is interesting to note that, unlike deposition, chromium dissolves in the chromic acid without sulphates and that it dissolves at the lower rate (103.0%) compared to Sargent bath (105.2%). Also, chromium deposited from an MSA bath dissolves at the *same rate* in 240 g/ℓ CrO_3 uncatalysed bath (105.7%) as compared with Sargent bath (105.1%).

However, by doubling the content of sulphuric acid to 5.0 g/ℓ in Sargent bath (Experiment. No. 10 in Table 51) the dissolution current efficiency is increased to 108.4% indicating that excess sulphate presumably does have some "activating" effect

Anodic current efficiencies that are consistently higher than 100% are an indication that the dissolution reaction is not a straight forward: $Cr^{o} \rightarrow Cr^{6+} + 6e$ oxidation and that a secondary reaction is also taking place, probably partial oxidation to a lower valence state and possible non electrochemical dissolution. QCM experiments in the next section corroborate this assumption.

Exper. No.	**Type of Bath (dissolution)**	**Type of Bath (deposition)**	**Dissolution Curr.Density (Adm^{-2})**	**Anodic Curr. Efficiency (ACE), %**	**Average Anodic Curr. Efficiency** (ACE). %
1	250 g/ℓ CrO_3 2.5 g/ℓ H_2SO_4 (SB)	(SB) t = 55° C CCD =*50 Adm^{-2}*	50	102.27 106.20 103.91 105.35 102.60 107.05 104.69 109.79	105.2
2	SB	(SB) t = 55° C CCD =*50 Adm^{-2}*	50	104.78 103.91 103.52 104.17 105.51 107.57 106.20	105.1
3	SB	(SB) t = 55° C CCD =*50 Adm^{-2}*	5	104.73 102.88 109.37 104.07 109.37 100.75 108.71 108.71 106.06	106.0
4	SB + 5.0 g/ℓ MSA	(SB) t = 55° C CCD =*50 Adm^{-2}*	50	103.78 104.07 106.78 106.55 109.27 109.53 105.35	106.5

Table 51. Average Anode Current Efficiency of Chromium Dissolution under DC Conditions.

Exper. No.	Type of Bath (dissolution)	Type of Bath (deposition)	Dissolution Curr.Density (Adm^{-2})	Anodic Curr. Efficiency (ACE). %	Average Anodic Curr. Efficiency (ACE). %
5	SB + MSA	SB + MSA t = 55° C CCD = 50 Adm^{-2}	50	103.52 103.26 10352 108.16 104.40 106.20 106.52 109.46 105.07 103.68 107.18 106.36	105.7
6	SB + MSA	SB + MSA t = 55° C CCD = 50 Adm^{-2}	5	107.01 102.61 105.13 102.61 102.34	104.1
7	SB	t = 70° C ACD=30 Adm^{-2}	50	107.45 101.57 103.10 103.43 105.88 105.23	103.6

Table 51. (Continued)

Experiment. No.	**Type of Bath (dissolution)**	**Type of Bath (deposition)**	**Dissolution Curr.Density Adm^{-2}**	**Anodic Curr.Effiiciency** (ACE), %	**Average Anodic Curr. Efficiency** (ACE), %
8	250 g/ℓ CrO_3	SB t = 55° C CCD = *50 Adm^{-2}*	50	101.29 102.21 101.29 105.61 102.47 102.99 105.74 103.39 102.47	103.0
9	250 g/ℓ CrO_3	SB + MSA t = 55° C CCD = *50 Adm^{-2}*	50	104.89 107.67 108.48 104.56 105.87 105.79 105.48 105.61 107.26	105.7
10	250 g/ℓ CrO_3 5.0 g/ℓ H_2SO_4	SB t = 55° C CCD = *50 Adm^{-2}*	50	110.44 105.48 113.71 108.74 107.31 105.61 109.63 105.87 109.14	108.4

Table 51. (Continued)

To investigate the influence of cracks on dissolution efficiency chromium was deposited from SB and SB + MSA baths with unipolar pulses (PC mode). It is well recognised that PC mode produces deposits with few if any cracks.

Comparison of tables 51 and 52 indicates that there are only slight differences in anodic current efficiencies and therefore there is no support offered for the claims on the influence of the cracks on the anodic current efficiency[126,127].

Exper. No.	**Type of Bath (dissolution) (55^0 C) ACD = 50 *Adm^2***	**Type of Bath (deposition) (55^0 C) CCD= 50*Adm^2***	**Deposition & Dissolution Time Periods** t_c t_p	**DC Average Anodic Curr. Efficiency** (ACE), %	**PC Average Anodic Curr. Efficiency** (ACE). %
1	SB + MSA	SB + MSA	20s 100ms	103.95	104.95
2	SB + MSA	SB + MSA	20s 400ms	102.32	104.00
3	SB	SB	20s 100ms	103.15	103.5
4	SB	SB	20s 400ms	102.15	104.20

Table 52. Average Anode Current Efficiency of PC deposited and DC and PC anodically dissolved chromium .

II.4.4.d Quartz Crystal Microballance (QCM) Determination of Chromium Anodic Dissolution in the Sargent Bath.

1. *Equipment:*

PAR 273 (AG&G, Princeton, N.J.) potentiostat/galvanostat driven by PAR 175 programmer was used in conjunction with QMC made by Intricon (Model 751001G1). Standard glass corrosion cell was used as a reaction vessel. Previously heavy chromium plated steel strips were used as cathodes and lead wire as anode. Due to the highly stressed deposits , gold plated quartz crystals often shattered during deposition at room temperature and subsequent experiments were done at 55^0 C.

2. *Determination of QMC sensitivity:*

The relationship between the frequency change and mass change is determined experimentally. Acid copper plating solution is used to calibrate the QCM since it has nearly 100% current efficiency. Figure 171 is the plot between frequency change of the QMC during copper deposition at -7.5mA (over 0.33 cm^2 electrode area) vs. time. The mass change for copper (M = 63.5) is calculated from the passed charge according to the following fundamental relationship:

$$\text{rate of mass change } \left(\frac{\Delta m}{\text{time}}\right) =$$

$$i \bullet \frac{1}{nF} \bullet M = 7.5 \cdot 10^{-3} \bullet \frac{1}{96500 \bullet 2} \cdot 63.5 = 2.468 \bullet 10^{-6} \text{g/s} \qquad <103>$$

From Figure 171 the slope is determined as -341.68 Hz/s. We can now evaluate the experimental sensitivity of the QCM according to:

$$\text{Sensitivity factor} = \frac{-341.68}{2.468 \bullet 10^{-6}} = -1.38 \bullet 10^8 \text{ Hz/g} \qquad <104>$$

3. *Chromium deposition at 20° C*

Figure 173 shows the frequency change during chromium deposition under applied current of -100 mA (c.d. is 350 mA/cm^2) vs. time. The slope of the line is -715.12 Hz/s. From the sensitivity factor the mass change of the electrode is calculated according to:

$$\text{Mass change from QCM} = \frac{-715.12}{-1.38 \bullet 10^8} = 5.18 \bullet 10^{-6} \text{g/s.}$$

We can find the mass change from the amount of charge passed for chromium (M = 52) for $Cr^{6+} \rightarrow Cr^0$ reaction; from Faraday's law :

$$\text{Mass change from charge passed} = \frac{1}{96500 \bullet 6} \bullet 52 = 8.98 \bullet 10^{-6} \text{ g/s.}$$

It is obvious that the cathode current efficiency would be:

$$\text{CCE} = \frac{\text{Mass change from QMC}}{\text{Mass change from charge passed}} = \frac{5.18 \bullet 10^{-6}}{8.98 \bullet 10^{-6}} = 57\%$$

4. *Chromium deposition and dissolution at 55^0 C:*

i. Deposition:

Figure 172 shows the frequency change of the QCM (for deposition at -100 mA and dissolution at 100 mA) vs. time. The slope of the deposition cycle is -188 Hz/s. By applying the same analysis as in part 3 we can find the current efficiency for Cr deposition at 55^0 C .

$$\text{Mass change from QCM} = \frac{-188}{-1.38 \bullet 10^8} = 1.362 \bullet 10^{-6} \text{g/s.}$$

$$\text{Mass change from charge passed} = 0.1 \bullet \frac{1}{96500 \bullet 6} \; 52 = 8.98 \bullet 10^{-6} \text{ g/s.}$$

$$\text{CCE} = \frac{\text{Mass change from QMC}}{\text{Mass change from charge passed}} = \frac{1.362 \bullet 10^{-6}}{8.98 \bullet 10^{-6}} = 15\%$$

ii. Dissolution:

The slope of the dissolution part is 1337.2 Hz/s. The anode current efficiency would be:

$$\text{ACE} = \frac{\text{Mass change from QMC}}{\text{Mass change from charge passed}} = \frac{1337.2}{1.38 \bullet 10^8} = 9.68 \bullet 10^{-6} \text{ g/s.}$$

Mass change from charge passed $= 0.1 \bullet \frac{1}{96500 \bullet 6} \bullet 5\,2 = 8.98 \bullet 10^{-6}$ g/s.

$$ACE = \frac{\text{Mass change from QMC}}{\text{Mass change from charge passed}} = \frac{9.68 \bullet 10^{-6}}{8.98 \bullet 10^{-6}} = 108\%$$

Because the current efficiency is higher than 100%, it is postulated that part of chromium must dissolve in either from Cr^{2+} or Cr^{3+} valent state. To find out how much would dissolve as Cr^{2+} state the following calculation is made:

If the amount dissolved as Cr^{6+} is **x** and the amount dissolved as Cr^{3+} is **(1-x)**, then based on 100% current efficiency, one can solve the following equations:

$$\text{Mass change from QCM} = \frac{1337.2}{1.38 \bullet 10^{8}} = 9.68 \bullet 10^{-6} \text{ g/s.} \qquad <105>$$

$$\text{Mass change from charge passed} = 0.1 \frac{1}{96500 \bullet [6x + 3(1-x)]} \bullet 52 \qquad <106>$$

For 100% efficiency the mass changes from QCM and Charge passed are equal ,i.e.,

$$0.1 \bullet \frac{1}{96500 \bullet [6x + 3(1-x)]} \bullet 52 = 9.68 \bullet 10^{-6}; \ \mathbf{x} = 0.85 \qquad <107>$$

The solution of equation <107> indicates that 85% of dissolved chromium is a Cr^{6+} state and the remainder is in Cr^{3+} state. The second possible situation is the assumption that part of the chromium dissolves as Cr^{6+} and the remaining part dissolves as Cr^{2+} state. A similar equation as <106> above can be solved for the Cr^{2+} case:

$$0.1 \bullet \frac{1}{96500 \bullet [6x + 2(1-x)]} \bullet 52 = 9.68 \bullet 10^{-6}; \ \mathbf{x} = 0.89 \qquad <108>$$

indicating that it can be assumed that 89% of chromium is dissolved as Cr^{6+} state and 11% is dissolved as Cr^{2+} state.

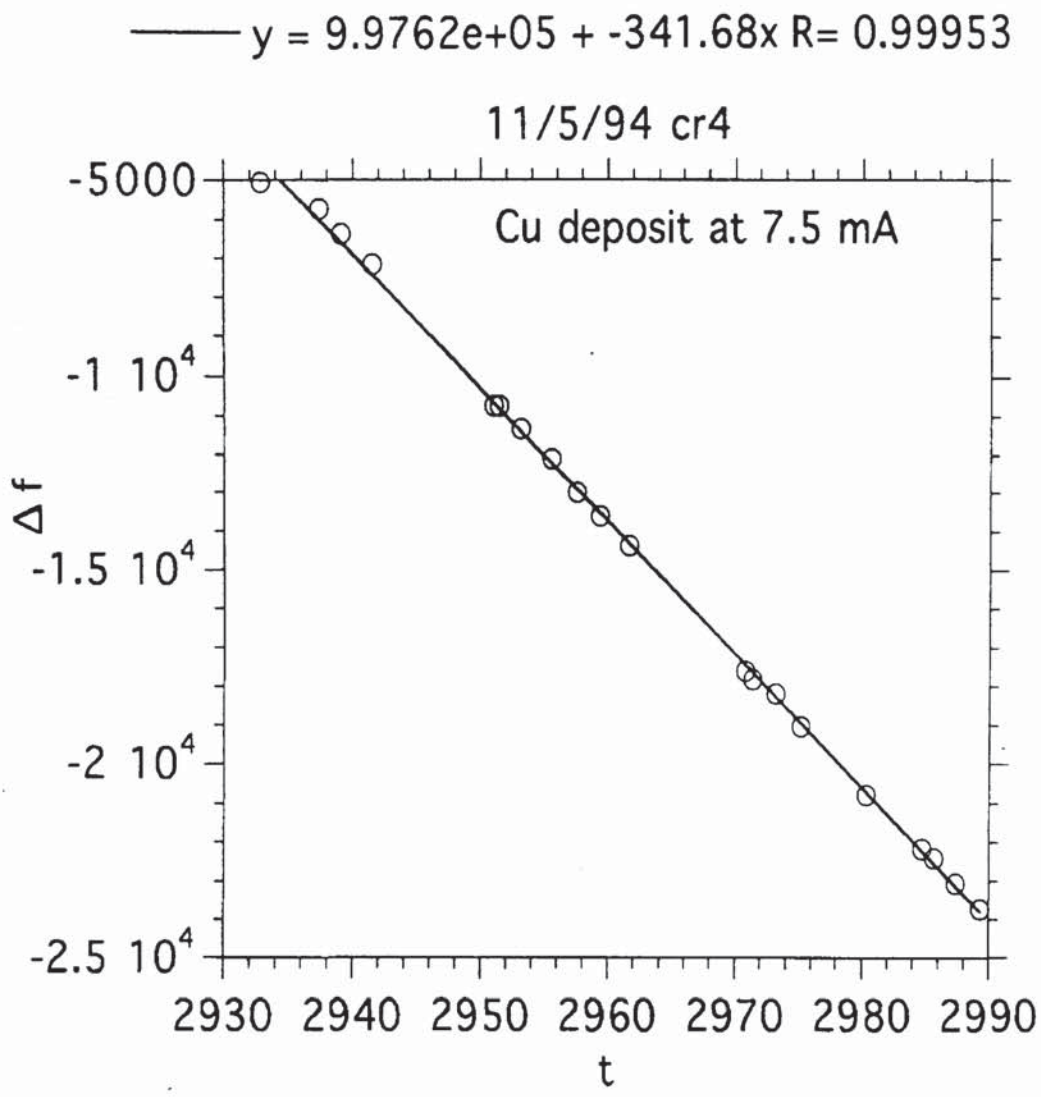

Figure 171. Calibration Curve for QCM Experiment.

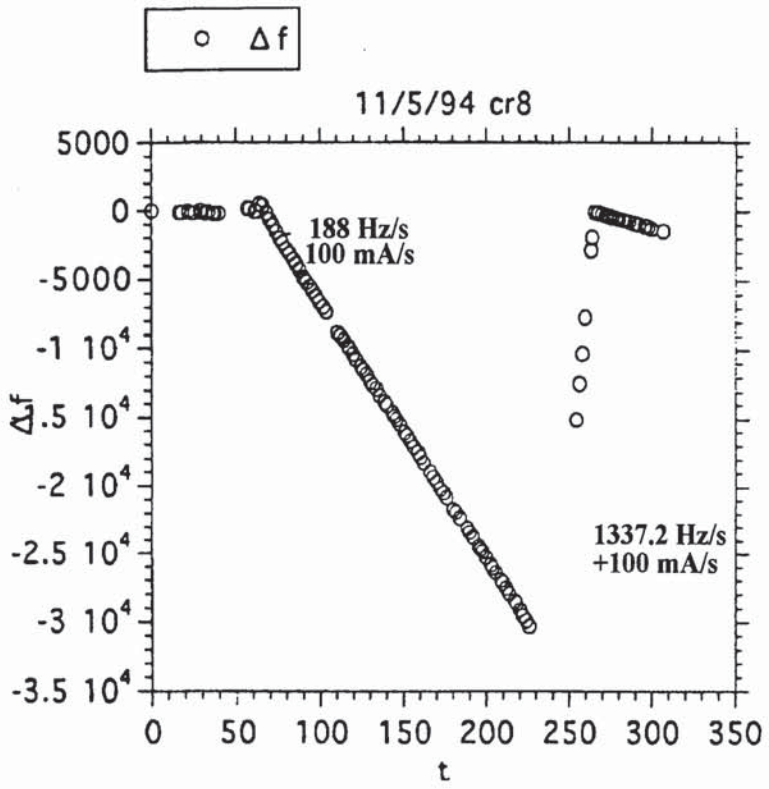

Figure 172. Frequency Change vs. Time at (55^0 C).

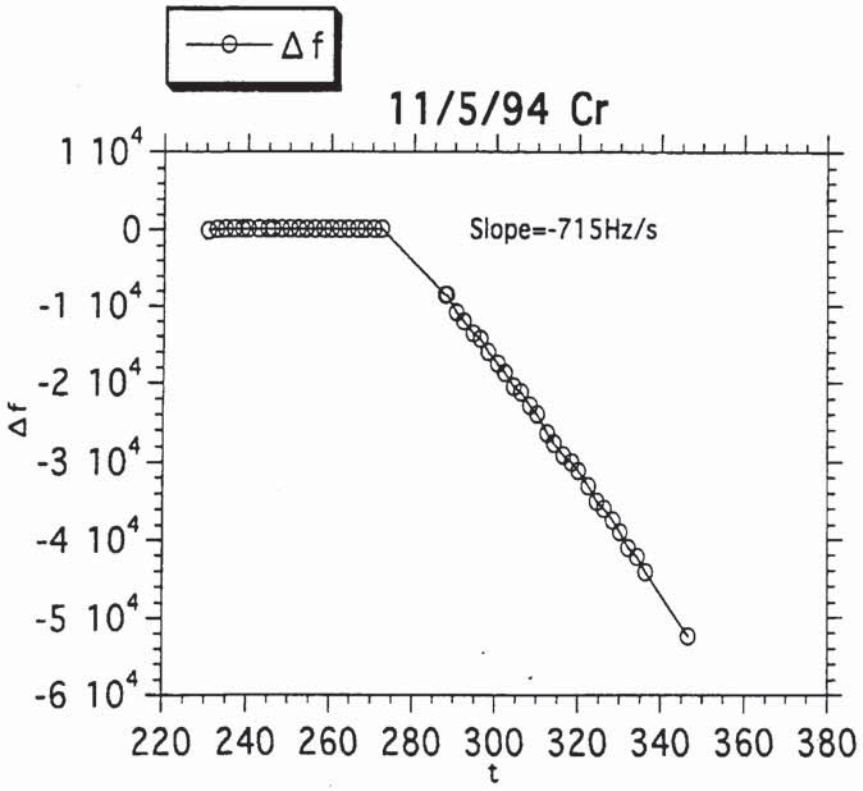

Figure 173. Frequency Change vs. Time at (20^0 C).

II.4.5e ANODIC DISSOLUTION OF CHROMIUM IN THE PRC MODE

Comparing the data given in Figures 174 and 175, it can be seen that during the anodic cycle of chromium dissolution, the electrode surface layers become reduced in the amount of sulphates present, whereas during the cathodic cycle is increased. The thickness of the oxide layer formed during anodic polarisation of electrodeposited chromium and its oxygen content are increased compared to the one formed during cathodic polarisation. However, during steady state deposition of chromium, Cr^{3+} and sulphate ions are continuously present in the liquid cathode film (L-film), the former as a product of incomplete reduction of $Cr^{6+} \rightarrow Cr^{3+}$ and later as a product of discharged chromous-bisulphate complex from which the metallic chromium is deposited and sulphate (or bisulphate) ion is regenerated.

The Cr^{3+} amount ought to be sufficient to keep equilibrium between rate of $Cr(OH)_3$ formation (a component of the cathodic film) and its dissolution. Sulphate ions liberated from the chromus-sulphate complex will diffuse back toward the outside surface of the cathodic film and then diffused further toward the bulk of the solution. Sulphate content ought to be sufficient to catalyse ("activate") a cathodic film reaction and to ensure the completion of Cr^{6+} to Cr^0 reduction reaction. The regulation of Cr^{3+} and sulphate concentrations is possible under the Periodically Reversed Current (PRC) regime.

The investigation of Cr^{3+} fraction that is forming during the anodic period of PRC mode was performed by RRDE technique. Experimental details are presented in a paper prepared for publication[7] . The Cr^{3+} fraction was found to depend on anodic current density i_a and the time of anodic period t_a as seen from Table 53. The Cr^{3+} fraction decreases with increasing anodic current density and increase with an increase of t_a. One then can select i_a, i_c, t_a and t_c independently in such a manner that chromium plating process will proceed with maximum CCE.

From the results presented, chromium plating in the PRC mode must proceed at high enough anodic current density (or high potential), at which the excess of Cr^{3+} ions formed in cathodic period is oxidised to Cr^{6+} . At the same time accumulated Cr^{3+}- sulphate complexes have to be removed from the cathode surface film and by having a sufficient anodic time period which will allow them to diffuse back into the bulk of the plating

solution. In other words, the anodic period t_a should be sufficiently long to allow diffusion of the sulphates in the complex with Cr^{3+} back into the bulk of the solution and yet short enough not to produce an excessive anodic dissolution rate which will affect the total PRC cathode current efficiency.

Obviously, it is not possible to regulate the Cr^{3+} and sulphate concentrations in the L-film during the direct current (DC) regime, since at steady state, cathodic current and cathodic time are, by definition, constant. Under DC conditions, Cr^{3+} is continuously forming and accumulating in the cathodic film where some sulphate ions stay incorporated in the surface film during the steady state Cr electrodeposition as complexes. This consequently slows down the rate of the main deposition reaction ($Cr^{6+} \rightarrow Cr^{0}$) and therefore decreasing the CCE. Clearly, this absence of the regulation of the concentration of those two components of the cathode film in the DC regime and possibility of overcoming that in the PRC mode explain the proven fact that chromium plating proceeds faster in the PRC mode, where the Cr^{3+} and sulphate content can be controlled and independently regulated with proper selection of i_c, i_a, t_c, and t_a values, resulting in an overall increase of CCEs in the PRC mode as compared to DC conditions.

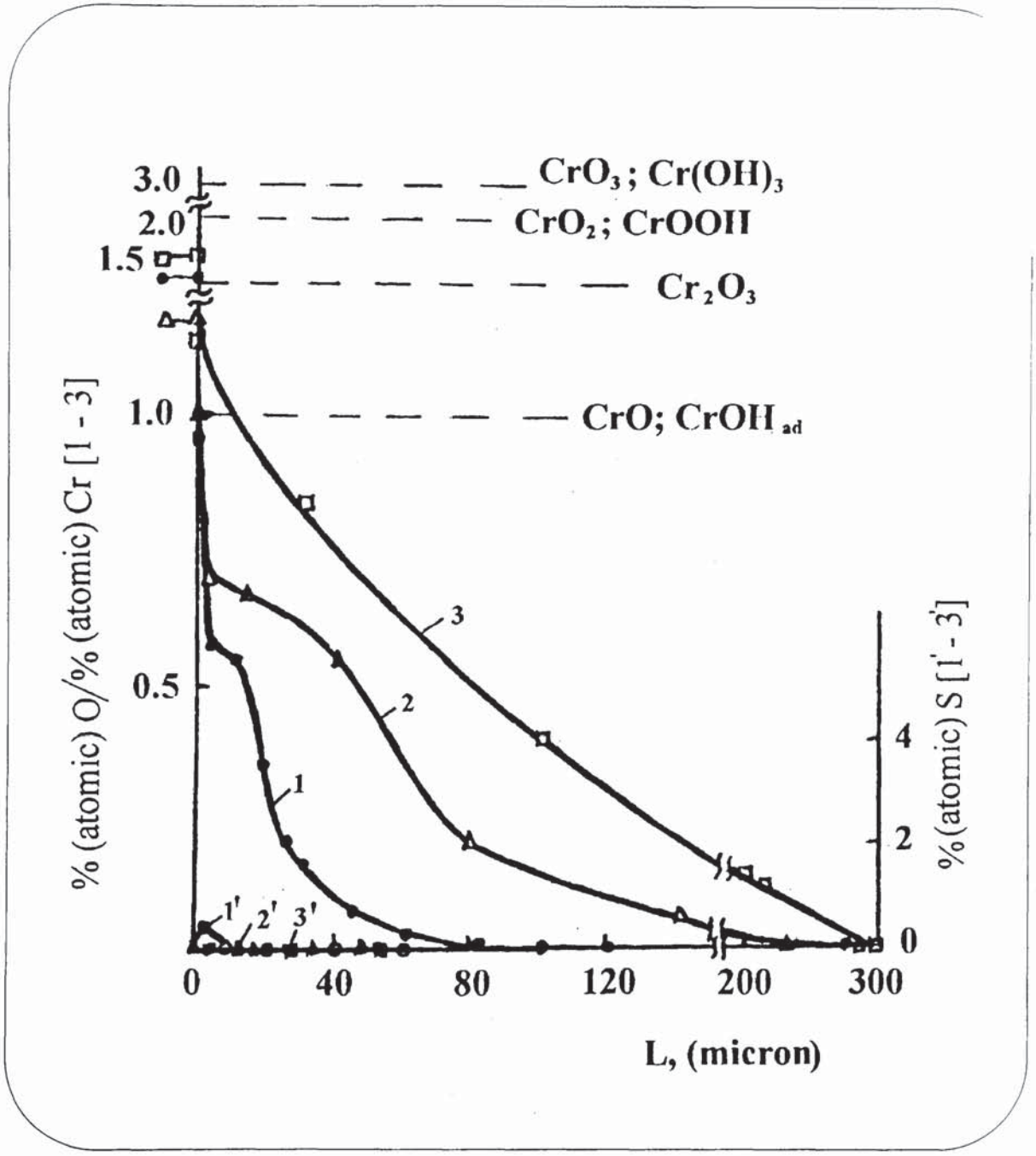

Figure 174. Change of oxygen and chromium atomic content ratio (1-3) and sulphur atomic content (1'-3') on oxide film depth of electrodeposited Cr before (1,1') and after (2, 2' ,3, .3') steady state anodic polarisation at a potentials of + 1.39 V (2,2') and 1.62 V (3, 3') in the Sargent bath (55^0 C).

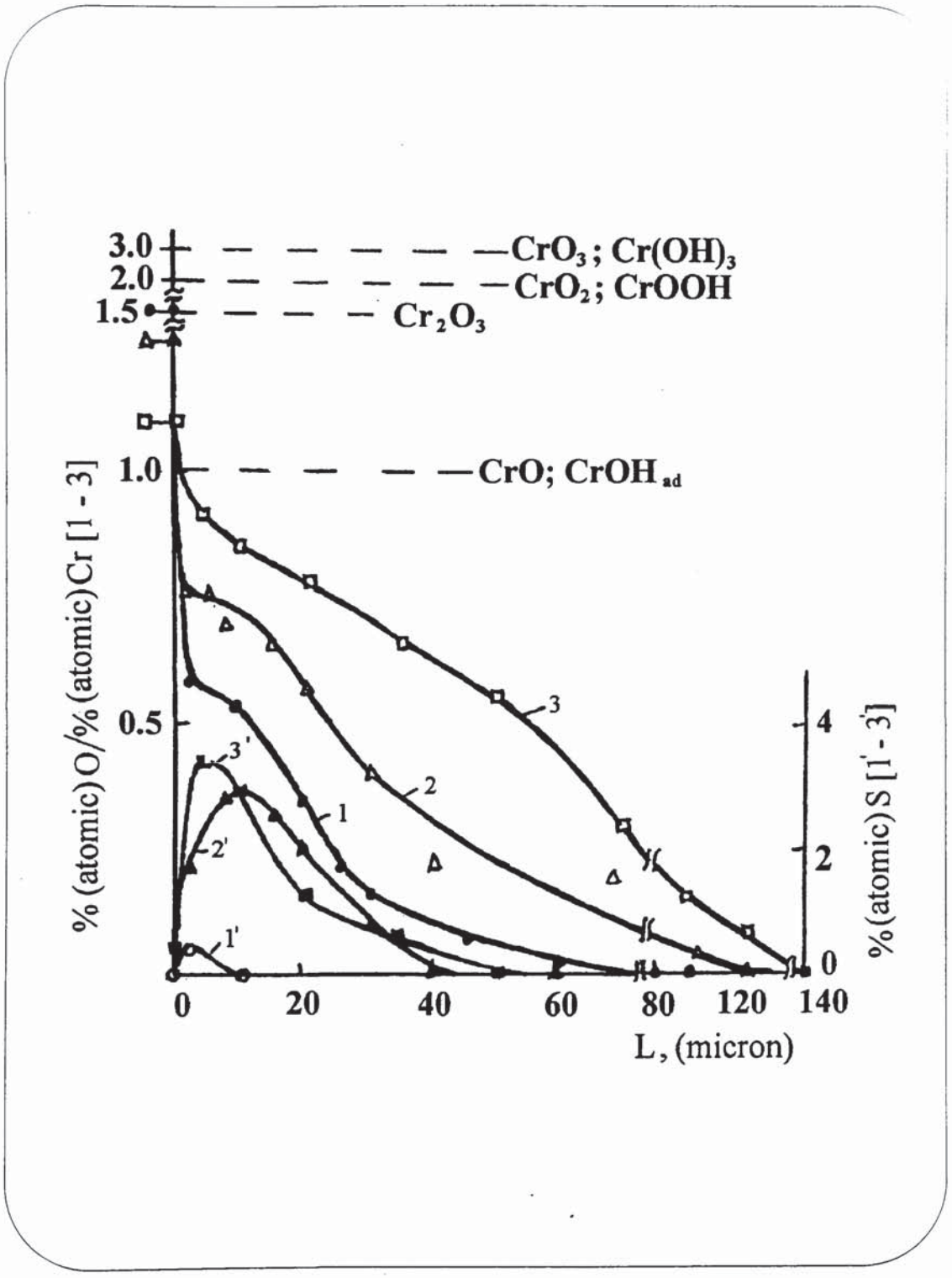

Figure 175. Change of oxygen and chromium atomic content ratio (1-3) and sulphur atomic content (1'-3') on oxide film depth of chromium electrodeposited at 50 Adm^{-2} 55^0 C, in SB before (1,1') and after (2, 2' ,3, 3') cathodic polarisation , between 0.00 V and -1.00 V, during the first (2, 2'), and the second cycles (3, 3') in the Sargent bath at 25^0 C. dE/dt = 0.100 V/s.

T (° C)	t_c / t_a (sec/sec)	E_c = -1.00 V i_c = - 0.05 Acm^{-2}	E_a = + 1.35 V i_a = 0.05 Acm^{-2}	E_c = - 0.90 V i_c = - 0.30 Acm^{-2}	E_a = + 1.47 V i_a = 0.30 Acm^{-2}	E_c = - 0.94 V i_c = - 0.50 Acm^{-2}	E_a = + 1.50 V i_c = 0.50 Acm^{-2}	E_c = - 1.02 V i_c = - 0.70 Acm^{-2}	E_a = + 1.53 V i_a = 0.70 Acm^{-2}
$i_{cr^{3+}}/i_d \cdot 100(\%)$									
40	300/5	5.60		2.06		0.89		0.77	
	120/2	5.30		2.02		0.88		0.63	
	60/1	5.30		-		-		-	
50	60/1	2.39		1.38		0.58		0.34	
55	300/5	4.50		1.60		0.47		0.30	
	120/2	1.94		0.39		0.37		0.28	
	60/1	0.14		0.22		0.17		0.11	

Table 53. Cr^{3+} fractions formed during polarization of Cr^0 in the SB under PRC mode; ω = 1400 rpm; E = + 1.85 V.

PART THREE

CONCLUSIONS AND RECOMMENDATIONS FOR FURTHER WORK

III.1 CONCLUSIONS.

a. General

Aqueous solutions of chromic acid (CrO_3) present an extremely complex system containing a mixture of chromates, bichromates and polychromates, in ratios that are depending on the CrO_3 concentration. In almost all previous research a gross simplification has been made in assumption that the chromium anion involved in chemical and electrochemical reactions is bichromate ion.

J. P. Hoare in his papers first recognised that the anion involved is actually the trichromate ion, which, due to its large size, considerably changes the overall picture of deposition mechanisms. Unfortunately, he retired from General Motors Research Laboratories soon after publishing his last paper in 1984, and his important contributions were left unfinished. His pivotal point on the presence of trichromate ions was not substantiated completely, and a number of researchers tended to ignore his proposed mechanism of chromium electrodeposition.

During this research it has been necessary to conduct a comprehensive literature search. Newer reference data were found which largely support Hoare's claim of the presence of trichromates in chromic acid solution of plating strength (1.5 - 2.5 M). Perhaps due to ambiguity of the chemistry involved, research on chromium deposition mechanisms attracted relatively few researchers in the Western scientific community.

Electrodeposition with Periodically Reversed Current (PRC), a relative newcomer in the electrodeposition field, offers a number of advantages and new opportunities for practising electroplaters. Alloys can be modulated with regard to the composition of alloying elements; bright deposit can be obtained without separate brightening additives, throwing power can be greatly improved and physical properties can be changed. Deposition rates can be increased due to the improvement of the crystallisation conditions of the metal being deposited for the processes where the charge transfer is a rate determining step; mass transport limitations/for processes under diffusion control can be reduced or eliminated. Electrocrystallisation conditions can be improved due to increased frequency of crystal nucleation with resulting decrease of crystals' growth rate, increasing of surface energy homogeneity and dissolution of dendrites or other surface imperfections by

anodic component of the current. For diffusion limited processes, practical current density can be increased due to the increase of the amplitude of the cathodic component of PRC current which can offset any reduction in total deposition rate due to anodic dissolution.

PRC permits anode activation in systems where passivation would occur with conventional DC since during the anodic cycle any oxide/hydroxide or insoluble salts present on the anodes can be dissolved and anodic current densities increased.

In the case of chromium, the PRC mode offers particular advantages. Physical properties can be modified by applying multilayered DC (hard, but porous) plus PRC (somewhat softer, but pore-free) composites with the combined effects of having hard top layer and a greatly improved corrosion resistance provided by the softer lower layer.

Inherent weaknesses of electroplated chromium such as poor throwing power and low current efficiency are definitely improved in PRC mode. Since every percentage of increase of current in efficiency translates directly in decrease in energy consumption and also in process time, benefits are obvious. However, the most important benefits come from ecological and health aspects. Increased efficiency reduces the amount of hydrogen bubbles that carry toxic chromic acid as a mist that has to be collected, scrubbed and exhausted.

b. New Contributions

1. The section on chemistry of chromium is a valuable contribution toward its better understanding. Complexity of reactions that are simultaneously proceeding in the cathode layer, formation of the chromium complexes in the various valence states, and presence and the role of two films that are present in the cathode layer are analysed. In Figure 7, the sequences of the whole cathodic process in all its complexity are presented for the first time in the form of a block diagram.

2. The theoretical aspects of PRC deposition, which are otherwise available in the literature only in the scattered fragments are presented in Section 1.3 in order to better understand rather complex mathematical treatments. Existing theory of K. I. Popov is expanded.

3. The development of high-efficiency catalysts confirmed that PRC mode increases efficiency, both in the case of standard Sargent type baths and in the case of baths catalysed with organic type or inorganic catalysts. All the experimental baths under development

presented in this thesis were used in a pilot six-litre small production tank with very satisfactory results including a number of successful production runs. This qualified them to be above the level of research curiosities.

4. Methane disulphonic acid was found to be superior to methane sulphonic acid due to the reduced rate of attack on lead anodes. The inorganic catalytic system - $KBrO_3/KIO_3$ mixture produced high efficiencies and sound deposits, particularly in PRC mode.

5. The governing parameter in PRC mode was confirmed to be the anodic/cathodic coulombic charge ratio, rather than the ratio of anodic to cathodic time periods. With optimum coulombic charge ratio the PRC mode produced efficiencies in the high 20% range.

6. Indium as a secondary catalyst produced no increase in efficiency but rather exceptionally smooth deposits, even in the presence of extraordinary high sulphate contents (13:1 ratio). It is unfortunate that the price of the indium is high and this disqualifies it as an ideal source for adjustment of sulphates in Sargent type baths rather than a conventional barium carbonate method. The latter produces barium sulphate sludge which always contains unwanted residual chromic acid that must be disposed of as toxic sludge.

7. Uranium salts of below hazardous radiation level produced very bright, almost brilliant coatings.

8. The deposition mechanism with all its complexity was studied in detail using time-controlled (linear and cyclic potential polarisation sweeps) and mass-controlled (rotating disc electrode) systems. The role of the sulphates in the formation of the complexes present in the cathode film are elaborated upon and suggestions on the possible reactions involved are offered.

9. The electrochemical kinetics of the reaction of incomplete $Cr^{6+} \rightarrow Cr^{3+}$ reduction is presented and clearly proved that it consists of diffusion and kinetically-controlled components.

10. Four different secondary catalysts were analysed and compared with Sargent bath under different potential sweep rates and cathode rotation speeds. Increase in current efficiencies for co-catalysed baths are obviously related to reduction of maximum current with sweep rates and rotation rates. Reducing of the rate of incomplete reduction $Cr^{6+} \rightarrow Cr^{3+}$ reaction produces an increase of the rate of the main, complete reduction reaction :

$Cr^{6+} \rightarrow Cr^{0}$ (deposition) which then dictates increase in cathodic current efficiency as well as energy efficiency for the overall deposition process.

11. Electrochemical kinetics of MSA and DMSA co-catalysed systems are analysed from the theoretical standpoint and compared with the Sargent bath for different CrO_3 concentrations, CrO_3/H_2SO_4 ratios and different temperatures.

12. Figure 116 clearly proves that chromic acid and sulphuric acid have opposite effects on the $Cr^{6+} \rightarrow Cr^{3+}$ reaction. While increase of H_2SO_4 content at constant CrO_3 concentration increases maximum rate, decrease of CrO_3 concentration at constant H_2SO_4 concentration increases the maximum current. This explains why there must be a compromise; the optimum chromic acid/sulphuric acid ratio is well known to be 100:1.

13. The important practical aspect - ability of plating bath co-catalysed with alkyl sulphonic acid to operate with maximum efficiency at higher temperatures - is also demonstrated in respect to maximum current.

14. Determination of electrochemical reaction order further corroborated the fact that the reaction $Cr^{6+} \rightarrow Cr^{3+}$ follows the mechanism involving the mixed kinetic control and that is limited by the diffusion step and addition of the first electron.

15. The study of hydrogen evolution reactions that are simultaneously proceeding on the chromium electrode revealed that MSA does not influence the hydrogen evolution reaction.

In connection with the previously established fact that MSA is also a weak catalyst for $Cr^{6+} \rightarrow Cr^{3+}$ reaction, it is concluded that the proven increase in cathode current efficiency must be due to MSA influence on the state and physicochemical properties of L-film and the reactions that are proceeding within the film.

16. Chromium dissolution reactions, similar to deposition reactions, are rather complex. The precise anodic dissolution efficiency was needed in order to calculate more precisely actual PRC efficiency and to help in understanding the PRC deposition mechanism.

17. Results from weight difference revealed that anodic current efficiency (ACE) is consistently higher than 100%, indicating the existence of other reactions in addition to $Cr^{0} \rightarrow Cr^{6+}$ dissolution reaction. Beside the slight influence of temperature, there is also the influence of anodic current density.

18. From gravimetric determination of ACE, it could be seen that additions of 5g/l MSA had no effect on the ACE of the Sargent bath. Unexpectedly , unlike deposition, Cr dissolves in uncatalised CrO_3 solution (103%). Quartz Crystal Microbalance results are in principle the most accurate and they gave ACE results of 108% for 55^0C bath at 35 Adm^{-2}

III.2 RECOMMENDATIONS FOR FUTURE WORK

The complexity of chromium chemistry and electrochemistry can keep many future researchers occupied. Due to the apparent practical significance, optimum thickness ratio of DC and PRC layers should be found in order to combine increased efficiency and corrosion protection when plating composites and still be in the bright range.

Due to the presence of three simultaneous electrochemical reactions and two cathodic films, standard electrochemistry should be coupled with one *in situ* analytical technique in order to study it's complexity in the most possible depth, particullarly the formation and influence of the liquid cathode film on all three reactions. Once these reactions are better understood, efforts can be concentrated to minimise unwanted reactions ($Cr^{6+} \rightarrow Cr^{3+}$ and $2H+ H_2$) and optimise $Cr^{6+} \rightarrow Cr^0$ reaction. Raman Laser Spectroscopy is almost a perfect answer. Some preliminary work done here and presented in the Appendix proved that this can be done without great obstacles. Liquid Ion Chromatography should be explored in order to separate and identify Cr^{6+} and Cr^{3+} complexes with sulphates. L-film should be separated from the cathode in order to be analysed using, e.g., freezing or drainage methods. Long range electrolysis of $KBrO_3/KIO_4$ mixture as secondary catalysts could be done in order to explore its stability and influence of reduction products, if any. Stable alkyl sulphonic and carboxylic acid could be found to be used as co-catalyst. Ethane hydroxy sulphonic acid results proved that 40% efficiency is obtainable if the catalyst is stable to oxidation.

Another area where there is dire need for more understanding is oscillatory behaviour of CrO_3 /H_2SO_4 system. Electrochemical oscillations recently attracted more attention in the studies of electropolishing systems where anodic reactions are proceeding through a thick anodic layer which is constantly forming and dissolving, even in the steady state. Since, in the case of chromium deposition, similar thick cathodic film exists, oscillations are observed (in a few older studies) during the initial period (1-3 seconds) before the steady state is reached. Current and potential transient step techniques could give us more insight into the mechanism of formation and the role of liquid cathodic film formation and thus better control over partial reduction reaction $Cr^{6+} \rightarrow Cr^{3+}$ and complete reduction reaction $Cr^{6+} \rightarrow Cr^0$ which, in turn, are responsible for overall current efficiency.

PART FOUR

LIST OF REFERENCES

IV. LIST OF REFERENCES

1. W. Mertz and K. Schwartz, *Arch. Biochem. Biophys.* **58,** (1995), 504.
2. Cotton and Wilkinson, "Advanced Inorganic Chemistry.", Interscience. NY., 3rd.ed., 1963.
3. J. Koppel, *Z. Anorg. u. Allgem. Chem.* **45,** (1905), 359.
4. F. Hein and S. Herzog in "Handbook of Preparative Inorganic Chemistry", Vol. 2, Academic Press, N.Y. 2nd. addition (1965), pp. 1361-1370.
5. *Inorganic Synthesis*, McGraw-Hill, N.Y., Vol 10, (1967), p 26.
6. P. Leisner, G. Bench-Nielson ,P. Moller, *J. Appl. Electrochem.***23**, (12), (1993) 1232.
7. N.V. Mandich and N. V. Vyazovikina, to be published.
8. M. Okuyama, M. Kawasaki and K. Ito, *Electrochim. Acta*, **30**, (1985), 757.
9. M. S. El-Basiouny and S. Haruyama, *Corros. Sci.*, **17**, (1977), 405.
10. A. Cotton and Wilkinson, "Advanced Inorganic Chemistry", 5th. ed., J. Willey & Sons, Inc., N.Y., (1985), pp. 679-697.
11. "Kirk-Othmer Encyclopedia of Chem.Technology", 4 ed., Willey, N.Y., V. 6, p.267.
12. F. Basolo and R. G. Pearson, "Mechanisms of Inorganic Reactions", J. Wiley & Sons, N.Y., (1967), pp. 141-145.
13. L. Spicia, H. Stoeckli-Evans, H. Marty R. Giovanoli., *Inorg.Chem.*, **26**, (1987), 474.
14. L. Spicia and W. Marty, ibid **25**, (1986), 266.
15. D. Rai, et al., *Inorg. Chem.*, **26**, (1987), 474.
16. D.E. Pennington and A. Haim, *Inorg. Chem.*, **5**, (1966), 1887.
17. M.R. el-Sharif, S. Ma, C.U.Chisholm, *Trans. Inst. Met. Finish.*, **73**, (1), (1995), 19.
18. M.R. el-Sharif, A. Watson, C.U.Chisholm, *Trans. Inst. Met. Finish.*, **66**, (1988), 34.
19. A. Smith, A. Watson, D. Waughan, *Trans. Inst. Met. Finish..*, **71**, (3), (1993), 106.
20. M.R. el-Sharif, S. Ma, C.U.Chisholm and A. Watson, SUR/FIN 95, Baltimore, Md. (1995)
21. J.C. Blair: "Comprehensiuve Inorganic Chemestry", Vol.3, Pergamon Press, (1970).
22. J.E. Earley and R.D. Cannon, "Aqueous Chemistry of Chromium(III)" in *Transition Metal Chemistry,* **1**, Marcel Dekker, N.Y., (1966), p. 64.
23. H. Stunzi, L. Spicia, F. P. Rotzinger and W. Marty, *Inorg. Chem.*, **28**, (1989), 66.
24. E. Serfas, E. Theis, T. Thovensen, *J. Amer. Leather Chem. Assoc.*, **43**, (1948), 132
25. E. Serfas, G. Wilson and E. Thesis, *J. Amer. Leather Chem. Assoc.*, **44**, (1949), 647.

26. J. W. Mellor, "A Comprehensive Treatise on Inorganic and Theoretical Chemistry," Vol. II, Longmans, London, (1931).
27. W. Smith, K. Pitzer and W. Lather, *J.Amer.Chem. Soc.*, **50**, (1937), 2642.
28. M. Shriai and Y. Matsumoto, *J. Chem. Educ.*, **54**, (10), (1971), 609.
29. G. Michel and R. Cahay, *J. Raman Spectroscopy*, **17**, (1986), 76.
30. M. J. Udy,"Chromium", Vol.1, Reinhold Publ. Co., N.Y., (1956).
31. G. Michel and R. Machiroux, *J. Raman Spectroscopy*, **14**, (1983), 22.
32. T. Radnai and C. Dorgai, *Electrochim. Acta*, **37**, (7), (1992), 1239.
33. J. S. Stephens and D. W. J. Cruickshank, *Acta Crystall.*, Ser. B **626**, (1970), 222.
34. A. Martins and G. Carpeni, *J. Chim. Phys.*, **60**, (1963), 534.
35. J. P. Hoare, *Plat. Surf. Finish.*, **76**, (9), (1989); *J. Electrochem. Soc.* **126**, (2), (1979), 190.
36 J. P. Hoare and M. A. La Boda, *J. Electrochem. Soc.*, **132**, (4), (1985, 798.
37. J.-L. Fang, N.-J. Wu, Z.-W. Wang, *J. Appl. Electrochem.*, **23**, (5), (1993), 495.
38. A. Radwan, A. El-Kiar, H. Farag, G. Sedahmed, *J. Appl. Electrochem.*, **22**, (12), (1922), 1161.
39. D. Landolt, R. Acosta, R. H. Mullar, C. W. Tobias, *J. Electrochem. Soc.*, **117**, (1970), 839.
40. H. Voght, *Electrochem. Acta.*, **32** (1987), 633.
41. T. C. Saiddington, G. R. Hoey, *J. Electrochem. Soc.*, **120**, (1973), 1475.
42. V. Guro, M. Schluger, O. Khodzhaev and Sh. Ganiev, *Elekrokhimiya*, **30**, (2), (1994), 251.
43. Z. A. Soloveva, Yu. V. Kondashov and S. V. Vashchenko, *Elekrokhimiya*, **30**. (2) (1994), 228.
44. K. Yosida, A. Suzuki, K. Doi, K. Arai, *Kinzoku Hyomen Gijutsu*, **30**, (1979), 338.
45. H. Kimura and T. Hayashi, *Denki Kagaku*, **37**, (1969), 5.
46. M. Nagayama and T. Izumitani, *Kinzoku Hyomen Gijutsu*, **21**, (1970), 505.
47. J. Levitan, *J. Electrochem. Soc.*, **111**, (3) , (1964), 286.
48. H. Okada, *Kinzoku Hyomen Gijutsu*, **11**, (1960), 623; *Kinzoku Kagaku* **4**, (1967), 1
49. K. Yoshida, Y. Tsukahara, and K. Koyama, *Kinzoku Hyomen Gijutsu,* **30**, (9), (1979), 457.
50. K. Nichicara, R. Kurachi, H, Nishi and K. Tabata, ibid, **39**, (3), (1988), 203.

51. G. W. Jernstedt, *Steel and Metal Finish.*, **20**, (1947), 100.
52. G. W. Jernstedt, *Steel Processing*, **33**, (1947), 479 and 498.
53. G. W. Jernstedt, *Plating*, **35**, (7), (1948), 708.
54. G. W. Jernstedt, *Westinghouse Engineer*, **7**, (1947), 89.
55. G. W. Jernstedt, *U. S. Patent 2.47,755, (1949),* 2.245,340 (1948), 2.636,850 (1953).
56. H. H. Wan, R.-Y. Chang, W.-L. Yang, *J. Electrochem. Soc.*, **140**, (5), (1993), 1380.
57. J. Wang, D. Balamurugan, D.-T. Chin, *J. Applied. Electrochem.*, **22**,(3), (1992), 290.
58. K.-M. Jeong, C.-K. Lee, H.-J. Sohn, *J. Electrochem. Soc.*, **139,** (7), (1992), 1927.
59. T. Pearson, J. K. Dennis, *J. Applied Electrochem.*, **20**, (2), (1990), 196.
60. T. Pearson, J.K. Denis, J. Houlsaton and M. Dorey, *Trans. Inst. Met. Finish.*, **69**, (1), (1991), 9.
61. S. Kruglikov,T.Yurchuk, A.Fedotova, *Electroplat.Surface Treat.*,**1**, (3-4) (1992) 60.
62. C. Kollia, F. Kotzia, N. Spyrellis, *Electrodep. Surf. Treat.*, **1**, (5-6), (1992), 23.
63. C. Kollia and N. Spyrellis, *Surf. Coat. Techn.*, **58,** (2), (1993), 101.
64. R.S. Safulin, I. Valeeve and I. Adbulin, *Zasht. Metallov,* **18,** (2), (1982), 300.
65. I. Valeeve,, I. Adbulin , R. S. Safulin, and A. Liberman, ibid.,**17,** (5), (1981), 603.
66. W. Kim, R. Weil, *Surf. Coat. Techn.*, **31**, (1987), 143.
67. T.P. Sun, C.C. Wan and Y.M. Shy, *Met. Finish,* **76**, (5), (1970), 33.
68. F. Kotzia, C. Kollia and S. Spyrellis, *Trans. Inst. Met. Finish.*, **71**, (1), (1993), 34.
69. G. Heilman, *U. S. Patent* 3.586.6
70. V. A. Knamaev, *Zashchtita Metallov, 17*, (3), (1981), 365.
71. L. Sjogren, B. Asthner, L. Liljestrand, L. B. Revay. *Plat.Surf. Finish.*, **73**, (3), (1986), 70.
72. P. Leisner, G. Bech-Nielson, P. Moller, *J. Appl. Electrochem.*, **23**, (1993), 1232.
73. P. Leisner, D. Ulrich, P. Moller, *Plat. Surf. Finish.*, **79**, (7), (1993), 1232.
74. W. Clauberg, *Metalloberflache*, 43, (1989), 9.
75. M. Sutter, *Surfaces*, 24, (5), (1985), 174.
76. Y. P. Lin, J. E. Selman, *J. Electrochem. Soc.*, 138, (1991), 3525.
77. W. H. Safranek, H. R. Miller, *U. S. Patent* 3,005,759 (10/24/1961).
78. A. Cohen, *German Patent No. 75,482*, (1893).
79. P. Baeyens, *Trans. Inst. Met. Finish.*, **31**, (1954), 429.
80. A. Hickling, H. P. Rothbaum, *Trans. Inst. Met. Finish.*, **34**, (1957), 53.

81. J. W. Dini, *Met. Finish.*, **51**, (6), (1963), 52.

82. H. Y. Cheh, *J. Electrochem. Soc.*, **118**, (7), (1971), 1132.

83. H. Y. Cheh, *J. Electrochem. Soc.*, **118**, (4), (1971), 551.

84. A. M. Pesco, H. Y. Cheh, *J. Electrochem. Soc.*, **136**, (2), (1989), 408.

85. T. R. Rosenbrugh, W. J. Miller, *J. Phys. Chem.*, **14**, (1910), 816.

86. K. J. Vetter, "Electrochemical Kinetics". Academic Press, NY, (1967).

87. D. T. Chin, *J. Electrochem. Soc.*, **130**, (1983), 1651.

88. K. I. Popov, M. D. Maksimovic, M. S. Simic, *Surf. Technol.*, **16**, (1982), 209.

89. K. I. Popov, M. D. Maksimovic, M. S. Simic, *Surf. Technol.*, **17**, (1982), 125.

90. K. Viswanathan, H. Y. Chech, *J. Electrochem. Soc.*, **126**, (1979), 398.

91. P. Leisner, G. Bech-Neilsen, P. Moller, "Scandinavian Pulse Plating Symposium", Lyngby, Denmark (Feb.1992).

92. K. I. Popov, D. C. Totovski, M. D. Maksimovic, *Surf. Technol.*, **19**, (1983), 181.

93. V. Chernenko, A. Rysakov, Z. Preistkaya, *Elektrokhimiya*. **4**, (5), (1968), 519.

94. L. Domnikov, *Met. Finish.*, **59**, (4), (1969), 59.

95 J. Mann, *Trans. Inst. Met. Finish*, **56**, (2), (1978), 70.

96. H. L. Pinkerton and J. W. Smith, *Plating*, **59**, (7), (1972), 672.

97. M. I. Ismail, *J. Appl. Electrochem*, **9**, (1979), 407.

98. R. L. Zeller and U. Landau, *Plat. Surf. Finish*, **78**, (12), (1991), 59.

99. M. B. Hammond and G. B. Bowman, *U. S. Patent.* 2. 989.446, (1961).

100. D. Grimmelt, M. Schwartz, K. Nobe, *J. Electrochem. Soc.* **140**, (4), (1993), 973.

101. B. N. Popov, K.-M. Yin, R. E. White, *J. Electrochem. Soc.*, **140**, (5), (1993), 1321.

102. K. Popov, B.A. Mitrovic, M.G. Pavlovic and B.V.Toperic, *J. Appl. Electrochem.*. **20**, (1), (1990), 50.

103. R. Audubert, *French Patent No. 932,039*, (1948).

104. A. Y. Rykova, "Isslodovaiye korrozii metallov pod papryazheniyem", (from Collection: Study of Corrosion of Metals Under Stress). State Scientific and Technical Publishing House of Literature on Machinery, 1953, (Russian).

105. L. Ya. Bogorad. "Chromium Plating with Periodic Change of the Current Direction," in *Tekhnologiya transpornogo mashinostroyeniya.*, **2**, (1957), 32, (Russian).

106. A. V. Pamfilov, A. I. Lopushanskaya, B. A. Gru., *Ukr. Khim. Zhurn.* (Ukrainian Chem. J.), **26**, (1), (1960), 31, (Russian).

107. M. A. Shluger, N. M. Kazakov, in "Protective Metallic Coatings and Corrosion of Metals." Publisher: Akad. Nauk SSSR, Leningrad, (1965). (Russian).

108. N. Maslov, *D. Sc. Dissertation*, Moscow State Univ., 1960, as cited in reference 98.

109. M. V. Filin, as cited in reference 110.

110 G. T. Bakhvalov, "Novaya Teknologiya Electrozdeniya: Reversirovanite Toka V Galvanostegi", Metallyrgiya Publishing House, Moscow, (1966), p 93. (Russian).

111. P. I. Kryzhanovskiy, "Electrolytic Depositioin of Chromium under the Action of an Alternating Current with a Varying Ratio of the Cathode and Anode Components," *Collection of Scientific Works of the Krivoy Rog Mining Institute*, **10**, (1971).

112. M. A. Shluger, *Vestnik Mashinostroenia*, **5**, 1954. (Russian).

113. N.Golubov, A. Golubova, *Technol. Organ. Proizv.*, **13,** (2) (1972) 66, (Russian).

114. N. T. Vagramyan, *Izv. Akad. Nauk Arm. SSR*, **6,** (6), (1963), 54, (Russian).

115. C. Colombini, "Use of Pulse Rectifiers in Hard Chromium Plating," 2nd Pulse Plating Symposium, AESF, Chicago, (1981).

116. B. Sutter, J. Reby, G. Vasseur, *Cetim Information*,# **99**, (Fevrier 1987); also, M. Sutter, *Surfaces*, **24**, (May 1985), 174.

117. C. Colombini, *Galvanotechnik,* **7a**, (1988), 2869..

118. B. Petrovic, P. Jovanovic, M. Stojanovic, "Lectures at the Seminar Sponsored by European Academy for Surface Technology", Belgrade, Serbia, 1992, (ISBN 86-82151-01-4).

119. R. Kirshnan, S. Criveeraraghvan, S. Natarajan, *Met. Finish.*, **91,** (10), (1993), 65.

120. H. R. Carveth, B. E. Curry, *J. Phys. Chem.*, **9**, (1905), 23.

121. M. A. Mitskus and D. I. Sklenikaite in "Electrodeposition of Metals", (Proceedings of 10th Lithuanian Conference of Electrochemists, held on 12-13 Dec. 1968). Translated from Russian by Israel Program for Scientific Translations, Jerusalem, 1970, p. 65.

122. R. H. Roberts, W. J. Shutt, *Trans. Faraday Soc.,* **34**, (1938), 1455.

123. Th. Heumann, F. W. Diekotter, *Z. Elekrochem.*, **62**, (1958), 745.

124. Th. Heumann, H. S. Panesaer, *J. Electrochem Soc.,* **110,** (6), (1963), 628.

125. M. S. El-Basicony, S. Horuyama, *Corr. Sci.,* **17**, (1977), 405.

126. M. B. Cherkez in "Theory and Practice of Chromium Electroplating," Publisher: Akademia Nauk SSSR, Moskva, (1957), p. 122.

127. M. A. Shluger, *Ibid.*, p. 101-121.

128. E. Deltombe, N. de Zoubov, M. Pourbaix in "Atlas of Electrochemical Equilibria in Aqueous Solution", M. Pourbaix, editor, NACE, Houston, TX (1974).

129. T. Hurlen, S. Hornkjol, E. Guldbransen, *Electrochim. Acta.*, **38**, (5), (1993), 643.

130. N. Vyazovikina, V. Kamushenko and Krapivka, *Russ. J. Electrochem.*, **30**, (8), (1994), 1039.

131. W. Lou and K. Ogura, *Electrochim. Acta*, **40**, (1995) 667.

132. M. Seo, R. Furuichi, G. Okamoto, N. Sato, *Inst. Met. Trans. Jpn.* **16**, (1975), 519.

133. N V Mandich and N. V. Vyazovikina, to be published.

134. K. Kanazawa and J. G. Gordon, *Anal. Chem.*, **57**, (1985), 1770.

135. T. Nomura, O. Hattori, *Anal.Chem. Acta.*, **115**, 323, (1980); **124**, (1981), 81; **131**, (1991), 131.

136. P. L. Komash and G. J. Bastians, *Anal. Chem.*, **52**, 1929, (1980).

137. S. Bruckenstein and Shay "1983 Abstracts" , 1983 Pittsburg Conference and Exposition, Atlantic City, New Jersey, (March 1983).

138. R. J. Byrne, P. Lloyd and W. J. Spencer, *J. Acoust. Soc. Am.*, **43**, 232, (1968).

139 G. Z. Sauberey, *Physic Verhandl.* **8**, 113, (1957); *Z. Phys.*, **155**, (1959). 206.

140. S. W. Wenzel, and R. M. White, *Appl. Phys. Lett.*, **54**, 1976, (1989).

141 C. Lu, in "Applications of Piezoelectric Quartz Microbalances", Elsevier, Amsterdam, (Editors: E. Lu and A.W. Czandema), (1984).

142. J Weng: "Analytical Electrochemistry.", VCH Publishers (1994).

143. A. Weissberger and B. Rossiter, "Physical Methods in Chemistry," Volume I, part II-a Willey-Interscience, New York, (1971).

144. P.T. Kissinger and W. R. Heineman , "Laboratory Techniques in Electroanalytical Chemistry, Marcel Deckker, NY, (1996).

145. P. A. Christensen and A. Hamnet, "Techniques and Mechanisms in Electrochemistry", Blackie Academic, NY (1994).

146. E. Gileadi, "Electrode Kinetics" VCH Publishers (1993).

147. R. N. Adams, "Electrochemistry of Solid Electrodes", Chap.4, Dekker; N. Y, (1960).

148. V. Levich, "Physicochemical Hydrodynamics", Prentice-Hall;Englewood Clifts., NJ, (1962).

149. V. Levich, *Acta Physicochim. USSR.* ,**17**, (1942), 257-307, **19**, (1944), 117-132, 133-138.

150. V. Levich, *Zh. Fiz. Khim.*,**18**, (1944), 335-355; **22**, (1948), 570-585, 711-729.

151. A.C. Riddiford, "Advan. Electrochem. Electrochem. *Eng".*, **4**, (1966), 46-116.

152. Bard and Faulkner. "Electrochemical Methods", Wiley; NY, (1980), Ch..8, p. 283.

153. Y. Pleskov and V. Filinovski: "The Rotating Disc Electrode". Consultants Bureau, N.Y. (1976).

154. C. Bret and A. Bret, "Electrochemistry: Principles, Methods and Applications." Oxford Univ. Press, Oxford (1993).

155 W. J. Albery, M. L. Hitchman, "Ring-Disc Electrodes": Clarendon, Oxford, (1971).

156. J. A. Abys. "Proceedings from Second AES Symp. on Economic Use of and Substitution for Precious Metals in the Electronics Industry", Danvers, MA (Oct. 5-6, 1982).

157. D. Tench, C. Ogden, *J. Electrochem. Soc.,* **125,** (2), (1978), 194.

158. D. Tench, C. Ogden, *J. Electrochem. Soc.,* **125,** (2), (1978), 1218.

159. C. Ogden, D. Tench, *Plat. Surf. Finish.,* **66**, (9), (1979), 30.

160. R. Haak, C. Ogden, D. Tench, *Plat. Surf. Finish.,* **69,** (4), (1981), 52.

161. R. Haak, C. Ogden, D. Tench, *Plat. Surf. Finish.*, **70,** (4), (1981), 55.

162. M. Paunovic, R. Arndt, *J. Electrochem. Soc.*, **130,** (4), (1983), 334.

163. J. Horkans, *J. Electrochem. Soc.*, **130,** (1), (1980), 311.

164. Yu-Po Lyn, J.R. Selman, *J. Electrochem. Soc.*, **140,** (5), (1993), 1299.

165. T. Mimani, S. Mayanna, N. Munichadraian, *J. Appl. Electrochem*, **23** (1993), 334.

166 E. Vales, R. Pollina, E. Gomes, *J. Appl. Electrochem.*, **23**, (5), (1993), 508.

167. R. Berlazzoli, D. Pletcher, *Electrochim. Acta*, **38**, (5), (1993), 1673.

168. R. Crousier, I. Bimaghra, *J. Appl. Electrochem.*, **23**, (8), (1993), 775.

169. M. McCormick and S, J. Dobson, *J. Appl. Electrochem.*, **17**, (1987), 303.

170. J. P. Hoare, *J. Electrochem. Soc.*, **130,** (7), (1983), 1476.

171. J. Lin Cai, and D. Pletcher, *J. Appl. Electrochem.,* **13**, (1983), 235.

171-a J. Lin Cai, and D. Pletcher, *J. Appl. Electrochem.,* **13**, (1983), 245.

172. J. P. Hoare, "Proceedings of 71st. AESF Annual Conference", N.Y. (1984).

173. M. McCormick, M.A. Pate, D. Howe, *Trans. Inst. Metal Finish,* **63**, (1) (1985) ,34.

174. B. Popov, R. White, D. Slavkov, Z. Koneska, *J. Electrochem Soc.,* **139**, (1), (1992).

175. F. K. Sautter, *J. Electrochem.* Soc., **110**, (6), (1963), 557.

176. R. V. Willams, P. W. Martin, *Trans. Inst. Metal Finish.*, **42**, (1964), 182.

177. J. P. Joung, Research Directorate, Weapons Laboratory Rock Island Arsenal, Ill. Report NB SIR 74-615, (1994).

178. J. P. Joung,, *Plat. Surf. Finish.*, **62**, (4), (1975), 348,

179. L. H. Wagner, R. P. Erikson, *NTIS* publication AAD No. 74-14103 W.

180. C. A. Adison, E. C. Kedward, *Trans. Inst. Metal Finish,* **55**, (2), (1977), 41.

181. R. Narayan and S. Singh, *Met. Finish.*, **89**, (3), (1983), 45.

182. R. Narayan and B. H. Narayana, *J. Electrochem. Soc.* ***128***, (8), (1981), 1704.

183. G. R. Kamat, *Plat. Surf. Finish.*, **66**, (6), (1979), 56.

184. O. Berkh, S. Eskin and J. Zahavi, *Plat. Surf. Finish.*, **81**, (3), (1994), 62.

185. R. Saifulin and R. Khalilova, *Electrokhimiya.*, **43**, (6), (1970), 63.

186. R. Bazzard and R. Boden, *Trans. Inst. Metal Finish.*, **50**, (2), (1972), 63.

187. N. Guglielmi, *J. Electrochem. Soc.*, **119**, (8), (1972), 1009.

188. A. Kariaaper and J. Forester, *Trans. Inst. Met. Finish.*, **52**, (1974), 87.

189. J. L. Valdes and H. Y. Cheh, *J. Electrochem. Soc.*, **134**, (7) , (1987), 223.

190 Y. Takaya, K. Terashima, T. Yinegishi and Y. Yatsunaga, *Kinzoky Hyomen Gijutsy*, **38,** (5), (1987), 185.

191. Y. Takaya, M. Matsunaga n and T. Otaka, *Plat. Surf. Finish.*, **74**, (10), (1987), 70.

192. S. V. Vashenko, Z. A. Soloveva, *Electrodep. Surf. Treat.*, **4**, (1994), 45 (Russian).

193. H. Chessin and K. Newby, *U.S. Patent* 4. 588,481, (1986).

194. K. Newby, *U.S.Patent* 5.176,813 (1/5/1993).

195. M.J.Law and H. Jones, *U.S. Patent, 3. 713,999,* (1973).

196. J. P. Hoare, "Proceedings of 71st. AESF Annual Conference", Indianapolis, (1983).

196-a. M. Constantin, E. Gruenwald, C. Varhely, *Galvanotechnik*, **82**, (11), (1991), 3819.

197. F. Aoun , *U.S. Patent* 3,654.101. (1972).

197-a. H. Chessin *U.S. Patent*, 4,472.249, (1984).

198. H. Dillenberg, *U.S. Patent* 4. 093,552, (1978).

199. W. Roggendorf, *U.S. Patent,* 3. 418,220, (1968).

200. W.W. Scott, A. A. Birsiri, W.G. Gregory, *U.S. Patent,*1. 9936,186, (1935).

201. H. Fry, *British Patent* 798,950, (1958).

202. A.T. Vagramyan, M.A. Zhamagortsyants, "Electrodeposition of Metals and Inhibiting Adsorption", Translated from Russian by U.S. Dept. of Commerce, 1969. (TT 72-51030).

203. W.H. Safranek and R.W. Hardy, *Plating*, **47**, (9), (1960), 1027.

204. A. Davidson and Y.N. Sadana, *Plating*, **58**, (10), (1971), 1007.

205. R. Wolker and S. Duncan, *Metal Finish,* **80,** (11), (1982), 59.

206. B. Lovrecek and V. Markovac, *J. Electrochem. Soc.*, **109**, (8), (1962), 727.

207. B. Lovrecek and V. Markovac, *J. Electrochem. Soc.*, **112,** (5), (1965), 520.

208. S. A. Levitskaya, *Izv. Vyssh. Ocheb. Zaved. Khim. Khim. Tekhol.*, **19**, (1968), 1971.

209. L. Pospisil and R. DeLevie, *J. Electrochem. Soc.*, **25,** ( ) (1970), 245.

210. V.V. Lovse and A.I. Molodov, *Dokl. Akad. Nauk SSSR*, **130,** (1963), 111.

211. V.V. Lovse and A.I. Molodov, *Itogi Nauki, 8,(1972), 25.*

212 J. Gabriel, *Galvanotechnik*, **58**, (11), (1967), 802.

213. M. Shluger and A.N. Kabina, *Electrodep. Surf. Treat.* **3** (4) (1994), 11, (Russian).

214. M. Kasaaian and J. Dash, *Plat. Surf. Finish.*,**71**, (11), (1984), 66.

215. S. Hoshino, H. Laitinen and G. Hoflund, *J. Electrochem. Soc.*, **33**, (4), (1986), 681.

216. R-Y. Tsai and S-T. Wu, *ibid*, **137**, (10), (1990), 3057.

217. S. V. Vashenko and Z. A. Soloveva, *Russian J. Electrochem.*, **30**, (2), (1994), 220.

218. V. Formichev, E. Moskvicheva and A. Ozerov, *Zasht. Metall.*, **12**, (1), (1982), 133.

219. W. Korbach and W. Mc. Mullen, *U.S. Patent* 4.828,656 (5/3/1989).

220. H. Chessin and M. Best, *U.S.Patent* 3.758,390, (9/11/1973).

221. R. M. Woodsand and D. Moul, *U.S. Patent* 3.418,221 (12/24/1968).

222. J. Gabriel, *Galvano*, **35**, (1967), 901.

223. J. Doskar and J. Gabriel, *Met. Finish.*, **65**, (3), (1967), 71.

224. S. Hoshino, S. Nazkada and G. Hoflund, Proceedings of AESF 80th. Technical Conference, SUR/FIN 93, (Anahaim, Cal.ifornia, (1993).

225. M. A. Shluger, *Zhurnal Priklandnoi Khimii*, **33** (6) (1960), 1355.

226. Z. A. Soloveva and A.T. Vagramyan., *Zh. Fiz. Khimii,* **36** (1962) 152.

227. D. Reinkowski and C. A. Knorr, *Z. Elektrochem.* **58** (9) (1954) 709.

228. H. Gerisher and M. Kappel, *ibid*, **61** (4) (1957) 463.

229. H. Kimura, T. Hayashi, *Denki Kagaku*, **39** (11) (19761) 892.

230. N. D. Ivanov, *Elektrokhimiya,* **8** (7) (1972) 1041.

231 J. J. Lingane and I. M. Kolthoff, *J. Amer. Chem. Soc.* **62,** (1940) 852.

232. A. Pamfilov and A. Lopushanskaya, *Ukrain. Khim. Zh.* **22,** (1956) 578.

233. G. Shteinberg and V. Bagotski, *Dokl. AN SSSR,* **115,** (3) (1957) 568.

234. M. Mitskus and Y. Matulis, *Trudy AN LitSSR, Ser.* B, **3,** (30) (1962) 31.

235. Z. Soloveva and A. M. Lapshina, *Elekrokhimiya*, **2,** (7) (1966) 767.

236. H. Feigl and C. A. Knorr, *Z. Elekrokhem.*, **63,** (2) (1956).

237. M. Frey and C. A. Knorr, *Z. Elekrokhem.*, **60,** (9/10) (1956) 1093.

238. G. Gabrielson, *Met. Finish.* **53,** (5) (1955) 56.

239. S. Senderoff , *Met. Finish.* **48,** (9) (1950) 71.

240. S. Shuttleworth, *J. Soc. Leather Trade Chemists*, **38,** (1954) 58.

241. Y. Matulis and M. Mitskus, *Trudy AN LitSSR, ser.B*, **3,** (1) (1958) 39.

242 A.T. Vagramyan and D. Usachev, *Zh. Fiz. Khimii*, **32,** (8) (1958) 1908.

243. H. Gerischer and M. Kappel, *Z. Electrochem.,* **64,** (1960) 235.

244. T. Dickinson, A. Powey and P. Sherwood, *J. Chem. Soc. Farad. Trans.*, **72,** (1976) 686.

245. Z. A. Soloveva and Yu. S. Petrova, *Zhurnal Prikaldnoi Khimii*, **34**, (8) (1961), 1752.

246. U. Adziev and Z. A. Soloveva, *Dokl. Nauk SSSR*, **273**, (1983), 116.

247. L. Solodkova, Y. Makarychev, Z. A. Soloveva, *Elekrokhimiya*, **24**, (6), (1988), 116.

248. J. O'. M Bockris and A. Ready, "Modern Electrochemistry", Plenum , NY.(1977).

249, E. A. Efimov, *Electrodep. Surf. Treat.*, (Russian), **3**, (4) (1994) 14.

250. E. A. Efimov and L.D. Tok, *Elekrokhimiya*, **27**, (1), (1991), 161.

251. E. A. Efimov, L.D. Tok and T. Tverdina, *Elekrokhimiya*, **25,** (10), (1988), 1398.

252. F.I. Danilov and M. N. Ben-Ali, *Elekrokhimiya*, **24**, (4), (1988), 438.

PART FIVE

APPENDIX

V.1 LIST OF SYMBOLS

Symbol	Description	Dimension
A	Atomic mass	g/mol
A	Surface area; electrode area	dm^2, ft^2
b	Tafel slope	V
c, C	Concentration	mol/l
c_{ad}	Surface concentration of adatom/adion	mol/dm
c_e	Concentration at the electrode	mol/l
c_o	Bulk concentration	mol/l
C	Coulombs	A •sec
CE	Current efficiency	%
D	Difussion coefficient	cm^2/s
E	Electrode potential vs. nhe	V
f	Frequency	Hz
F	Faraday's number, 96500	C/mol
HV	Vickers hardness	kg/mm
i, j	Current density	A/dm
i_a	Anodic current density in PRC	A/dm^2
i_c	Cathodic current density in PRC	A/dm^2
i_{dc}	Current density in DC	A/dm^2
i_j	Limiting current density in DC	A/dm^2
i_{ave}	Average current density	A/dm^2
$i_{l,ave}$	Average limiting current density	A/dm^2
i_p	Pulse current density	A/dm^2
$i_{p,l}$	Limiting pulse current density	A/dm^2
I	Electric current	A
K	Specific conductivity of electrolyte	Ω/m
m	Mass	kg; gr
M	Molecular mass	g/mol
n	Number of electrons transferred per metal ion	egv./mol
z	Number of electrons transferred per metal ion	egv./mol
q	Charge density	C/dm^2
q_a	Charge density in anodic period in PRC	C/dm^2
q_c	Charge density in cathodic period in PRC	C/dm^2
Q	Electric charge	C
Q_a	Charge of the anodic period in PRC	C
Q_c	Charge of the cathodic period in PRC	C
R	Gas constant, 8.314	J/(mol K)
R_c	Crystallisation resistance	Ω
R_d	Diffusion resistance	Ω
R_e	Omic resistance of the electrolyte	Ω
R_p	Polarisation resistance	Ω
R_r	Reaction resistance	Ω
R_t	Charge-transfer resistance	Ω

Symbol	Description	Dimension
t	Temperature	°C
t	Time	s
T	Absolute temperature	° K
T	Cycle time in PC ($t_{on} + t_{off}$)	s (ms)
T	Cycle time in PRC ($t_a + t_c$)	s
t_a	Anodic pulse time in PRC	s
t_c	Cathodic pulse time in PRC	s
T_{off}	Off-time in PC	s
T_{on}	Pulse time in PC	s
TP	Throwing power	%
Wa	Wagner number	-
T	Duty cycle	-

θ	Duty cycle	-
δ	Thickness of diffusion layer	cm
δ_n	Thickness of the Nernst diffusion layer	cm
δ_s	Thickness of the stationary diffusion layer	cm
η	Overvoltage	V
η_c	Crystallisation overvoltage	V
η_{con}	Concentration overvoltage	V
η_d	Diffusion overvoltage	V
$\eta_{m,ave}$	Average overvoltage	V
η_r	Reaction overvoltage	V
η_t	Charge-transfer overvoltage	V
θ_1, θ_a	Anodic pulse time	s (ms)
θ_2, θ_c	Cathodic pulse time	s (ms)
ν	Kinematic viscosity of fluid	cm^2/s
ν	Scan rate	mV/s
γ	Hydrodynamic boundary layer	cm
ω	Rotation speed	s^{-1} (rpm)
ω	Angular velocity	s^{-1}
α	Transfer coefficient	-
ξ	PRC Cycle Efficiency	%

V.2 NOMENCLATURE AND DEFINITIONS

Anodic current efficiency in PRC: ξ_a

The ratio of the actual weight deplated to the weight that should be deplated during the *anodic portion of PRC* cycle expressed as percent.

Anodic pulse duration: T_a, t_a, θ_2

Duration of the anodic pulse in *bipolar pulse* plating.

Average current density: I_m, $i_{ave.}$

In unipolar (PP) pulse plating the average current density is expressed as,

$$i_{ave} = \frac{i_p T_{on}}{T} = \quad \cdot p$$

Average limiting pulse current density: $i_{m,l}$, $i_{lim.}$

The average current density in plating with limiting pulse current density in *unipolar pulse plating* the average limiting pulse current density is expressed as:

$$i_{m,l} = i_{p,l} \frac{T_{on}}{T} = i_{p,l} \cdot p$$

Average overvoltage: η_{ave}

Average overvoltage in non stationary plating.

Bipolar pulse (Pulse Reverse):

Current waveform containing both anodic and cathodic current pulses.

Cathodic current efficiency in PRC: ξ_c

The ratio of the actual weight plated to the weight that should be plated during the *cathodic portion of PRC cycle* expressed as percent.

Cathodic pulse time: t_c , t_{on}

Duration of a cathodic pulse in unipolar (PC) or bipolar pulse plating (PRC).

Charge-transfer overvoltage: η_t **:**

Hindrance of transport charge carriers through the electrical double layer leads to charge-transfer overvoltage.

In the Tafel region: $\eta_t = a + b \log i$

Charge-transfer resistance: R_t

Hindrance of the charge-transfer reaction. $R_t = \frac{d\eta_t}{dc}$

In the Tafel region: $R_t = \frac{b}{2.3}$

Composition modulated alloy (CMA) coating:

Multi-layered coatings of very thin layers of two different alloys (or metals).

Concentration overvoltage: η_{conc}

Voltages, which are a consequence of deviations from bulk values of concentration near the electrode, that is diffusion and the reaction overvoltage. ($\eta_{conc} = \eta_d + \eta_r$)

Convection:

Motion in the electrolyte. Convection can be natural (motion driven by differences in density) and forced (agitation).

Covering power:

The covering power expresses the ability of an electrodeposition process to deposit at low current densities.

Crystallisation overvoltage: η_c

Hindrance of incorporation of atoms into lattice crystals leads to crystallisation overvoltage.

Crystallisation resistance: R_c

Hindrance of the process by which atoms are incorporated into crystal lattice.

Current efficiency: θ, *CE*, ξ

The current efficiency is the portion of the total current utilised in the deposition process. The rest of the current will usually produce hydrogen.

Cycle time: T

Duration of a cycle ($t_{on} + t_{off}$) in PC or ($t_a + t_c$) in PRC deposition process.

Deplating (anodic) current density: i_a

The current per unit work area, while the work is *anodic*, usually expressed in amperes per square foot or amperes per square decimetres.

Diffusion:

Mass transfer driven by a concentration gradient (chemical potential gradient).

Diffusion overvoltage: η_d

Diffusion overvoltage appears when the supply of reactant at the electrode is rate-determining when current flows.

Diffusion resistance: R_d

Hindrance of transfer of reactant at the electrode surface.

Duplex coating:

Duplex coating can be electrodeposited in a one-step process by *non stationary (PC or PRC) plating*. Only the current waveform has to be changed when two different layers are to be deposited.

Duty cycle: T, θ

The part of the cycle when the current is used for plating.

$$T = \frac{t_{on}}{t_{on}+t} \quad \text{(for PC)} \quad \text{or} \quad T = \frac{t_c}{t_c+t} \quad \text{(for PRC)}$$

Effective plating current density: i_e ·

The plating current density of the PRC cycle multiplied by the cycle efficiency.

Electrical double layer:

Dipole molecules and ions are arranged in a more ordered structure at the electrode surface than in the electrolyte. Water molecules and non-hydrated ions (mostly anions) are absorbed at the surface in an outer layer. The two layers in the interface act as an electric capacitance.

Faradaic current density: i_F

The current density, which drives the electron transfer reactions. The Faradaic and the Capacitive current density add up to the *total current density*.

Electrochemical equivalent:

The number of grams of metal deposited by one coulomb of electricity.

Frequency: f

Number of cycles per time unit.

Limiting current density: i_l

The current density at which the depositing metal ion will be fully depleted at the electrode surface.

Macroprofile:

At diffusion controlled deposition the surface is a macroprofile, when the dimension of the roughness is larger than the thickness of the diffusion layer. In this case the thickness of the diffusion layer is even and an even deposition is expected, assuming that fluctuations in the hydrodynamic conditions do not disturb the diffusion layer (especially at the corners and edges).

Metal distribution:

The same as throwing power.

Microprofile:

At a diffusion controlled deposition the surface is a microprofile, when the dimension of the roughness is smaller than the thickness of the diffusion layer. In this case protrusions are favoured for the deposition due to reduced diffusion resistance.

Migration: Mass transfer driven by an electric gradient.

Multiplex coating:

Coating consisting of several layers. A multiplex coating can be electrodeposited in a one-step process by *non stationary plating.* Only the current waveform has to be changed when two or more layers are deposited. See also composition modulated alloy (CMA) coating and Duplex coatings.

Off-time: t_{off}

Duration of period, where the current is switched *off.*

Ohmic resistance of the electrolyte: R_c

The electric resistance of the electrolyte.

Overvoltage: η

The potential deviation from equilibrium potential.

Percent levelling:

The ratio of the decrease of the surface roughness, as measured in micrometers, of the plated metal to the original surface roughness, expressed as a percent.

Percent reverse coulombs: $Q_a / Q_c \times 100$

The ratio of the deplating coulombs to the plating coulombs expressed as a percent.

Periodic reverse cycle time: $T = t_c + t_a$

The complete cycle time consisting of a plating time followed by a deplating time.

Plating coulombs: $Q_c = t_c\, i_c$ or $Q_{on} = t_{on} + i_{on}$

The plating current in amperes multiplied by the plating time in seconds.

Plating current density: i_c or i_{on}

The current per unit work area, while the work is *cathodic*, usually expressed in amperes per square foot or amperes per square decimetres.

Plating time: t_c or t_{on}

The time of the PRC or PC cycle whenever the work is *cathodic*, that is, the time that metal is being deposited.

Polarisation resistance: R_p

The total resistance in the electrochemical process. Polarisation resistance is the sum of electrolyte, charge-transfer, crystallisation, reaction and diffusion resistance. Often the electrolyte resistance is not included in the polarisation resistance, Thus:

$$R_p = \Sigma \quad R_e + R_t + R_r + R_d$$

PRC cycle efficiency:

The *net* time of plating [plating time minus (deplating time x percent reversal current)] divided by the total cycle time (assuming 100% switching efficiency; that is, instantaneous switching)

Primary current distribution:

Current distribution is only determined by the *electrolyte resistance*. The geometry has an important influence on the material distribution under conditions with primary current distribution

Pulse current density: i_p; i_{on}; j_p

Current density of a current pulse, during *on* time for PC plating.

Pulse limiting current density: $i_{p,l}$; i_l; $j_{p,l}$

The current density at which the depositing metal ion will be fully depleted at the electrode at the end of each pulse.

Pulse plating: (PC)

Electrodeposition of metals by pulsing (interrupted) current of unipolar nature.

Pulse reverse plating: (PRC)

Electrodeposition of metals with bipolar current. Plating (cathodic) pulses are followed with deplating (anodic) pulses.

Pulse time: T_{on} , t_i , t_{on}

Duration of a current pulse in non stationary plating.

Reaction overvoltage: η_r

Overvoltage caused by non-charge transfer reactions (chemical reactions).

Reaction resistance: R_r

Hindrance of a non-charge transfer reactions (chemical reactions).

Secondary current distribution:

Current distribution determined by *both* the electrolyte and activation resistance. When the activation resistance is relatively greater (large Wagner number) the influence of geometry on the material distribution is relatively small. The Wagner number decreases with increasing current density under conditions with secondary current distribution.

Superimposed pulse:

Unipolar pulse plating with *two current levels*. (See Figure 1a).

Tertiary current distribution:

Current distribution determined by *electrolytic activation and diffusion resistance.* The Wagner number increases to an infinite value when the current density approaches the limiting current density. An even metal distribution should therefore be expected at diffusion controlled deposition, but the diffusion layer then has to be absolutely even.

Throwing power:

The throwing power describes the ability of the plating solutions to distribute the metal in a deposition process; it is the number derived from deviation of the actual metal distribution from the primary current distribution.

Total current:

The applied current, which is divided into the *capacitive* and *Faradaic current*.

Transition time: τ

The pulse time at which the depositing metal ion will be fully depleted at the electrode at the end of the pulse under the given conditions of pulse current and off-time.

Unipolar pulse:

Current waveform containing only cathodic (or anodic) pulses. (See Figure 1).

Wagner number: W_a

The Wagner number is the ratio of the sum of the activation, the crystallisation, reaction, diffusion and the electrolyte resistance. The Wagner number describes the current distribution in a deposition process. A high Wagner number represents a relatively even current distribution. $Wa = \frac{\sum R\text{-}R_e}{R_e}$

V.3 PUBLICATIONS AND U.S. PATENTS BY AUTHOR

1. N. V. Mandich, "pH-metric Determination of Succinic Acid in Non-Aqueous Solutions," (title translation) *Dipl. Ing. Thesis*, University of Belgrade, Serbia, (1970).

2. N. V. Mandich, "Nastajanje i otklanjanje karbonata i razlaganje cijanida iz cijanidnih rastvora za galvanizaciju," *Zast. Mater.* **31**, (4), (1990), 151. (Serbia).

3. N. V. Mandich, "Pulse Plating of Acid Gold for Electronic Contacts," AESF 4th. International Pulse Plating Symposium, (Orlando, 1990).

4. N. V. Mandich, "Metal Finishing Education and Research in the U.S.A," *Trans. Inst. Met. Finish*, **69**, (1), (1991), 3.

5. N. V. Mandich, "Carbonate Formatiion and Removal of Cyanide Decomposition from Cyanide Plating Solution," *Trans. Inst. Met. Finish.*, **70**, (1), (1991), 41.

6. N. V. Mandich, "Electroless Catalyst Bath Optimization," *Plating Sur. Fin..*, **78**, (12), (1991), 50.

7. N. V. Mandich, "Electrodeposition of Thin Films of Gold by Pulsating DC Current," *M. Sc. Thesis*, Roosevelt University, Chicago, IL, (1991).

8. S. S. Djokic and N. V. Mandich, "Effect of Tartarate on Electrodeposition of Ni-Fe Alloy, "Proceedings of 78th. AESF Technical Conference, (Toronto, 1991).

9. N. V. Mandich, "Removal of Contaminants in Chromium Plating Solutions Via Porous Pot Method," Proceedings of AESF Hard Chromium Plating Workshop (Orlando, 1992).

10. R. Sidhu, G. A. Krulik, and N. V. Mandich, "Contribution Toward Understanding the Phenomenon of Pink Ring," *Plating Surf. Finish.*, **79**, (6), (1992), 74.

11. N. V. Mandich and G. A. Krulik, "Effect of Selected Metals on Electroless Plating Catalyst", *Trans. Inst. Met.Finish,"* **70**, (3), (1992), 117.

12. N. V. Mandich and G. A. Krulik, "Substitution of Hazardous for Non-Hazardous Process Chemicals in the Printed Circuit Industry," *Met. Finishing*, **90**, (11), (1992), 49.

13. N. V. Mandich and G. A. Krulik, "A Novel Biogenic Nickel Source for Electroless Nickel Plating," *Met. Finishing"*, **90**, (3), (1992), 9.

14. N. V. Mandich, "Electroless Gold Plating with Use of Solid (External) Nickel Catalyst," Proceedings of 79th. AESF Technical Conference, (Atlanta, 1992).

15. N. V. Mandich and G. A. Krulik, "Evolution of a Process: 50 Years of Electroless Nickel," *Met. Finishing*, **40**, (5), (1992), 25.

16. N. V. Mandich and G. A. Krulik, "The Mechanisms of Catalytic Processes in Electroless Plating," *Trans. Inst. Met. Finish.*, **70**, (3), (1992), 111.

17. N. V. Mandich and G. A. Krulik, "On the Mechanisms of Plating on Plastics," *Plating Surf. Finish.*, **80**, (11), (1993), 68.

18. N. V. Mandich and G. A. Krulik, "R&D in Year 2020," *Electrodep. Surf. Treat.* (Russian), **2**, (6), (1993), 62.

19. N. V. Mandich and G. A. Krulik "A High Efficiency Electroless Gold Plating Bath," *Electrodep. Surf. Treat. (*Russian*)*, **4**, (2), (1993), 27.

20. N. V. Mandich and G. A. Krulik, "Chemistry of Modern Permanganate Etch System for Printed Circuit Board Production," *Plating Surf. Finish.*, **78**, (12), (1993), 56.

21. N. V. Mandich and G. A. Krulik, "Fundamentals of Electroless Copper Bath Operations on Printed Circuit Boards," *Met. Finishing*, **91**, (1), (1993), 33.

22. N. V. Mandich and G. A. Krulik, "Fundamentals of Hydrogen Embrittlement," *Met. Finishing*, **91**, (3), (1993), 54.

23. N. V. Mandich and G. A. Krulik, "Selecting and Troubleshooting Chemical Conversion Coating - I," *Finishing (U.K.),* **17**, (11), (1993), 26.

24. N. V. Mandich, "EMI Shieldinig by Electroless Plating of ABS Plastics," *Plating Surf. Finish.*, **8**, (19), (1994), 60.

25. N. V. Mandich and D. Tuomi, "Morphological and Chemical Comparisons of Electroless Copper and Nickel Film Growth," *Trans. Inst. Met. Finish.,* **72**, (2), (1994), 72.

26. N. V. Mandich and G. A. Krulik, "Selecting and Troubleshooting Chemical Conversion Coating - II," *Prod. Finish (U.K.)*, **47**, (1), (1994), 20.

27. N. V. Mandich, "Chemistry of Solvent Conditioning Prior to Permanganate Etching of PCBs," *Trans. Inst. Met. Finish.*, **72**, (1), (1994), 41.

28. N. V. Mandich, "Removal of Metallic Impurities in Chromium Plating Solutions by Electrocoagulation," AESF Chromium Colloquium (Orlando, 1994).

29. N. V. Mandich, "Theoretical Considerations in Pulse Reverse Plating," Proceedings of 81st. AESF Technical Conference, (Indianapolis, 1994).

30. G. A. Krulik and N. V. Mandich, "Metallic Coatings,"in *Kirk-Othmer Encyclopedia of Chemical-Technology, Vol. 8*, 4th ed., pp 258-291 Willey, NY, (1995).

31. N. V. Mandich and R. Tuszynski, "Metalizing of Plastics" in: *Engineered Materials Handbook,* ASM International, pp. 356-364 (1995)

32. N. V. Mandich, "Chemistry of Chromium," Proceedings of 82nd. AESF Technical Conference, (Baltimore, 1995).

33. N. V. Mandich, "Troubleshooting in Zinc and Cadmium Plating," *Electrodep. Surf. Treat.* (Russian). (Submitted for publication), (1996).

34. N. V. Mandich, "Metalizing of Ceramic," *Electrodep. Surf. Treat.* (Submitted for publication), (1996)

35. N. V. Mandich, "Practical and Theoretical Aspects of Chromium Activation and Reverse Etching " AESF Chromium Colloquium, Cleveland, OH, (1996).

36. N. V. Mandich, "The Mechanisms of Chromium Plating II," Proceeding of 83rd. AESF Technical Conference (Cleveland, OH, 1996), (submitted for publication)

37. F. Altmayer and N. V. Mandich "Processing parts prior to chromium plating", chapter from AESF training book: *Chrome Plating for Engineering Application*, AESF, Orlando, FL. (1996)

38. N. V. Mandich, and N. V. Vyazovikina, "Kinetics and Mechanisms of the Chromium Anodic dissolution in the Chromium Plating Solution in the Transpassive Range," *J. Electrochem. Soc.*, (to be submitted)

39. G. A. Krulik and N. V. Mandich, "Waste Stabilisation Composition for Safer Storage of Cyanide Solutions for Reclaim," U. S. Patent Appl. #743,203 (8/91).

40. G. A. Krulik and N. V. Mandich, "Waste Treatment Composition Containing Magnesium for Treatment of Alkaline Organic Polymer Waste Solution," U. S. Patent Appl. #753,136, (9/20/91).

41. G. A. Krulik, N. V. Mandich, and R. Sidhu, " Regeneration of Iron-Based Metal Stripper Compositions," *U. S. Patent* #5,212,138, (5/18/93).

42. G. A. Krulik and N. V. Mandich, "Low Corrosivity Catalyst for Activation of Copper for Electroless Nickel Plating," *U. S. Patent* #5,212,138, (5/18/93).

43. G. A. Krulik and N. V. Mandich, "Low Corrosivity Catalyst for Containing Ammonium Ions for Activation of Copper for Electroless Nickel Plating," *U. S. Patent* #5,219,815, (6/15/93).

44. G. A. Krulik and N. V. Mandich, "Electroless Gold Plating Composition," *U. S. Patent* #5,232,492, (8/3/93).

45. N. V. Mandich, G. A. Krulik, and R. Sidhu, "Improved Process for Elimination of Pink Ring Effect in Multilayer Printed Boards Processing," U. S. Patent Appl. #886,010, (5/20/92).

46. N. V. Mandich, G. A. Krulik, and R. Sidhu, "Novel Electroless Silver Plating Solution," *U. S. Patent* # 5,322,553 (6/21/94).

47. G. A. Krulik, N. V. Mandich, and R. Sidhu, "Plating Rate Improvement for Electroless Silver and Gold Plating, *U. S. Patent* # 5,318,621, (6/7/94).

48. R. Sidhu, N. V. Mandich, and G. A. Krulik, "Solder and Tin Stripper Composition," *U. S. Patent* #5,512.201 (4/30/96).

49. G. A. Krulik, N. V. Mandich, and R. Sidhu, "Regeneration and Recycle of Ammoniacal Copper Etchant," U. S. Patent Appl. # 08-141,513 (10/27/93).

50. G. A. Krulik, N. V. Mandich, and R. Sidhu, "Control of Regeneration of Ammoniacal Copper Etchant," U. S. Patent Appl. # 08-447,811, (5/23/95).

51. G. A. Krulik, N. V. Mandich, and R. Sidhu, "Solder Stripper Recycle and Reuse," *U. S. Patent* # 5, 505.872 (04/09/1996).

52. G. A. Krulik, N. V. Mandich, and R. Sidhu, "Recycle Process for Regeneration of Ammoniacal Copper Etchant," U. S. Patent Appl. # 08-447,752, (5/13/95).

```
                ORIGINAL DATA ACQUIRED: 01/31/96 AT 10:23:54 BY CTO
                                        --------   --------   ---

FILE HISTORY:
-------------
THIS FILE IS AN ORIGINAL FILE

COMMENTS:
---------
  Methane sulfonic acid (MSA); technical grade
  Standard material
  Chrome plating project
  Y/NB-6214 p 79

ACQUISITION CONDITIONS:
-----------------------
NUMBER OF SCAN REGIONS:1
NUMBER OF SCANS:1

      FROM          TO          SPACING       TIME       HV1(V)
       Rcm-1        Rcm-1        Rcm-1       (SEC)
       24.997     3998.997         2.000     1.000         1700

DATA STORAGE                     :ACCUMULATIVE
REFERENCE WAVELENGTH :  514.53200 NM
DATA TAKEN FROM PCHANNEL(S)      :1
ENTRANCE SLIT                    :LATERAL
EXIT SLIT                        :LATERAL
SPECTROMETER OPERATION           :SIMPLE
SAMPLING                       : MACRO

USER PARAMETERS:
----------------
   Laser wavelength, nm: 514.532
   Laser power, mW: 150
   Slits, microns(1,2,3,4): 500
   Sampling method: Leitz 125x
   Date: 01/31/96

INSTRUMENTAL PARAMETERS:
------------------------
SPECTROMETER: U1000              GRATING: 1800 G/MM
DETECTOR 1: C31034          DETECTOR 2:

                ORIGINAL DATA ACQUIRED: 01/31/96 AT 10:23:54 BY CTO
                                        --------   --------   ---
PEAKS POSITION IN RCM-1       PEAKS INTENSITY IN CTS/SEC
-----------------------------------------------------------

   POSITION        INTENSITY          POSITION        INTENSITY

      344.997        12927.00           1424.997        13506.00
      550.997        13076.00           2944.997        11302.00
      784.997        14277.00           3026.997        14920.00
      972.997        10992.00
     1048.997        14932.00
```

Table 54. Laser Raman Spectroscopy Operational Data

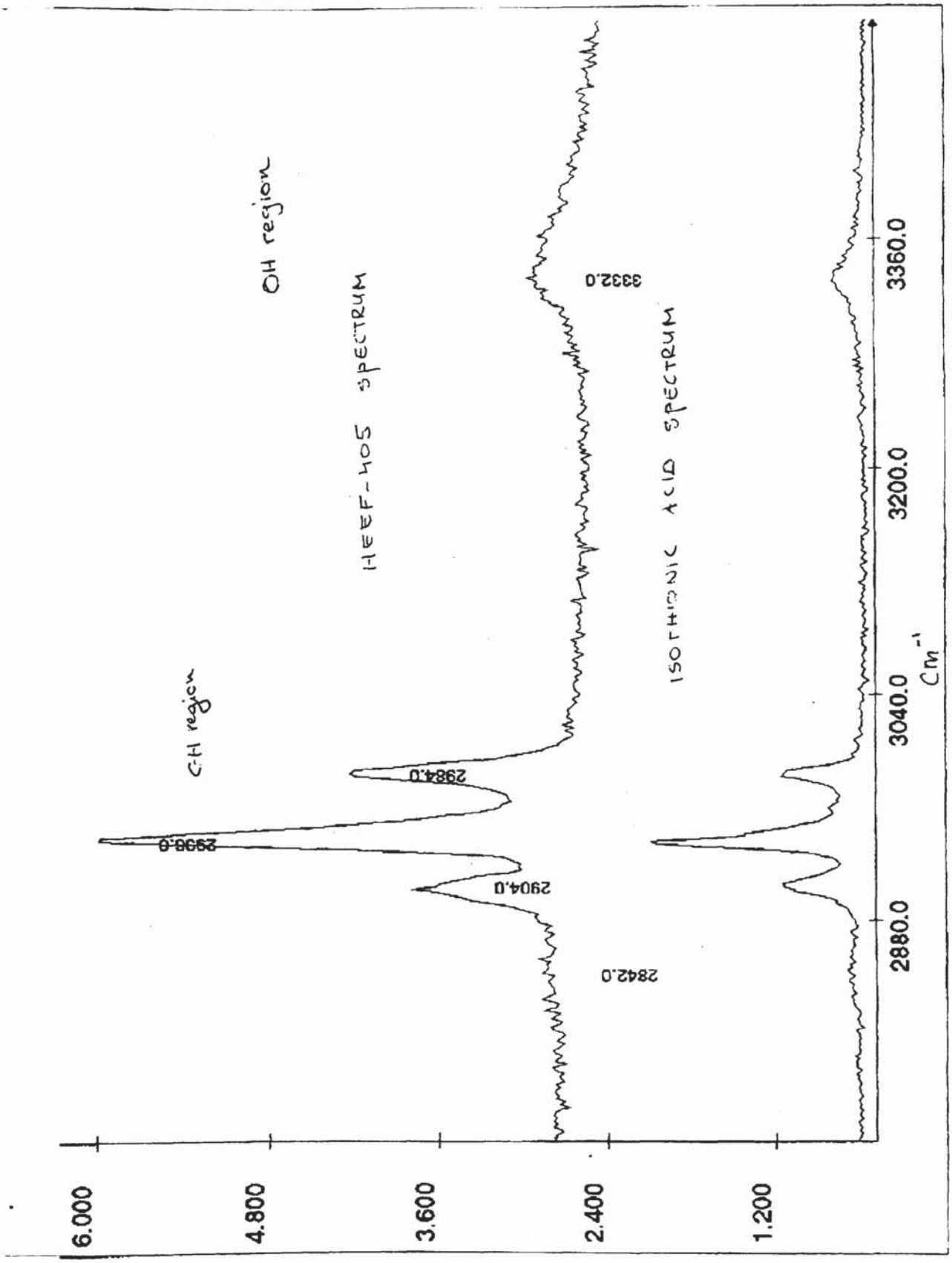

Figure 176. Laser Raman spectrum of Heef-405.

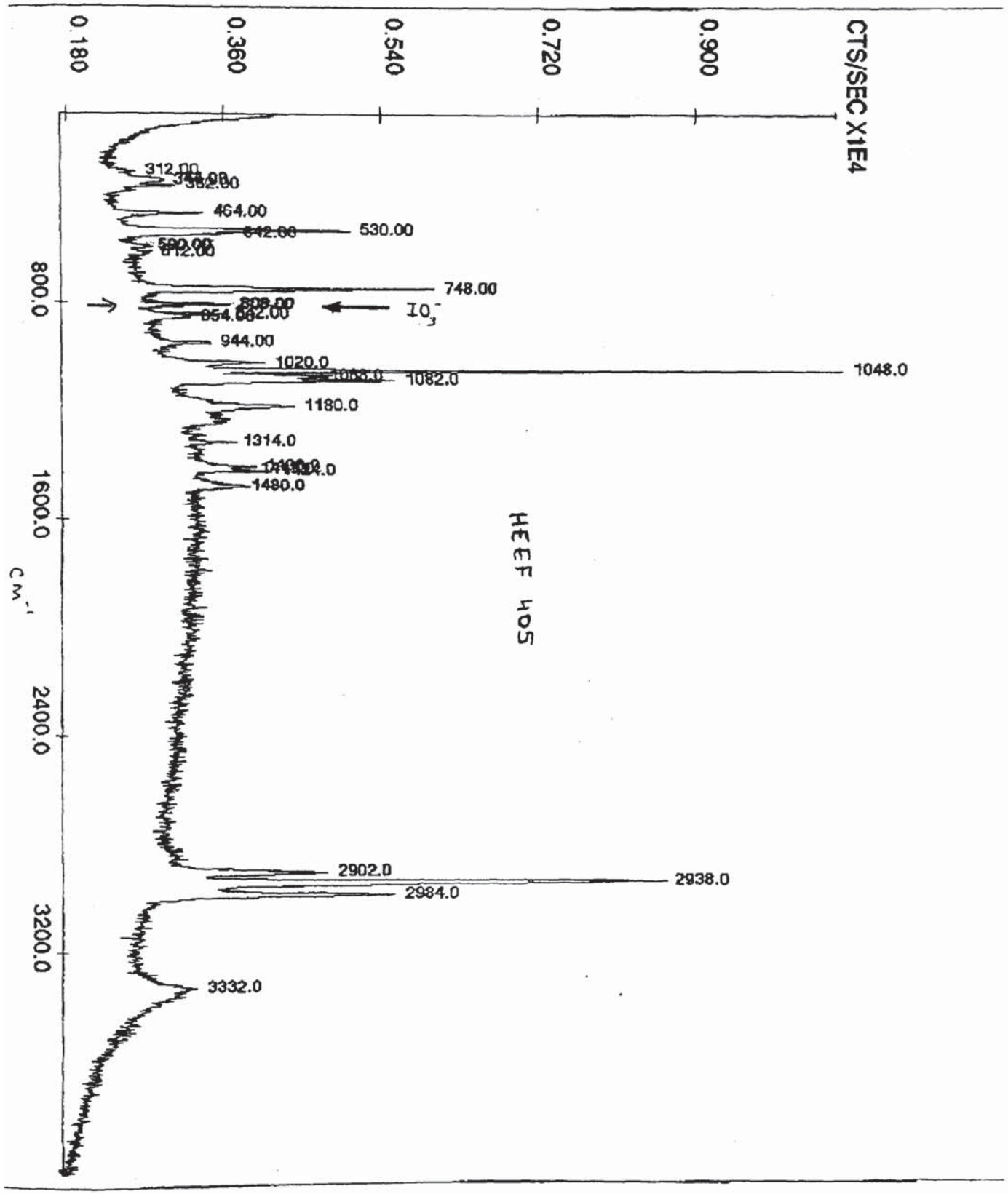

Figure 177. Laser Raman spectrum of Heef-405 indicating presence of IO_3 ion.

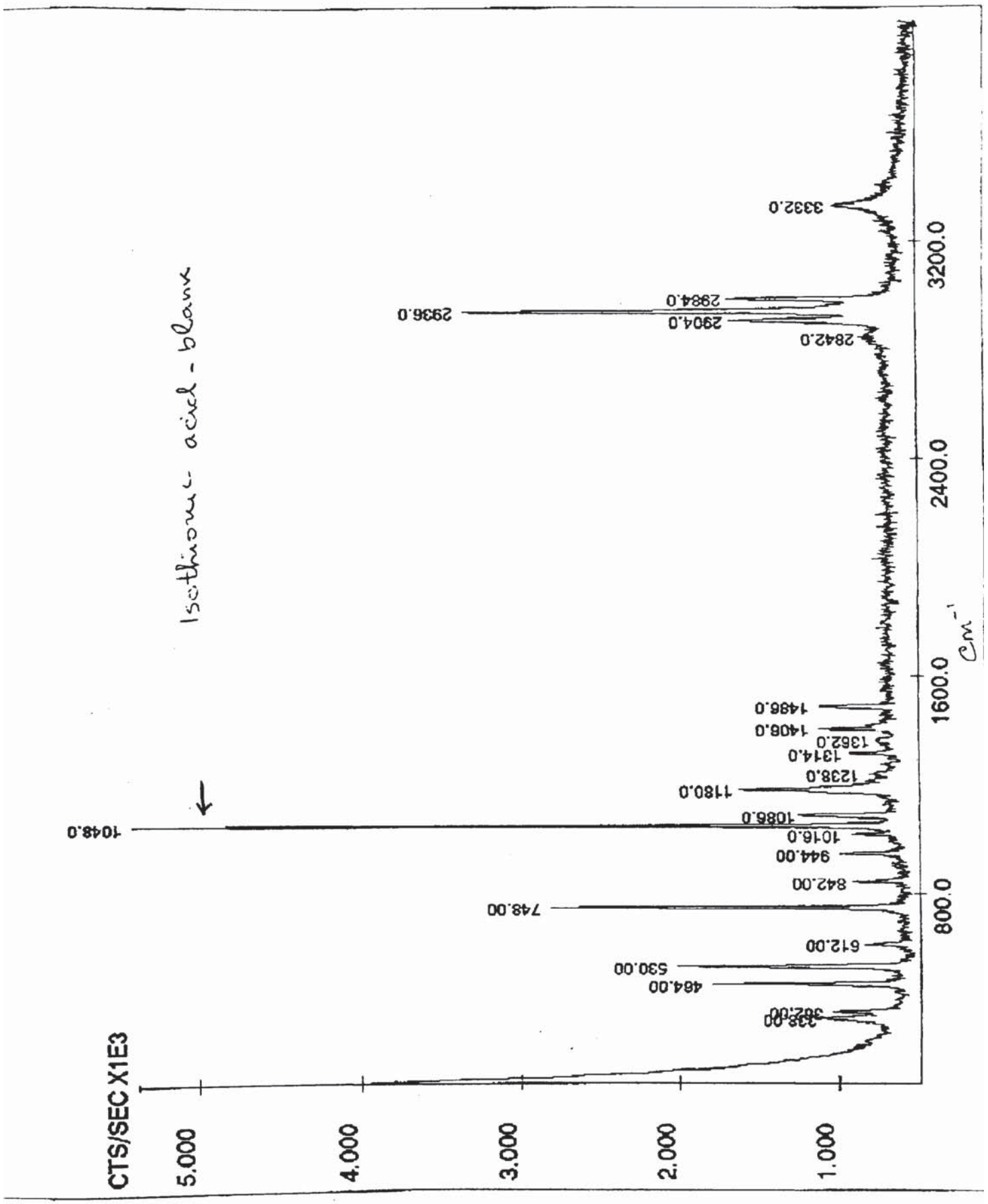

Figure 178. Laser Raman spectrum of isothionic acid.

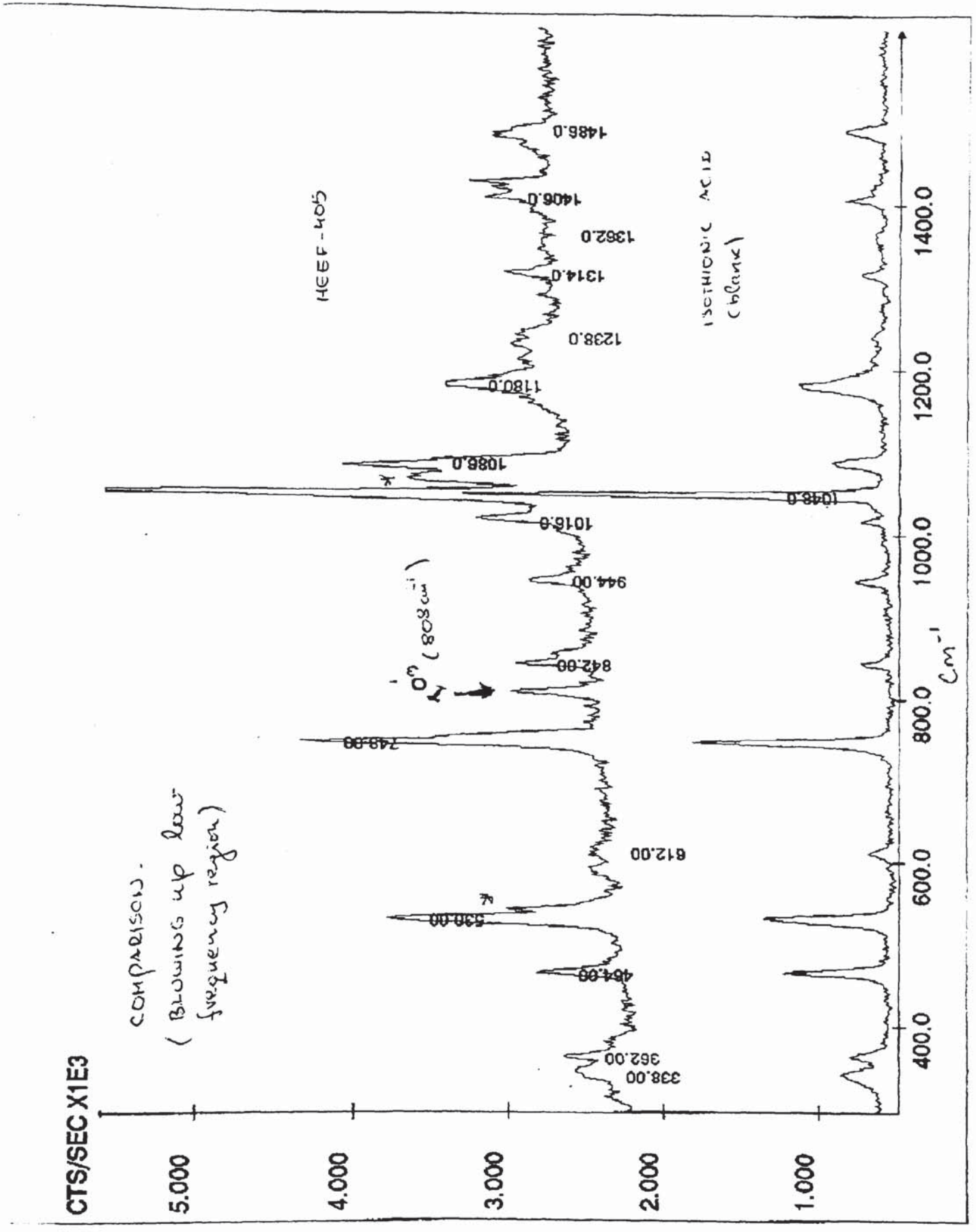

Figure 179. Laser Raman spectrum (low frequency range) of HEEF-405 (top) and isothionic acid (bottom).